

2009-01-21

Development and Validation of a Modified Clean Agent Draining Model for Total Flooding Fire Suppression Systems

Todd M. Hetrick
Worcester Polytechnic Institute

Follow this and additional works at: <https://digitalcommons.wpi.edu/etd-theses>

Repository Citation

Hetrick, Todd M., "Development and Validation of a Modified Clean Agent Draining Model for Total Flooding Fire Suppression Systems" (2009). *Masters Theses (All Theses, All Years)*. 121.
<https://digitalcommons.wpi.edu/etd-theses/121>

This thesis is brought to you for free and open access by [Digital WPI](#). It has been accepted for inclusion in Masters Theses (All Theses, All Years) by an authorized administrator of Digital WPI. For more information, please contact wpi-etd@wpi.edu.

DEVELOPMENT AND VALIDATION OF A MODIFIED CLEAN AGENT DRAINING MODEL FOR TOTAL FLOODING FIRE SUPPRESSION SYSTEMS

A Masters Thesis Submitted to the Faculty of the
WORCESTER POLYTECHNIC INSTITUTE
in partial fulfillment of the requirements for the
Degree of Master of Science in
Fire Protection Engineering

AUGUST 2009

Todd M. Hetrick

Approved:

Professor Ali S. Rangwala, Advisor

Professor Jose L. Torero, Co-Advisor

Professor Kathy A. Notarianni,
Co-Advisor & Head of Department

This document has been revised from its original form

Revisions have been made to Appendix B, *Hold Time Model Derivation*, to provide further theoretical development of the subject hold time models.

As all things are,
for mother and father.

Abstract

This project analyzes the validity of theoretical models used to predict the duration (hold time) for which a halon-replacement suppression agent will remain within a protected enclosure. Two current models and one new formulation are investigated; the *sharp descending interface* model (as applied in NFPA 2001, Annex C), the *wide descending interface* model (implemented in ISO 14520.1, Annex E), and the *thick descending interface* model (introduced herein). The thick interface model develops the *characteristic thickness*, ω , as an additional input parameter. Experimental data from 34 full-scale tests designed to characterize the discharge and draining dynamics of seven clean extinguishing agents (CEA) is used to assess model validity. For purposes of model validation the characteristic thickness is regressed from the experimental data although further work may be required to establish the independence of this parameter to other system design and environmental variables.

Results show that the wide and sharp interface models' validity is highly sensitive to the threshold of agent concentration decay being modeled; whereas the thick interface prediction method demonstrates increased robustness at any modeled threshold. When the hold time is defined as a 15% decay in agent concentration, experimentally obtained hold time values are roughly 10% shorter than sharp interface predictions, 60% longer than wide interface predictions, and 30% longer than the thick interface model predicts.

Acknowledgments

This research effort was begun under the auspices of the NFPA 2001 Technical Committee on Gaseous Fire Extinguishing Systems. Experimental work was made possible in thanks to the generous donations of suppressant agents, system hardware, system design specifications, of 3M Company, Ansul Incorporated, Chemetron Fire Systems, Fike Corporation, Kidde-Fenwal Incorporated. Additionally, Fike Corporation provided a modern test facility and multiple technicians aiding in making this effort possible. Gas sampling instrumentation was provided by 3M Company, Ansul Incorporated, Chemetron Fire Systems, DuPont Fluoroproducts, Fike Corporation, and Sevo Systems. Equipment for and execution of all door fan integrity testing was provided by Retrotec Incorporated.

The authors' appreciation for the keen foresight and efficiency of attendees to the test phase is gratefully recognized. Contributing members of the research team include Dale Edlebeck, Colin Genge, Eric Haberichter, Howard Hammel, Gene Hill, Daniel Hubert, Dai Heming, Jim Marquedant, Mark McLelland, Richard Niemann, Paul Rivers, John Schaefer, Seth Sienkiewicz, Brad Stilwell, and Bob Whiteley.

Without the encouragement and assistance of Paul Rivers this study would not have been realized. The extended efforts of Michael Barrera and John Woycheese in the first year allowed for the success this project has found today.

I would like to thank my advisor, Professor Ali S. Rangwala, for his consistency and philosophy which is always a great source of motivation to me. Discussions with faculty and fellow students at Worcester Polytechnic Institute are graciously acknowledged.

Contents

Title Page	i
Abstract	iv
Acknowledgments	v
Contents	vi
List of Figures	ix
List of Tables	xviii
Nomenclature	xix
1 Introduction	1
2 Analysis of Hold Time Models	3
2.1 Introduction	4
2.2 Background & Theoretical Considerations	5
2.3 Experimental Apparatus & Instrumentation	14
2.4 Experimental Results and Analysis	17
2.5 Summary and Conclusions	28
2.6 Recommendations for Future Work	29
Bibliography	30
3 Validating A Modified Hold Time Model	32
3.1 Introduction	33
3.2 Theoretical Background	34

3.3	Experimental Background	36
3.4	The Agent Distribution Profile	38
3.5	Validation Results & Prediction Error	45
3.6	Conclusions	50
	Bibliography	52
4	Conclusions	55
5	Recommendations for Future Work	57
	Appendices	59
A	Test Bed & Instrumentation	60
A.1	Test Bed & Leakage Characteristics	61
A.2	Total Flooding System Design	66
A.3	Instrumentation & Environmental Variables	69
B	Hold Time Model Derivation	73
B.1	Physical Phenomena & The Agent Distribution Profile	74
B.2	The Equivalent Height - Part I	77
B.3	Summarized Theoretical Assumptions	78
B.4	Conservation of Mass - The General Solution Form	79
B.5	Orifice Flow & The Door Fan Enclosure Integrity Test	81
B.6	Development of the Governing Equation	82
B.7	The Dimensionless Governing Equation	85
B.8	Rendering a Hold Time Dimensionless	88
B.9	The Equivalent Height - Part II	90
C	Agent Concentration Data	95
D	Ambient Pressure Data	108
E	Nozzle Pressure Data	125
F	Ambient Temperature Data	133
G	The Lower Leakage Fraction	146

<i>CONTENTS</i>	viii
H The Agent Concentration Profile	158
I The Regressed Agent Profile Slope	165
J Hold Time Model Evaluation	175

List of Figures

2.1	Sharp interface hydrostatic pressure schematic	8
2.2	Wide interface hydrostatic pressure schematic	9
2.3	Theoretical hold time vs. the lower leakage fraction	11
2.4	Schematic of the test enclosure	15
2.5	Example of ambient pressure data	19
2.6	The transient correlated value of F	20
2.7	Example of agent concentration data	22
2.8	The ideal agent concentration profile	23
2.9	The observed agent concentration profile	23
2.10	Plot of observed hold time versus predicted v.1	25
2.11	Plot of observed hold time versus predicted v.2	27
3.1	Theoretical agent concentration profiles	36
3.2	Schematic of the test bed	37
3.3	Typical observed agent distribution profiles	39
3.4	Theoretical agent distribution profiles	40
3.5	Diagram of interface thickness analysis	41
3.6	Interface thickness versus time	42
3.7	Regressed characteristic thickness by test	44
3.8	Regressed characteristic thickness by agent type	45
3.9	Model validation plots by theory type	48
A.1	Schematic of the test bed	62
A.2	Upper vent duct system	63
A.3	Lower vent duct system	64
B.1	Sharp interface hydrostatic diagram	75
B.2	Wide interface hydrostatic diagram	76

B.3	Thick interface hydrostatic diagram	77
B.4	Dimensionless hold time versus the flow exponent n	88
B.5	Dimensionless interface height versus time for set values of n	88
B.6	Dimensionless sharp, wide, and thick interface theories	93
C.1	Agent concentration data for test no. 1 (HFC-227ea)	96
C.2	Agent concentration data for test no. 2 (HFC-227ea)	96
C.3	Agent concentration data for test no. 3 (HFC-227ea)	96
C.4	Agent concentration data for test no. 5 (HFC-227ea)	97
C.5	Agent concentration data for test no. 6 (FK-5-1-12)	97
C.6	Agent concentration data for test no. 7 (FK-5-1-12)	97
C.7	Agent concentration data for test no. 8 (FK-5-1-12)	98
C.8	Agent concentration data for test no. 9 (FK-5-1-12)	98
C.9	Agent concentration data for test no. 10 (FK-5-1-12)	98
C.10	Agent concentration data for test no. 11 (IG-541)	99
C.11	Agent concentration data for test no. 12 (IG-541)	99
C.12	Agent concentration data for test no. 13 (IG-541)	99
C.13	Agent concentration data for test no. 14 (IG-541)	100
C.14	Agent concentration data for test no. 15 (IG-541)	100
C.15	Agent concentration data for test no. 16 (HFC-125)	100
C.16	Agent concentration data for test no. 17 (HFC-125)	101
C.17	Agent concentration data for test no. 18 (HFC-125)	101
C.18	Agent concentration data for test no. 19 (HFC-125)	101
C.19	Agent concentration data for test no. 20 (HFC-125)	102
C.20	Agent concentration data for test no. 21 (HFC-227ea)	102
C.21	Agent concentration data for test no. 22 (HFC-227ea)	102
C.22	Agent concentration data for test no. 23 (HFC-227ea)	103
C.23	Agent concentration data for test no. 28 (HFC-23)	103
C.24	Agent concentration data for test no. 29 (HFC-23)	103
C.25	Agent concentration data for test no. 30 (HFC-23)	104
C.26	Agent concentration data for test no. 31 (HFC-23)	104
C.27	Agent concentration data for test no. 32 (IG-55)	104
C.28	Agent concentration data for test no. 34 (IG-55)	105
C.29	Agent concentration data for test no. 35 (IG-55)	105
C.30	Agent concentration data for test no. 36 (IG-55)	105
C.31	Agent concentration data for test no. 38 (IG-55)	106
C.32	Agent concentration data for test no. 40 (IG-55)	106
C.33	Agent concentration data for test no. 42 (IG-100)	106

C.34 Agent concentration data for test no. 43 (IG-100)	107
D.1 Ambient pressure data for test no. 1 (HFC-227ea)	110
D.2 Ambient pressure data for test no. 2 (HFC-227ea)	110
D.3 Ambient pressure data for test no. 3 (HFC-227ea)	110
D.4 Ambient pressure data for test no. 5 (HFC-227ea)	111
D.5 Ambient pressure data for test no. 6 (FK-5-1-12)	111
D.6 Ambient pressure data for test no. 7 (FK-5-1-12)	111
D.7 Ambient pressure data for test no. 8 (FK-5-1-12)	112
D.8 Ambient pressure data for test no. 9 (FK-5-1-12)	112
D.9 Ambient pressure data for test no. 10 (FK-5-1-12)	112
D.10 Ambient pressure data for test no. 11 (IG-541)	113
D.11 Ambient pressure data for test no. 12 (IG-541)	113
D.12 Ambient pressure data for test no. 13 (IG-541)	113
D.13 Ambient pressure data for test no. 14 (IG-541)	114
D.14 Ambient pressure data for test no. 15 (IG-541)	114
D.15 Ambient pressure data for test no. 16a (HFC-125)	114
D.16 Ambient pressure data for test no. 16b (HFC-125)	114
D.17 Ambient pressure data for test no. 17a (HFC-125)	115
D.18 Ambient pressure data for test no. 17b (HFC-125)	115
D.19 Ambient pressure data for test no. 18a (HFC-125)	115
D.20 Ambient pressure data for test no. 18b (HFC-125)	115
D.21 Ambient pressure data for test no. 19a (HFC-125)	115
D.22 Ambient pressure data for test no. 19b (HFC-125)	115
D.23 Ambient pressure data for test no. 20a (HFC-125)	116
D.24 Ambient pressure data for test no. 20b (HFC-125)	116
D.25 Ambient pressure data for test no. 21a (HFC-227ea)	116
D.26 Ambient pressure data for test no. 21b (HFC-227ea)	116
D.27 Ambient pressure data for test no. 22a (HFC-227ea)	116
D.28 Ambient pressure data for test no. 22b (HFC-227ea)	116
D.29 Ambient pressure data for test no. 23a (HFC-227ea)	117
D.30 Ambient pressure data for test no. 23b (HFC-227ea)	117
D.31 Ambient pressure data for test no. 24 (HFC-227ea)	117
D.32 Ambient pressure data for test no. 25a (HFC-227ea)	117
D.33 Ambient pressure data for test no. 25b (HFC-227ea)	117
D.34 Ambient pressure data for test no. 26 (HFC-227ea)	118
D.35 Ambient pressure data for test no. 27 (HFC-23)	118
D.36 Ambient pressure data for test no. 28a (HFC-23)	118

D.37 Ambient pressure data for test no. 28b (HFC-23)	118
D.38 Ambient pressure data for test no. 29a (HFC-23)	119
D.39 Ambient pressure data for test no. 29b (HFC-23)	119
D.40 Ambient pressure data for test no. 30a (HFC-23)	119
D.41 Ambient pressure data for test no. 30b (HFC-23)	119
D.42 Ambient pressure data for test no. 31a (HFC-23)	119
D.43 Ambient pressure data for test no. 31b (HFC-23)	119
D.44 Ambient pressure data for test no. 32a (IG-55)	120
D.45 Ambient pressure data for test no. 32b (IG-55)	120
D.46 Ambient pressure data for test no. 33 (IG-55)	120
D.47 Ambient pressure data for test no. 34a (IG-55)	120
D.48 Ambient pressure data for test no. 34b (IG-55)	120
D.49 Ambient pressure data for test no. 35a (IG-55)	121
D.50 Ambient pressure data for test no. 35b (IG-55)	121
D.51 Ambient pressure data for test no. 36 (IG-55)	121
D.52 Ambient pressure data for test no. 37 (IG-55)	121
D.53 Ambient pressure data for test no. 38a (IG-55P)	122
D.54 Ambient pressure data for test no. 38b (IG-55P)	122
D.55 Ambient pressure data for test no. 39 (IG-55P)	122
D.56 Ambient pressure data for test no. 40a (IG-55P)	122
D.57 Ambient pressure data for test no. 40b (IG-55P)	122
D.58 Ambient pressure data for test no. 41 (IG-55P)	123
D.59 Ambient pressure data for test no. 42a (IG-100)	123
D.60 Ambient pressure data for test no. 42b (IG-100)	123
D.61 Ambient pressure data for test no. 43a (IG-100)	123
D.62 Ambient pressure data for test no. 43b (IG-100)	123
D.63 Ambient pressure data for test no. 44 (IG-100)	124
E.1 Nozzle pressure data for test no. 1 (HFC-227ea)	126
E.2 Nozzle pressure data for test no. 2 (HFC-227ea)	126
E.3 Nozzle pressure data for test no. 3 (HFC-227ea)	126
E.4 Nozzle pressure data for test no. 4 (HFC-227ea)	126
E.5 Nozzle pressure data for test no. 5 (HFC-227ea)	126
E.6 Nozzle pressure data for test no. 6 (FK-5-1-12)	126
E.7 Nozzle pressure data for test no. 7 (FK-5-1-12)	127
E.8 Nozzle pressure data for test no. 8 (FK-5-1-12)	127
E.9 Nozzle pressure data for test no. 9 (FK-5-1-12)	127
E.10 Nozzle pressure data for test no. 10 (FK-5-1-12)	127

E.11	Nozzle pressure data for test no. 11 (IG-541)	127
E.12	Nozzle pressure data for test no. 12 (IG-541)	127
E.13	Nozzle pressure data for test no. 13 (IG-541)	128
E.14	Nozzle pressure data for test no. 14 (IG-541)	128
E.15	Nozzle pressure data for test no. 15 (IG-541)	128
E.16	Nozzle pressure data for test no. 16 (HFC-125)	128
E.17	Nozzle pressure data for test no. 17 (HFC-125)	128
E.18	Nozzle pressure data for test no. 18 (HFC-125)	128
E.19	Nozzle pressure data for test no. 19 (HFC-125)	129
E.20	Nozzle pressure data for test no. 20 (HFC-125)	129
E.21	Nozzle pressure data for test no. 21 (HFC-227ea)	129
E.22	Nozzle pressure data for test no. 22 (HFC-227ea)	129
E.23	Nozzle pressure data for test no. 23 (HFC-227ea)	129
E.24	Nozzle pressure data for test no. 24 (HFC-227ea)	129
E.25	Nozzle pressure data for test no. 25 (HFC-227ea)	130
E.26	Nozzle pressure data for test no. 26 (HFC-227ea)	130
E.27	Nozzle pressure data for test no. 28 (HFC-23)	130
E.28	Nozzle pressure data for test no. 29 (HFC-23)	130
E.29	Nozzle pressure data for test no. 30 (HFC-23)	130
E.30	Nozzle pressure data for test no. 31 (HFC-23)	130
E.31	Nozzle pressure data for test no. 32 (IG-55)	131
E.32	Nozzle pressure data for test no. 33 (IG-55)	131
E.33	Nozzle pressure data for test no. 34 (IG-55)	131
E.34	Nozzle pressure data for test no. 36 (IG-55)	131
E.35	Nozzle pressure data for test no. 37 (IG-55)	131
E.36	Nozzle pressure data for test no. 38 (IG-55P)	131
E.37	Nozzle pressure data for test no. 39 (IG-55P)	132
E.38	Nozzle pressure data for test no. 40 (IG-55P)	132
E.39	Nozzle pressure data for test no. 41 (IG-55P)	132
E.40	Nozzle pressure data for test no. 42 (IG-100)	132
E.41	Nozzle pressure data for test no. 43 (IG-100)	132
F.1	Ambient temperature data for test no. 1 (HFC-227ea)	134
F.2	Ambient temperature data for test no. 2 (HFC-227ea)	134
F.3	Ambient temperature data for test no. 7 (FK-5-1-12)	134
F.4	Ambient temperature data for test no. 8 (FK-5-1-12)	135
F.5	Ambient temperature data for test no. 9 (FK-5-1-12)	135
F.6	Ambient temperature data for test no. 10 (FK-5-1-12)	135

F.7	Ambient temperature data for test no. 11 (IG-541)	136
F.8	Ambient temperature data for test no. 13 (IG-541)	136
F.9	Ambient temperature data for test no. 14 (IG-541)	136
F.10	Ambient temperature data for test no. 15 (IG-541)	137
F.11	Ambient temperature data for test no. 17 (HFC-125)	137
F.12	Ambient temperature data for test no. 18 (HFC-125)	137
F.13	Ambient temperature data for test no. 21 (HFC-227ea)	138
F.14	Ambient temperature data for test no. 22 (HFC-227ea)	138
F.15	Ambient temperature data for test no. 23 (HFC-227ea)	138
F.16	Ambient temperature data for test no. 24 (HFC-227ea)	139
F.17	Ambient temperature data for test no. 25 (HFC-227ea)	139
F.18	Ambient temperature data for test no. 26 (HFC-227ea)	139
F.19	Ambient temperature data for test no. 27 (HFC-23)	140
F.20	Ambient temperature data for test no. 28 (HFC-23)	140
F.21	Ambient temperature data for test no. 29 (HFC-23)	140
F.22	Ambient temperature data for test no. 30 (HFC-23)	141
F.23	Ambient temperature data for test no. 31 (HFC-23)	141
F.24	Ambient temperature data for test no. 32 (IG-55)	141
F.25	Ambient temperature data for test no. 33 (IG-55)	142
F.26	Ambient temperature data for test no. 34 (IG-55)	142
F.27	Ambient temperature data for test no. 35 (IG-55)	142
F.28	Ambient temperature data for test no. 36 (IG-55)	143
F.29	Ambient temperature data for test no. 37 (IG-55)	143
F.30	Ambient temperature data for test no. 38 (IG-55P)	143
F.31	Ambient temperature data for test no. 39 (IG-55P)	144
F.32	Ambient temperature data for test no. 40 (IG-55P)	144
F.33	Ambient temperature data for test no. 41 (IG-55P)	144
F.34	Ambient temperature data for test no. 42 (IG-100)	145
F.35	Ambient temperature data for test no. 43 (IG-100)	145
F.36	Ambient temperature data for test no. 44 (IG-100)	145
G.1	Correlated value of F for test no. 16 - Inst. #1 (HFC-125)	149
G.2	Correlated value of F for test no. 17 - Inst. #1 (HFC-125)	149
G.3	Correlated value of F for test no. 18 - Inst. #1 (HFC-125)	149
G.4	Correlated value of F for test no. 19 - Inst. #1 (HFC-125)	150
G.5	Correlated value of F for test no. 20 - Inst. #1 (HFC-125)	150
G.6	Correlated value of F for test no. 21 - Inst. #1 (HFC-227ea)	150
G.7	Correlated value of F for test no. 21 - Inst. #2 (HFC-227ea)	151

G.8	Correlated value of F for test no. 22 - Inst. #2 (HFC-227ea)	151
G.9	Correlated value of F for test no. 23 - Inst. #1 (HFC-227ea)	151
G.10	Correlated value of F for test no. 23 - Inst. #2 (HFC-227ea)	152
G.11	Correlated value of F for test no. 25 - Inst. #1 (HFC-227ea)	152
G.12	Correlated value of F for test no. 25 - Inst. #2 (HFC-227ea)	152
G.13	Correlated value of F for test no. 29 - Inst. #1 (HFC-23)	153
G.14	Correlated value of F for test no. 30 - Inst. #1 (HFC-23)	153
G.15	Correlated value of F for test no. 31 - Inst. #1 (HFC-23)	153
G.16	Correlated value of F for test no. 32 - Inst. #1 (IG-55)	154
G.17	Correlated value of F for test no. 32 - Inst. #2 (IG-55)	154
G.18	Correlated value of F for test no. 34 - Inst. #1 (IG-55)	154
G.19	Correlated value of F for test no. 34 - Inst. #2 (IG-55)	155
G.20	Correlated value of F for test no. 35 - Inst. #1 (IG-55)	155
G.21	Correlated value of F for test no. 38 - Inst. #1 (IG-55P)	155
G.22	Correlated value of F for test no. 38 - Inst. #2 (IG-55P)	156
G.23	Correlated value of F for test no. 40 - Inst. #1 (IG-55P)	156
G.24	Correlated value of F for test no. 42 - Inst. #1 (IG-100)	156
G.25	Correlated value of F for test no. 42 - Inst. #2 (IG-100)	157
G.26	Correlated value of F for test no. 43 - Inst. #1 (IG-100)	157
G.27	Correlated value of F for test no. 43 - Inst. #2 (IG-100)	157
H.1	Agent concentration profile for test no. 1 (HFC-227ea)	159
H.2	Agent concentration profile for test no. 2 (HFC-227ea)	159
H.3	Agent concentration profile for test no. 3 (HFC-227ea)	159
H.4	Agent concentration profile for test no. 5 (HFC-227ea)	159
H.5	Agent concentration profile for test no. 6 (FK-5-1-12)	159
H.6	Agent concentration profile for test no. 7 (FK-5-1-12)	159
H.7	Agent concentration profile for test no. 8 (FK-5-1-12)	160
H.8	Agent concentration profile for test no. 9 (FK-5-1-12)	160
H.9	Agent concentration profile for test no. 10 (FK-5-1-12)	160
H.10	Agent concentration profile for test no. 11 (IG-541)	160
H.11	Agent concentration profile for test no. 12 (IG-541)	160
H.12	Agent concentration profile for test no. 13 (IG-541)	160
H.13	Agent concentration profile for test no. 14 (IG-541)	161
H.14	Agent concentration profile for test no. 15 (IG-541)	161
H.15	Agent concentration profile for test no. 16 (HFC-125)	161
H.16	Agent concentration profile for test no. 17 (HFC-125)	161
H.17	Agent concentration profile for test no. 18 (HFC-125)	161

H.18	Agent concentration profile for test no. 19 (HFC-125)	161
H.19	Agent concentration profile for test no. 20 (HFC-125)	162
H.20	Agent concentration profile for test no. 21 (HFC-227ea)	162
H.21	Agent concentration profile for test no. 22 (HFC-227ea)	162
H.22	Agent concentration profile for test no. 23 (HFC-227ea)	162
H.23	Agent concentration profile for test no. 28 (HFC-23)	162
H.24	Agent concentration profile for test no. 29 (HFC-23)	162
H.25	Agent concentration profile for test no. 30 (HFC-23)	163
H.26	Agent concentration profile for test no. 31 (HFC-23)	163
H.27	Agent concentration profile for test no. 32 (IG-55)	163
H.28	Agent concentration profile for test no. 34 (IG-55)	163
H.29	Agent concentration profile for test no. 35 (IG-55)	163
H.30	Agent concentration profile for test no. 36 (IG-55)	163
H.31	Agent concentration profile for test no. 38 (IG-55P)	164
H.32	Agent concentration profile for test no. 40 (IG-55P)	164
H.33	Agent concentration profile for test no. 42 (IG-100)	164
H.34	Agent concentration profile for test no. 43 (IG-100)	164
I.1	Regressed agent profile slope for test no. 1 (HFC-227ea)	166
I.2	Regressed agent profile slope for test no. 2 (HFC-227ea)	166
I.3	Regressed agent profile slope for test no. 3 (HFC-227ea)	166
I.4	Regressed agent profile slope for test no. 7 (FK-5-1-12)	167
I.5	Regressed agent profile slope for test no. 8 (FK-5-1-12)	167
I.6	Regressed agent profile slope for test no. 9 (FK-5-1-12)	167
I.7	Regressed agent profile slope for test no. 10 (FK-5-1-12)	168
I.8	Regressed agent profile slope for test no. 15 (IG-541)	168
I.9	Regressed agent profile slope for test no. 16 (HFC-125)	168
I.10	Regressed agent profile slope for test no. 17 (HFC-125)	169
I.11	Regressed agent profile slope for test no. 18 (HFC-125)	169
I.12	Regressed agent profile slope for test no. 19 (HFC-125)	169
I.13	Regressed agent profile slope for test no. 20 (HFC-125)	170
I.14	Regressed agent profile slope for test no. 21 (HFC-227ea)	170
I.15	Regressed agent profile slope for test no. 22 (HFC-227ea)	170
I.16	Regressed agent profile slope for test no. 23 (HFC-227ea)	171
I.17	Regressed agent profile slope for test no. 28 (HFC-23)	171
I.18	Regressed agent profile slope for test no. 29 (HFC-23)	171
I.19	Regressed agent profile slope for test no. 30 (HFC-23)	172
I.20	Regressed agent profile slope for test no. 31 (HFC-23)	172

I.21	Regressed agent profile slope for test no. 32 (IG-55)	172
I.22	Regressed agent profile slope for test no. 34 (IG-55)	173
I.23	Regressed agent profile slope for test no. 35 (IG-55)	173
I.24	Regressed agent profile slope for test no. 36 (IG-55)	173
I.25	Regressed agent profile slope for test no. 38 (IG-55P)	174
I.26	Regressed agent profile slope for test no. 40 (IG-55P)	174
J.1	Model validation plots for all FK-5-1-12 tests	176
J.2	Model validation plots for all HFC-125 tests	177
J.3	Model validation plots for all HFC-227ea tests	178
J.4	Model validation plots for all HFC-23 tests	179
J.5	Model validation plots for all IG-541 tests	180
J.6	Model validation plots for all IG-55 tests	181
J.7	Model validation plots for all agent types	182

List of Tables

2.1	Gas sampling probe locations	17
2.2	Experiment configuration parameters	18
3.1	Summary values of the regressed dimensionless interface width	46
3.2	Experimental error relative to predicted values	50
A.1	Experimental leakage configuration parameters	65
A.2	Total flooding system design parameters	67
A.3	Environmental parameters & data sources retained	70

Nomenclature

A	Theoretical orifice area [m ²]
A_F	Enclosure floor area [m ²]
A_i	Orifice area for gas flowing into enclosure [m ²]
A_{LL}	Summed orifice area of all lower leakages [m ²]
A_o	Orifice area for gas flowing out of enclosure [m ²]
A_T	Total theoretical orifice area in the orifice flow equation [m ²]
A_{UL}	Summed orifice area of all upper leakages [m ²]
C	Combined coefficient in the orifice flow equation [s ²ⁿ⁻¹ /m ²ⁿ⁻³]
C_d	Discharge coefficient in the orifice flow equation [-]
C_o	Discharge coefficient for the orifice described by A_o [-]
C_U	Unit conversion constant in the orifice flow equation [s ²ⁿ⁻¹ /m ²ⁿ⁻¹]
c_i	Initial clean agent volume concentration [Vol. %]
c_f	Final clean agent volume concentration [Vol. %]
F	Lower leakage fraction, Eqs. 2 & 4 [-]
\tilde{F}	Dimensionless ratio of out flow and inflow orifice areas [-]
g	Acceleration due to gravity [9.81 m/s ²]
H_o	Enclosure maximum height [m]
H_e	Equivalent interface height [m]
H_i	Interface height [m]
H_{np}	Neutral plane height [m]
H_p	Protected height [m]
$\tilde{H}_{SDI_{2004}}$	Dimensionless height for the sharp interface theory of the 2004 NFPA publication [-]
$\tilde{H}_{SDI_{2008}}$	Dimensionless height for the sharp interface theory of the 2008 NFPA publication [-]
\tilde{H}_{tp}	Dimensionless transition elevation at which the thick interface changes piecewise behavior [-]

\tilde{H}_{WDI}	Dimensionless height for the wide interface theory of published in ISO 14520-1 [-]
k_1	Orifice flow coefficient from the door fan integrity test [$\text{m}^{2+3n}/\text{kg}^n$]
k_2	Regressed equivalent leakage area [m^2]
n	Orifice flow exponent in the orifice flow equation [-]
ΔP_{LL}	Pressure difference (with reference to ambient) across enclosure boundary at lowest leak elevation [Pa]
ΔP_{UL}	Pressure difference (with reference to ambient) across enclosure boundary at highest leak elevation [Pa]
P_{in}	Absolute ambient pressure inside the enclosure [Pa]
P_{out}	Absolute ambient pressure outside the enclosure [Pa]
Q	Flow in the orifice flow equation [m^3/s]
t_0	Start of the hold time [s]
t_c	Characteristic drain time [s]
t_f	End of the hold time [s]
\tilde{t}_1	Dimensionless hold time used when n is variable [-]
\tilde{t}_2	Dimensionless hold time used when $n = 0.5$ [-]
V_c	Characteristic drain rate [m^3/s]
V_i	Flow into the enclosure [m^3/s]
V_o	Flow out of the enclosure [m^3/s]

Greek Symbols

β_1	Dimensionless coefficient used when n is variable [-]
β_2	Dimensionless coefficient used when $n = 0.5$ [-]
ρ	Fluid density in orifice flow equation [kg/m^3]
$\tilde{\rho}$	Dimensionless density parameter [-]
ρ_{ag}	Clean extinguishing agent vapor density at 21°C [kg/m^3]
ρ_{air}	Density of air; 1.202 in NFPA & 1.205 in ISO standards [kg/m^3]
ρ_{mix}	Agent and air mixture density [kg/m^3]
ω	Characteristic thickness of the agent-air interface in the thick descending interface model [$(\Delta H/H_{max}) / (\Delta C/C_{max})$] [-]

Abbreviations

FK	Fluoroketone
HFC	Hydrofluorocarbon

LIST OF TABLES

xxi

IG	Inert gas
ISO	International Standards Organization
NFPA	National Fire Protection Association

Chapter 1

Introduction

Total flooding fire suppression systems are currently installed and armed for activation in high-value, enclosed spaces all over the world. Prior to enforcement of the Montreal Protocol, which instituted broad restrictions on the emissions of ozone depleting compounds, Halon 1301 was the common suppressant of choice. Today's industry provides an array of halon-replacement agents termed as clean extinguishing agents. These agents are generally divided into two categories: halocarbon-compounds and inert gases. The difference in vapor densities of the CEA relative to the air surrounding the protected enclosure provides the driving force for agent leakage and concentration decay. Due to the increased molecular weights of many modern agents they tend to drain from the protected enclosure much more rapidly than their halogenated ancestors. The transition in CEA usage, however, has not been paralleled by an equally radical modernization of the physical theory used to design and model these systems' function. Model validation studies using halon-replacement agents have not, until now, been completed for the public in full scale.

This project documents an extensive, full-scale test program designed to characterize the draining behavior of seven prevalent CEAs. The experimental findings are used to validate analytical models that are universally applied in designing total flooding systems based on specified performance criteria. Herein it is found that the *sharp descending interface model*, espoused in NFPA 2001, and the *wide descending interface model*, adopted in ISO 14520, typically provide inadequate predictions of CEA retention times because the model assumptions are not analogous to the users' performance criteria.

Each model introduces simplified assumptions for where CEA accumu-

lates in the protected enclosure as a function of elevation. Increased prediction accuracy is obtained in the present study by reformulating this model assumption to more closely represent the draining behavior observed in the experimental measures. Coined as the *thick descending interface model*, this analytical tool requires the user to input an additional parameter, which specifies the maximum interface thickness. For the purposes of model validation this parameter is extracted from the experimental data although further work may be required to establish the independence of this parameter to other system design and environmental variables.

The experimental program documented throughout was initiated under the auspices of the NFPA 2001 technical subcommittee on gaseous fire extinguishing systems. Prototypical work was completed with the agent HFC-227ea by Fike Corporation in the fall of 2005 at their test facility in Blue Springs, Missouri. The same test bed (4.9 m tall and 100 m³) was then used in the fall of 2006 with FK-5-1-12, HFC-125 and IG-541. Support garnered by the Fire Suppression Systems Association (FSSA) lead to additional testing in the late summer of 2007 with HFC-227ea, HFC-23, IG-100 and IG-55. The sizes of enclosure penetrations available for agent draining were independently controlled at the upper and lower of compartment elevation. Agent concentrations across elevation comprise primary measurements although ambient pressure, temperature, and relative humidity are also documented.

Experimental findings from testing in 2006 alone are presented in the first chapter of this document which was previously published in Fire Technology. Experimental results from 2005, 2006 and 2007 are presented in the second and final chapter which is dedicated primarily to introducing the newly formulated thick descending interface model. Because each of these two chapters is intended for publication purposes, they are each concise and may leave some questions unanswered. The included appendices are expected to meet this need by providing extended documentation of the implemented experimental measures and measurements acquired.

Chapter 2

Analysis of Hold Time Models for Total Flooding Clean Extinguishing Agents¹

Abstract

This study documents the experimental results of a research program designed to evaluate the validity of the widely published hold time prediction models found in NFPA 2001, Annex C and ISO 14520-1, Annex E. The models discussed in these standards obtain a measure of the equivalent leakage area, which, when coupled with ‘worst case’ assumptions, can be used to determine the minimum hold time. Three hold time prediction theories are adopted from these standards for validation; a wide descending interface model as implemented in ISO 14520-1 and two sharp descending interface models from the 2004 and 2008 publications of NFPA 2001.

The experimental program is comprised of fifteen tests conducted in a 103 m³ test enclosure. Three commercially available clean agents are selected to span a wide range of agent vapor densities including FK-5-1-12, HFC-125, and IG-541. A series of holes were drilled through enclosure boundaries at upper and lower elevations which were opened or closed as a means of regulating the amount of leakage area for any given test. Vertical profiles of agent concentration and ambient pressure are used to evaluate the agent concentration distribution, rates of agent draining, and the effective lower leakage fraction.

¹Previously Published in Fire Technology.

Received: May 18, 2007 / **Accepted:** February 15, 2008 / **Published online:** April 1, 2008 / **Published in print:** September, 2008

A nondimensional hold time is used to compare experimental results involving differing agent types and leakage areas. Results show that empirical values of the hold time are up to 50% longer than the theoretical hold time predictions when evaluated as the time to reduce the agent concentration to half its initial value. When evaluated as a 15% drop in concentration the model validity is significantly reduced. Under this condition, empirical hold time values are up to 50% shorter than the predictions of the sharp descending interface models and up to 100% longer than the wide descending interface model.

Keywords: hold time, retention time, total flooding, clean agent, validation study

2.1 Introduction

The goal of this study is to validate industry-standard hold time prediction models as they apply to a variety of clean extinguishing agents. Total flooding fire suppression involves the discharge of a clean extinguishing agent that is typically required to provide protection within the design envelope for a minimum ten minute period. The ‘fan integrity test’ encompasses the test method and leakage modeling used to evaluate the total flooding system design with respect to the ‘hold time’ or ‘retention time’ requirement. The hold time is defined as the period of time required for the clean agent concentration to drop to a specified threshold (usually 80% of the initial discharge concentration) at a specified height in the enclosure (often chosen as the point of highest combustibles or at 75% of the maximum enclosure height) [1]. The Authority Having Jurisdiction (AHJ) can set the hold time requirement accounting for both the cooling of potential ignition hazards and emergency response.

In this study, a 103 cubic meter experimental enclosure is used to observe leakage flows through enclosure boundaries. The upper and lower leakage areas are varied to determine the effect on hold times of three commercially available gaseous suppression agents: FK-5-1-12, HFC-125, and IG-541. Previous studies evaluating the observed agent leakage after discharge show that model predictions are often inaccurate; resulting in both overly conservative and optimistic hold time approximations [2], [3], [4].

NFPA 2001, Annex C and ISO 14520-1, Annex E contain enclosure integrity design standards, which are chosen for comparative analysis in this

paper due to the prevalent adoption and use around the world. Extensive modifications have been submitted to the current version of NFPA 2001 that was published in 2004. An updated version of the NFPA design standard will be published early in 2008. Comparative analysis in this paper will utilize both NFPA publications to further help in understanding these changes. In addition, the empirical data is compared to the theory employed in the 2006 publication of ISO 14520-1.

2.2 Theoretical Considerations

The development of a theoretical model to predict clean agent hold times must begin with a general description of the physical phenomena in question. Once the governing forces of the phenomena are isolated a series of simplifying model assumptions are made and a quantitative model built. Existing theory is then presented in a dimensionless form as employed in the data analysis portions of this paper.

Upon activation, the valves on all agent storage containers attached to the total flooding fire suppression system open simultaneously. The clean extinguishing agent, propelled by the high storage pressure, flows through the connected pipe network to one or more points of discharge into the design envelope (nozzles). Inert gases used as clean agents rapidly expand, cooling the temperature of the pipe network and ultimately the mixture of air and agent inside the design envelope. Because fluoroketone agents such as FK-5-1-12 and hydrofluorocarbons such as HFC-125 are stored as liquids under pressure it is expected that these agents undergo rapid vaporization and expansion in the pipe network and immediately after discharging through the system nozzle.

Following the turbulent discharge a relatively uniform mixture of clean agent and air remains inside the design envelope. The bulk gas temperature is significantly lower than that of the air surrounding the enclosure. Given enough time, it is likely that the agent and air will stratify. As well, for agents such as IG-541 that are actually mixtures of multiple constituents (52% N₂, 40% Ar, 8% CO₂), the potential for partitioning and eventual stratification of the agent itself does exist.

The agent and air mixture mass density, inside the design envelope, is generally greater inside the enclosure than the density of air surrounding it. This density disparity exerts a positive hydrostatic pressure on the lower en-

closure boundaries and a negative interior-to-exterior pressure differential at upper enclosure boundaries. These pressure differentials drive a convective flow of agent-air mixture out lower leakages in the enclosure, which is volumetrically balanced by fresh air flowing in upper leakages. This is the only transport method considered in evaluating the global rate at which agent drains from the enclosure.

In order to condense the involved physics into an analytical solution, the following assumptions are made. (1) Thermal effects are ignored. The agent-air mixture resulting after the discharge event and the air surrounding the enclosure are both assumed to exist at standard atmospheric temperature (21°C). Further, the thermal affects produced during a real fire incident will not be considered in this study. (2) Species diffusive transport is either neglected or assumed to mix at an infinitesimal rate in known proportions. An immediate result of this assumption is that agents comprised of multiple species do not partition. The variation in the treatment of diffusive transport is addressed in this work. (3) The leakage areas in enclosure boundaries are assumed to exist at only two locations: the extremes of upper and lower elevation. The agent draining and fresh air replacement therefore occurs through one upper orifice and one lower orifice. (4) For the purposes of this paper bias pressures are not considered².

Assumption (2) leaves the reader with an unclear interpretation of how species diffusion is to be treated. The primary difference between various models used to predict agent distribution lies in the assumption of agent diffusion employed [1]. Depending upon the assumed behavior of species diffusion a distinct *agent distribution profile* will result. Due to this, in the remainder of this paper the assumed agent distribution profile is frequently used in reference to the species diffusion assumption.

Three different theoretical hold time models are discussed in NFPA 2001 and ISO 14520-1: the *sharp descending interface model*, *wide descending interface model*, and *continuous mixing model*. Each theoretical model implements a zone model analysis in which each zone is modeled as a homogeneous mixture. However, each model uses a different assumption for the agent distribution profile, thereby predicting slightly different agent concentrations

²Bias pressures are typically created by HVAC systems; resulting in either a static or dynamic pressure differential between the enclosure's interior and exterior. Observation and mathematical handling of bias pressures is integrated into the published editions of NFPA 2001 and ISO 14520-1. Bias pressures were eliminated from the test enclosure in this study; and thus, are not included in the theoretical derivations.

through the hold time as a function of elevation.

Two of these three models employ a stratified agent distribution assumption. The sharp descending interface model assumes that as the column of agent-air mixture leaks out lower enclosure boundaries a sharp interface forms between inflowing fresh air and the agent-air mixture. Across this interface, species diffusion is not accounted for. The wide descending interface model assumes that incoming air mixes with the upper edge of the column of agent-air mixture; resulting in a linear decay from full concentration at the interface height, H_i , to a 0% concentration at the enclosure's maximum height, H_0 . The continuous mixing model assumes that the enclosure's volume is homogeneous throughout the hold time; resulting in infinitely fast mixing between inlet fresh air and the resident agent-air mixture. According to typical design practices this model is not applied unless there is good reason to believe that the agent-air mixture would readily mix with the influx of fresh air. In this study, mechanical mixing was not provided in any tests conducted; thus, application of the continuous mixing model is not used. Further discussion of this model and its applicability to modeling clean agent hold times is reported elsewhere [1], [2], [5].

Schematics of the two stratified agent distribution profile assumptions, the sharp descending interface and wide descending interface, with the resulting hydrostatic pressure profile are shown in Figures 2.1 and 2.2, respectively. In each, the assumed hydrostatic pressure profile of the atmosphere is given as P_o and that of the agent-air mixture inside the enclosure as $P_i(t)$. The height of the interface is given as H_i and the neutral plane, H_{np} , denotes that elevation where inside and outside pressures are equal.

Figures 2.1 and 2.2 show how the species distribution assumption defines the agent distribution profile. As well, only two leakage areas exist, at the upper left and lower left of the figure. The model is one dimensional in space as a function of elevation (the leakages are not actually located in the corners of the room). Each figure shows how the pressure differential between interior and exterior conditions is evaluated as a function of the hydrostatic pressure profile at the elevations of inlet and outlet leakages. Based upon the magnitude of these two pressure differentials the gas flow through leakages is modeled according to well-established theory on orifice flow [5].

The sizes of the leakage areas at the upper and lower elevations of the enclosure play a significant role in governing the draining rate of the agent-air mixture. To relate the theoretical model to a real-world scenario a method of assessing the amount of leakage area in an existing structure must be

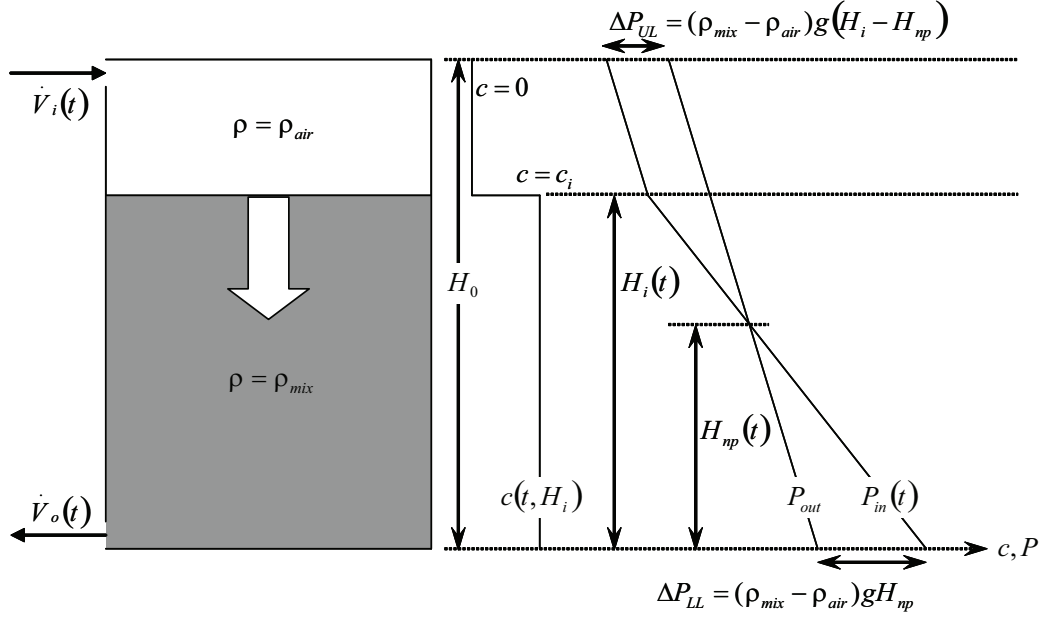


Figure 2.1: Sharp descending interface hydrostatic pressure profile. As shown in the figure, a sharp interface forms between inflowing fresh air and the agent-air mixture.

adopted.

One method of evaluating the total amount of open leakage area in enclosure boundaries is to perform a *fan integrity test*. The test procedure consists of a calibrated fan that infuses or removes air from the enclosure at a known flow. The corresponding increase or decrease in enclosure pressure relative to atmospheric is then measured for a series of fan flows. The pairs of values are used in a regression and fit to Equation (2.1),

$$Q = C \left(\frac{2\Delta P}{\rho} \right)^n, \quad (2.1)$$

in order to find the unknown values of the total leakage area, A_T , and the flow exponent, n . Q is the fan flow, ΔP is the pressure differential from atmospheric, ρ is the density of air and n is the flow exponent. The coefficient, C , is equal to $A_T C_d C_U$; where, A_T is the total leakage area, C_d is an orifice discharge coefficient, and C_U is a constant based on the value of

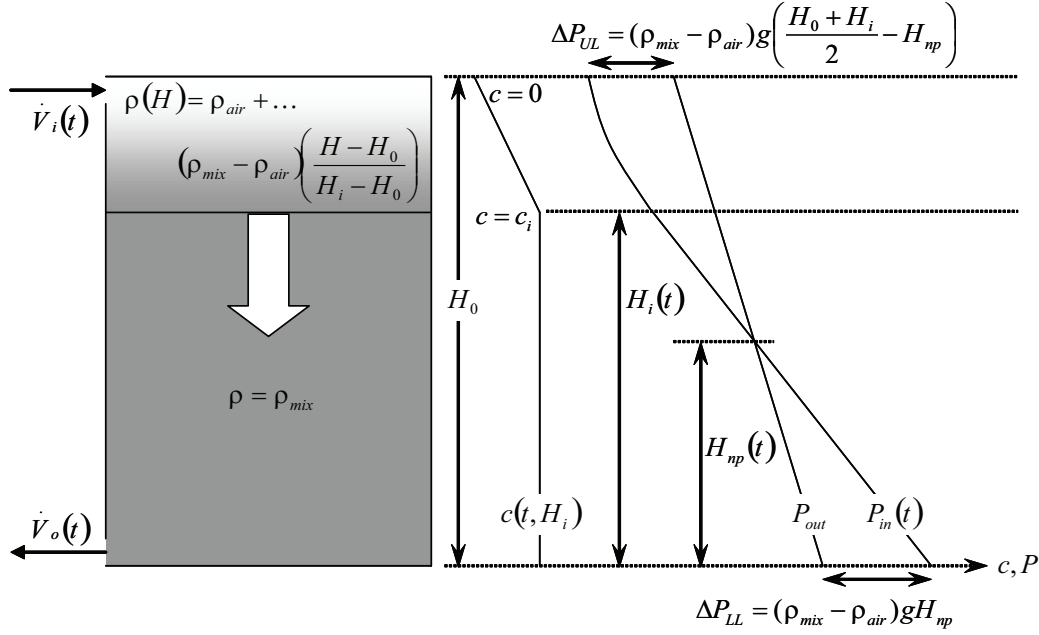


Figure 2.2: Wide descending interface hydrostatic pressure profile. Incoming air mixes with the upper edge of the column of agent-air mixture; resulting in a linear decay from full concentration at the interface height, $H_i(t)$, to a 0% concentration at the enclosure's maximum height, H_0 .

the flow exponent, n , and the units being used [7]. Typically, a value of 0.61 is used for C_d which represents the ratio of the actual flow to the theoretical maximum flow through a sharp-edged circular orifice.

The 2004 edition of NFPA 2001 uses a slightly modified version of Equation (2.1), where the flow exponent, n , is fixed ($n = 0.5$). With this assumption the door fan test does not need to be completed at a series of fan flows. Instead, the total leakage area is obtained by performing the fan integrity test at a single flow. A value of 0.5 indicates turbulent flow and a value of 1.0 indicates laminar flow [1]. When solved for, the flow exponent, n , represents a leakage area-weighted average value, which approximately describes the total enclosure leakage flow. These variations in the fan integrity test and implementation of the orifice flow equation constitute a major theoretical disparity between the 2004 and 2007 editions of NFPA 2001. The theory discussed in the 2006 ISO 14520-1 uses a variable flow exponent.

Each model makes an assumption that leakage areas exist in two locations only; at the extremes of enclosure height, upper and lower. Often the fan integrity test is used to determine the total area of all leakages although no information is gained from this procedure about the actual location of these enclosure penetrations. Without further information, both NFPA 2001 and ISO 14520-1 stipulate that the designer shall assume that 50% of the total measured leakage area is located at the ceiling's elevation and 50% located at the floor.

The distribution of leakage area between upper and lower locations may be referred to as the *lower leakage fraction*, given as F , and evaluated as Equation (2.2),

$$F = \frac{A_{LL}}{A_{LL} + A_{UL}}. \quad (2.2)$$

A_{LL} and A_{UL} denote the summed leakage areas for all lower and upper leakages, respectively. The combination of the lower leakage fraction and the total enclosure leakage area includes all the necessary variables needed to define the leakage configuration in the hold time model.

If an equal split of leakage area between upper and lower extremes is not assumed it is difficult to determine the lower leakage fraction. The selection of a value for this model input parameter requires great prudence as the output hold time is more sensitive to it than any other input parameter. Figure 2.3 shows the significance of the lower leakage fraction F , by plotting the clean agent hold time (introduced later in this section) as a function of the lower leakage fraction. It is observed that the hold time prediction approaches infinity as the value of F approaches 0 or 1. For this reason, ISO 14520-1 Annex E prohibits F values less than 0.15 or greater than 0.85 because the prediction of retention time becomes unrealistically long under these conditions.

In the present study the hydrostatic pressure profile was recorded at a series of heights inside the test enclosure including the elevations of inlet and outlet leakages. These measurements are correlated using the orifice flow equation to observe the effective lower leakage fraction throughout the hold time. Gas flow through enclosure leakage pathways is described by Equation (2.1). Upon rearrangement, this may be solved for the leakage cross sectional area as shown in Equation (2.3)³,

³The flow exponent, n , has been set to 0.5 because the orifice flow equation will only

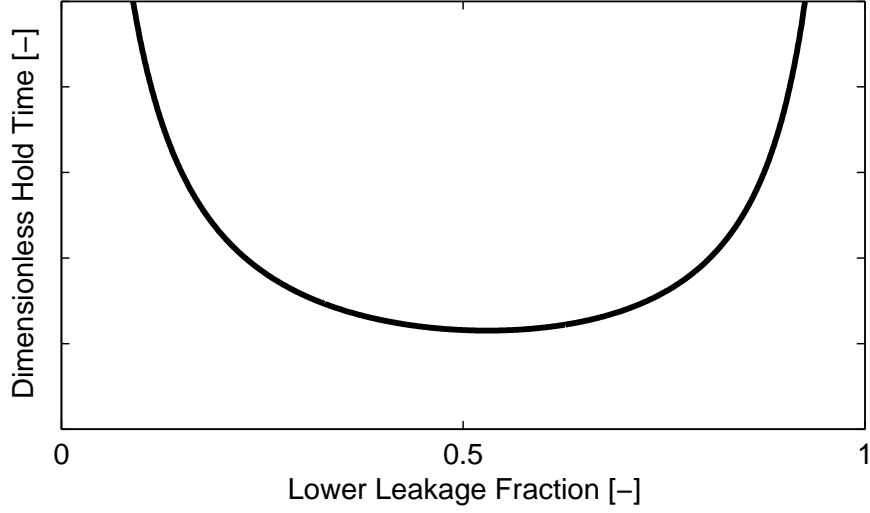


Figure 2.3: Hold time prediction as a function of the lower leakage fraction, F , defined in Equation (2.2).

$$A = \frac{Q}{C_d C_U} \sqrt{\frac{\rho}{2\Delta P}}. \quad (2.3)$$

Assuming that upper and lower leakages are not equally sized, this equation may be used to describe each leakage area individually, which is then substituted to solve for the lower leakage fraction, F , given as Equation (2.2). Applying mass conservation, it can be shown that the volumetric flow of gas through upper leakages is balanced by that flowing through lower leaks ($Q_{LL} = Q_{UL}$). Further, if the coefficients of discharge and unit correction constants at both upper and lower leakage areas are assumed to be equal then Equation (2.2) can be modified to result in Equation (2.4) given by,

$$F = \frac{1}{1 + \sqrt{\frac{\rho_{UL}\Delta P_{LL}}{\rho_{LL}\Delta P_{UL}}}}. \quad (2.4)$$

Depending on the agent type and concentration the values of the bulk gas densities flowing through lower and upper leakages are known parameters. A represents the area of a real orifice when this condition is satisfied [1].

ters. The pressure differentials at upper and lower leak locations are recorded throughout the hold time. Through implementation of these ambient pressure data sets correlated empirical values of the lower leakage fraction, F , are calculated and plotted as a function of time in the Experimental Results section.

The three theoretical models' governing equations are presented in the following. The most extensive model is presented first. Subtle assumptions are later introduced that result in the other hold time models in question.

The wide descending interface model requires one additional input compared to the sharp descending interface model. This allows prediction of the hold time for a specified concentration drop rather than simply the moment at which a sharp interface instantaneously passes. The sharp descending interface model was replaced by the wide descending interface model in the 2006 edition of ISO 14520-1, Annex E. This theoretical model is expanded upon elsewhere [5], [8].

The wide descending interface model is given as Equation (2.5). A dimensionless form is derived in order to facilitate direct comparisons between various test configurations:

$$\tilde{H}_{WDI} = [1 - \beta_1 \tilde{t}_1]^{\frac{1}{1-n}}, \quad (2.5)$$

where

$$\begin{aligned} \tilde{H}_{WDI} &= \frac{H_e}{H_0}, \quad H_e = H_0 - (H_0 - H_p) \frac{c_i}{2c_f}, \quad \tilde{F} = \left(\frac{A_o}{A_i} \right) = \frac{F}{1-F}, \quad \tilde{\rho} = \frac{\rho_{air}}{\rho_{mix}}, \\ \tilde{t}_1 &= (t - t_0) \frac{C_o A_o g^n}{A_f H_0^{n-1}}, \quad \beta_1 = (1 - n) \left(\frac{2(1-\tilde{\rho}^{-1})}{1+\tilde{\rho}^{-1}\tilde{F}^{1/n}} \right), \end{aligned}$$

and

$$\rho_{mix} = \rho_{ag} \left(\frac{c_i}{100} \right) + \rho_{air} \left(\frac{100-c_i}{100} \right).$$

The dimensionless parameters found to govern the rate of interface descent include the ratio of the equivalent height to the enclosure's maximum height, \tilde{H}_{WDI} , the ratio between the outlet and inlet leakage areas, \tilde{F} , and the ratio of the agent-air mixture density relative to the density of ambient air, $\tilde{\rho}$. The equivalent interface height, H_e , is given as a function of the enclosure's maximum height, H_0 , the protected height, H_p , and the initial and final agent concentrations, c_i and c_f , respectively. The hold time is thus evaluated as the time at which a specified concentration (c_f) exists at

a specified height (H_p). The dimensionless hold time is given as \tilde{t} . β_1 is a combined dimensionless coefficient. The vapor densities of atmospheric air and the agent-air mixture are ρ_{air} and ρ_{mix} , respectively.

The two remaining models are both stratified, sharp descending interface models. The 2008 edition of NFPA 2001, Annex C espouses a sharp interface model that uses a variable value of the orifice flow exponent, n , as implemented in the wide interface theory, above [9]. The above theory may be simplified into the 2008 edition of the sharp interface theory by setting the agent concentration at the end of the hold time, c_f , equal to one half the initial concentration, c_i (resulting in: $H_e = H_p$). By redefining the dimensionless height parameter as the ratio of the actual interface height to the enclosure's maximum height the intent of the 2008 edition of NFPA 2001, Annex C is met. Equation (2.6) shows this model in dimensionless form as

$$\tilde{H}_{SDI_{2008}} = [1 - \beta_1 \tilde{t}_1]^{\frac{1}{1-n}}, \quad (2.6)$$

where

$$\tilde{H}_{SDI_{2008}} = \frac{H_i}{H_0}.$$

The final remaining body of sharp descending interface theory was published in the 2004, and prior editions of NFPA 2001, Annex C [10]. The subtle disparity between the 2004 and 2008 editions of NFPA 2001 lies in the application of the orifice flow equation. In the theoretical models above the orifice flow exponent, n , was a variable model input parameter. The 2004 edition of NFPA 2001 assumes that n is equal to 0.5. Equation (2.7) gives the dimensionless governing equation for the simple, sharp descending interface model as

$$\tilde{H}_{SDI_{2004}} = [1 - \beta_2 \tilde{t}_2]^2, \quad (2.7)$$

where

$$\tilde{H}_{SDI_{2004}} = \frac{H_i}{H_0}, \tilde{t}_2 = (t - t_0) \left(\frac{C_o A_o}{A_F} \right) \left(\frac{g}{H_0} \right)^{1/2}, \beta_2 = \left[\frac{1 - \tilde{\rho}^{-1}}{2(1 + \tilde{\rho}^{-1} \tilde{F}^2)} \right]^{1/2}.$$

This can be derived from the sharp interface model given in Equation (2.6) by introducing the assumption that n equals 0.5. The derivation of this equation is published elsewhere [3], [4].

2.3 Experimental Apparatus & Instrumentation

All testing reported herein was conducted at the Fike Corporation test facility in Blue Springs, Missouri, USA, in the same enclosure with no significant modifications made between test sessions. A schematic of the experimental enclosure is shown in Figure 2.4. Internal dimensions are 4.61 m (181.5 in) by 4.62 m (181.75 in) by 4.88 m. (192 in) in height, which totals 103.8 m³ (3640 ft³) in volume. Construction consists of 5.1 cm by 20.3 cm (2 in by 8 in) wood studs on 40.6 cm (16 in) centers with two interior layers of 15.9 mm (⁵/₈ in) plywood and one layer of fiberglass sheeting as an interior finish. Intentional leakage area was supplied in two forms; (1) 84 drill holes 2.5 cm (1 in) diameter about the upper and lower enclosure boundaries and (2) a ceiling vent for discharge pressure venting of inert agents⁴. All drill holes are offset from lower and upper boundaries by 30.5 cm (12 in) and equally distributed across each wall facing such that a nominal 10 upper and 10 lower holes exist per wall. A floor drain is located in the room's center that was closed by means of an existing ball valve.

For each clean agent tested, a series of controlled leakage area configurations were simulated by plugging and/or unplugging drill holes. Dense rubber stoppers were used to plug holes from the inside where they made a reliable seal with the fiberglass sheeting. Each specified leakage configuration was accomplished in such a way as to produce a *symmetrical* leakage pattern. For example, an experiment with 16 open drill holes would be accomplished by opening a single hole at ¹/₃ and ²/₃ of the wall width on each wall, upper and lower.

The experimental chamber is located in a facility that has a footprint greater than five times that of the test enclosure. This ensures that the exiting flow of clean agent vapor does not pool about the test enclosure thereby diminishing the column pressure driving flow out lower leakages. Additionally, the surrounding enclosure minimizes pressure gradients produced by external wind flow that could have otherwise affected the enclosure's leakage

⁴Experiments 2, 3 and 4 from the IG-541 test set involve relatively 'tight' leakage configurations. In these tests only, there was concern for the potential of over pressurization. Tests 2 & 3 left the ceiling vent open throughout the discharge and retention time. In Test 4 the ceiling vent was closed within a few seconds after the clean agent discharge ended. For all other tests this vent remained sealed closed.

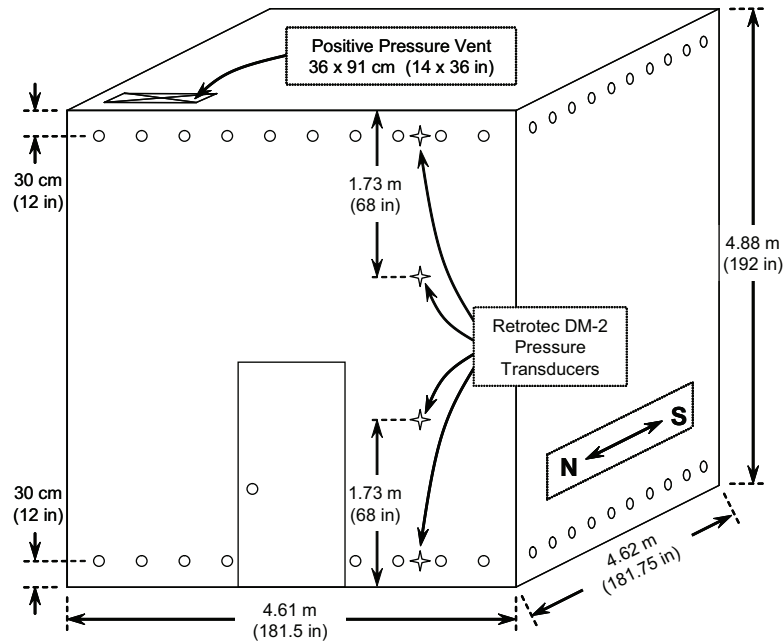


Figure 2.4: Schematic of the test enclosure. Ambient pressure probes and controllable leakage areas are shown. The positive pressure relief vent was allowed to open only for select IG-541 tests.

behavior. Ambient pressure probes reflect the brief openings of facility doors throughout the hold time, but do not persist long enough to significantly affect clean agent retention times. No HVAC ducting traverses through the test chamber; eliminating the potential for bias pressures. As well, a controlled introduction of bias pressure is not investigated in this study.

Environmental variables were otherwise uncontrollable. All testing was completed within August and September, 2006. Ambient temperatures and pressures did not vary drastically, as this period of time is fairly temperate where Fike's facility is located. Peak pressures during halocarbon clean agent discharges have been shown to have a strong inverse relationship with the ambient relative humidity levels. Typical electronic control rooms are maintained at approximately 55% RH [11]. For all non-inert agent testing completed the enclosure was purged with dry compressed air until the relative humidity level dropped to less than 40%. Clean agent system cylinders, valve assemblies, discharge nozzles and other design parameters were provided by

each system manufacturer. The manufacturers also specified the discharge volume concentrations and cylinder pressures used in testing according to typical design practices⁵.

Measured quantities include nozzle and ambient pressures, gas species vapor concentrations, and enclosure air temperatures⁶. Nozzle pressures are retained as a means to ensure proper agent delivery and to diagnose potential problems in system design. Ambient pressures are recorded to document (1) the peak pressure pulses generated during agent discharge and (2) the hydrostatic pressure profile throughout the hold time. The present study focuses on the later, leaving the topic of room integrity for future research. Clean agent volume concentrations are used to observe the drop in agent concentration as a function of height and time. Enclosure air temperature measurements are used to further analyze the applicability of neglecting this variable in hold time predictions (as prescribed by NFPA 2001 and ISO 14520-1 design standards).

Inert gas vapor concentrations are correlated indirectly from measurements of enclosure oxygen content using cartridge *fuel cell* sensors. Two Nova 320 and one Nova 320 S-3 O₂ gas analyzers were used in the test phase. Combined, this provided the ability to monitor five elevations for IG-541 tests.

Fluoroketone and hydrofluorocarbon agent vapor concentrations are observed by means of a gaseous thermal conductivity measurement technique. This is accomplished with two Tuure analyzers, two Perco analyzers, and one Tripoint gas analyzer. Proper calibration was only available for the agent FK-5-1-12 as sampled by the Tripoint instrument. All five instruments were calibrated for linearity however as a basis on which to shift and scale the data to peak and baseline at the correct reference values. Agent concentration data for FK-5-1-12 and HFC-125 tests inherently carries a larger uncertainty level due to this lack of thorough calibration⁷.

Table 2.1 lists the installation elevations of the sampling probes used in

⁵Reference Table 2.2 for a listing of critical test configuration parameters.

⁶The enclosure's ambient pressure, temperature, and nozzle pressure were typically recorded for a 60 second duration during agent discharge. Ambient pressure transducers were used throughout the test duration only for the HFC-125 test series.

⁷Tuure and Perco gas analyzers' output circuitry was non-invasively monitored throughout operation. The ability to analyze the instruments' electrical activity rather than a small, strip-chart printout greatly enhanced the author's ability to ensure greater precision in these measurements.

Table 2.1: Gas sampling probe locations

Gas Sample Probe Installation Height (Percent of Maximum Enclosure Height)		
FK-5-1-12	IG-5-4-1	HFC-125
86%	86%	84%
81%	76%	73%
76%	57%	68%
68%	47%	63%
61%	37%	57%
51%		47%
47%		36%
37%		

each experimental test set. All probes sampled air from a vertical axis offset 61 cm (24 in) to the east of the central enclosure axis. Gas sampling probes were terminated at various elevations in the enclosure; bracketing the range of potential protected heights.

A total of fifteen tests are included in the present study; five by three clean agent types. Table 2.2 lists the critical experimental setup parameters used for each test. The leakage configuration is described empirically using the door fan integrity test. The value of the lower leakage fraction (column 7) is used in calculating the theoretical hold time predictions. Further information on these values is found in the Experimental Results section. It should be noted that the door fan integrity test data shown for IG-541 tests 2, 3 and 4 is a duplication of the data obtained during FK-5-1-12 testing. A large-enough door fan system was not available for these tests, since the overpressure relief vent was open. As such, the door fan data has been taken from FK-5-1-12 tests where an equal number of lower leakage holes were left open.

2.4 Experimental Results and Analysis

An analysis of the differential pressure measurements is used to evaluate the actual, effective value of the lower leakage fraction throughout the hold time. This parameter is then used as an input to the theoretical models to ensure that hold time predictions for any given test are as accurate as possible.

Two Retrotec DM-2 digital manometers were used to record pressure

Table 2.2: Experimental setup & measured leakage parameters

Clean Agent Type	Test ID (by agent)	Discharge Concentration (Vol. %)	# Open Upper Holes	# Open Lower Holes	Additional Open Leakages	Lower Leakage Fraction (-)	Door Fan Integrity Test - Inflow		Door Fan Integrity Test - Outflow	
							n (-)	k (l/s/Pa ⁿ)	n (-)	k (l/s/Pa ⁿ)
FK-5-1-12	1	4.2	16	16	N/A	0.50	0.550	19.29	0.531	21.65
FK-5-1-12	2	4.2	41	41	N/A	0.50	0.503	49.38	0.572	35.01
FK-5-1-12	3	4.2	8	8	N/A	0.50	0.587	10.45	0.745	5.75
FK-5-1-12	4	4.2	4	4	N/A	0.50	0.617	7.12	0.594	6.77
FK-5-1-12	5	4.2	7	7	N/A	0.50	0.560	10.69	0.618	8.21
HFC-125	1	8.0	41	41	N/A	0.51	0.503	49.38	0.572	35.01
HFC-125	2	8.0	16	16	N/A	0.51	0.550	19.29	0.531	21.65
HFC-125	3	8.0	8	8	N/A	0.50	0.587	10.45	0.745	5.75
HFC-125	4	8.0	4	4	N/A	0.49	0.617	7.12	0.594	6.77
HFC-125	5	8.0	24	8	N/A	0.34	0.550	19.29	0.531	21.65
IG-541	1	36.8	41	43	N/A	0.51	0.499	45.75	0.518	43.89
IG-541	2	36.8	16	16	overpressure vent	0.50	0.550	19.29	0.531	21.65
IG-541	3	37.0	16	8	overpressure vent	0.50	0.587	10.45	0.745	5.75
IG-541	4	36.8	16	16	vent open during discharge only	0.50	0.550	19.29	0.531	21.65
IG-541	5	41.0	41	43	N/A	0.51	0.499	45.75	0.518	43.89

differentials at the elevations of upper and lower leakage areas. Although only operated throughout the HFC-125 test series, these instruments obtained valuable, high precision measurements at very low differential pressures as shown in Figure 2.5. For approximately ten minutes a transient behavior is observed where the temperature of the gas mixture inside the enclosure is gradually warming towards that of the air surrounding the test enclosure. After this time period the pressure differential across enclosure boundaries at the elevation of upper leakages stabilizes at a lower limit. This indicates that fresh air is flowing into the upper region of the enclosure. At this moment the positive pressure delta across lower leakages forces a flow of agent-air mixture out of the enclosure. As time progresses, agent continues to drain from the enclosure; serving to minimize the magnitude of the hydrostatic column pressure inside the enclosure relative to that of typical, atmospheric conditions.

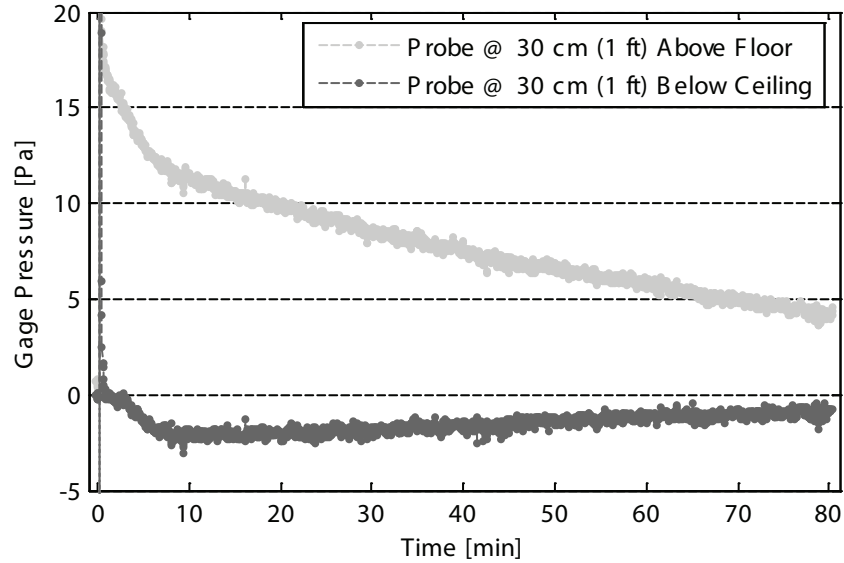


Figure 2.5: Hydrostatic pressure profile throughout the hold time (HFC-125, test #5). The pressure delta across enclosure boundaries is measured at the elevations of upper and lower leakages.

The pressure data is correlated using Equation (2.4) to experimentally determine the effective lower leakage fraction, F . The vapor densities of the gases flowing through upper and lower leakages are calculated by assuming an

air temperature of 21°C. Figure 2.6 shows the plotted result of this correlation as applied to the entire data set in Figure 2.5.

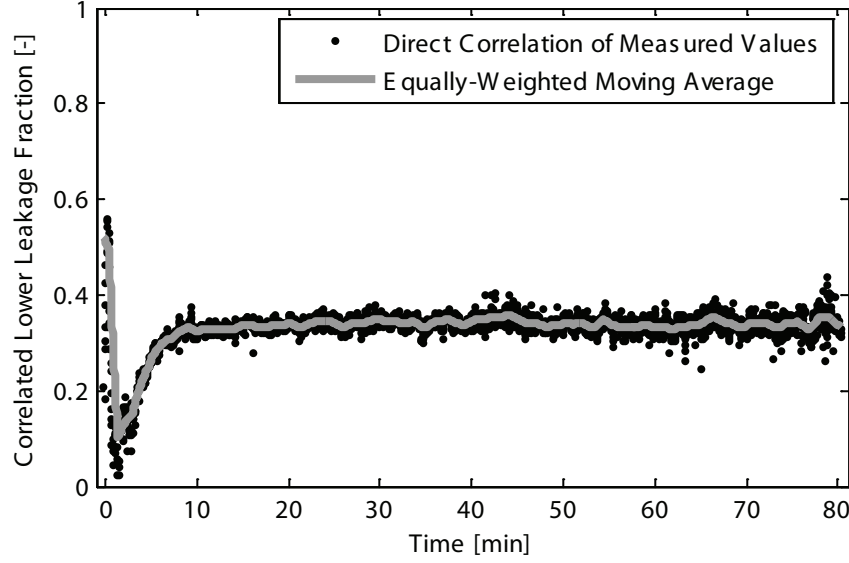


Figure 2.6: Correlated effective lower leakage fraction throughout the hold time (HFC-125, test #5). The correlation's limits are met only after the thermal transients have stabilized (~ 10 min). After then, the lower leakage fraction is observed to be nominally constant throughout the hold time.

This correlation proves to be a powerful tool in evaluating the actual, effective lower leakage fraction. The correlating equation was derived previously by assuming that volumetric flows through upper and lower leakages were equal. Figure 2.6, shows that this condition is not satisfied until approximately 10 minutes into the hold time. During this initial time period, the lower leakage fraction is close to a value of 1; and not 0 as shown in Figure 2.6. The flows through upper and lower leakages are not equal during this time period because the agent-air mixture inside the enclosure is gradually expanding as it warms to the temperature of air surrounding the enclosure. Following this transient period, the correlation shows the lower leakage fraction to retain a nearly constant value throughout the test's duration. The amount of data spread gradually increases as the magnitude of the hydrostatic column pressure inside the enclosure is lessened (while the precision of the differential pressure transducers remains the same).

The steady-state value of the lower leakage fraction in Figure 2.6 is found to be approximately 0.34. The plot is generated using data from a test with 8 drill holes open at the lower end of the enclosure and 24 open at the upper. Given this leakage configuration, an intuitive guess of the lower leakage fraction would be approximately 0.25 although this is quite different from the correlated value. This is because the test enclosure, like all enclosures, has uncontrollable leakages distributed randomly about the enclosure boundaries and not *only* at the polar extremes of the experimental envelope's elevation. Thus, the actual lower leakage fraction is a function of both the controlled leakage and the uncontrolled leakage areas. As such, even though the controllable leakage resulted in a lower leakage fraction of 0.25, the lower leakage fraction of all leak areas resulted in a value of approximately 0.34. This is indicative that the lower leakage fraction of the uncontrollable leakages is much greater than 0.25 and likely near to 0.5. The theoretical hold time predictions will be calculated with the correlated values of the lower leakage fraction as inputs to provide the most accurate application of the theory.

Agent concentration measurements were made with a variety of instruments. For each, an exhaustive effort is made to ensure that the recorded values are interpreted, filtered and scaled into engineering units according to that prescribed by well-established measurement theory⁸. Note that the recorded values are from a *relative* measurement technique which results in the inability to measure units of *absolute* concentration. An example of the finalized agent concentration data sets is provided in Figure 2.7. Measurement uncertainty is likely less than $\pm 10\%$ of full scale, however, an investigation of measurement error bounds and propagated uncertainty in the calculated quantities is yet to be completed.

The present study seeks to validate the theoretical predictions of clean agent hold times according to the sharp descending interface and wide descending interface models. As previously discussed, the primary difference between these is the assumption of agent distribution within the design envelope. Because agent concentration is measured for a range of heights, the

⁸Proper calibration of all gas sampling instrumentation was not available. A relative measurement technique was implemented in the scaling of agent concentration data. Recorded values were scaled into engineering units based on a zero value (a 30 second average of sampled fresh air before discharge) and a full-scale value (an average of = 90 seconds of data acquired after agent discharge had ended and readings had stabilized). Data traces exhibiting suspect behavior or failing to return to baseline values after the test duration are discarded.

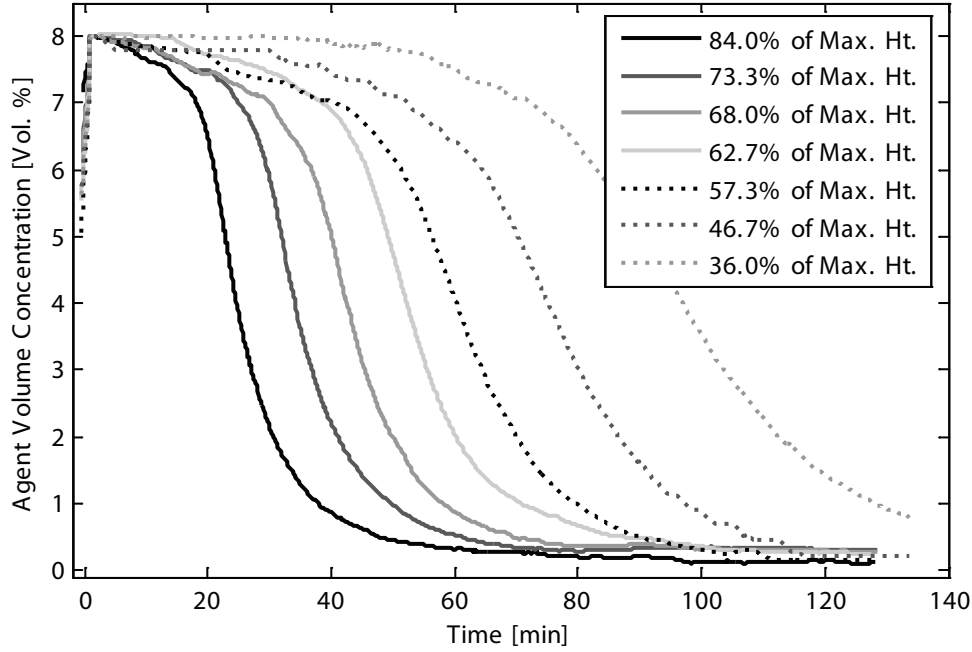


Figure 2.7: Example of agent concentration data

actual agent distribution profile at any moment during the retention time is known. Side-by-side comparisons of the actual agent distribution to the idealized distributions employed in the models are a tactical way of evaluating the applicability of the models' assumptions.

Figure 2.8 graphically depicts the idealized assumption of the agent distribution profile as employed in the theoretical hold time models. Examples of the empirical, or, effective agent distribution profile for each of the three agents tested is shown in Figure 2.9. In each figure the data traces represent instantaneous *snapshots* in time where a progression in time is indicated by a lighter shade of gray.

A comparison of Figure 2.8 and 2.9 shows that the empirical agent distribution profile lies in between the sharp and wide interface assumption. As shown in Figure 2.9, the effective agent distribution profile for each of the three agents tested does not fit the assumption of either idealized agent distribution assumption. The clean agent vapor takes on a highly-stratified form for all three agents. The interface width, roughly interpreted as the change in height (y-axis) for a given data series (moment in time), appears

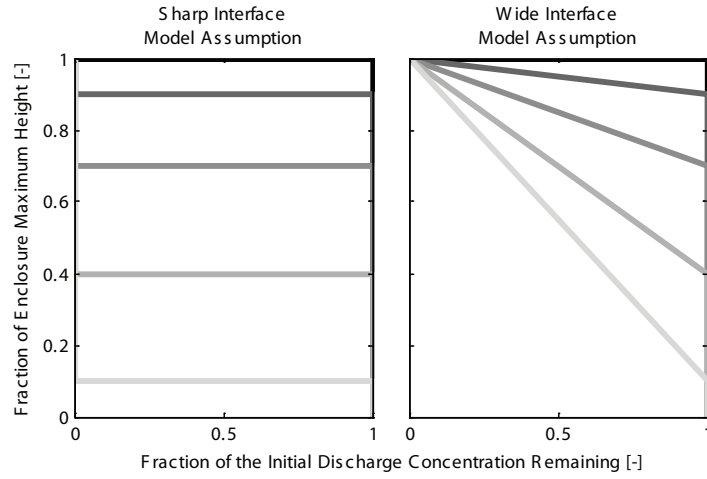


Figure 2.8: Idealized assumptions of the agent distribution profile as applied in the theoretical models. Each data trace represents an instantaneous snapshot in time where a lighter shade of gray indicates a progression in time.

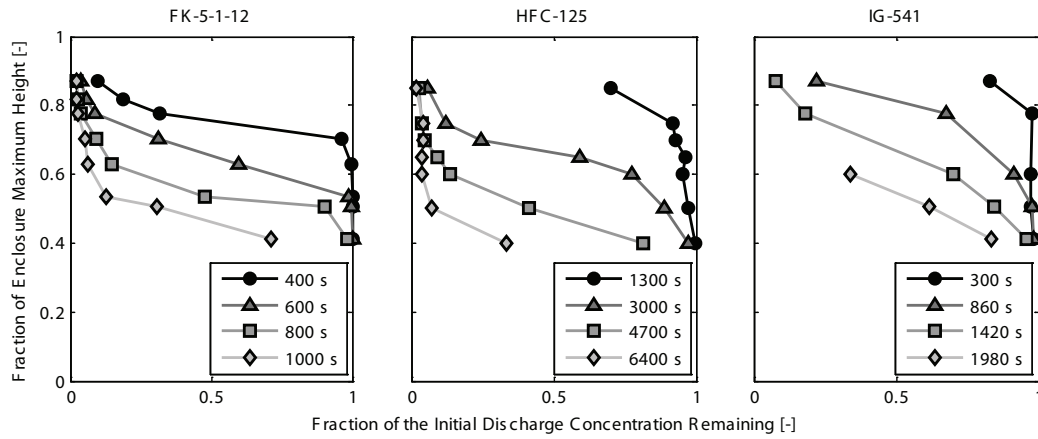


Figure 2.9: Examples of the effective agent distribution profile for all tested agents. Each agent shows a significant tendency to stratify in the enclosure. Neither the idealized sharp or wide interface assumptions accurately model the agent distribution for all three agent types.

to take on a different value for the different agent types. Comparatively, it can be concluded that the interface width shares an inverse relationship with

the agent-air mixture density (a value that decreases in magnitude from left to right in Figure 2.9).

The validity of the hold time models to the experimental data can be analyzed by plotting the theoretical hold time prediction versus the empirically derived hold time duration. Comparison plots are presented where the data series are grouped by agent type and by the applied theoretical model. As well, in each figure, two charts are found where the same data set has been analyzed twice; accounting for the ability to evaluate the hold time at various concentration thresholds.

Figure 2.10 shows the dimensionless theoretical hold time prediction plotted with respect to the dimensionless empirical hold time where the data series are grouped by agent type. Either axis ranges from 0 to 1 where the interface can be imagined as traveling from the ceiling of the test enclosure (at dimensionless time = 0) to the floor of the enclosure (at dimensionless time = 1). For each test conducted a series of agent concentration measurements are taken across a range of elevations. Each instrument provides a single empirical value of the hold time duration where probes at upper elevations result in nondimensional hold times nearer to a 0 value and lower elevations tend towards values of 1. In Figure 2.10 each data point is plotted three times; once as rendered dimensionless by the wide interface theory, and twice by the different sharp interface theories. In the following, the data is presented again with the data series regrouped by theory type to elucidate the disparity of these triplicate data points.

The uppermost chart in Figure 2.10 shows the hold time evaluated at the time when there is a 15% reduction from the initial discharge concentration. The lower chart differs in that the hold time is evaluated for a 50% reduction in clean agent concentration.

The method of evaluating the hold time has an affect on both the empirical and theoretical hold times. Empirical values of the hold time are found by locating the moment in time, for any given instrument's recorded data trace, at which the agent concentration is found to drop below the specified concentration reduction threshold. The obtained value of the empirical hold time is then rendered dimensionless according to the three theoretical models, which results in slightly varying values for each.

The theoretical hold time is a function of the concentration reduction (below the initial discharge concentration) only when considering the wide interface theory. ISO 14520-1, Annex E limits the applicability of the wide descending interface to concentration reduction thresholds ranging up to 50%

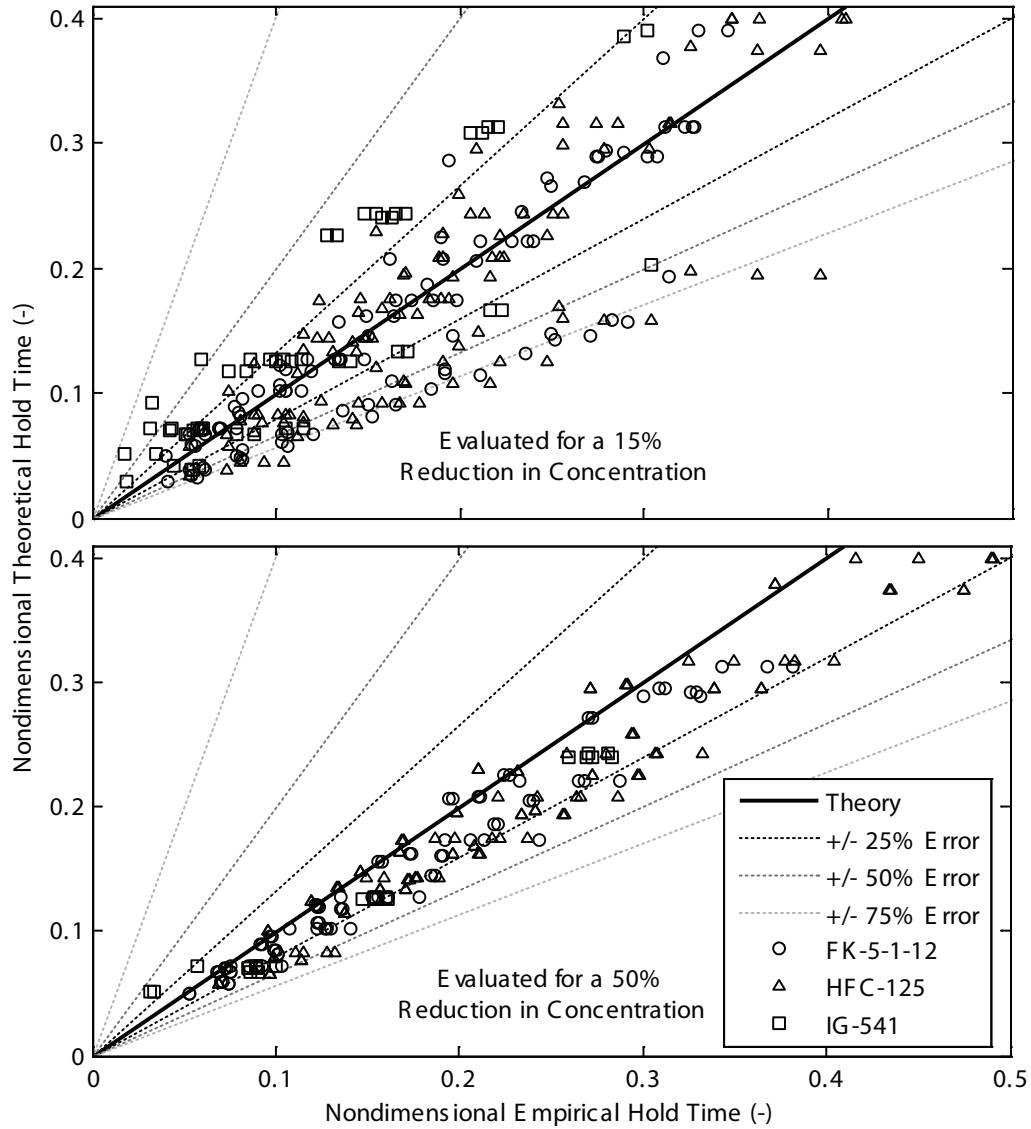


Figure 2.10: Validation plots of the nondimensional theoretical hold time versus the nondimensional empirical hold time with data series grouped by clean agent type. Plotted values are calculated as the quantity βt . The hold time is evaluated for a 15% reduction in concentration in the upper chart and a 50% reduction in the lower chart. Error lines represent the percent deviation from the theoretical hold time prediction.

although the theoretical derivation is actually formulated to predict reductions ranging up to 100%. The sharp descending interface theories do not implement the percent concentration reduction as an input variable. As such, data points in the upper and lower charts of Figure 10 that have been rendered dimensionless according to the sharp interface theories have the same values on either chart's y-axis.

Figure 2.10 shows the degree of correlation observed for one agent type versus another. In the lower chart the data points are equally scattered; indicating that the theory works well for a range of agent types when the hold time is evaluated as a 50% reduction in concentration. The IG-541 data points in the upper chart lie in the upper-left of the chart. This indicates that the degree of interdiffusion between IG-541 and inflowing fresh air may be greater for this agent than the others; resulting in a more rapid initial decrease in agent followed by a more gradual bulk draining of agent (indicated by better correlation exhibited in the lower chart).

Data points found below the theory line represent a conservative condition where the agent is observed to drain more gradually from the enclosure than predicted by the theory. Conversely, data points above this line represent an overly optimistic condition where the agent is found to drain more rapidly than the theory predicts. It is observed that when evaluated at a 50% concentration reduction the large majority of the data is in the conservative domain of the chart; generally with an error magnitude less than 50%. The validity of the hold time predictions is diminished when applied to predict a 15% reduction from the initial, discharge concentration. The upper chart in Figure 2.10 demonstrates this with a widely scattered data pattern which ranges from nearly 50% error in the overly optimistic region to over 75% error in the conservative direction. Generally speaking, the validity of the hold time models for all three agents is drastically reduced when the hold time is not evaluated as a 50% reduction in concentration. The data pairs plotted in Figure 2.10 are presented again in Figure 2.11 with the data series regrouped according to the theory applied in nondimensionalizing the data.

In the lower chart of Figure 2.11 the data tends to lie below the line of perfect correlation, or theory curve when the hold time is evaluated as a 50% reduction from the initial, discharge concentration. The group of data points for any of the three types of applied theory appears to be equally scattered. Although not clearly portrayed in the lower chart, depending on the value of the flow exponent, n , the sharp interface theory used by the 2004 edition of NFPA 2001 consistently predicts shorter hold times than the

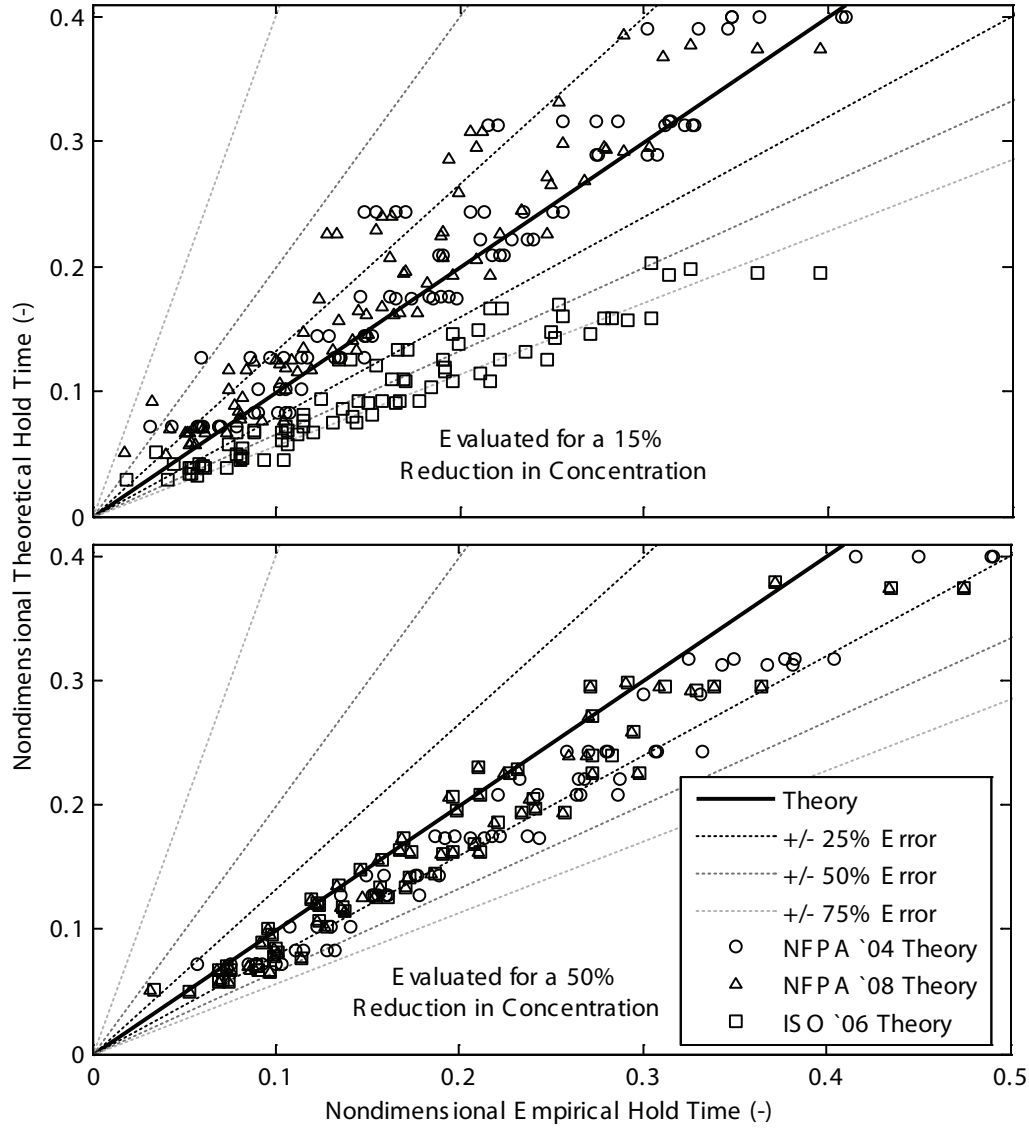


Figure 2.11: Validation plots of the nondimensional theoretical hold time versus the nondimensional empirical hold time with data series grouped by theory type. Plotted values are calculated as the quantity $\beta \tilde{t}$. The hold time is evaluated for a 15% reduction in concentration in the upper chart and a 50% reduction in the lower chart. Error lines represent the percent deviation from the theoretical hold time prediction.

2008 version of this theory. As explained in the Background and Theoretical Considerations section, when evaluated at a 50% concentration reduction the wide descending interface theory of ISO 14520-1 collapses into the sharp interface theory found in the 2008 edition of NFPA 2001. Due to this, data points for these two theories consistently overlap in the lower chart of Figure 2.11.

When the hold time is evaluated at a 15% reduction in concentration a clear trend is observed. The data is not equally scattered about the chart any more. Rather, a distinct separation between the sharp interface and wide interface theories is found. The sharp interface theories typically result in an overly optimistic prediction of the hold time. The empirical hold time deviates from the theoretical prediction by around 25% in most cases and may range beyond 75% error (especially for the case of IG-541). Conversely, the wide descending interface theory provides overly conservative hold time predictions. The data indicate that actual clean agent retention times evaluated for a 15% concentration reduction threshold are typically longer than and up to twice as long in duration as the wide descending interface theory predicts (as incorporated in the 2006 edition of ISO 14520-1).

2.5 Summary and Conclusions

This paper documents the findings of a research program designed to experimentally evaluate the applicability of the widely published hold time prediction models found in NFPA 2001, Annex C and ISO 14520-1, Annex E. Fifteen experiments involving a variety of enclosure leakage configurations are presented for three clean extinguishing agents; FK-5-1-12, HFC-125 and IG-541. Experimental results are modified to a dimensionless form to permit direct comparison between tests. Results indicate that the actual hold time is longer than the theoretical hold time prediction when evaluated as the time it takes for the agent concentration to drop to 50% of the initial discharge concentration. Under this condition, empirical hold times are typically up to 50% shorter than the theoretical prediction.

The accuracy of theoretical hold time predictions diminishes greatly when the hold time is evaluated as a 15% reduction in agent concentration. Theoretical predictions according to the sharp descending interface theories are typically overly optimistic; resulting in empirical hold times up to 50% shorter than the predicted value. The wide descending interface theory typ-

ically results in overly conservative hold time estimates; yielding empirical values up to 100% longer than the theoretical value.

2.6 Recommendations for Future Work

A limited selection of clean extinguishing agents was included in this research program. Test data for other predominant agents on the market today should be investigated. Test results for the clean agent HFC-227ea were inconclusive. This agent should be tested again under more controlled conditions.

The majority of all tests completed involved target hold times much larger than the typical field requirement of 10 minutes. The inert gas agent IG-541 was tested for target hold times ranging from 15 to 73 minutes. To better determine the applicability of the hold time prediction theory of NFPA and ISO design standards the target value of 10 minutes needs to be more directly bracketed.

The worst consistency between empirical and theoretical evaluations of the hold time occurred when the upper and lower leakage areas were not equal. Further investigation of this parameter as a source of prediction error is warranted.

Nearly all structures are subject to bias pressure whether intentional (i.e. HVAC design, smoke control pressurization) or not (i.e. stack effect). A controlled introduction of positive and negative bias pressure from high and low elevations should be investigated.

If feasible, the legacy hardware incorporated for halocarbon gas sampling should be calibrated in order to convert the relative measurement technique to an absolute one. The various pressure transducers used simultaneously in testing deviate significantly from one another. More accurate means of monitoring the enclosure pressure profile should be obtained for any future testing.

The cooling affect of a clean agent discharge and resultant temperature change is not accounted for in the models, which may lead to measurable errors in the predicted hold time. Further analysis of these transient thermal effects is warranted.

Bibliography

- [1] Dewsbury, J., and Whiteley, R.A. “Review of fan integrity testing and hold time standards,” Fire Technology, Vol. 36, No. 4, pp. 249-265, Nov. 2000.
- [2] DiNenno, P.J., and Forssell, E.W. “Evaluation of the door fan pressurization leakage test method applied to Halon 1301 total flooding systems,” Journal of Fire Protection Engineering, Vol. 1, No. 4, pp. 131-140, 1989.
- [3] Mowrer, F. “Analysis of vapor density effects on hold times for total flooding clean extinguishing agents,” Halon Options Technical Working Conference, 16th Proceedings, Albuquerque, New Mexico, pp. 1-12, May 2006.
- [4] O’Rourke, S.T. “Analysis of hold times for gaseous fire suppression agents in total flooding applications,” Masters Thesis, University of Maryland, College Park, MD, 2005.
- [5] Dewsbury, J. and Whiteley, R.A. “Extensions to standard hold time calculations,” Fire Technology, Vol. 36, No. 4, pp. 267-278, Nov. 2000.
- [6] Emmons, H.W. “Vent flows, chapter 2-3,” The SFPE Handbook of Fire Protection Engineering, 3rd Ed., NFPA, Quincy, MA, 2002.
- [7] Saum, D., Saum, A., Messing, M. and Hupman, J., “Pressurization air leakage testing for Halon 1301 enclosures,” Substitutes and Alternatives to Chlorofluorocarbons and Halons, Washington, D.C., 1988.

- [8] “ISO 14520-1: Gaseous fire extinguishing systems - physical properties and system design - part 1: general requirements,” International Standards Organization, Geneva, Switzerland, Annex E, 2006.
- [9] “NFPA 2001: Standard on clean agent fire extinguishing systems,” National Fire Protection Association, Quincy, MA, Annex C, 2008.
- [10] “NFPA 2001: Standard on clean agent fire extinguishing systems,” National Fire Protection Association, Quincy, MA, Annex C, 2004.
- [11] Genge, C. “Preventing excessive enclosure pressures during clean agent discharges,” Halon Options Technical Working Conference, 15th Proceedings, Albuquerque, New Mexico, pp. 1-16, May, 2005.

Chapter 3

Validation of a Modified Hold Time Model for Total Flooding Fire Suppression¹

Abstract

This study analyzes the validity of theoretical models used to predict the duration (hold time) for which a halon-replacement suppression agent will remain within a protected enclosure. Two current models and one new formulation are investigated; the *sharp descending interface* model (as applied in NFPA 2001, Annex C), the *wide descending interface* model (implemented in ISO 14520.1, Annex E), and the *thick descending interface* model (introduced herein). Experimental data from 34 full-scale tests designed to characterize the discharge and draining dynamics of seven clean extinguishing agents (CEA) are used to validate the thick descending interface model. Results show that the validity of the wide and sharp interface models is highly sensitive to the threshold of agent concentration decay being modeled; whereas the thick interface prediction method is not greatly susceptible to this input parameter. When the hold time is defined as a 15% decay in agent concentration, experimentally obtained hold time values are roughly 10% shorter than sharp interface predictions, 60% longer than wide interface predictions, and 30% longer than the thick interface model predicts.

¹This chapter is currently a manuscript under review in Fire Safety Journal.

3.1 Introduction

Total flooding fire suppression systems deluge an enclosure with a gaseous suppressant such that combustion cannot be supported for an extended period of time. Systems consist of one or more pressurized fire suppressant storage vessels, a delivery pipe network, a discharge nozzle(s), and an adequately sealed, protected enclosure. Following system activation, the agent is allowed to flow to the nozzle and become dispersed throughout the design envelope. Typical applications include data processing and telecommunication facilities, museums, banks, clean rooms, and hospitals. The fire suppressant (agent), or clean extinguishing agent (CEA), is required to remain within the protected enclosure for 10 minutes [1]. This allows for manual fire suppression measures and cooling of potential ignition sources. Systems are approved for installation only after sufficient evidence is provided to authorities that the minimum hold time requirement will be met. Design standards published by the National Fire Protection Association (NFPA) and the International Standards Organization (ISO) provide simplified physical models that predict any system's hold time expectation. This is an evaluation of the time at which the agent concentration at a specified height falls to a specified concentration threshold. Although either design standard advocates nearly identical sets of model input data and methods for gathering this data the hold time prediction of the NFPA model is usually twice that of the ISO model². This difference deserves attention which is offered in this study.

Each theoretical model espouses a simplified assumption for species diffusivity, which results in different assumptions for agent distribution within the design enclosure. This assumption is responsible for the difference in hold time predictions and also each theoretical model's name. The *sharp descending interface*, published in NFPA 2001, Annex C, assumes that the agent does not diffuse at all. ISO 14520.1, Annex E advocates the *wide descending interface*, which assumes that agent diffuses instantaneously in known proportions. In this study, the assumption for gas species diffusivity is reformulated as a piecewise combination of the *sharp* and *wide* theories. The proposed assumption allows for greater general agreement between the

²This comparison is made for a typical height (75% of room height) and concentration threshold (85% of the initial discharge concentration). NFPA 2001 defines the hold time as the time when 85% of the initial discharge concentration remains [2] while Dewsbury & Whiteley, speaking about typical European practices under ISO 14520, propose a typical system expectation as 80% of the discharge concentration [3].

theory and experimental results.

3.2 Theoretical Background

The sharp descending interface and the wide descending interface models combine well established theory on orifice flow and *worst case* assumptions to model the decay of CEA concentration as a function of time and elevation. Theoretical considerations and model construction are discussed elsewhere [1, 3, 4, 5, 6, 7, 8, 9].

Theoretical hold time models assume that the discharge process results in a homogeneous mix of CEA and air throughout the enclosure's volume. Previous studies have investigated the correctness of this presumption [10, 11]. The bulk addition of gas species to the enclosure creates a risk of over-pressurization. As well, some modern CEAs vaporize as part of the discharge process. This consumes large amounts of latent energy and results in a drop in temperature and sometimes an under-pressurization risk. Discharge-related pressure transients are not considered in the hold time models as the hold time effectively does not begin until the discharge event ends. Consideration for the risk of enclosure implosion/explosion is available in the literature [12, 13, 14]. The thermal transients produced during agent discharge are not considered in the hold time models. Following discharge, the enclosure's contents are assumed to be at the same temperature as the gas surrounding the enclosure. This assumption can result in an under-prediction of the agent draining rate. At the same time, the models assume that fresh air begins flowing into the design enclosure immediately following agent discharge, which is not consistent with actual conditions either. During the period of agent-air warming, directly following agent discharge, the agent-air mix gradually expands, thus not allowing the influx of fresh air into the enclosure during this period. The first condition serves to lengthen the predicted hold time duration while the latter results in shortened hold time predictions. It should be noted that excess agent is designed into the total flooding system to account for the agent mass that escapes the enclosure during the discharge event itself.

The sharp and wide interface models rely upon the *fan integrity* test to gather critical model input data. This is a non-invasive method for evaluating air tightness (or leakiness) of an enclosure. A calibrated fan is used to pressurize or depressurize an enclosure. The resulting pressure change across

enclosure boundaries and volumetric flow through the fan are used to measure the total amount of leakage area. Judicious treatment is given to the test method and uncertainty considerations in the literature [15, 16]. ISO and NFPA procedures vary slightly in how the results from fan inflow and outflow testing are averaged. These deviations, however, are nearly negligible in terms of overall model validity [4, 17].

Most agents available in the market have vapor densities greater than that of atmospheric air. Due to hydrostatic pressure differences between the agent-air mix and the gas surrounding the protected enclosure the agent will tend to drain out lower leakages while atmospheric air flows in through upper leakages. The magnitude of the pressure differential driving this agent draining process depends upon where the agent accumulates throughout the hold time. The fan integrity test measures the combined area of all leakages about enclosure boundaries but gives no knowledge of actual leak locations. The hold time models assume that leakages exist only in the compartment's ceiling and floor but not in the surrounding walls. This results in the maximum possible hydrostatic pressure that drives agent draining. When the distribution of total leakage between upper and lower elevations is not known, it is assumed to exist, in half, at either elevation. This nominally provides a worst case scenario; allowing for the most rapid agent draining.

Figure 3.1 shows the agent concentration profiles in three hold time models considered in this study. The thick interface model is a newly proposed model developed in this study.

Assuming that gas species do not diffuse results in an infinitesimally thin interface between inflowing fresh air and the agent-air mix resulting after discharge. The wide interface model assumes that inflowing fresh air mixes instantaneously with the agent-air mixture to form a linear decay of agent concentration from the leading edge of the interface, H_i , to the uppermost elevation in the protected enclosure, H_0 . These two conditions represent theoretical extremes of a stratified model formulation. In this study gas diffusivity is formulated such that it provides a compromise between the sharp and wide models. The *thick descending interface* model assumes that the interface has a characteristic thickness across which the agent concentration is assumed to decay linearly. At time zero the interface does not exist. As fresh air begins to flow in it mixes with the top of the column of agent air, forming a linear concentration decay through elevation. Given enough time, the interface grows to a maximum characteristic thickness and begins to descend towards the floor. When the leading edge of the interface reaches the

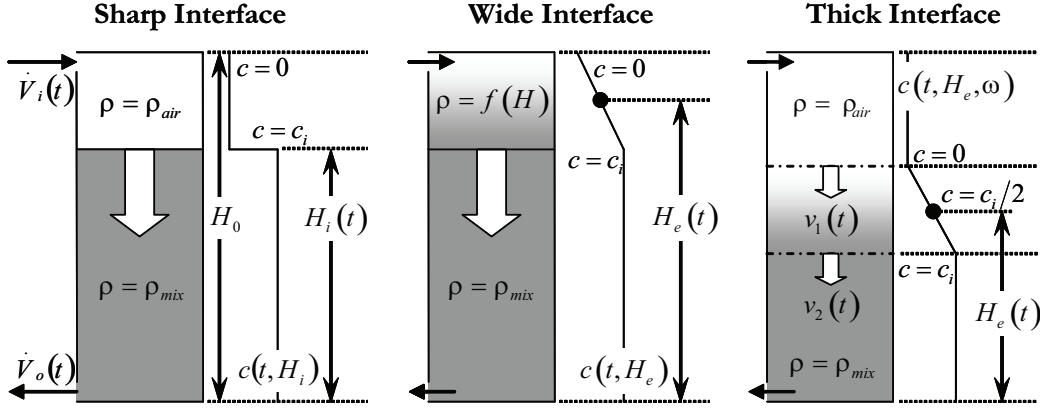


Figure 3.1: Concentration distribution of agents in the sharp and wide interface models. The thick interface model is a new model proposed in this study. The thickness of the interface is estimated from test data of 34 full scale tests.

floor's elevation the interface gradually begins to decay in thickness. Eventually, the interface disappears, all agent has drained from the enclosure, and only fresh, atmospheric air remains.

The interface thickness arises from a balance between gravity and gas diffusion. The resulting agent profile from these forces is transient and forms a highly nonlinear interface between two gas species. The clean agent type, enclosure dimensions, enclosure obstacles, plumes above heat sources, and leaks located at various elevations in the walls pose too many unknowns. Given our current state of knowledge, a concise theoretical formulation for the characteristic thickness is not possible and as such, the characteristic thickness must be evaluated experimentally. After conducting 34 tests on 7 agent types, it is found that the characteristic thickness is a constant in time and also nominally has the same value for various agent types [5].

3.3 Experimental Background

All experiments are conducted in a 4.6 x 4.6 x 4.8 m (15 x 15 x 16 ft) high test enclosure. A schematic of the test bed is given in Figure 3.2. A series of 2.5 cm (1 in) diameter holes are drilled about the enclosure's boundaries at

30 cm (1 ft) offsets from the floor and ceiling elevations. For each experiment dense rubber stoppers are added to or removed from these drill holes to control the total amount of upper and lower leakages provided for agent draining. The entire test bed and instrumentation design is modeled after the small scale prototypical work completed by Mowrer [8].

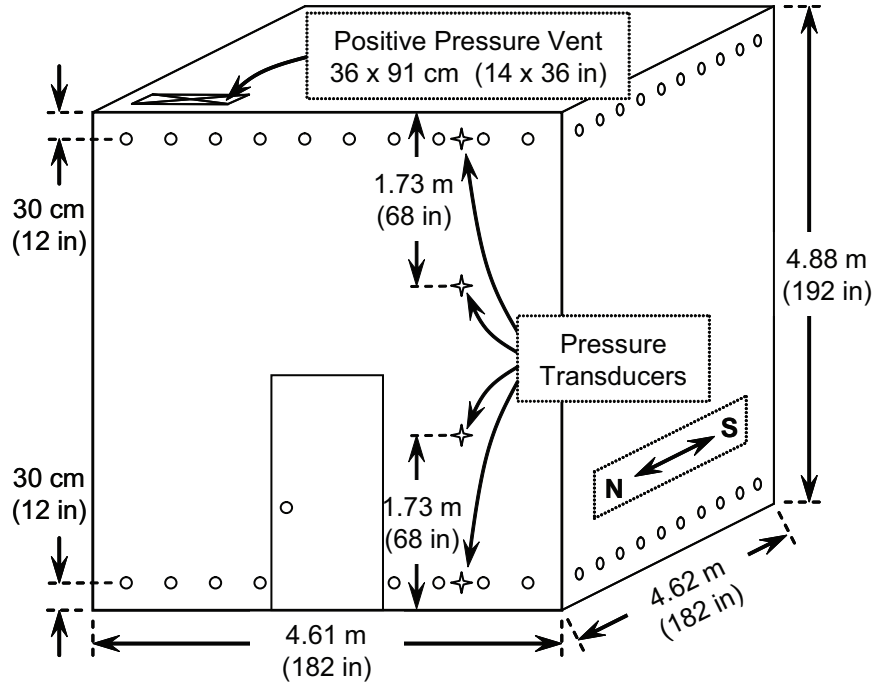


Figure 3.2: Schematic of the test bed. Ambient pressure probes and controllable leakage areas are shown. Temperature and gas sampling probes (not shown) are located 60 cm (2 ft) east of the central axis.

Ambient pressure, temperature, and CEA volume concentrations are monitored inside the test enclosure at a series of elevations. This instrumentation layout parallels the theoretical hold time models in that they are resolved in two dimensions; temporally and spatially in the direction of gravity. The procedure for each experiment begins with a ‘fan integrity test,’ previously introduced. The fan integrity test is performed before and after each hold time test’s execution to ensure that the leakage configuration did not appreciably change during the period of agent discharge. Information gained from

this test measure is used as input data to the theoretical models in making hold time predictions.

The test enclosure is not thermally controlled although the relative humidity is dropped to approximately 40% before test initiation. Fires are not introduced in any experiments, which is consistent with total flooding design objectives that mandate rapid fire detection and system activation before the fire has become a significant threat. The total flooding fire suppression system is manually activated and the CEA allowed to flow through a pipe network to a discharge nozzle inside the test enclosure. After agent discharge the enclosure is left undisturbed for a sufficient period of time to allow for observation of agent draining.

Previously, the data set is used to validate two versions of the sharp descending interface model and one version of the wide descending interface model [4]. It is found that the observed hold time is typically shorter than the sharp interface models' prediction by up to 50% and longer than the wide interface hold time prediction by up to 100%. These figures do not include the uncertainty introduced by the fan integrity test and gas sampling instrumentation.

3.4 The Agent Distribution Profile

The agent distribution profile is the major differentiating factor between the three theoretical hold time models considered in this study. The applicability of each theoretical assumption can be ascertained through direct comparisons of the ideal and observed agent distribution profiles.

Figure 3.3 shows the observed agent distribution profile for each of the seven clean agents tested. The data set from a single, representative test for each agent is plotted. Each data series represents a single instant in time. The progress in time is depicted by lighter shades of gray in Figure 3.3. The time step between data series in each subfigure is a constant, but varies for each subfigure; depending upon the total duration of the test from which each plot originates. Data is presented in the elevation range for which gas sampling instrumentation is installed. At each plotted time step, the installation height for a given instrument and the agent concentration recorded at that instant is shown in Figure 3.3.

Figure 3.4 shows the ideal height-concentration relationship predicted by the models' simplified species diffusivity assumptions. Plotted data series

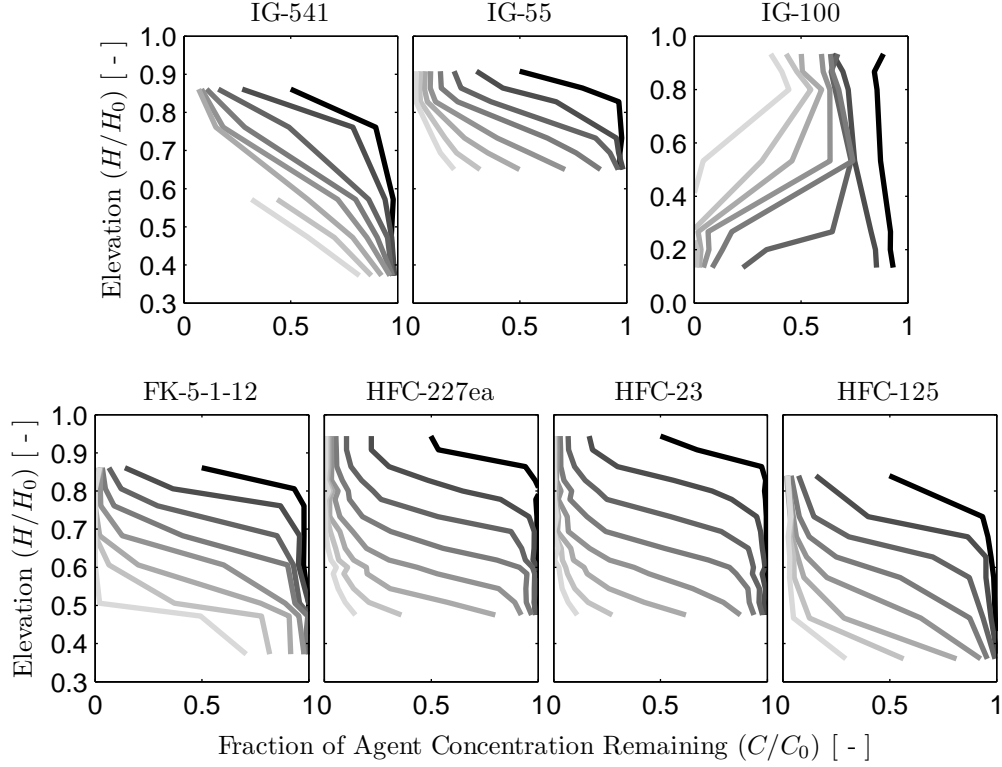


Figure 3.3: Typical observed agent distribution profiles

represent an instantaneous *snapshot* in time where an advance in time is denoted by lighter shades of gray. Because Figures 3.3 and 3.4 share the same axes, direct, graphical comparisons between the observed and predicted agent distributions for various agent types can be made.

Figures 3.3 and 3.4 show that the sharp interface model does not represent actual conditions. All agents have a distinguishable *thickness*; denoted by the change in elevation as a data trace spans from left to right (zero to full agent concentration). The wide interface model shows more reasonable agreement for agents IG-541 and IG-55 but predicts a far greater interface thickness than is observed for all other agent types. Figure 3.3 and 3.4 also show that the thick interface model developed in this study shows good agreement with experimental data for all agent types (except IG-100). However, the thick interface model relies on knowledge of the characteristic thickness. In this

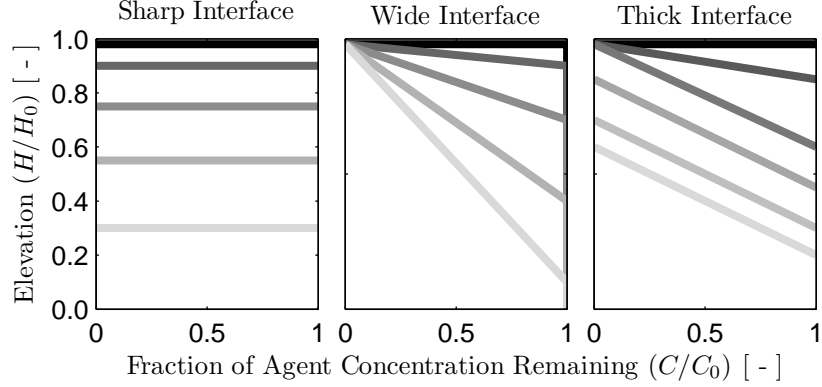


Figure 3.4: Theoretical agent distribution profiles.

study, the experimental data is regressed with the objective of quantifying the observed characteristic thickness as a function of time and agent type.

It should be noted that agent IG-100 does not match any of the models. IG-100 is pure nitrogen, which has a vapor density less than that of atmospheric air. The agent gathers at lower elevations initially because the agent is cold (denser than air due to discharge and expansion) and then gathers at upper elevations as it thermally acclimates to the fresh air within the enclosure. IG-100 therefore does not show a stratified distribution and is not considered for further analysis in this study.

Figure 3.5 illustrates a method of assessing the time resolved interface thickness. HFC-23 experimental data is used as a sample case to analyze the thick interface model proposed in this work³. The relationship between elevation and concentration is assumed to be linear. At each time step a linear regression is computed for all data points that exist within a concentration range of 15% to 85%. Inclusion of all available data points would skew the linear regression and result in poor interface representation. Additionally, at each time step a linear regression is computed with at least 3 data points (no regression lines appear for the uppermost and lowermost data series).

The slope of the regressed line (hollow dotted lines),

³This experiment's data is arbitrarily chosen for demonstration purposes in Figures 3.4, 3.5 and 3.6. The sharp interface model is used to predict a 13 minute hold time; indicating that this particular test is similar to typical total flooding systems in use today.

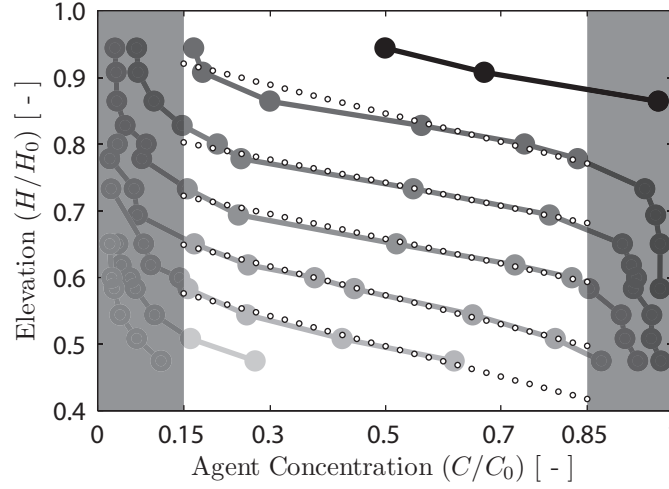


Figure 3.5: Diagram of interface thickness analysis procedure.

$$\omega = \frac{(\Delta H/H_{max})}{(\Delta C/C_{max})},$$

is equal to the dimensionless interface thickness. This procedure is repeated at each data acquisition time step (5 second intervals in this study) to determine the dependency of the interface thickness to time. Figure 3.6 shows the regressed dimensionless interface thickness as a function of the dimensionless time for the HFC-23 data set. Periodically, vertical jumps are observed as the regression is performed at sequential time steps due to the sampling probe entering (or exiting) the region of regressed data (in this case from 15% to 85% of the concentration scale). In general, the dimensionless interface thickness ranges between 0.15 and 0.25. This represents an interface thickness between 15% and 25% of the enclosure's maximum height.

Figure 3.6 shows that the interface thickness is a constant and does not change with time. One would expect that the agent-air interface region will widen with time; however, this is not well supported in Figure 3.6. The affect of test duration and agent type on the mean value of the regressed characteristic thickness is accomplished by summarizing the interface thickness regression results in the format of box plots discussed below.

A series of box plots are presented in Figure 3.7 that summarize the results from the entire test campaign. Each box plot is constructed from a population of data that includes the regressed characteristic thickness from

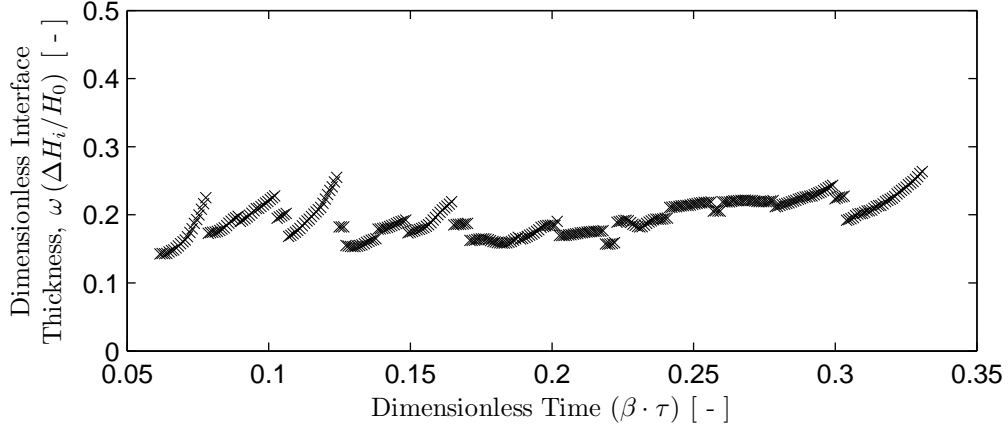


Figure 3.6: Dimensionless interface thickness versus dimensionless time. It is observed that the characteristic thickness is relatively constant as the agent drains out of the enclosure. The nondimensionalization is discussed elsewhere [5].

each time step of a single experiment's agent concentration data (ie. a single box plot in Figure 3.7 represents the entire set of plotted data values in Figure 3.6). Some experiments yield no characteristic thickness information because sufficient gas sampling instrumentation was not available. These experiments are not included in Figure 3.7; leaving a total of 26 charted data sets out of 34 conducted hold time tests. Box plot construction does not assume that the data population is distributed in any predictable way. Rather, it serves to graphically describe the population in terms of the median value (red line inside box), lower and upper quartile values (lower and upper box bounding edges), the range wherein the majority of data values lie (black 'whiskers' extending 1.5 times the interquartile range⁴ above or below the box), and outlier data points, or the data plotted beyond the whiskers (red crosses). Because the population size is not described within the box plot it is included as a separate gray data trace on the rightmost y-axis.

Based on the kinetic theory of gases, the interface thickness should depend on differences in molecular weight between gas species and air [18]. In

⁴The interquartile range (IQR) represents the population data values that are within the 2nd and 3rd quartiles. For example, the population {1,2,3,4,5,6,7,8} results in an IQR of 3 to 6.

addition, the degree of interdiffusion between agent and air (the interface region) should increase with time. The effects of these two parameters are analyzed by ordering the box plots in blocks by agent type (sectioned by black vertical lines) and by the respective test's duration (gauged by the predicted sharp interface hold time at 75% of maximum height, listed on the x-axis). Blocks of agent type progresses from left to right in descending order of the agent-air mixture density. It is expected that interface thickness will follow an upward trend from left to right as the stratifying affect of gravity becomes less powerful. Within each agent type division the individual tests' box plots are ordered from shortest to longest test duration. Here again, one would expect a trend of increasing interface thickness as test duration (or agent diffusion) advances.

Neither of the expected trends introduced above are well supported by Figure 3.7. The agents HFC-125 and IG-55 demonstrate a broadening of the interface region (thickness of the interface) as test duration increases. HFC-23 shows constancy as test duration increases, and FK-5-1-12 and HFC-227ea demonstrate an unpredictable relationship between these two variables. The agent IG-541 stands out due to the tightness of the interquartile range (box extents) and the observation that median value (red line) is drastically different than that of any other test's data. A low level of confidence should be placed in this finding however in that there are no other IG-541 experiments to compare this finding against and because the IG-541 data population size is so limited.

Figure 3.7 does not reveal an inverse relationship between the observed, characteristic thickness and the agent-air mixture vapor density as previously hypothesized. This possibility can be investigated further by regrouping the available data into categories by agent type alone. Figure 3.8 provides a new series of box plots that summarizes all the regressed characteristic thickness data by clean agent type. Again however, there is little evidence to support the hypothesis that the characteristic thickness increases as agent molecular weight decreases (a variable that decreases from left to right).

The interquartile range (upper and lower box edges) for each agent type shown in Figure 3.8 overlaps the respective range of nearly every other agent type (with the exception of IG-541). This indicates that the data population represented by each box plot is probably not statistically different from one another. In order to derive an appropriate value of the characteristic thickness an average value must be obtained. The mean, standard deviation, and population size of each data set, categorized by agent type, is shown in

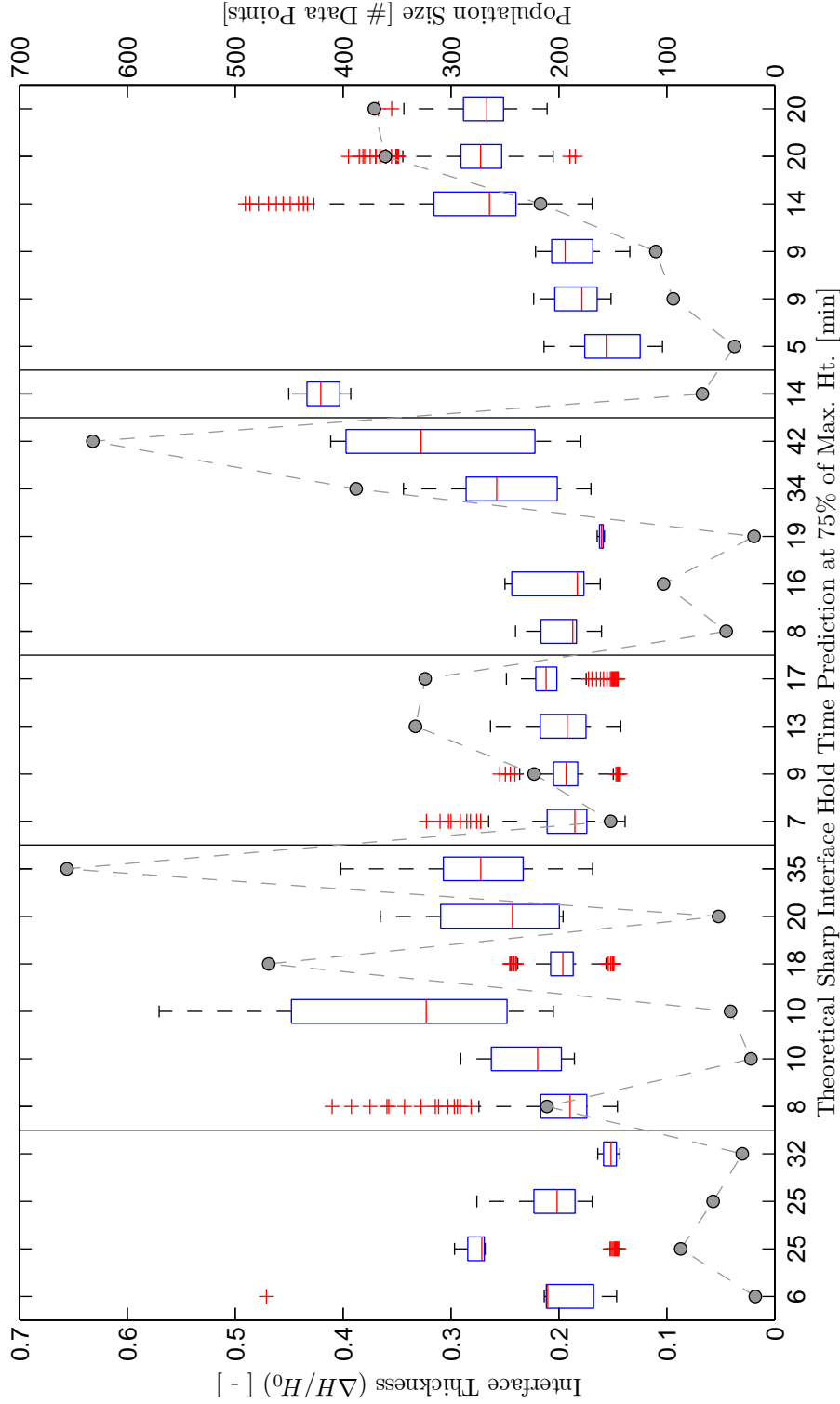


Figure 3.7: Box plots of the dimensionless interface thickness for all conducted tests. Each section of the chart represents a single agent type that is ordered from left to right according to decreasing magnitude of the agent-air mixture density relative to that of atmospheric air (buoyant driving force of agent draining). Each box plot summarizes the data from a single test, which are ordered by the predicted test duration (x-axis value) within each agent type section. Population sizes for each summary box plot are in gray on the rightmost y-axis.

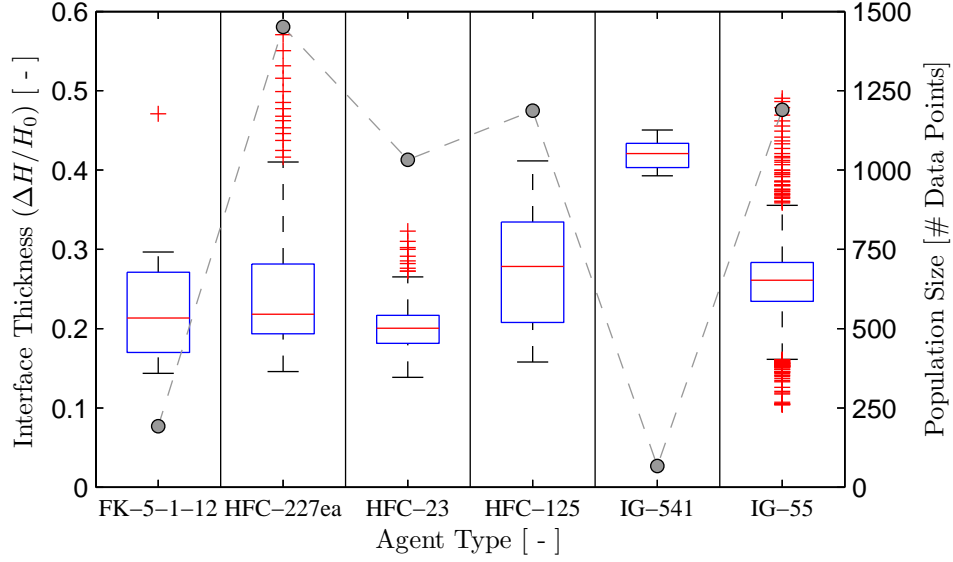


Figure 3.8: Box plots of the dimensionless interface thickness categorized by clean agent type. Each section of the chart represents a single agent type that is ordered from left to right according to decreasing magnitude of the agent-air mixture density relative to that of atmospheric air (buoyant driving force of agent draining). Population sizes for each summary box plot are in gray on the rightmost y-axis.

Table 3.1. The final row in Table 3.1 represents metrics for the entire data population, regardless of agent type. It is found that the mean value of the characteristic interface thickness can be roughly represented as 0.25 ± 0.07 (or 25% of the maximum enclosure elevation $\pm 7\%$).

For the purposes of this study and eventual presentation of model validity this value is chosen to represent a characteristic interface thickness and is used as an input variable to the thick descending interface model; regardless of agent type or test duration.

3.5 Validation Results & Prediction Error

The validity of any of three hold time models considered in this study depends on the users understanding of what a *hold time* is. Previously, the hold time

Table 3.1: Summary values of the regressed dimensionless interface width

Agent Type	Mean Value	Standard Deviation	Population [# data points]
FK-5-1-12	0.22	0.06	192
HFC-125	0.27	0.08	1187
HFC-227 _{ea}	0.24	0.06	1451
HFC-23	0.20	0.03	1032
IG-541	0.42	0.02	67
IG-55	0.26	0.06	1190
All Agents	0.25	0.07	5119

was defined as the duration required for the agent concentration to decay to a specified threshold at a specified elevation. Clearly, a user understanding the hold time to be 50% decay in agent concentration should expect the hold time at any given height to be longer than that for a 15% drop. NFPA 2001 requires that a minimum, 85%⁵ of the initial agent concentration must remain at the hold time (at the elevation of highest combustibles) [2]. ISO 14520 does not provide such guidance but does specify the applicable range of the model use to be 50% to 100% agent remaining at the hold time [19]. Regardless of what has been stated about model applicability, this study establishes new guidance based upon extensive, full scale, experimental evidence.

The hold time model is validated by comparing the theoretical and experimentally observed hold times as shown in Figure 3.9. In order to provide direct comparisons between experiments with various agent types and differing amounts/distributions of leakages the hold time is best expressed in dimensionless units⁶. Due to the semi-subjective nature of the hold time, three plots are provided; each assuming a different threshold for agent concentration. The elevation threshold at which the hold time is defined need not be incremented in the plots below as all elevations are simultaneously visualized (a dimensionless hold time value of 0 represents the hold time at

⁵Note that the theoretical construct of a ‘sharp interface’ as implemented in NFPA 2001’s sharp descending interface model is best understood as representing a 50% drop in agent concentration.

⁶Both experimental and theoretical values of the hold time are charted as the quantity $(\beta \cdot \tilde{t})$, which is presented in depth elsewhere [4].

the maximum elevation and a value of 1 represents the hold time at the minimum elevation).

A line of ‘exact correlation’ and dashed lines representing incremented error thresholds are included in each subplot of Figure 3.9. Data values on the line of exact correlation represent when experimental and theoretical hold times are equal. The error threshold lines represent percent deviations in the experimentally observed hold time values relative to the theoretical prediction. Data points lying below the line of perfect correlation represent a conservative condition where the experimental hold time duration is longer than the predicted value. Data values above this line represent a non-conservative scenario where the models predict an overly optimistic hold time.

All experimental hold time values are depicted three times in each plot; once for each of three hold time models under consideration. Plotted data points are colored by theory type and assume a marker shape based on agent type. The affect of agent type on model validity is difficult to discern. In general, no particular agent type can be observed to stand out from the others. This indicates that the clean agent type being modeled does not have a significant affect on model validity. On the other hand, the theoretical model used has a significant impact on model validity.

A significant portion of the data shown in Figure 3.9a lies in the non-conservative region (above the 45° solid line). The newly introduced, thick descending interface model is shown to provide more accurate predictions of the hold time for a 15% drop in agent concentration than the other existing theories. Thick interface data points (black) populate the region of the axes between that of the sharp and wide theories. Hold times at lower left (measurements taken from upper elevations) are commonly one-and-a-half to two times the predicted value but as the interface descends to approximately one half of the enclosure height (advancing to the upper right) the data center at the line of exact correlation.

The thick interface was introduced as behaving like the wide interface as the thickness initially develops and then transferring to that of the sharp interface’s descent once the characteristic thickness is met. This crossover in behavior is apparent in Figure 3.9a. Initially, the thick interface data overlaps that of the wide interface and eventually it is observed to populate a different region of the chart. This appears to occur at a dimensionless theoretical time of ~ 0.05 , which represents the interface passing an elevation of $\sim 85\%$ of maximum enclosure height.

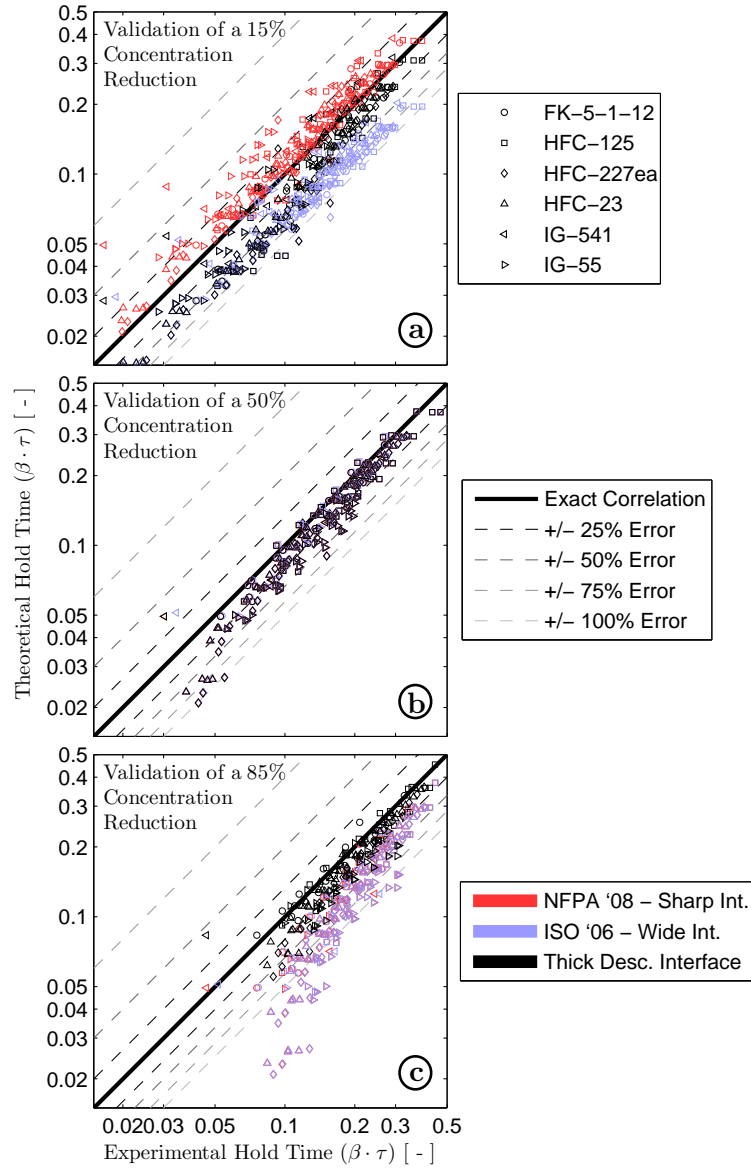


Figure 3.9: Validation plots of the dimensionless theoretical hold time versus the dimensionless experimental hold time for a 15%, 50% and 85% decay in agent concentration. Plotted values are calculated as the quantity $(\beta \cdot \tilde{t})$. Error lines represent percent deviations from the theoretical hold time prediction.

The wide descending interface model (ISO 14520) results in experimental hold times that are up to 75% longer than the predicted values when the hold time is regarded as a 15% decay in concentration. This overly conservative trend is mostly constant through time/elevation as the interface descends and results in system designers not being able to justify whether a 10 minute hold time can be met; even when many total flooding systems can easily retain the necessary clean agent concentration for this duration.

Figure 3.9b assumes the hold time to represent a 50% decay in agent concentration. Because each of the three theories model this concentration threshold equally, most data points directly overlap one another. ISO and NFPA standards adopt slightly different values of the vapor density of agents, the density of atmospheric air, and methods of measuring the amount of leakage present in an existing structure. Due to this, slight jitter is observed between wide and thick data points. The thick interface model is operated with the same assumptions as the sharp interface model, thus perfectly overlapping all of these data points (no red data visible).

Figure 3.9c assumes the hold time to represent an 85% decay of the initial agent concentration or, in other words, only 15% of the total agent remains in the enclosure. From an industrial application, an 85% decay of agent is usually not applicable. However, hold time results are presented in this case as well to demonstrate the versatility of the thick descending interface model. In Figure 3.9c, the plotted theoretical hold time values of the sharp and wide theories are the same as those in Figure 3.9b. Either of these existing theories do not support a 15% agent remaining input value and therefore are not meant to be applicable in this range.

Table 3.2 provides supplemental quantitative measures of model validity. Each data value presented in Figures 3.9a, b and c is first computed as an error level relative to the theoretical prediction and then summarized in three quantities; the mean, cubic mean, and standard deviation. The mean and standard deviation should be fairly intuitive to the reader and the cubic mean is understood to represent an always-positive measure of the total deviation of all experimental hold times from the theoretical prediction.

The third column of Table 3.2, where the hold time represents a 15% decay in agent concentration, is most relevant to a design scenario. In the sharp interface theory, actual hold times can be roughly $13\% \pm 14\%$ shorter than predicted values with a total average error of 19%. This justifies the graphical observation in Figure 3.9a where most data points lie above the 45° solid line. The thick interface model is more applicable than the wide

Table 3.2: Quantitative summary of experimental error relative to the theoretical prediction

Quantitative Measure	Theory Type	Concentration Decay at the Hold Time		
		15%	50%	85%
Cubic Mean (Percent Error)	Sharp Interface	19%	27%	99%
	Wide Interface	61%	28%	99%
	Thick Interface	42%	27%	24%
Mean (Percent Error)	Sharp Interface	-13%	20%	76%
	Wide Interface	56%	20%	77%
	Thick Interface	31%	20%	16%
Standard Deviation (Percent Error)	Sharp Interface	14%	19%	63%
	Wide Interface	24%	19%	63%
	Thick Interface	28%	19%	18%

interface model if similar metrics are considered. Both theories provide predictions that are typically conservative (mean error is positive) even when considering the standard deviations from this mean value. The thick interface model presented in this study provides hold time predictions that are a lot less conservative than that of the wide interface theory however. Experimental hold times are longer than thick interface model predictions by $31\% \pm 28\%$ compared to $56\% \pm 24\%$ for the wide interface model. As well, it is interesting to note that the thick interface models agent draining with increasing accuracy as the agent concentration threshold is set lower (moving from left to rightmost column in Table 3.2).

3.6 Conclusions

This study questions the validity of two prevalent models used to predict the duration for which a modern, halon-replacement agent will remain within a protected enclosure. A novel model formulation is introduced and shown to provide more accurate predictions of agent draining dynamics than either of the existing methods. The results of a recent experimental campaign including seven common clean agent varieties and 34 full scale tests are used to assess model validity.

The applicability of a single differentiating factor between the three con-

sidered models - the profile of agent distribution through elevation - is investigated. The assumption taken for this concentration profile constitutes a titular basis for each considered model. The sharp interface model assumes that fresh air and agent stratify across an infinitesimally thin interface (published in NFPA 2001). The wide interface model assumes a linear concentration gradient across the air-agent interface width, which has a thickness that ultimately spans the total height of the design enclosure (published in ISO 14520). The modified model formulation, proposed as the *thick descending interface* model assumes an interface of known thickness. This constitutes an additional input parameter, the *characteristic thickness*, ω , which is extracted from the experimental data by linear regression for use in this study.

Within this study, and typical to the industry, the hold time is defined as the duration required for the agent concentration to decay 15% of its initial value at a set elevation within the design enclosure. Experimentally observed hold times at elevations between 95% and 40% of total enclosure height are generally longer than the thick interface model predictions by $\sim 30\%$. These same values are longer than the wide interface by $\sim 60\%$ and shorter than the sharp interface theory by $\sim 10\%$. The last of these findings is a cause for alarm in that the sharp interface model is providing non-conservative hold time predictions.

Bibliography

- [1] Dewsbury, J. and Whiteley, R.A. “Extensions to standard hold time calculations,” Fire Technology, Vol. 36, No. 4, pp. 267-278, Nov. 2000.
- [2] “NFPA 2001: Standard on clean agent fire extinguishing systems,” National Fire Protection Association, Quincy, MA, Annex C, 2008.
- [3] Dewsbury, J., and Whiteley, R.A. “Review of fan integrity testing and hold time standards,” Fire Technology, Vol. 36, No. 4, pp. 249-265, Nov. 2000.
- [4] Hetrick, T. “Analysis of hold time models for total flooding clean extinguishing agents,” Fire Technology, Vol. 44, No. 3, pp. 239-261, Sept. 2008.
- [5] Hetrick, T. “Development and Validation of a Modified Clean Agent Draining Model for Total Flooding Fire Suppression Systems,” M.S. thesis, Worcester Polytechnic Institute, Worcester, MA, 2008.
- [6] Saum, D., Saum, A., Messing, M. and Hupman, J. “Pressurization air leakage testing for Halon 1301 enclosures,” Substitutes and Alternatives to Chlorofluorocarbons and Halons, Washington, D.C., 1988.
- [7] DiNenno, P.J., and Forssell, E.W. “Evaluation of the door fan pressurization leakage test method applied to Halon 1301 total flooding systems,” Journal of Fire Protection Engineering, Vol. 1, No. 4, pp. 131-140, 1989.
- [8] Mowrer, F. “Analysis of vapor density effects on hold times for total flooding clean extinguishing agents,” Halon Options Technical Working Conference, 16th Proceedings, Albuquerque, NM, pp. 1-12, May 2006.

- [9] O'Rourke, S.T. "Analysis of hold times for gaseous fire suppression agents in total flooding applications," M.S. thesis, University of Maryland, College Park, MD, 2005.
- [10] Black, B., Maranghides, A., Sheinson, R., Peatross, M., and Smith, W. "Real scale halon replacement testing aboard the ex-USS Shadwell: post fire suppression compartment characterization," Halon Options Technical Working Conference, 6th Proceedings, Albuquerque, NM, pp. 1-12, May 1996.
- [11] Maranghides, A., Black, B., Sheinson, R., Friderichs, T., and Peatross, M. "Discharge system modifications: real scale halon 1301 replacement testing," Halon Options Technical Working Conference, 6th Proceedings, Albuquerque, NM, pp. 1-12, May 1996.
- [12] Genge, C. "Preventing excessive enclosure pressures during clean agent discharges," Halon Options Technical Working Conference, 15th Proceedings, Albuquerque, NM, pp. 1-16, May, 2005.
- [13] Harry, L., Meltzer, J., Robin, M. "Development of room pressure in the discharge of FM-200 compared to the strength of various structural components," Halon Options Technical Working Conference, 7th Proceedings, Albuquerque, NM, pp. 1-12, May, 1997.
- [14] Robin, M., Forssell, E., and Sharma, V. "Pressure dynamics of clean agent discharges," Halon Options Technical Working Conference, 15th Proceedings, Albuquerque, NM, pp. 1-11, May, 2005.
- [15] Sherman, M., Palmiter, L. "Uncertainties in fan pressurization measurements," Airflow Performance of Building Envelopes, Components and Systems, ASTM STP 1255, American Society for Testing and Materials, Philadelphia, PA, pp. 266-283, 1995.
- [16] Sherman, M. "The use of blower-door data," Indoor Air, Vol. 5, Issue 3, pp. 215-224, 1995.
- [17] Hetrick, T., Rangwala, A. "Analysis of hold time models for total flooding clean extinguishing agents," Fire Suppression and Detection Research and Applications A Technical Working Conference (SUPDET 2008), Orlando, FL, March, 2008.

- [18] Vincenti, W., Kruger, C. Introduction to physical gas dynamics. New York, Wiley, 1965.
- [19] “ISO 14520-1: Gaseous fire extinguishing systems - physical properties and system design - part 1: general requirements,” International Standards Organization, Geneva, Switzerland, Annex E, 2006.

Chapter 4

Conclusions

Total flooding fire suppression systems are designed and installed according to the prescriptive measures established in widely accepted standards. The preceding chapters question the applicability of the methods of NFPA 2001 and ISO 14520 as applied to the surplus of halon-replacement agents available in today's marketplace. Both of these design standards include a method for estimating the duration of time (hold time) that a gaseous suppressant, or clean extinguishing agent, will remain within the protected enclosure following discharge. Results obtained from 34 full-scale experiments are used to validate the predictive capability of these models. It is found that the *sharp descending interface model* of NFPA 2001 typically provides non-conservative predictions of the hold time and that the *wide descending interface model* of ISO 14520 provides overly conservative hold time predictions.

The inadequacy of the analytical models stated above is partially mitigated through use of the *thick descending interface model*; proposed in the second chapter of this document. This model reformulates the simplifying assumption for where the suppressant accumulates within the design enclosure as resolved in elevation. A result of this is the need for users to define an additional input parameter, the characteristic interface thickness. For the purposes of model validation herein this parameter is regressed from the experimental data although further work may be required to establish the independence of this parameter from other system design and environmental variables.

The experimentally observed hold time is found to be shorter than sharp interface model predictions by $\sim 10\%$, longer than wide interface predictions by $\sim 60\%$, and longer than thick interface model predictions by $\sim 30\%$. These

figures reflect findings specific only to the experimental findings documented herein. Further, they represent the combined predictive capacity at any elevation within the range of 40% to 95% of the full scale experimental enclosure height and apply only when the hold time is defined as representing a 15% decay in agent concentration from the discharge concentration.

Chapter 5

Recommendations for Future Work

Nearly all structures are subject to bias pressure whether intentional (i.e. HVAC design, smoke control pressurization) or not (i.e. stack effect). A controlled introduction of positive and negative bias pressure from high and low elevations should be investigated.

The worst consistency between empirical and theoretical evaluations of the hold time often occurs when the upper and lower leakage areas are not equal. Further investigation of this parameter as a source of prediction error is warranted.

Many of the instruments used in collection of agent concentration measurements could not be properly calibrated. A objective procedure for interpretation and scaling of these data sets is implemented herein. Future testing should use more modern instrumentation such as the Halonizer used by the Federal Aviation Administration for approvals testing of clean agents inside nacelles.

The cooling affect of a clean agent discharge and resultant temperature change is not accounted for in the models, which may lead to measurable errors in the predicted hold time. Additionally, transient temperature data at various locations in the x-y plane and in elevation is sparse in this study. Further analysis of these transient thermal effects is warranted.

The agent concentration profile in elevation is not perfectly modeled by a linearized, maximum slope maxim as introduced in Chapter 3. As well, the characteristic maximum slope parameter used for hold time calculation purposes herein for the thick descending interface model is based on an empirical

regression. A means of formulating this input parameter based upon known system design variables would be ideal. Otherwise, this parameter needs to be estimated based on consistent, known behavior or acceptable validity of calculated hold time predictions.

Appendices

Appendix A

Test Bed & Instrumentation

This appendix serves to document extended information about the test bed configuration and instrumentation setup that has not been properly addressed in the papers for publication included in Chapters 2 and 3. The paper previously published in Fire Technology (Chapter 2) presents results only from the first phase of testing; in the summer of 2006. Four prototypical tests were conducted in the fall of 2005 that were not included in the paper due to the author's not having witnessed their execution. An additional test phase in the summer of 2007 is not, until now, elaborated upon although the collected data is presented for analysis in Chapter 3. In result, the following of this appendix discusses and documents quite a bit of new information.

The publication of Chapter 2 in Fire Technology in conjunction with live presentations to key audiences garnered financial support for a second phase of testing in the summer of 2007. An extended team of industry specialists representing a wealth of clean extinguishing agents and system design practices was assembled. The support and generosity of these associates provided for nearly a two-fold increase in instrumentation and doubled the total number of tests conducted. Credited to the continuance of this research campaign the cumulative test matrix now includes a collection of clean extinguishing agents that spans the widest range of agent vapor densities available on the market; inclusive of pure nitrogen, which is a special case in that it is less dense than atmospheric air itself. Creative problem solving allowed the new research team to non-destructively modify the test enclosure to allow for extremely leaky configurations. Allowing extra leakage provided for meeting a primary research goal ascertained following the conclusion the first test phase; to perform tests for various agent types where the target hold time

of the test system adequately matches the applicable range of usage in real world applications. Additionally, this allowed for further observation of the leakage phenomenon when unequal leakages were allowed to exist at the test enclosure's upper and lower elevations.

In the summer of 2007 a second phase of full scale testing was conducted in the same test enclosure as that used in the 2005 and 2006 test campaigns. Further experimental setup modifications provided for 2007 testing is documented in the following. As well, a review of all conducted tests' leakage configurations, total flooding system designs, operated instrumentation, and influential environmental variables is provided.

A.1 Test Bed & Leakage Characteristics

Owned and operated by Fike Corporation, the test enclosure is of the typical design used for clean extinguishing agent approvals testing per UL 2166. It is located inside a larger warehouse to reduce exposure to stray wind pressures. The diagram in Figure A.1 contains the enclosure's external dimensions, ambient pressure transducer locations, and available leakage pathways. The enclosure volume is 103.8 m^3 (3665 ft^3) measuring 461 cm by 462 cm by 488 cm in height (181.5 x 181.75 x 192 in). A series of 2.54 cm (1 in) diameter drill holes are located about the outer walls; offset from the floor and ceiling elevations by 30 cm (1 ft) on center. These holes are provided with dense rubber stoppers that may be inserted or removed as desired for a particular test configuration.

Testing of agents with a vapor density very near to that of atmospheric air requires more available leakage pathways in order to yield a shorter agent draining time. With all the plugs removed from available leakages clean agents such as IG-55 and IG-100 yield predicted hold times of 19 and 165 minutes, respectively (when evaluated at 75% of the maximum enclosure height). These hold time durations are excessively long and do not apply to the typical design goals of installed systems. In order to meet the research objective of performing tests that are applicable to the typical range of use in the field it was necessary to add additional venting through enclosure boundaries. Further permanent alteration of the test bed was undesirable to the owner. The research team required additional venting that was both evenly distributed about the planar dimensions and only distributed in elevation at the upper and lower extremes. As such, the research team was forced to seek

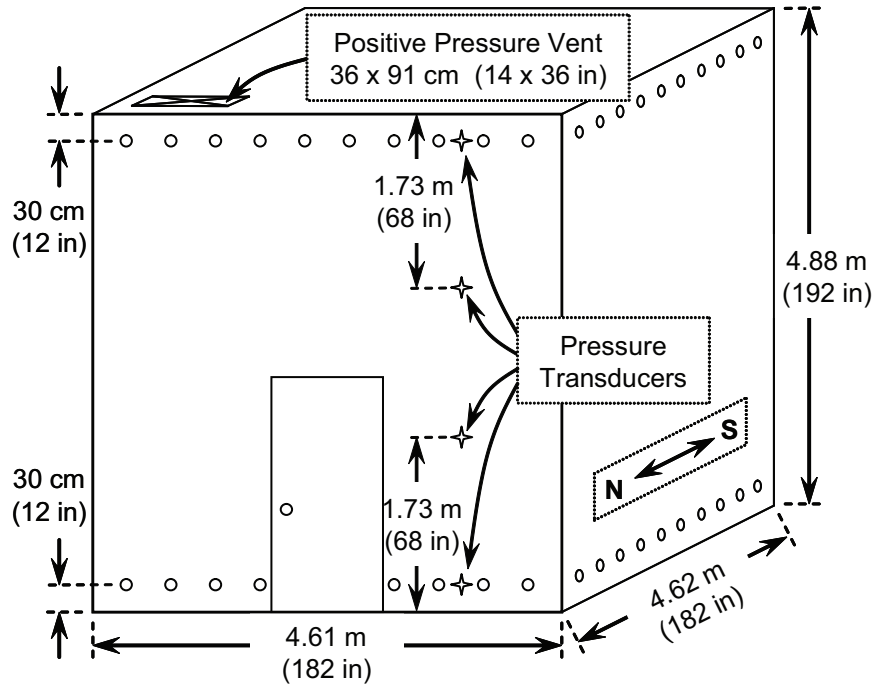


Figure A.1: Schematic of the test bed. Ambient pressure probes and controllable leakage areas are shown. Temperature and gas sampling probes (not shown) are located 60 cm (2 ft) east of the central axis.

out a novel way to meet their needs.

Two sealed access panels were provided at the upper and lower of the east enclosure wall. These panels were replaced with well-seated plywood panels through which a 30 cm (1 ft) diameter hole was cut. These new leakages were located very near to the extremes of the enclosure's elevation and were significantly large enough to provide for minimum IG-55 and IG-100 predicted hold times of 7 and 58 minutes, respectively.

The new leakages were required to be distributed evenly about the planar dimensions of the test enclosure. Sections of 30 cm (1 ft) diameter HVAC ducting were used to accomplish this. The majority of clean agents tested had vapor densities greater than that of atmospheric air; meaning that they would drain through lower enclosure boundaries as fresh air flowed in through upper leakages. Due to this, a more sophisticated duct-system was designed for the additional upper leakage. Ducting was terminated at four locations in

the planar view at the upper-most elevation; located in the center of each of four fourths of the total planar area. Duct ends were capped over the lower 50% of the opening and left open for gas flow through the upper 50%.

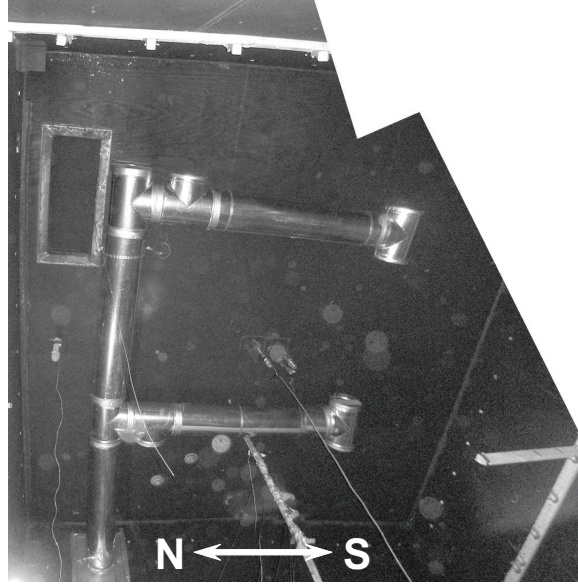


Figure A.2: Upper vent duct system

The lower additional leakage was ducted through a single pathway to the center of the planar view at the lowest possible elevation and left uncapped. Figures A.3 & A.2 are photographs of the HVAC duct installations from the vantage of the northwest corner. Duct openings are assumed to nominally match the elevations of the other drilled leakages about enclosure walls. Friction losses in the vented gas were assumed negligible as the volumetric flows during test durations were of minimal magnitude.

A complete collection of experimental leakage configurations all tests conducted is available in Table A.1. The entire test campaign spanning from the prototypical tests conducted in the fall of 2005 to the first and second phases of testing in the summer of 2006 and 2007 constitutes a sum of 44 conducted tests. Nine of the test numbers in Table A.1 are short duration tests where only ambient pressures were recorded (not a hold time test). Test number 4 is a null test, yielding no usable ambient pressure or agent concentration data. A total of 34 hold time tests exist, or those where agent

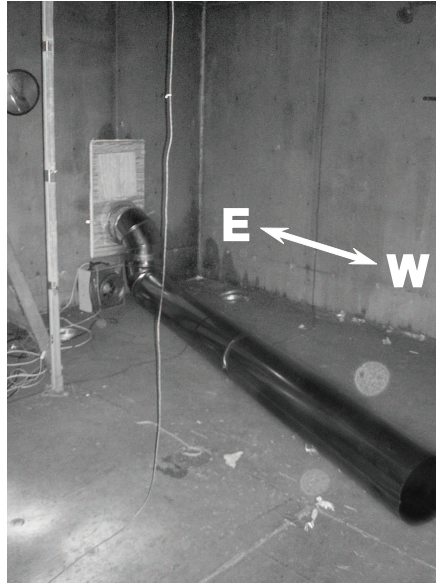


Figure A.3: Lower vent duct system

volume concentrations are also monitored for an extended duration.

The second and third columns of Table A.1 list the number of 2.54 cm (1 in) drill holes left unplugged about the upper or lower of the enclosure. For select test numbers the fifth column lists any additional leakages that may have been provided. The additional ducting system, described previously, was left fully open to gas flow twice and restricted twice by installing an 18.46 in² circular orifice plate at the outer duct termination point.

Calculation of theoretical hold time predictions is performed using much of the information presented in the remainder of Table A.1. The Lower Leakage Fraction (LLF), F , described by Equation 2.2 is tabulated in the sixth and seventh columns of Table A.1. The first is the theoretical value based on the set leakage configuration.

Column seven gives the mean of the steady-state, lower leakage fraction correlation as implemented with Equation 2.4. The correlated LLF value is

Table A.1: Experimental leakage configuration parameters

Test Number	Clean Agent Type (ASHRAE)	# Open Upper Holes	# Open Lower Holes	Additional Open Leakages	Lower Leakage Fraction	Lower Leakage Fraction	Door Fan Test Data - Inflow		Door Fan Test Data - Outflow		Total Leak Area
					(set to)	(correlated)	n	k _i	n	k _i	
					[-]	[-]	[-]	[l/s/Pa ⁿ]	[-]	[l/s/Pa ⁿ]	[cm ²]
0	-	-	-	-	N/A	0.51	0.740	2.817	0.672	2.626	79
1	HFC-227ea	27	27	-	0.50	0.50 ¹	0.558	26.900	0.546	28.500	432
2	HFC-227ea	27	27	-	0.50	0.50 ¹	0.558	26.900	0.546	28.500	432
3	HFC-227ea	14	14	-	0.50	0.50 ¹	0.650	11.300	0.658	11.800	269
4	HFC-227ea	8	8	-	N/A	N/A	-	-	-	-	-
5	HFC-227ea	4	4	-	0.50	0.50 ¹	0.617	7.124	0.594	6.770	134
6	FK-5-1-12	16	16	-	0.50	0.50 ¹	0.550	19.286	0.531	21.649	304
7	FK-5-1-12	41	41	-	0.50	0.50 ¹	0.503	49.376	0.572	35.014	613
8	FK-5-1-12	8	8	-	0.50	0.50 ¹	0.587	10.454	0.745	5.752	189
9	FK-5-1-12	4	4	-	0.50	0.50 ¹	0.617	7.124	0.594	6.770	134
10	FK-5-1-12	7	7	-	0.50	0.50 ¹	0.560	10.691	0.618	8.212	169
11	IG-541	41	43	-	0.51	0.51 ¹	0.499	45.745	0.518	43.893	589 ⁴
12	IG-541	16	16	overpressure vent	0.50	0.50 ¹	0.550	19.286	0.531	21.649	1230 ⁴
13	IG-541	16	8	overpressure vent	0.50	0.50 ¹	0.587	10.454	0.745	5.752	1846 ⁴
14	IG-541	16	16	vent open during discharge only	0.50	0.50 ¹	0.550	19.286	0.531	21.649	1898
15	IG-541	41	43	-	0.51	0.51 ¹	0.499	45.745	0.518	43.893	589
16	HFC-125	41	41	-	0.50	0.51	0.503	49.376	0.572	35.014	613
17	HFC-125	16	16	-	0.50	0.51	0.550	19.286	0.531	21.649	304
18	HFC-125	8	8	-	0.50	0.50	0.587	10.454	0.745	5.752	189
19	HFC-125	4	4	-	0.50	0.49	0.617	7.124	0.594	6.770	134
20	HFC-125	24	8	-	0.25	0.34	0.550	19.286	0.531	21.649	304
21	HFC-227ea	32	32	-	0.50	0.51	0.542	36.452	0.510	41.335	547
22	HFC-227ea	11	12.5	-	0.53	0.50	0.648	12.338	0.541	17.750	273
23	HFC-227ea	4	4	-	0.50	0.47	0.629	7.174	0.637	7.792	160
24	HFC-227ea	1	1	-	N/A	N/A	0.693	4.641	0.649	4.663	116
25	HFC-227ea	1	1	-	N/A	N/A	0.693	4.641	0.649	4.663	116
26	HFC-227ea	1	1	-	N/A	N/A	0.693	4.641	0.649	4.663	116
27	HFC-23	43	42	1/2 of a 11.8" dia hole	N/A	N/A	0.507	77.917	0.507	79.977	1031
28	HFC-23	41	41	-	0.50	0.52 ²	0.545	44.098	0.524	48.248	671
29	HFC-23	30	30	-	0.50	0.50	0.546	33.131	0.523	36.621	506
30	HFC-23	20	20	-	0.50	0.50	0.548	24.344	0.531	25.351	368
31	HFC-23	15	15	-	0.50	0.48	0.591	17.142	0.588	16.416	303
32	IG-55	43	43	HVAC system fully open	0.50	0.39 ³	0.469	158.924	0.575	126.384	1971
33	IG-55	43	43	Open Upper duct w/ orf. plate on Lower	N/A	N/A	0.497	120.040	0.518	115.183	1539
34	IG-55	43	43	18.46 sq.in. orf. on Upper & Lower Vent	0.50	0.48 ³	0.519	73.547	0.504	76.930	1001
35	IG-55	43	43	-	0.50	0.52	0.519	49.637	0.553	45.750	699
36	IG-55	30	30	-	0.50	0.49 ²	0.551	31.588	0.526	34.179	486
37	IG-55	41	3	-	N/A	N/A	0.554	26.660	0.545	27.147	415
38	Pro-IG-55	43	43	18.46 sq.in. orf. on Upper & Lower Vent	0.50	0.50	0.519	73.547	0.504	76.930	1001
39	Pro-IG-55	43	43	-	N/A	N/A	0.532	48.826	0.531	50.287	712
40	Pro-IG-55	30	30	-	0.50	0.49	0.551	31.588	0.526	34.179	486
41	Pro-IG-55	43	5	-	N/A	N/A	0.548	29.300	0.523	31.304	442
42	IG-100	43	43	HVAC system fully open	0.50	0.57	0.469	158.924	0.575	126.384	1971
43	IG-100	43	43	-	0.50	0.46	0.532	48.826	0.531	50.287	711.891
44	IG-100	43	5	-	N/A	N/A	0.548	29.300	0.523	31.304	441.958

used as input data for all hold time predictions when available¹²³.

Columns 8 through 11 give the resultant door fan test data for a multi-point fan test. ISO and NFPA standards specify different methods of averaging the inflow and outflow test data into a single value of the flow exponent, n , and coefficient, k_1 . When the method specified by the 2008 publication of NFPA 2001 is assumed, the total leakage area found is that listed in the final column⁴.

A.2 Total Flooding System Design

To meet the industry best-practices for any tested clean agent, total flooding system suppliers / manufacturers were called upon for both design and installation at the test site. As part of their involvement, the majority of these institutions donated agent and delivery hardware to the test campaign. Table A.2 summarizes the total flooding system parameters used throughout all phases of testing. The first column gives the test reference number, used to link this table to others in this report. The third column gives the system manufacturer name along with the market name of their total flooding system. Tests 42 through 44 do not have a coined product name as this manufacturer does not actually market pure nitrogen as an extinguishant although their Argonite hardware is appropriately employed in these tests.

Clean extinguishing agents are stored in a pressurized vessel until the moment of discharge. In this state they are either stored as liquid under pressure or as a pressurized gas. Many of the liquid phase agents have been *super-pressurized* with added nitrogen. The nitrogen partially dissolves into the liquid agent, which can aid in accelerating the vaporization process, but

¹When pressure data is not available to achieve a steady-state LLF correlated value, the LLF is computed as an average between the set value and the background value (see test 0) weighted by the total leak areas of each.

²Due to lacking transient pressure data the correlated LLF for tests 28 and 36 is adopted from a similar test configuration.

³The irrational instrument behavior exhibited in Figures D.45, D.48, G.16, G.17, G.18 and G.19 casts doubt on the correlated LLF given for tests 32 and 34!

⁴The available door fan equipment for Tests 12 through 14 could not adequately pressurize the enclosure with this much leakage! Fan data is borrowed from FK-5-1-12 tests with an equal number of lower holes open. The leakage areas reported are 1/2 second averaged, point measurements with the available fan at full speed. This approximation is made for model validation purposes on the basis that the rate of agent draining is limited by the smaller of either the upper or lower total leakage areas.

Table A.2: Total flooding system design parameters

Test Number	Clean Agent Type (ASHRAE)	Hardware Manufacturer & Technology Name	Number of Suppressant Cylinders	Cylinder Internal Volume	Cylinder Pressure	Total Agent Mass	Disc. Time	Target Suppressant Concentration	Hold Time Prediction at 85% of Max Ht.
			[-]	[liter]	[bar]	[kg]	[s]	[Vol.%]	[min]
1	HFC-227ea	Fike / HFC-227ea	1	N/R	24.8	57.1	16.00	7.00	5.8
2	HFC-227ea	Fike / HFC-227ea	1	N/R	24.8	57.1	11.18	7.00	5.8
3	HFC-227ea	Fike / HFC-227ea	1	N/R	24.8	57.1	10.65	7.00	11.3
4	HFC-227ea	Fike / HFC-227ea	1	N/R	24.8	57.1	10.50	7.00	-
5	HFC-227ea	Fike / HFC-227ea	1	N/R	24.8	57.1	10.85	7.00	20.7
6	FK-5-1-12	Ansul / Sapphire	1	N/R	20.7	62.6	12.15	4.17	7.3
7	FK-5-1-12	Ansul / Sapphire	1	N/R	24.8	62.6	10.90	4.17	3.6
8	FK-5-1-12	Ansul / Sapphire	1	N/R	24.8	62.6	10.80	4.17	14.6
9	FK-5-1-12	Ansul / Sapphire	1	N/R	24.8	62.6	9.85	4.17	18.7
10	FK-5-1-12	Ansul / Sapphire	1	N/R	24.8	62.6	10.65	4.17	14.3
11	IG-541	Ansul / Inergen	4	80	150.0	67.3	25.70	36.82	8.7
12	IG-541	Ansul / Inergen	4	80	150.0	67.3	49.80	36.82	18.9
13	IG-541	Ansul / Inergen	4	80	150.9	67.7	45.70	37.01	46.3
14	IG-541	Ansul / Inergen	4	80	150.0	67.3	38.50	36.82	18.9
15	IG-541	Ansul / Inergen	4	80	N/R	77.5	64.70	40.97	8.3
16	HFC-125	Fike / ECARO-25	1	N/R	24.8	45.7	11.40	8.00	4.6
17	HFC-125	Fike / ECARO-25	1	N/R	24.8	45.7	10.00	8.00	9.3
18	HFC-125	Fike / ECARO-25	1	N/R	24.8	45.7	9.70	8.00	19.6
19	HFC-125	Fike / ECARO-25	1	N/R	24.8	45.7	10.20	8.00	24.5
20	HFC-125	Fike / ECARO-25	1	N/R	24.8	45.7	9.90	8.00	11.2
21	HFC-227ea	Chemetron / FM-200	1	65.96	24.8	48.5	9.40	6.04	4.6
22	HFC-227ea	Chemetron / FM-200	1	65.96	24.8	48.5	9.00	6.04	10.7
23	HFC-227ea	Chemetron / FM-200	1	65.96	24.8	48.5	9.60	6.04	20.0
24	HFC-227ea	Chemetron / FM-200	1	65.96	24.8	48.5	9.10	6.04	-
25	HFC-227ea	Chemetron / FM-200	1	65.96	24.8	48.5	9.90	6.04	-
26	HFC-227ea	Chemetron / FM-200	1	65.96	24.8	48.5	8.70	6.04	-
27	HFC-23	Kidde-Fenwal / FE-13	3	67.96	42.0	73.5	-	19.47	-
28	HFC-23	Kidde-Fenwal / FE-13	3	67.96	42.0	73.5	12.00	19.47	4.0
29	HFC-23	Kidde-Fenwal / FE-13	3	67.96	42.0	73.5	13.10	19.47	5.3
30	HFC-23	Kidde-Fenwal / FE-13	3	67.96	42.0	73.5	-	19.47	7.4
31	HFC-23	Kidde-Fenwal / FE-13	3	67.96	42.0	73.5	12.70	19.47	10.1
32	IG-55	Chemetron / Argonite	3	80.00	199.9	67.0	52.70	36.81	3.0
33	IG-55	Chemetron / Argonite	3	80.00	199.9	67.0	53.20	36.81	-
34	IG-55	Chemetron / Argonite	3	80.00	199.9	67.0	53.00	36.81	5.2
35	IG-55	Chemetron / Argonite	3	80.00	199.9	67.0	-	36.81	8.1
36	IG-55	Chemetron / Argonite	3	80.00	205.0	67.0	52.40	36.77	11.8
37	IG-55	Chemetron / Argonite	3	80.00	199.9	67.0	52.20	36.81	-
38	Pro-IG-55	Fike / PROINERT	3	80.00	199.9	67.0	57.60	36.77	5.2
39	Pro-IG-55	Fike / PROINERT	3	80.00	199.9	67.0	53.40	36.77	-
40	Pro-IG-55	Fike / PROINERT	3	80.00	200.0	67.0	53.40	36.77	11.8
41	Pro-IG-55	Fike / PROINERT	3	80.00	199.9	67.0	57.80	36.77	-
42	IG-100	Chemetron / N/A	3	80.00	199.9	56.1	46.60	37.22	6.5
43	IG-100	Chemetron / N/A	3	80.00	199.9	56.1	49.90	37.22	18.2
44	IG-100	Chemetron / N/A	3	80.00	199.9	56.1	-	37.22	-

primarily is used to drive the agent through piping networks to points of discharge in the design envelope. Table A.2 gives the number of storage cylinders required and the cylinders' internal volume in the fourth and fifth columns, respectively. Generally, inert gas agents (those with ASHRAE names beginning with IG) are those stored as gases under pressure and mandate much larger storage requirements.

The pressure of the stored agent is given as a gage pressure in the sixth column. The seventh column of Table A.2 lists the agent mass presumably delivered to the design enclosure for any given test. Non inert gas cylinders are filled by mass and the tests conclude with a weighing of the empty storage cylinder, which typically ascertained less than 1 kg of undelivered agent (assumed negligible due to a relative calibration technique used for all gas sampling instrumentation). Inert gas agent cylinders are filled by pressure, allowed to acclimate to room temperature, and then filled to pressure once again. Due to this, the listed agent mass for inert gas tests is actually calculated from the cylinder pressure per the ideal gas law.

Table A.2 lists the time required to deliver the clean agent into the design enclosure in the eighth column. These values are obtained by monitoring the pressure inside the delivery pipe network just upstream of the terminating nozzle. The method used to find this value is inspired by the definition provided by the 2008 publication of NFPA 2001; "the time required to discharge from the nozzles 95 percent of the agent mass." The integral of the square route of this data trace represents a unit-less value for the total volume of agent delivered through the nozzle. Agent discharge is assumed to cease when the value of this time-integral is equal to 95% of the total data trace's integral value. Tests without a value listed are due to instrument failure.

By invoking the methods of the 2008 edition of NFPA 2001 the delivered agent concentration is calculated in the ninth column. This value is assumed to be the actual delivered concentration existing throughout the enclosure following the turbulent discharge event. All gas sampling data traces are assumed to baseline at zero volume concentration before discharge and plateau at the calculated volume concentration after discharge (or after the instrument output signal plateaus). This relative measurement technique is required in nearly all cases due to inadequate instrument calibration. All oxygen analyzers used in the 2007 test campaign were recently calibrated and capable of making absolute measurements. To provide for consistency and impartiality in the data regression of various test data sets, even these data traces have been rescaled by the assumptions outlined above.

The predicted hold time at 85% of the enclosure’s elevation according to the 2008 edition of NFPA 2001 is given in the final column of Table A.2⁵. It was desired that the tests conducted span a range of hold time values adequately representing typical system installations. For the 3 to 46.3 min range of leakage configurations tested the mean predicted hold time is 11.9 min with a median value of 9.7 min. This covers the research team’s interest within the range of roughly 5 to 20 minute hold times.

A.3 Instrumentation & Environmental Variables

The test bed is housed in a larger warehouse of semi-controlled environment⁶. Ambient conditions are partially controlled and detailed upon in the following. Additionally, the types and amount of instrumentation provided throughout the test list are enumerated.

Because air conditioning is not provided to the facility the ambient temperature is uncontrollable. Table A.3 lists the approximate temperature inside the test enclosure prior to agent discharge in the sixth column. Additionally, the test date and time are given in Table A.3. When multiple temperature probes are provided, the reported value is a mean value of all data sources. Missing values indicate the absence of data sources.

For all non inert gas experiments the relative humidity is controlled. Prior to test execution a measurement of the relative humidity is taken and recorded in the fifth column of Table A.3. The ambient humidity level is understood to significantly affect ambient pressure fluctuations observed during the period of agent discharge. Efforts to dry the test bed environment aimed to drop the relative humidity below 40%. Controlling this environmental property is of great importance for the purpose of analyzing peak pressure fluctuations; however, it is not known to significantly affect the agent draining phenomena.

⁵The hold time prediction is evaluated at 15% of maximum enclosure height for IG-100 tests. This is due to them having gas phase densities lesser than regular atmospheric air; and thus, IT-100 is expected to drain out through upper leakage pathways.

⁶The primary purpose of the surrounding structure is to remove the influence of external wind pressures. When these dynamic wind-generated bias pressures are of significant magnitude the subject hold time models’ grounding assumptions are fully nullified and the models lose all applicability.

Table A.3: Environmental parameters & data sources retained

Test Number	Chronological Test Number	Date	Time (C.S.T.)	Relative Humidity	Mean Pre-Test Temperature	Number of Retained Data Traces by Instrument Type for Each Test ID						
				(%)	(°C)	Noz	# PT	# TC	# O2	# Tr	# Pr	# Tp
1	1	10/21/2005	-	-	24	X	1	1	-	3	-	-
2	2	11/9/2005	-	32.0	23	X	1	1	-	3	-	-
3	3	11/10/2005	-	28.0	-	X	1	-	-	3	-	-
4	4	11/22/2005	-	27.0	-	X	-	-	-	-	-	-
5	5	11/23/2005	-	27.0	-	X	1	-	-	2	-	-
6	6	8/28/2006	3:56:49 PM	36.0	-	X	0.5	-	-	4	-	3
7	7	8/29/2006	10:55:55 AM	36.0	23	X	0.5	1	-	5	3	-
8	8	8/29/2006	-	36.0	25	X	0.5	1	-	4	1	3
9	9	8/29/2006	-	36.0	24	X	0.5	1	-	-	1	2
10	10	8/30/2006	12:25:56 PM	36.0	24	X	0.5	1	-	4	1	3
11	11	8/30/2006	5:33:53 PM	N/A	24	X	0.5	1	5	-	-	-
12	12	8/30/2006	7:54:07 PM	N/A	-	X	0.5	-	5	-	-	-
13	13	8/31/2006	10:30:45 AM	N/A	20	X	0.5	1	2	-	-	-
14	14	8/31/2006	12:39:22 PM	N/A	21	X	0.5	1	5	-	-	-
15	15	8/31/2006	3:45:44 PM	N/A	22	X	0.5	1	5	-	-	-
16	16	9/26/2006	12:43:52 PM	38.0	-	X	2.5	-	-	2	3	2
17	17	9/26/2006	3:08:38 PM	38.0	27	X	4.5	1	-	2	3	2
18	18	9/27/2006	9:40:03 AM	38.0	23	X	4.5	1	-	2	3	2
19	19	9/27/2006	1:16:27 PM	38.0	-	X	4.5	-	-	2	3	2
20	20	9/27/2006	3:37:59 PM	38.0	-	X	4.5	-	-	2	3	2
21	33	7/12/2007	9:32:01 AM	39.5	25	X	5	4	2	3	5	5
22	28	7/11/2007	10:15:57 AM	38.0	25	X	5	4	2	3	5	5
23	29	7/11/2007	11:54:47 AM	38.0	26	X	5	3	2	3	5	5
24	31	7/11/2007	4:13:18 PM	26.5	28	X	5	4	-	-	-	-
25	30	7/11/2007	2:42:12 PM	38.0	26	X	5	4	-	-	-	-
26	32	7/11/2007	5:30:55 PM	87.0	25	X	5	4	-	-	-	-
27	27	7/11/2007	9:08:00 AM	38.0	25	-	4	4	-	-	-	-
28	23	7/10/2007	11:23:21 AM	38.0	28	X	2.5	4	-	3	5	4
29	26	7/10/2007	5:34:47 PM	38.0	29	X	5	3	2	3	5	5
30	24	7/10/2007	1:04:22 PM	38.0	28	-	3	3	2	3	5	5
31	25	7/10/2007	4:00:29 PM	38.0	29	X	5	3	2	3	5	5
32	39	7/12/2007	6:44:06 PM	N/A	29	X	5	4	7	-	-	-
33	40	7/12/2007	7:16:26 PM	N/A	28	X	4.5	4	-	-	-	-
34	41	7/13/2007	9:07:01 AM	N/A	26	X	4.5	4	7	-	-	-
35	21	7/9/2007	3:30:01 PM	N/A	31	-	4.5	4	6	-	-	-
36	44	7/13/2007	3:52:15 PM	N/A	28	X	3	4	7	-	-	-
37	22	7/9/2007	5:18:46 PM	N/A	29	X	4.5	4	-	-	-	-
38	42	7/13/2007	10:25:37 AM	N/A	26	X	5	4	6	-	-	-
39	37	7/12/2007	2:20:52 PM	N/A	26	X	5	4	-	-	-	-
40	43	7/13/2007	1:40:00 PM	N/A	28	X	3	4	7	-	-	-
41	36	7/12/2007	1:59:55 PM	N/A	26	X	5	4	-	-	-	-
42	38	7/12/2007	4:39:37 PM	N/A	29	X	5	4	7	-	-	-
43	35	7/12/2007	11:47:44 AM	N/A	25	X	5	4	7	-	-	-
44	34	7/12/2007	11:07:26 AM	N/A	25	-	4	4	-	-	-	-

The amount and type of instrumentation available for each test varies from the prototypical work of 2005 through the two additional test campaigns. After test completion the output from any given measurement source is inspected. Usually due to complete instrument failure or evidence of instrument malfunction, some collected data traces are discarded. This further results in a variable amount of retained data sources available for analysis for any given test⁷. Table A.3 lists the amount of data sources retained for each family of instrument types in columns 7 through 13.

The seventh column of Table A.3 reports whether enough data was obtained from the pressure transducer located just upstream of the nozzle in the pipe delivery network to document the discharge time. This data source is also used to troubleshoot clean agent delivery issues and additionally to observe the duration of agent discharge.

The number of ambient pressure transducers operated is provided in the eighth column. Two types of transducers are used; (1) needle-indicating, diaphragm-type, Magnehelic transducers, and (2) micro-diaphragm, logging digital manometers from Retrotec. The prior (1) is operated throughout agent discharge to monitor peak pressure fluctuations. One positive and one negative Magnehelic transducer in the span of 0 to ± 2750 gage Pa (11 in H₂O) are used. The latter variety (2) is precise to the one fourth of a Pascal in the range of ± 1200 Pa and is operated throughout agent draining to monitor the hydrostatic pressure profile (in elevation). The reported number of pressure transducer data sources is a sum of the number of Retrotec probes recorded in addition to a one half credit for each Magnehelic data source retained.

Column 9 reports the number of temperature data sources retained. A single probe is typically installed at one fourth room elevation in the center of the planar view. Tests conducted in 2007 utilize up to 4 thermocouple probes; installed at one half room elevation, at upper and lower leak elevations, and halfway through an open leakage at the upper elevation.

Table A.3 documents the number of recorded gas sampling data sources in columns 10 through 13. The first of these is for oxygen analyzers. These were all manufactured by Nova and include the 320, 320 S-3, and 314LBT models. Multiple 2007 tests use these for both inert gas and chemical suppressant types. Clean agent volume concentrations are expressed using an

⁷The degree to which any given agent type or individual test can be analyzed is a direct function of the number of data sources available for experimental observation.

oxygen reduction correlation. Columns 11 through 13 give the number of retained data sources from Tuure, Perco, and Tripoint instruments, respectively. These instruments offer up to three sampling channels per unit and operate on nearly the same internal hardware and design. Each brand indicates a separate generation of manufacturing spanning from the 1970's into the present and is listed in chronological manufacturing order. These devices were modified to output an electrical signal directly to a passive data acquisition interface rather than to print out on strip chart recorders. In this manner all scaling from millivolt output to engineering units was performed computer-side rather than by using the instruments calibration controls.

Appendix B

Hold Time Model Derivation

In the following of this appendix, stratifying-type, hold time models are derived in long-hand and rendered in dimensionless form. These include the *sharp descending interface* model of NFPA 2001, the *wide descending interface* model of ISO 14520, and the thick descending interface model, developed herein. Each of the models is based upon a hydrostatically-driven agent draining theory, which is implemented in each using identical theoretical assumptions. The models diverge from one another only in the assumption taken for the agent concentration distribution; modeled only as a function of elevation.

All three stratifying-type models assume that as agent drains from the enclosure, an equal volume of makeup air enters; replacing the former. In the case of the sharp interface theory, the fresh air is assumed to not mix with the agent-air mixture originally filling the enclosure's volume; creating an infinitesimally thin interface that translates through elevation with time. The wide interface theory assumes that a mixing region or interface forms between inflowing fresh air and the agent mixture. The wide interface has zero width initially, and eventually grows to span the enclosure's entire height. The interface is modeled as a linear relationship between concentration and elevation. The thick interface theory models the growth in interface thickness identically to the wide interface theory. At some point in time, the interface ceases to gain width; after which it remains at a maximum thickness as it continues to translate through elevation.

The thick interface theory necessitates an additional input parameter, ω , or the characteristic interface slope. In this study, the value of ω is obtained using experimental data from 34 tests utilizing 7 different clean extinguishing

agents.

As will be seen, the central governing theory can be derived independently of the assumed concentration distribution profile, which is then implemented as a final step by modifying the integration limit for which the governing equation is evaluated.

B.1 Physical Phenomena & The Agent Distribution Profile

Total flooding fire suppression systems deluge a protected envelope (‘enclosure’) with an extinguishing agent of sufficient quantity to ensure that sustained combustion cannot be supported. The clean extinguishing agent (‘agent’) is expected to disburse throughout the enclosure; protecting the entire volume. With the exception of pure nitrogen, all agents available on today’s market have vapor densities greater than that of atmospheric air (and thus, an agent that is heavier-than-air is assumed throughout save for the final equation presentations). The difference in gas densities between the agent and air mixture within the protected enclosure and that of regular atmospheric air surrounding this envelope provides the driving force of agent draining. If penetrations (‘leakages’) exist through the barriers of the enclosure, this buoyancy-generated force predictably drives agent out lower leakages and allows fresh air to flow in through upper leakages (and inversely for the case of lighter-than-air agents). The force driving agent draining will decay as the amount of agent remaining within the protected enclosure decays.

The objective of any considered agent draining model is to determine the time duration required for the agent concentration to decay to a specified threshold at a specified elevation threshold. This measure is hereafter referred to as the *hold time*. Thus, it is clear that the stipulation of these two thresholds necessitates a knowledge of where the agent accumulates within the enclosure. This necessity provides a differentiating and titular basis for the three analytical models considered in this study. Each assumes a unique relationship between agent concentration and elevation; hereafter referred to as the *agent distribution profile*. Figures B.1, B.2 and B.3 respectively provide the resulting hydrostatic pressure profile schematics for the sharp, wide, and thick agent distribution profile assumptions. The assumed knowledge of

the agent distribution profile allows for evaluation of the hold time or when a set concentration threshold is experienced at a set elevation threshold.

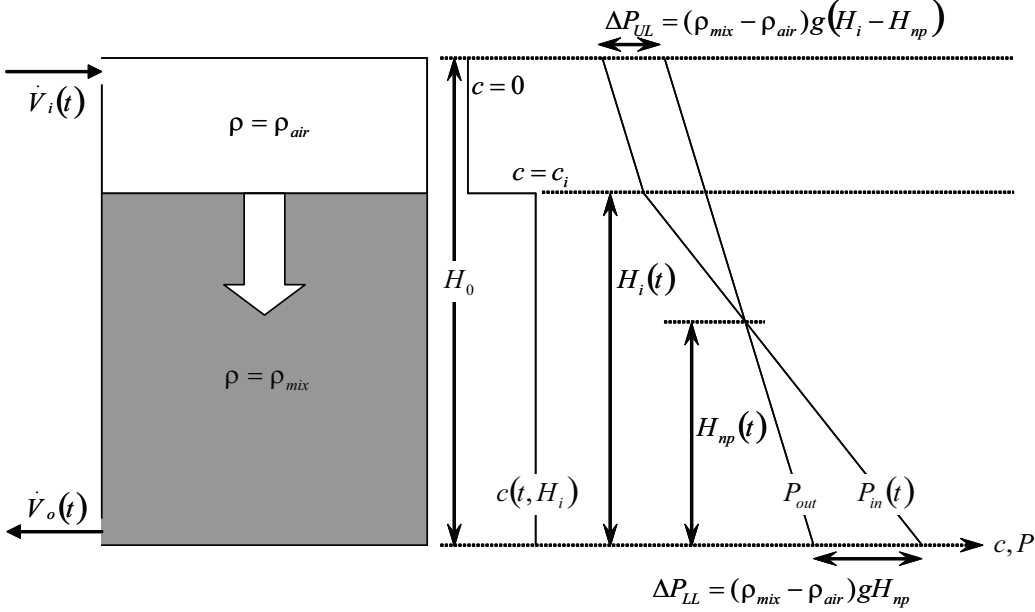


Figure B.1: Sharp interface hydrostatic pressure profile schematic

The *sharp* interface assumption is denoted by the neglect of gas species diffusion. As shown in Figure B.1, it results in an infinitesimally thin interface between the draining agent-air mixture region and the inflowing layer of fresh air. Agent concentration and ambient pressure share the x-axis in Figure B.1. Agent concentration is seen to exist at the initial concentration, c_i , from the floor's elevation up to the height of the interface, H_i . Above this elevation the volumetric agent concentration is equal to zero. The ambient pressure of air *outside* the enclosure, P_{out} , is linear in elevation and represents the weight of atmospheric air. The pressure *inside* the enclosure, P_{in} , is shown as a piecewise function that changes behavior at the elevation of the interface, H_i .

The *wide* interface assumption presumes that the agent-air mixture combines instantaneously with inflowing fresh air in known proportions. In essence, one half of the inflowing fresh air mixes with the top of the column of the agent-air mixture while the second half of inflowing fresh air

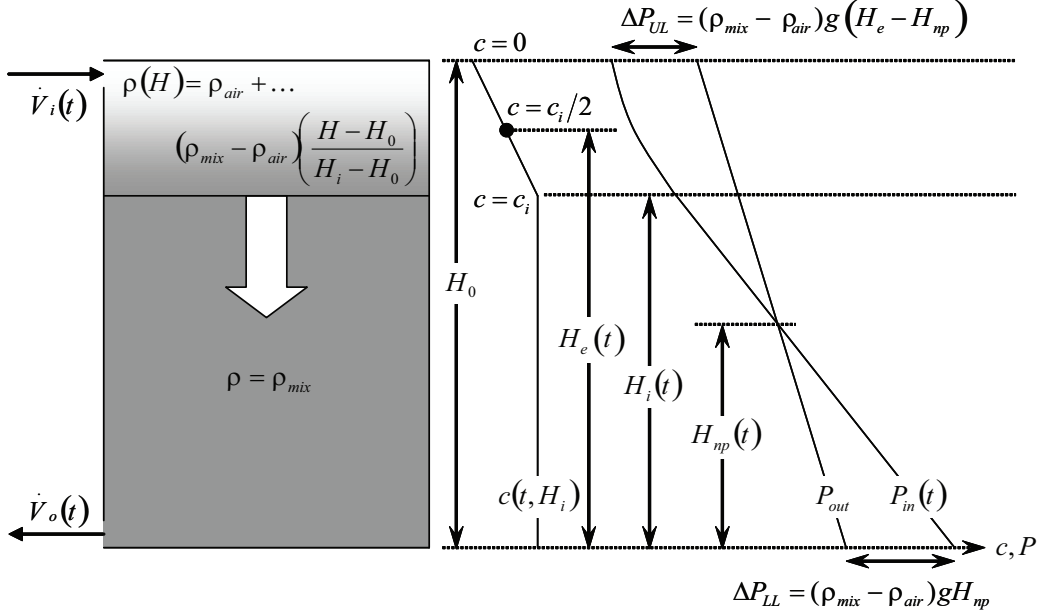


Figure B.2: Wide interface hydrostatic pressure profile schematic

remains, as such, above the agent-air mixture column. Figure B.2 depicts this assumption as resulting in a linear decay of concentration from the leading edge of the interface, H_i , to the maximum enclosure elevation, H_0 . The resulting ambient pressure inside the enclosure, P_{in} , is shown.

As is seen in Figure B.3 the *thick* interface assumption assumes that a linear change from full to nil concentration exists across a finite elevation range (from the leading interface edge, H_2 , to the trailing edge, H_1). This interface is defined by a maximum *characteristic thickness*, which is generally assumed to be a constant in time. Naturally, at time zero this thickness ($H_1 - H_2$) does not yet exist when the enclosure volume is flooded with a given agent concentration. As such, the thickness is expected to develop from nil thickness to the characteristic thickness in the same manner that the wide interface forms. Once the characteristic (maximum) thickness is developed, inflowing air is no longer assumed to mix with the agent-air mixture. Rather, the interface, as a constant construct, is assumed to descend through the enclosure's elevation. Again, the resulting ambient pressure inside the enclosure, P_{in} , is given.

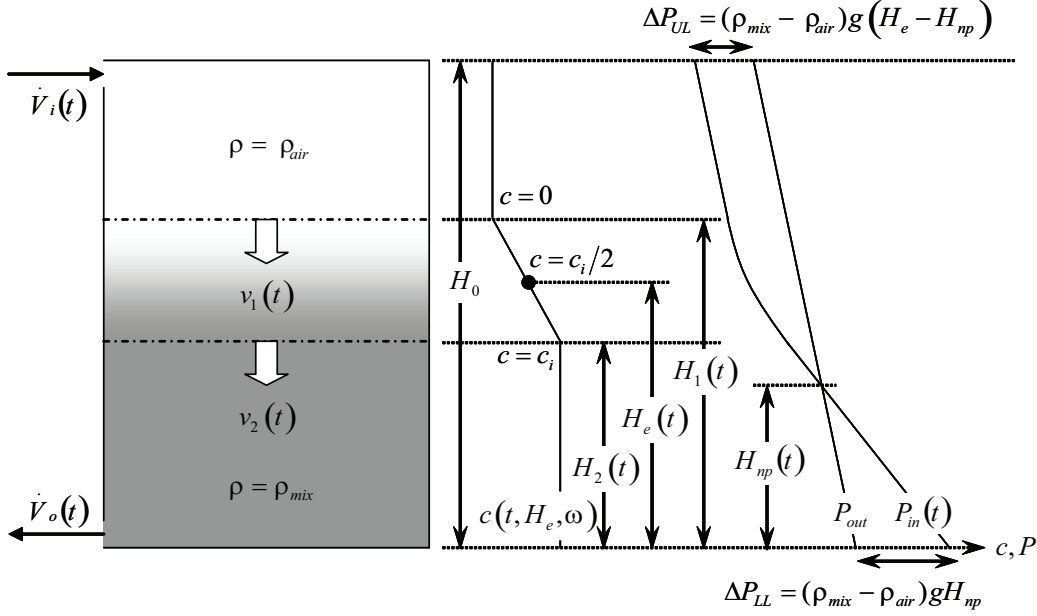


Figure B.3: Thick interface hydrostatic pressure profile schematic

As previously introduced, the difference in vapor densities between the agent-air mixture inside the design enclosure relative to that of the fresh atmospheric air surrounding this envelope provides the buoyancy-generated force driving agent draining through enclosure leakages. The magnitude of the induced pressure differential across the enclosure boundary at the upper and lower extremes of elevation is central to the model derivation and can be formulated through inspection of Figures B.1, B.2 and B.3. Additionally, each of three figures gives the magnitude of these pressure differentials, which is found to primarily be a function of the neutral plane height, H_{np} (the elevation at which ambient pressures inside and outside the enclosure are equal).

B.2 The Equivalent Height - Part I

The *equivalent height*, H_e , constitutes the elevation at which the hold time is evaluated in the analytical models. In the case of the sharp descending interface theory, the model is always evaluated at the interface height. For

the purposes of this derivation and consistency in terms, the sharp interface height shall be set equal to the equivalent height,

$$H_e = H_i. \quad (\text{B.1})$$

Ultimately, as is presented in Section B.9, the equivalent height is used to interpret between a set of hold time performance criteria (modeled concentration decay threshold, elevation threshold, and characteristic interface slope) and the elevation at which the model must be evaluated. It represents the elevation at which the sharp interface would equally represent the wide or thick interface in terms of total agent mass at any given time. As shown in Figures B.2 and B.3 the decay from full to nil concentration in the wide and thick models is always linear in elevation. Thus, the integral of this relationship will always result in the equivalent height being the elevation at one half the distance between the starting and ending elevations of concentration change. For the wide interface theory the equivalent height is always equal to

$$H_e = \frac{H_0 + H_i}{2}. \quad (\text{B.2})$$

Similiarly, this is given as,

$$H_e = \frac{H_1 + H_2}{2}, \quad (\text{B.3})$$

with regard to the thick descending interface model.

B.3 Summarized Theoretical Assumptions

A series of simplifying assumptions are employed in the hold time model derivations to provide for simple analytical solutions for use in the field. They are presented in the following list and will be referred to throughout the remainder of this appendix.

- As an initial condition, the event of agent discharge results in a homogeneous mixture of agent and air throughout the protected enclosure's volume.

- As an initial condition, the homogeneous mixture of agent and air is at thermal equilibrium with the atmospheric air surrounding the enclosure. No thermal sources or sinks are considered and all gases are assumed to exist at standard temperature and pressure (disregarding hydrostatic pressure variations).
- Each stratifying-type model considered assumes a specific agent distribution profile as a function of time (previously introduced in Section B.1). This is analogous to each model assuming a defined behavior of species gas diffusion, which is never governed by first principles.
- Leakages (penetrations) through enclosure boundaries are assumed to exist only in two locations; at the extremes of elevation, upper and lower.
- Gas flow through each (upper and lower) leakage is modeled according to the theory proposed by the ‘door fan enclosure integrity test.’ This generally assumes that each orifice can be modeled as an ideal, sharp-edged, circular orifice with a discharge coefficient of 0.61. Streamline flow is not always assumed as the volumetric gas flow is not always proportional to the square root of the pressure differential across the orifice.
- The protected enclosure is assumed to have a planar cross section of constant area through the enclosure’s height (structures of more complex geometry including sloped ceilings and variable planar areas in height are easily modeled but not dealt with herein).

B.4 Conservation of Mass - The General Solution Form

Model derivation begins with a conservation of mass equation, which will be shown to result in the general solution form. Only the mass of the agent-air mixture remaining within the enclosure need be conserved to yield the desired solution form.

Using a control volume analysis, the rate of change of the agent-air mixture mass inside the enclosure can be set equal to the rate at which the

agent-air mix passes through the control volume boundaries. As such we have

$$\frac{\partial}{\partial t} m_{mix} = \dot{m}_{mix,in} - \dot{m}_{mix,out}. \quad (\text{B.4})$$

At time zero the maximum amount of agent is present. As time progresses, agent is assumed to only drain from the enclosure. This implies that the agent-air mixture obeys both,

$$\dot{m}_{mix,in} = 0, \quad (\text{B.5})$$

and,

$$\dot{m}_{mix,out} = \rho_{mix} \dot{V}_o. \quad (\text{B.6})$$

Through substitution, Equation (B.4) is reformulated as,

$$\frac{\partial}{\partial t} m_{mix} = -\rho_{mix} \dot{V}_o. \quad (\text{B.7})$$

The volume rate of agent outflow, \dot{V}_o , must be related to the interface equivalent height, H_e . This can be established through inspection of the total mass of agent-air mixture inside the enclosure at any given time,

$$m_{mix} = \rho_{mix} A_F H_e. \quad (\text{B.8})$$

The time derivative of Equation (B.8) is,

$$\frac{\partial}{\partial t} m_{mix} = \rho_{mix} A_F \frac{\partial H_e}{\partial t}. \quad (\text{B.9})$$

Substitution of Equation (B.9) into Equation (B.7) results in,

$$\rho_{mix} A_F \frac{\partial H_e}{\partial t} = -\rho_{mix} \dot{V}_o, \quad (\text{B.10})$$

which can be rearranged into,

$$\frac{\partial H_e}{\partial t} = -\frac{\dot{V}_o}{A_F}, \quad (\text{B.11})$$

to yield the general solution form.

The above conserves only the mass of agent-air mixture. A very similar result,

$$\frac{\partial H_e}{\partial t} = -\frac{\dot{V}_i}{A_F}, \quad (\text{B.12})$$

is obtained when the exercise is repeated; conserving only the mass of fresh atmospheric air. By combining Equations (B.11) and (B.12) it is found that

$$\dot{V}_o = \dot{V}_i. \quad (\text{B.13})$$

This finding is made of use in the following section.

B.5 Orifice Flow & The Door Fan Enclosure Integrity Test

The door fan enclosure integrity test is used to measure the total, summed area of enclosure leakages (penetrations) in existing structures. The procedure begins with mounting a fan in any, typically sealed, orifice to the design enclosure (generally a window or door). The fan(s) is then operated at a series of volumetric flows and for each the generated pressure differential across enclosure boundaries is measured; resulting in a set of paired volumetric flows and pressure differentials $\{\dot{V}, \Delta P\}$. This, effectively, is the data pool generated by the door fan integrity test.

The paired series of flows and pressure differentials is then regressed as a power law function to the form

$$\dot{V} = k_1 \Delta P^n. \quad (\text{B.14})$$

The classical orifice flow equation,

$$\dot{V} = A_T C_d C_U \sqrt{\frac{2\Delta P}{\rho}}, \quad (\text{B.15})$$

is similar in form but differs in that the volumetric gas flow is always proportional to the square root of the pressure differential across the orifice. In order to allow for more direct modeling of the dynamic relationship exhibited between the experienced volumetric flow induced by various pressure differentials, Equation (B.14) provides an empirical measure of the orifice flow exponent, n .

The regressed orifice flow coefficient, k_1 , is actually a lumped parameter; combining all the constants of Equation (B.15) together. This primarily includes the total cross sectional area of the orifice, A_T , the orifice's coefficient of discharge, C_d , and a unit conversion term, C_U . Further meaning can be given to the orifice flow coefficient by noting the relation,

$$k_1 = A_T C_d C_U \left(\frac{2}{\rho} \right)^n. \quad (\text{B.16})$$

To relate the parameter, k_1 , found from the door fan integrity test to the the *equivalent leakage area*, A_{eq} , or the actual leak area available for gas flow, the parameter k_2 is introduced as

$$k_2 = \frac{k_1}{C_U} \left(\frac{\rho_{air}}{2} \right)^n; \quad (\text{B.17})$$

where $k_2 = A_{eq} = A_T C_d$. The subscript 'air' is given to the density term as it is assumed to be the gas species flowing through the orifice during the door fan test procedure.

B.6 Development of the Governing Equation

As is shown by Equation (B.11) the rate of descent of the equivalent interface height is the negative rate of agent outflow, \dot{V}_o , divided by the area of the enclosure floor, A_F . Being that the floor area is a known constant, only the rate of agent-air mixture outflow must be solved for.

The quantity, \dot{V}_o , can be found by beginning with a substitution of Equation (B.15) into Equation (B.13) for each of the inward and outward flows through enclosure boundaries (assumed to exist at the upper and lower of elevation extremes, respectively). Assuming the the upper and lower orifice flows are equally characterized results in cancellation of the unit conversion term, C_U ($C_{U,i} = C_{U,o}$), the discharge coefficient, C_d ($C_{d,i} = C_{d,o}$), and the orifice flow exponent, n ($n_i = n_o$). The parameter 2^n can also be canceled to yield

$$A_i \left(\frac{\Delta P_i}{\rho_i} \right)^n = A_o \left(\frac{\Delta P_o}{\rho_o} \right)^n, \quad (\text{B.18})$$

where the subscripts 'i' and 'o' designate the orifices of inward and outward flow, respectively. Rearranging for the pressure differential across the orifice

of gas inflow gives

$$\Delta P_i = \left(\frac{\rho_i}{\rho_o} \right) \left(\frac{A_o}{A_i} \right)^{\frac{1}{n}} \Delta P_o. \quad (\text{B.19})$$

A second formulation relating the upper and lower pressure differentials can be achieved by revisiting Figures B.1, B.2 and B.3. Each gives a formulation for the pressure differential across the enclosure boundary at the upper and lower elevation extremes, which are functions of the neutral plane height, H_{np} . These are repeated here as,

$$\Delta P_i = (\rho_{mix} - \rho_{air}) g (H_e - H_{np}), \quad (\text{B.20})$$

and,

$$\Delta P_o = (\rho_{mix} - \rho_{air}) g H_{np}, \quad (\text{B.21})$$

which are identical for all three considered theories when the definition of the equivalent interface height is applied to the sharp interface theory ($H_i = H_e$). Summation of Equations (B.20) and (B.21) results in

$$\Delta P_i + \Delta P_o = (\rho_{mix} - \rho_{air}) g H_e. \quad (\text{B.22})$$

For further clarity it can be assumed that fresh air flows through the inlet orifice ($\rho_i = \rho_{air}$) and that the agent-air mixture flows through the outlet orifice ($\rho_o = \rho_{mix}$). Equation (B.19) can be combined with Equation (B.22) and solved for the pressure differential across the orifice of outlet flow to yield

$$\Delta P_o = \frac{(\rho_{mix} - \rho_{air}) g H_e}{1 + \left(\frac{\rho_{air}}{\rho_{mix}} \right) \left(\frac{A_o}{A_i} \right)^{\frac{1}{n}}}. \quad (\text{B.23})$$

Substitution of Equation (B.23) into the classical orifice flow equation, Equation (B.15), with the flow exponent now set equal the empirical value, n , (instead of a value of 0.5) gives

$$\dot{V}_o = A_o C_d C_U \left\{ \left(\frac{2}{\rho_{mix}} \right) \left[\frac{(\rho_{mix} - \rho_{air}) g H_e}{1 + \left(\frac{\rho_{air}}{\rho_{mix}} \right) \left(\frac{A_o}{A_i} \right)^{\frac{1}{n}}} \right] \right\}^n; \quad (\text{B.24})$$

or a final formulation for the volumetric rate of gas outflow.

Substituting this into the general solution form, Equation (B.11), yields,

$$\frac{\partial H_e}{\partial t} = -\frac{A_o C_d C_U}{A_F} \left[\frac{2 \left(1 - \frac{\rho_{air}}{\rho_{mix}} \right) g H_e}{1 + \left(\frac{\rho_{air}}{\rho_{mix}} \right) \left(\frac{A_o}{A_i} \right)^{\frac{1}{n}}} \right]^n; \quad (\text{B.25})$$

a final governing equation in differential form.

Integration limits are defined for time, t , ranging from time zero, t_0 , to the time of the hold time, t_f . Through this time delta the interface is expected to descend from the maximum enclosure height, H_0 , to the set threshold of the equivalent height, H_e . Implemented as stated,

$$\int_{t_0}^{t_f} dt = - \int_{H_0}^{H_e} \frac{A_F}{A_o C_d C_U} \left[\frac{1 + \left(\frac{\rho_{air}}{\rho_{mix}} \right) \left(\frac{A_o}{A_i} \right)^{\frac{1}{n}}}{2 \left(1 - \frac{\rho_{air}}{\rho_{mix}} \right) g} \right]^n H_e^{-n} dH_e, \quad (\text{B.26})$$

results in the final governing equation,

$$t_f - t_0 = -\frac{A_F}{A_o C_d C_U (1 - n)} \left[\frac{1 + \left(\frac{\rho_{air}}{\rho_{mix}} \right) \left(\frac{A_o}{A_i} \right)^{\frac{1}{n}}}{2 \left(1 - \frac{\rho_{air}}{\rho_{mix}} \right) g} \right]^n (H_e^{1-n} - H_0^{1-n}), \quad (\text{B.27})$$

after integration.

In the case of clean extinguishing agents with vapor densities lesser than that of atmospheric air (such as pure nitrogen, given by the ASHRAE designation, IG-100) the model form varies slightly due to the agents bouyant tendency to drain out of upper leakages. Using the same definitions of the associated input parameters for the condition where $\rho_{mix} < \rho_{air}$ results in a final governing equation of the form,

$$t_f - t_0 = -\frac{A_F}{A_o C_d C_U (1 - n)} \left[\frac{1 + \left(\frac{\rho_{air}}{\rho_{mix}} \right) \left(\frac{A_o}{A_i} \right)^{\frac{1}{n}}}{2 \left(\frac{\rho_{air}}{\rho_{mix}} - 1 \right) g} \right]^n [(H_0 - H_e)^{1-n} - H_0^{1-n}], \quad (\text{B.28})$$

B.7 The Dimensionless Governing Equation¹

To provide for proper analysis of an experimental data set where the control variables are not always constant requires the use of nondimensional analysis. To render the governing equations, given as Equations (B.27) and (B.28), dimensionless, a *characteristic drain time*,

$$t_c = \frac{V_0}{\dot{V}_c}, \quad (\text{B.29})$$

is introduced as the ratio of the total volume enclosure, V_0 , to the *characteristic drain rate*,

$$\dot{V}_c = A_o C_d C_U \left[\left(\frac{2}{\rho_{mix}} \right) \left(\frac{\rho_{mix} g H_0}{2} \right) \right]^n,$$

which simplifies to,

$$\dot{V}_c = A_o C_d C_U (g H_0)^n. \quad (\text{B.30})$$

The characteristic drain rate, \dot{V}_c , represents a hypothesized, maximum agent draining rate. The form of Equation (B.30) assumes that when unrestricted the total hydrostatic pressure induced by a room completely flooded by a given agent-air concentration, $(\rho_{mix} g H_0)$, acts in half to drive agent outwards and in half to pull fresh air inwards².

Division of the actual hold time, $t_f - t_0$ by the characteristic drain time, t_c , yields a dimensionless time term³,

$$\tilde{t} = \frac{t_f - t_0}{t_c}. \quad (\text{B.31})$$

The characteristic drain time of Equation (B.29) can be reformulated through substitution of the characteristic drain rate, Equation (B.30), and the enclosure volume, V_0 , when given as $A_F H_0$, to yield,

¹The dimensional analysis presented herein is extended from the form proposed by Mower, et. al. (as applied to the hold time model espoused in the 2004 edition of NFPA 2001.)

²The stated hydrostatic pressure is not accurate in that it is really a function of the difference between the pressures existing inside and outside of the enclosure. The actual maximum theoretical differential pressure driving agent draining is then, $(|\rho_{mix} - \rho_{air}| g H_0)$, which would act in part to push agent out and in part to pull fresh air inwards.

³Due to the chosen form of the characteristic drain rate, \dot{V}_c , the value of the dimensionless time parameter, \tilde{t} , does not range from 0 to 1 as might be expected.

$$t_c = \frac{A_F H_0^{1-n}}{A_o C_d C_U g^n}. \quad (\text{B.32})$$

By way of the dimensionless time parameter, Equation (B.31), the characteristic drain time, Equation (B.32), can be substituted into the governing equation, Equation (B.27). After canceling terms and rearranging a modified form is obtained,

$$\tilde{t} = \frac{1}{(1-n)} \left[\frac{1 + \left(\frac{\rho_{air}}{\rho_{mix}} \right) \left(\frac{A_o}{A_i} \right)^{\frac{1}{n}}}{2 \left(1 - \frac{\rho_{air}}{\rho_{mix}} \right)} \right]^n \left[1 - \left(\frac{H_e}{H_0} \right)^{1-n} \right], \quad (\text{B.33})$$

The proximity of similar terms provides a convenient means of introducing additional dimensionless parameters. Meaningful analysis can be achieved through investigation of these parameters' sensitivity to and relationship with other model variables. These include a dimensionless density term,

$$\tilde{\rho} = \frac{\rho_{mix}}{\rho_{air}}, \quad (\text{B.34})$$

a dimensionless interface elevation,

$$\tilde{H} = \frac{H_e}{H_0}, \quad (\text{B.35})$$

and a dimensionless leakage area split term (between lower and upper leakages),

$$\tilde{F} = \frac{A_o}{A_i}. \quad (\text{B.36})$$

The *lower leakage fraction* (LLF),

$$F = \frac{A_{LL}}{A_{LL} + A_{UL}}, \quad (\text{B.37})$$

is formulated in Chapters 2 and 3 and is a direct result of assumption (4) in Section B.3⁴. Because $A_T = A_o + A_i$, the LLF is related to the dimensionless leakage area split by the progression

⁴Where the subscripts *LL* and *UL* stand for lower leakage and upper leakage, respectively.

$$\tilde{F} \Rightarrow \frac{F A_T}{(1-F) A_T} \Rightarrow \frac{F}{(1-F)}. \quad (\text{B.38})$$

Further implementation of the dimensionless terms given as Equations (B.34), (B.35) and (B.38) into Equation (B.33) results in a final nondimensional governing equation of the form,

$$\tilde{H} = (1 - \beta_1 \tilde{t})^{\frac{1}{1-n}}, \quad (\text{B.39})$$

where,

$$\beta_1 = (1-n) \left[\frac{2(1 - \tilde{\rho}^{-1})}{1 + \tilde{\rho}^{-1} \tilde{F}^{\frac{1}{n}}} \right]^n. \quad (\text{B.40})$$

The governing equation for lighter-than-air agent types, Equation (B.28), can be rendered dimensionless accordingly. For the condition where $\rho_{mix} < \rho_{air}$, the final nondimensional form is given as,

$$\tilde{H} = 1 - (1 - \beta_2 \tilde{t})^{\frac{1}{1-n}}, \quad (\text{B.41})$$

where,

$$\beta_2 = (1-n) \left[\frac{2(\tilde{\rho}^{-1} - 1)}{1 + \tilde{\rho}^{-1} \tilde{F}^{\frac{1}{n}}} \right]^n. \quad (\text{B.42})$$

The influence of the orifice flow exponent, n , should be noted as it alone depicts the difference between the 2004 and 2008 publications of the sharp descending interface theory of NFPA 2001. Figures B.4 & B.5 demonstrate the relationship between the dimensionless interface elevation, \tilde{H} , and the combined quantity, βt , when the orifice flow exponent, n , is variable.

It can be seen that as the value of n approaches 1, when the hold time is evaluated for any given elevation, the hold time tends towards a zero value (agent drains instantaneously when n equals 1). Classically, the value of n always equals 0.5 (NFPA 2001, 2004 edition and prior). A variable value of the orifice flow exponent, as measured during the door fan enclosure integrity test, allows for more accurate leakage modeling of real-world enclosures. Let it be borne in mind that due to the highly influential nature of n as an input parameter, its value should never be assumed in the absence of a calibrated, multi-point, enclosure integrity test.

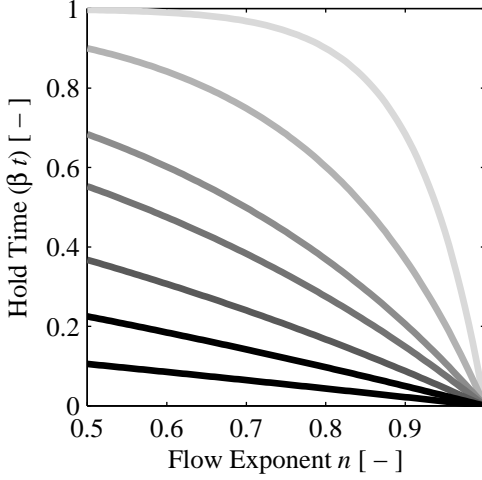


Figure B.4: Dimensionless hold time versus the flow exponent, n , for set values of the dimensionless interface height, \tilde{H} (value ranges from 0.8 to 0.5 as the shade lightens).

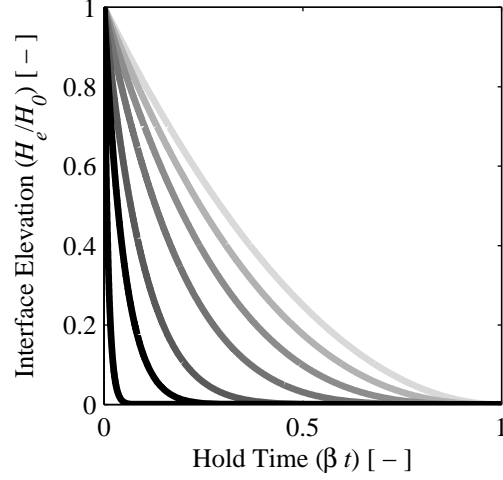


Figure B.5: Dimensionless interface centroid elevation, \tilde{H} , versus the dimensionless hold time, βt , for set values of n (value ranges from 0.5 to 0.99 as the shade darkens).

B.8 Rendering a Hold Time Dimensionless

Figures B.4 and B.5 show that the combined value, $\beta\tilde{t}$, ranges from 0 to 1. Plotting experimental hold time data for graphical analysis is made possible by computing the value of $\beta\tilde{t}$.

The experimental hold time, $t_f - t_0$, can be related to the combined parameter, $\beta\tilde{t}$. The dimensionless time term, Equation (B.31), through substitution of the characteristic time, Equation (B.32), can be formulated. When the value of β , given as Equation (B.40), is made a multiplicative coefficient of the dimensionless time, \tilde{t} , the result obtained is,

$$\beta_1 \tilde{t} = (1 - n) \left[\frac{2(1 - \tilde{\rho}^{-1})}{1 + \tilde{\rho}^{-1} \tilde{F}^{\frac{1}{n}}} \right]^n \left[\frac{A_o C_d (g H_0)^n}{A_F H_0} \right] (t_f - t_0). \quad (\text{B.43})$$

Thus, the experimental hold time ($t_f - t_0$) should be multiplied by the parameter,

$$(1 - n) \left[\frac{2(1 - \tilde{\rho}^{-1})}{1 + \tilde{\rho}^{-1} \tilde{F}_n^{\frac{1}{n}}} \right]^n \left[\frac{A_o C_d (gH_0)^n}{A_F H_0} \right], \quad (\text{B.44})$$

to obtain a dimensionless time quantity, $\beta \tilde{t}$, which ranges between a value of zero and one. This procedure essentially provides scaling of experimentally obtained hold time values by taking consideration for the effects of enclosure geometry, agent type, and leakage flow characteristics.

In the most recent editions of NFPA 2001 and ISO 14520 the value of the lower or upper leakage (A_o or A_i) is rarely calculated as a matter of routine. Rather, the fan data is regressed into the parameter k_1 and n , and a value of the lower leakage fraction, F , is either estimated as 0.5 or measured. For the ease of calculation, the leakage area term can be replaced by relating k_1 and F directly into Equation (B.44).

The value of $A_o C_D$ is alternatively formulated through use of Equations (B.16), (B.17), (B.37) and the given relationships, $k_2 = A_{eq} = A_T C_d$, and, $A_T = A_o + A_i$. In this manner, both A_o and A_i can be related to the relevant and known quantities,

$$A_o C_d = F k_2, \quad (\text{B.45})$$

and,

$$A_i C_d = (1 - F) k_2. \quad (\text{B.46})$$

Implementing Equation (B.45) into Equation (B.44) yields a final parameter,

$$(1 - n) \left[\frac{2(1 - \tilde{\rho}^{-1})}{1 + \tilde{\rho}^{-1} \tilde{F}_n^{\frac{1}{n}}} \right]^n \left[\frac{F k_2 (gH_0)^n}{A_F H_0} \right], \quad (\text{B.47})$$

which may be multiplied by the dimensional hold time to yield a dimensionless time value fit for inter-test, comparative analysis.

When working with experimental data for lighter-than-air agent types ($\rho_{mix} < \rho_{air}$), this parameter is equivalent to

$$(1 - n) \left[\frac{2(\tilde{\rho}^{-1} - 1)}{1 + \tilde{\rho}^{-1} \tilde{F}_n^{\frac{1}{n}}} \right]^n \left(\frac{(1 - F) k_2 (gH_0)^n}{A_F H_0} \right). \quad (\text{B.48})$$

B.9 The Equivalent Height - Part II

As presented in that above, there is no difference between the central governing theory of these models with respect to the hydrostatic driving forces and parameters characterizing enclosure leakage. The only difference between the sharp, wide and thick descending interface models is mathematically implemented through an adjustment to the end-of-integration limit, or elevation input value for which the hold time is evaluated.

The final dimensional governing equations, Equations (B.27–B.28), and their dimensionless forms, Equations (B.39–B.42), all rely upon the equivalent interface height, H_e , as an input parameter⁵. This is the elevation at which the hold time is evaluated for. Modification to this value allows for implementation of the wide and thick interface formulations⁶.

The equivalent height, H_e , has been stated as representing the elevation at which a wide or thick interface would be equally represented by a sharp interface in terms of total agent mass. The hold time theory, as derived in the preceding sections, introduces the integration limits for H as being H_0 to H_e . The value of the ending integration limit, H_e , may theoretically be in the range of 0 to H_0 . Thus, following this and from Equations (B.2–B.3) it follows that the dimensionless interface elevation, \tilde{H} , will always lie in the range of 0 to 1. Manipulation of the value, H_e , to adjust for a non-sharp-interface, elevation-concentration relationship can be easily achieved.

In the case of the wide interface, the model user is expected to implement the relationship,

$$\tilde{H} = 1 - \left(1 - \frac{H_p}{H_0}\right) \frac{c_i}{2c_f}, \quad (\text{B.49})$$

for agents heavier-than-air, and,

$$\tilde{H} = \frac{H_p}{H_0} \frac{c_i}{2c_f}, \quad (\text{B.50})$$

⁵The dimensionless form incorporates this parameter through the dimensionless interface elevation term, \tilde{H} .

⁶Manipulation of the interface elevation, model input is not necessary when modeling a sharp interface. The equivalent height does not exist in terms of the sharp interface theory. A result of the definition of the equivalent height term is that it is equal to the interface height if the interface has negligible thickness ($H_i = H_e$). Such extensions are required only by the wide and thick interface models.

for agents lighter than air. Effectively, to calculate \tilde{H} the user must know the protected height, H_p , for which, when a limiting concentration threshold, c_f/c_i , exists, the hold time will be assumed to have been reached.

The thick interface model user must know the desired concentration reduction from the initial value, c_i , to the value existing at the hold time, c_f . Extending beyond the wide theory however, the user must also input an appropriate value for the characteristic interface slope, previously given as⁷,

$$\omega = \frac{(\Delta H/H_{max})}{(\Delta C/C_{max})}. \quad (\text{B.51})$$

The thick interface model is introduced in Section B.1 as including traits of both the sharp and wide interface behavior. This is manifest here in that a piecewise formulation is necessarily used to determine the appropriate value of the elevation integration limit, \tilde{H} .

At time zero, the interface does not yet exist; forming only after fresh air is allowed to flow into the enclosure. The interface then behaves in three stages:

1. Gradually growing in width while maintaining a linear concentration-elevation gradient, which is fixed at a zero concentration at the elevation of inflowing fresh air. This stage persists until the maximum characteristic thickness (or the absolute value of the slope, ω) has been reached.
2. Maintaining constant width while descending through the enclosure's elevation; ascending in the case of agents lighter than air ($\rho_{mix} < \rho_{air}$).
3. Gradually decaying in width after the leading edge of the descending (or ascending) interface reaches the far enclosure boundary. This stage persists until the agent drains completely from the enclosure and the interface no longer exists.

⁷This parameter is investigated throughout much of Chapter 3. Its value for heavier-than-air agents is expected to range between 0 and -1, while for lighter-than-air agents it is assumed to range between 0 and 1. Inspection of the linear portions of the charted data series in Appendix H reveals that the slope is negative in the case of all tests conducted except for the agent IG-100, in which case the slope approaches a value of infinity (well beyond and in direct opposition to the theoretical model's range of applicability). Note that the regressed slope (or dimensionless interface thickness when assuming that the denominator, $(\Delta C/C_{max})$, always equals 1), is always plotted as a positive magnitude throughout Appendix I

Initially, the user should assume that the interface is in stage (2); modeled for all agent types with the relationship,

$$\tilde{H} = \frac{H_p}{H_0} - \omega \left(\frac{c_f}{c_i} - \frac{1}{2} \right). \quad (\text{B.52})$$

To determine whether the interface is in stage (1) or (3) the user must first evaluate the interface transition point,

$$\tilde{H}_{tp} = \left\lfloor \frac{\omega}{2} \right\rfloor. \quad (\text{B.53})$$

For heavier-than-air agents ($\rho_{mix} > \rho_{air}$), when the value of the dimensionless interface elevation, as calculated with Equation (B.52), is greater than one minus the interface transition point ($\tilde{H} > 1 - \tilde{H}_{tp}$) the interface is in stage (1). In this stage the interface behaves according to the wide interface formulation,

$$\tilde{H} = 1 - \left(1 - \frac{H_p}{H_0} \right) \frac{c_i}{2c_f}, \quad (\text{B.54})$$

previously given as Equation (B.49). The model user need then recalculate and implement the value of \tilde{H} as given by Equation (B.54).

When dealing with lighter-than-air agents the interface is in stage (1) if $\tilde{H} < \tilde{H}_{tp}$. Originally given as Equation (B.50), the wide interface form is then assumed as given by,

$$\tilde{H} = \frac{H_p}{H_0} \frac{c_i}{2c_f}. \quad (\text{B.55})$$

Stage (3) interface behavior exists for heavier-than-air agents if $\tilde{H} < \tilde{H}_{tp}$. The user should recalculate and implement \tilde{H} as,

$$\tilde{H} = \frac{H_p}{H_0} \left[2 \left(1 - \frac{c_f}{c_i} \right) \right]^{-1}. \quad (\text{B.56})$$

Lighter-than-air agents are in stage (3) when ($\tilde{H} > 1 - \tilde{H}_{tp}$). Under this condition, the following form is used,

$$\tilde{H} = 1 - \left(1 - \frac{H_p}{H_0} \right) \left[2 \left(1 - \frac{c_f}{c_i} \right) \right]^{-1}. \quad (\text{B.57})$$

This concludes the presentation and derivation of the hold time theory and evaluation criteria as implemented by the sharp, wide and thick interface hold time prediction models.

The disparity between the three models considered in this body of work is best illustrated with a side-by-side depiction of the dimensionless theory. Figure B.6 plots the dimensionless *interface* elevation as a function of the dimensionless time. The plotted series do not quite represent the interface itself, but rather a traveling point within the interface's domain that represents a fixed concentration reduction threshold.

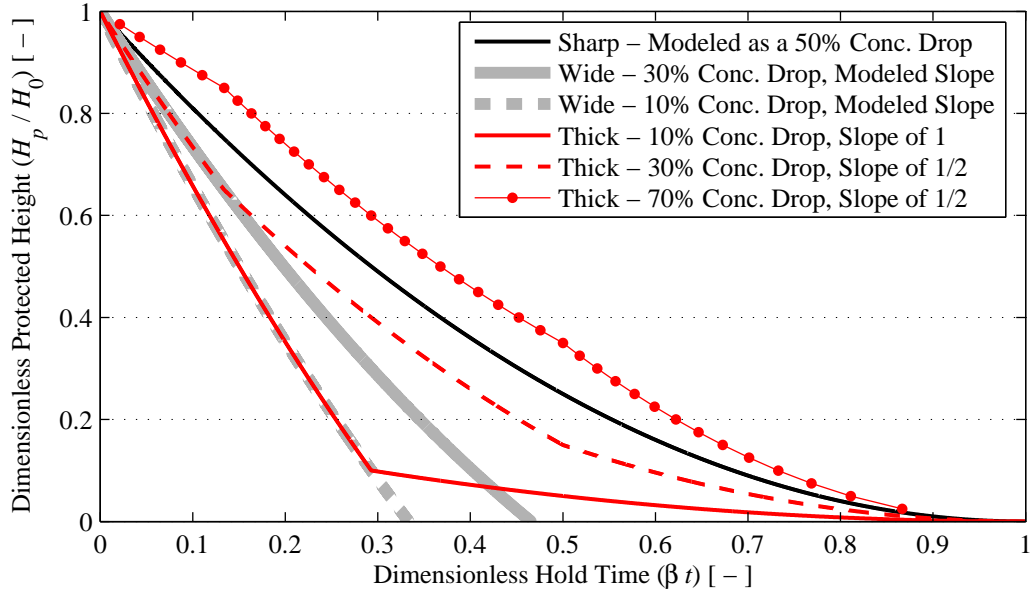


Figure B.6: Dimensionless hold time theory for the sharp, wide, and thick interface theories. The protected height of the descending interface is given as a function of time. Typical input parameters are used to demonstrate comparative hold time model behavior.

The sharp interface theory is represented by the solid black curve. Because the interface has no thickness, only one solution curve will ever exist.

The wide interface theory accepts one additional input parameter; a concentration reduction threshold. When this parameter is $1/2$, the model collapses into the sharp interface. The thickness of the wide interface is assumed to be, and modeled as, an ever increasing thickness. Observation of the two

thick, gray, data traces shows that when modeling concentration reductions of a lesser degree than the initial discharge concentration a much shorter hold time is predicted.

The three red data series represent the thick interface for three different sets of input parameters as are reported in the legend. The overall function is seen to be piecewise. There are only two segments to the first thick interface curve. This is due to a maximum, characteristic thickness (or slope value) of 1 (input as -1) being used; representing its maximum theoretical value⁸. The remaining two data traces exhibit three segments. From upper-left to lower-right these segments represent stages (1), (2) and (3), respectively. Initially, the curve is similar to the wide interface behavior, then transitioning to a translated portion of the sharp interface curve, and ultimately regressing back into a inverted wide interface behavior.

Depending upon the modeled concentration reduction and interface thickness it is apparent that the potential solution space of the hold time theory has been drastically increased. Figure B.6 shows the wide theory dropping below and to the left of the sharp theory curve. In essence, the progression from the sharp to wide theory has added the entire region to the lower-left of the sharp theory curve to the possible solution space⁹. The thick interface theory has further expanded this solution space to include the entirety of the plottable region. Worth noting here is that, as with any modeling theory, the accuracy of the outputs is entirely dependant upon the accuracy of the inputs. Such a flexible solution space is deserving of measured, repeatable, and reasonably conservative input parameters.

⁸When the characteristic thickness is input as -1 or 1, stage (2) behavior is never exhibited. Inversely, when the slope is input as 0, stage (1) and stage (3) behavior do not exist.

⁹In terms of the ISO 14520 implementation of the wide interface theory the model is not to be used for concentration reductions below 50%. To a certain degree, it can be argued that input parameters below this threshold are in fact stretching the model's physical applicability.

Appendix C

Agent Concentration Data

This and the following appendices serve to document all data types retained from the 2005, 2006 and 2007 test phases. Furthermore, with regard to Chapters [2](#) and [3](#), any relevant correlations, regressions, or calculations obtained through use of the raw data sets are presented.

This project is dedicated to the validation of models used to predict the hold time, or duration for which a gaseous clean extinguishing agent will remain within the protected envelope. Of all the data types retained the agent concentration measurements are of primary interest in directly analyzing the agent draining behavior. The following of this appendix presents all the scaled and filtered gas sampling data retained for analysis in this project.

Each figure indicates the test number and agent type. In analyzing the ensuing figures reference Tables [A.1](#), [A.2](#), and [A.3](#) to understand the contextual variables for each conducted test. Additionally, for each data series plotted, the legend displays the percent of room elevation at which the gas sampling probes were installed and which instrument and channel the data was originated from.

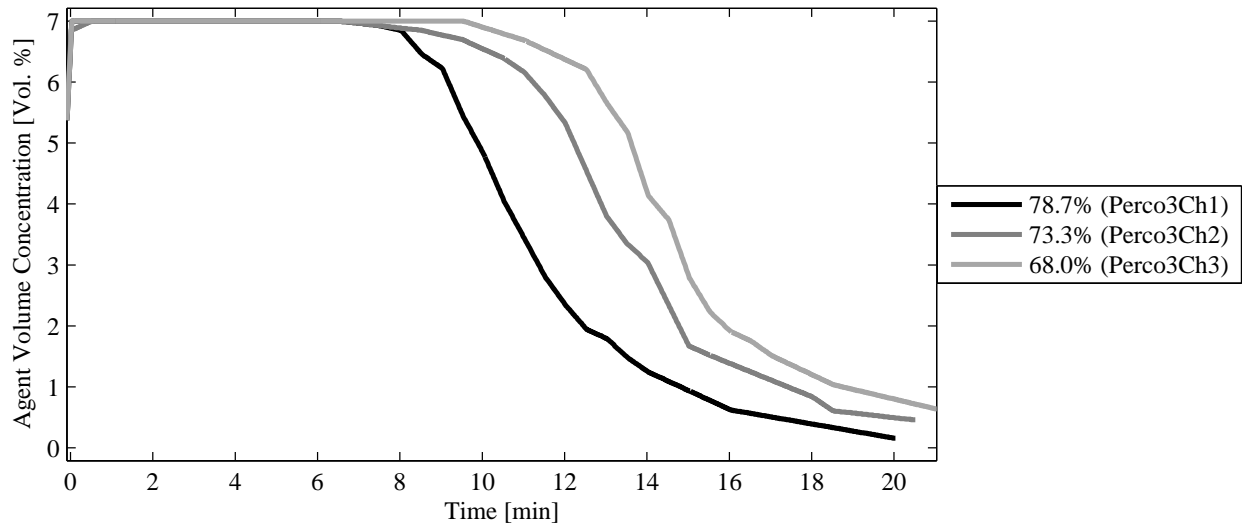


Figure C.1: Agent concentration data for test no. 1 (HFC-227ea)

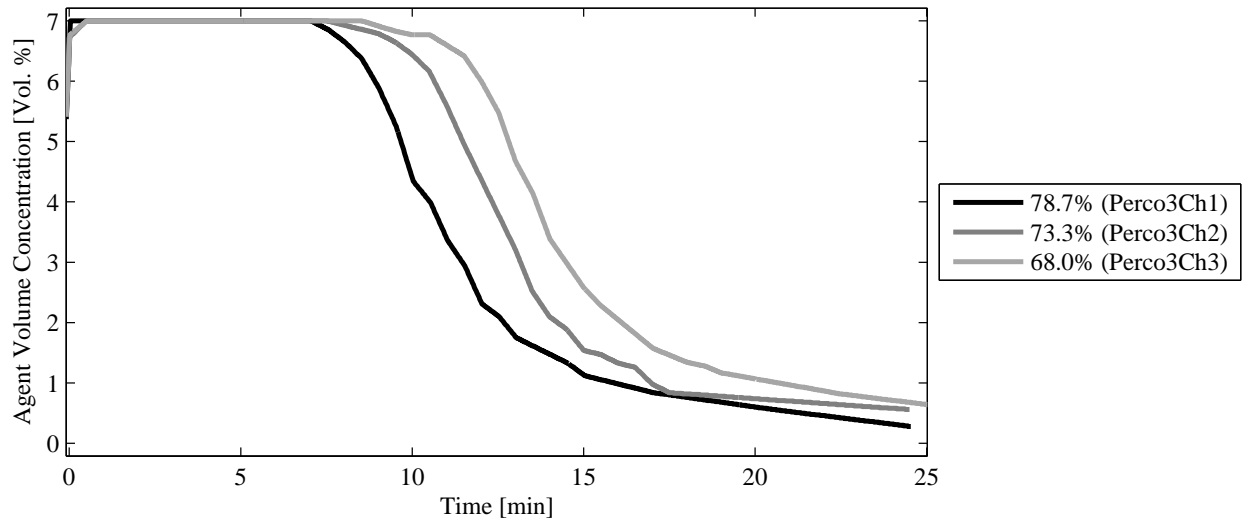


Figure C.2: Agent concentration data for test no. 2 (HFC-227ea)

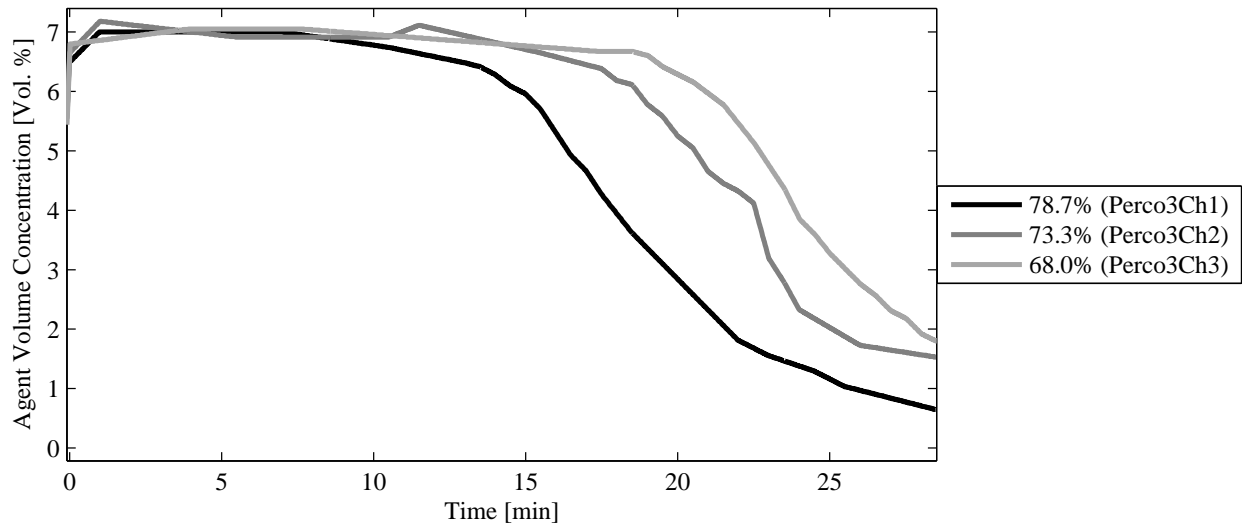


Figure C.3: Agent concentration data for test no. 3 (HFC-227ea)

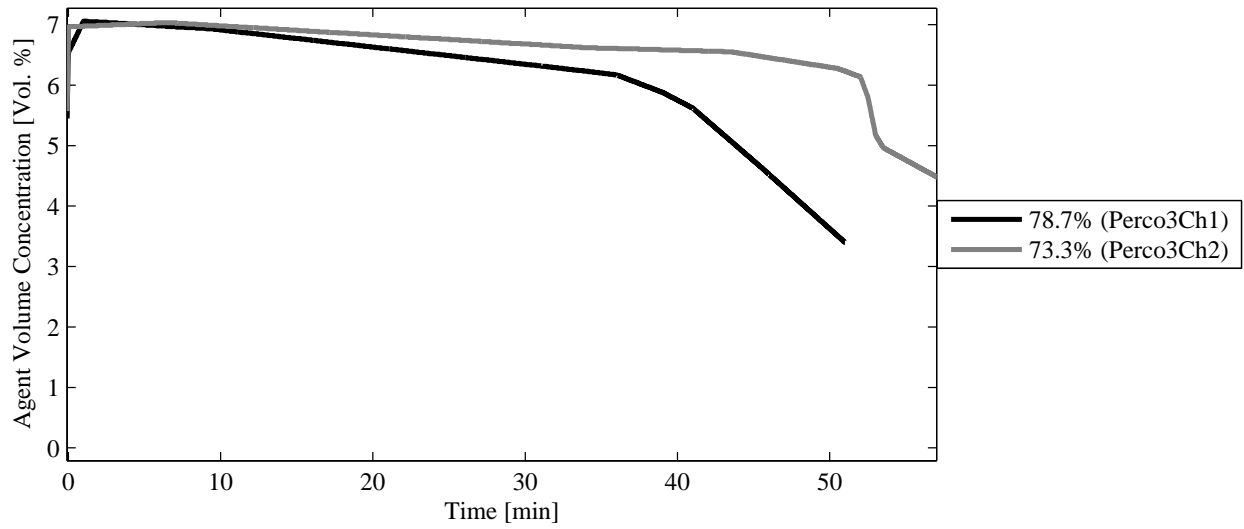


Figure C.4: Agent concentration data for test no. 5 (HFC-227ea)

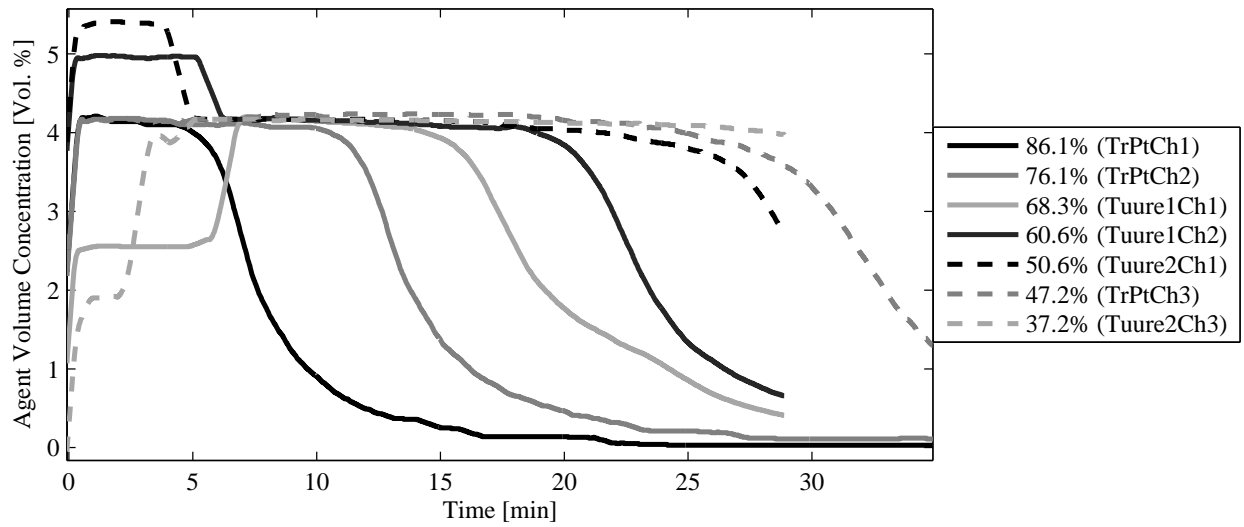


Figure C.5: Agent concentration data for test no. 6 (FK-5-1-12)

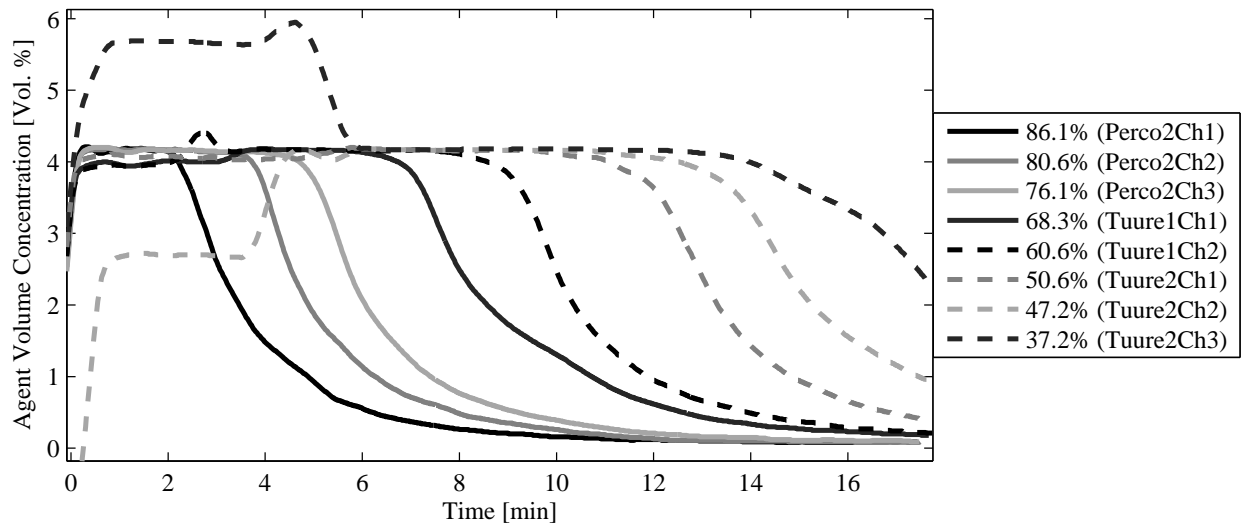


Figure C.6: Agent concentration data for test no. 7 (FK-5-1-12)

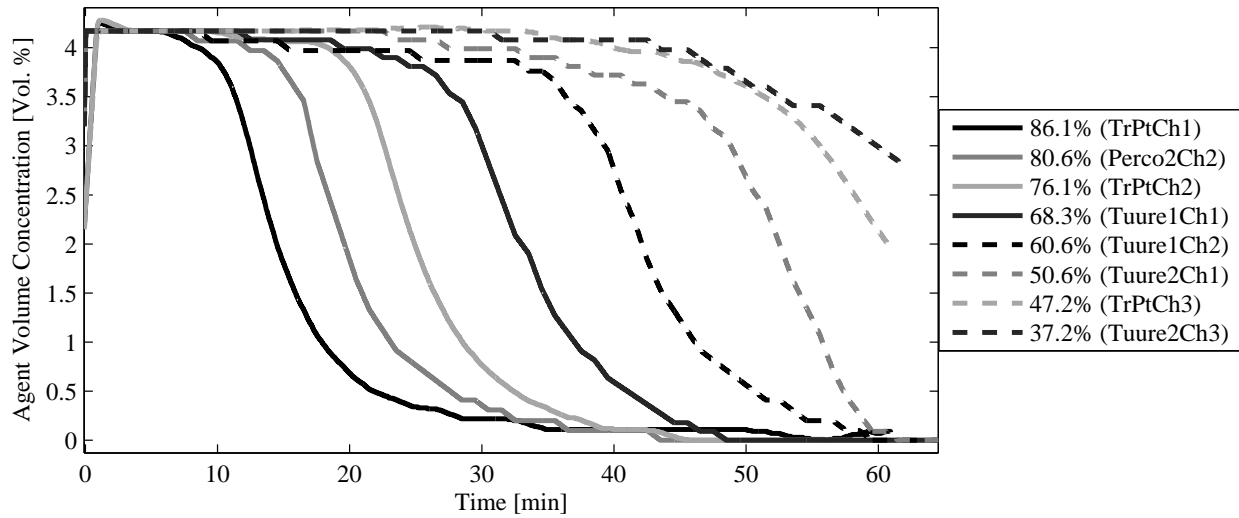


Figure C.7: Agent concentration data for test no. 8 (FK-5-1-12)

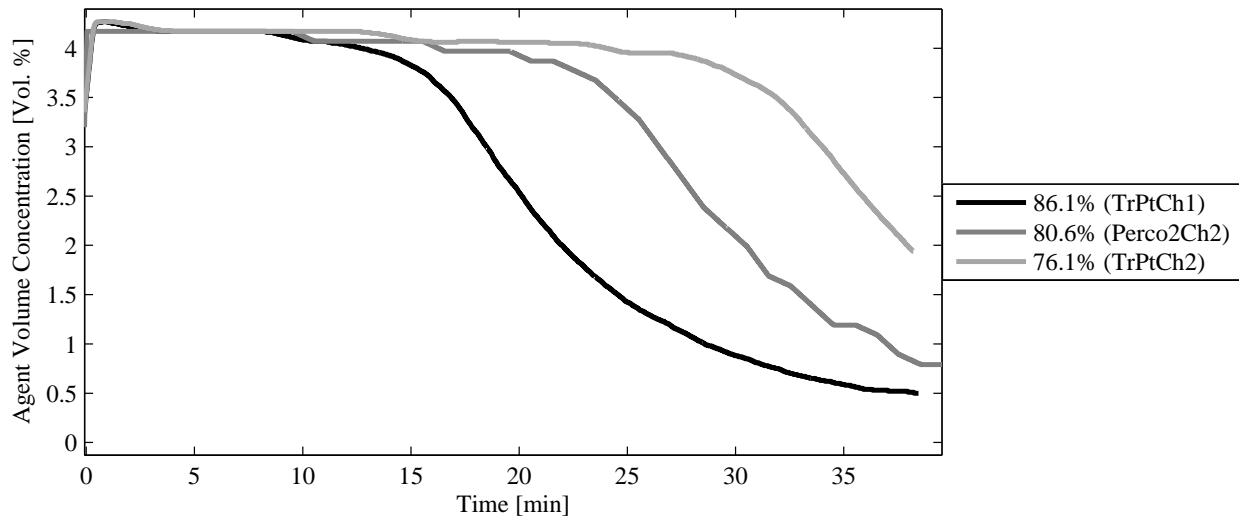


Figure C.8: Agent concentration data for test no. 9 (FK-5-1-12)

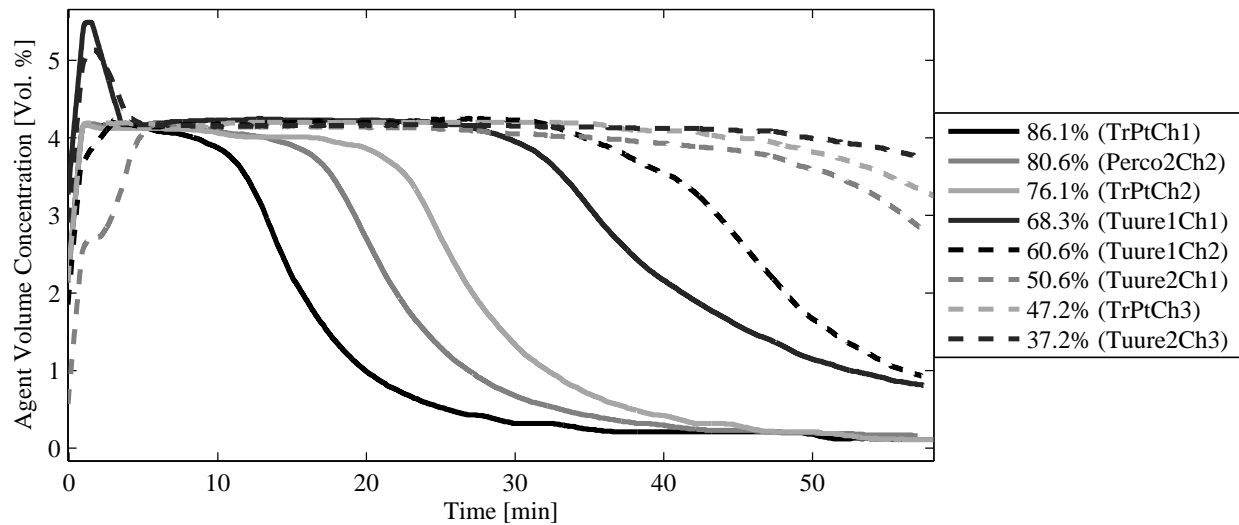


Figure C.9: Agent concentration data for test no. 10 (FK-5-1-12)

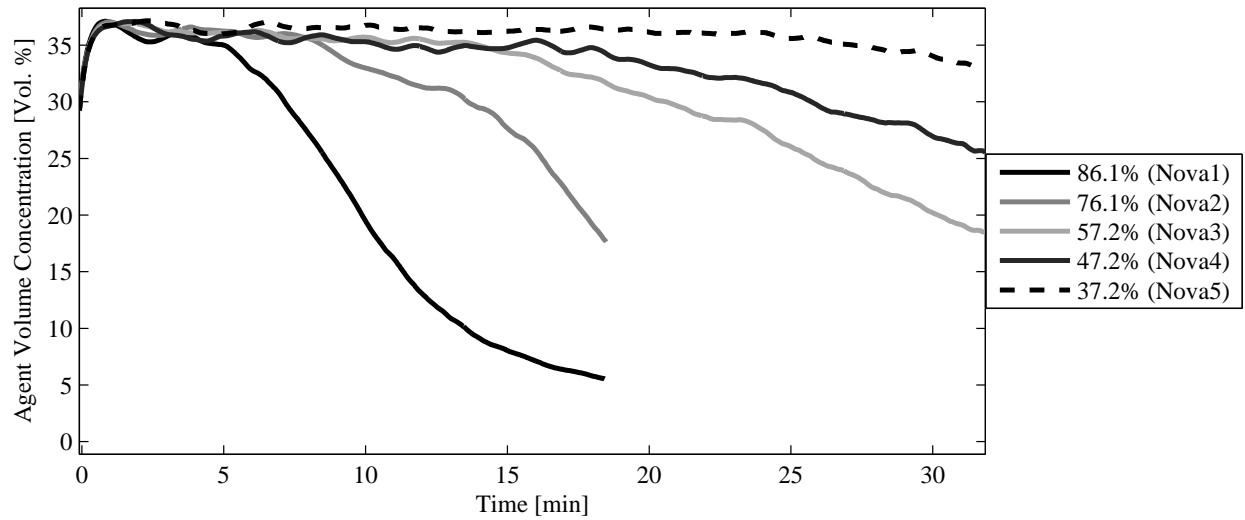


Figure C.10: Agent concentration data for test no. 11 (IG-541)

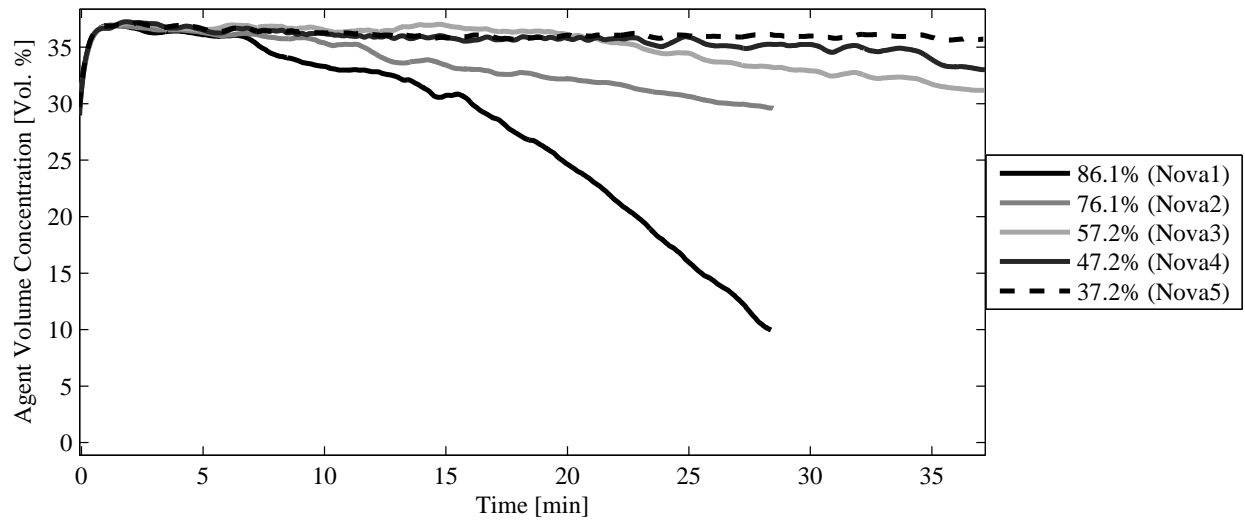


Figure C.11: Agent concentration data for test no. 12 (IG-541)

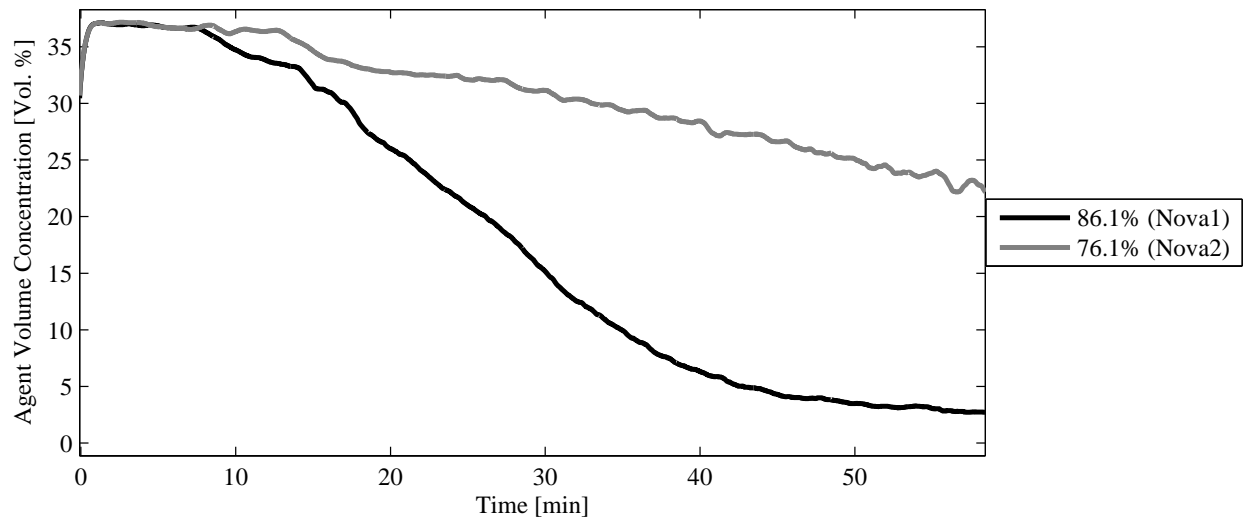


Figure C.12: Agent concentration data for test no. 13 (IG-541)

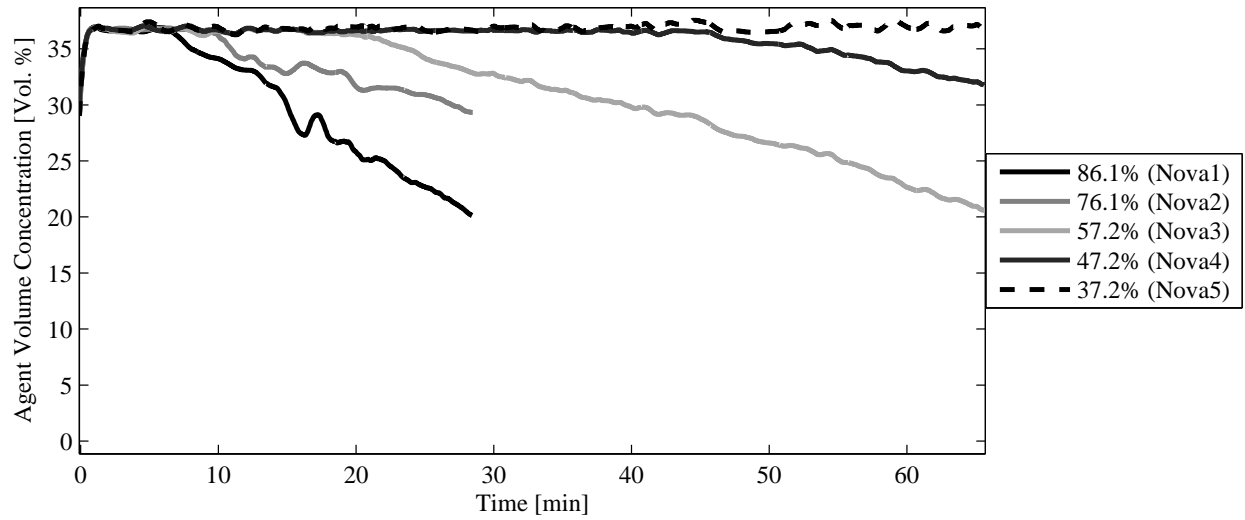


Figure C.13: Agent concentration data for test no. 14 (IG-541)

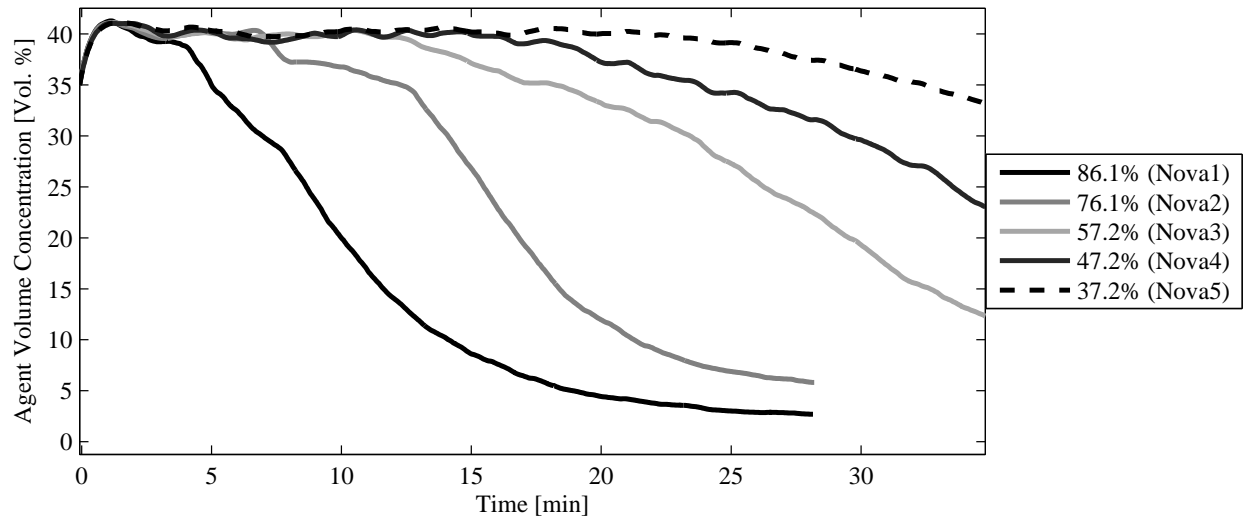


Figure C.14: Agent concentration data for test no. 15 (IG-541)

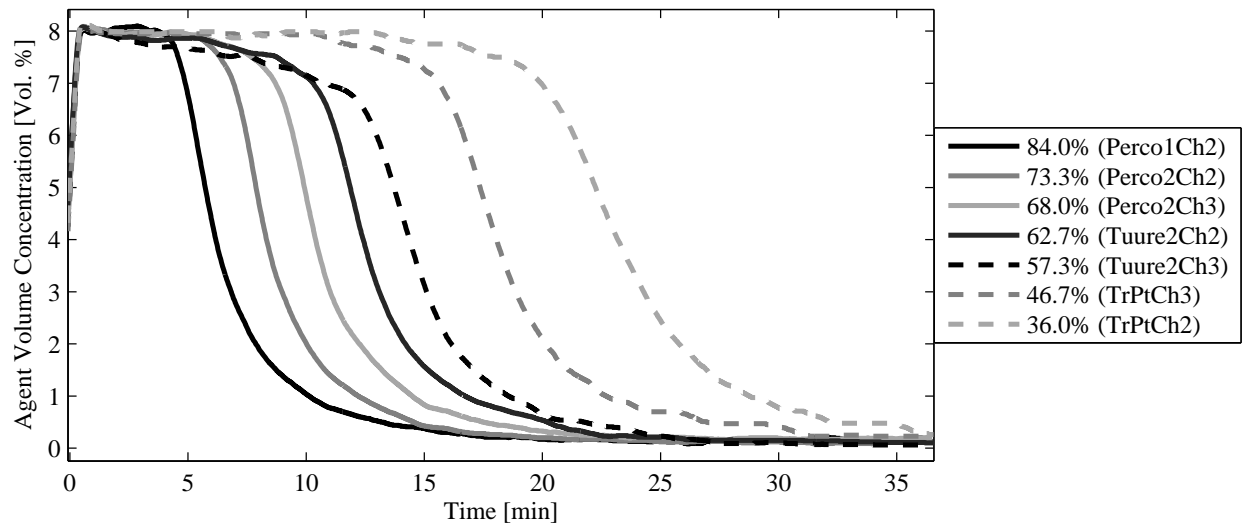


Figure C.15: Agent concentration data for test no. 16 (HFC-125)

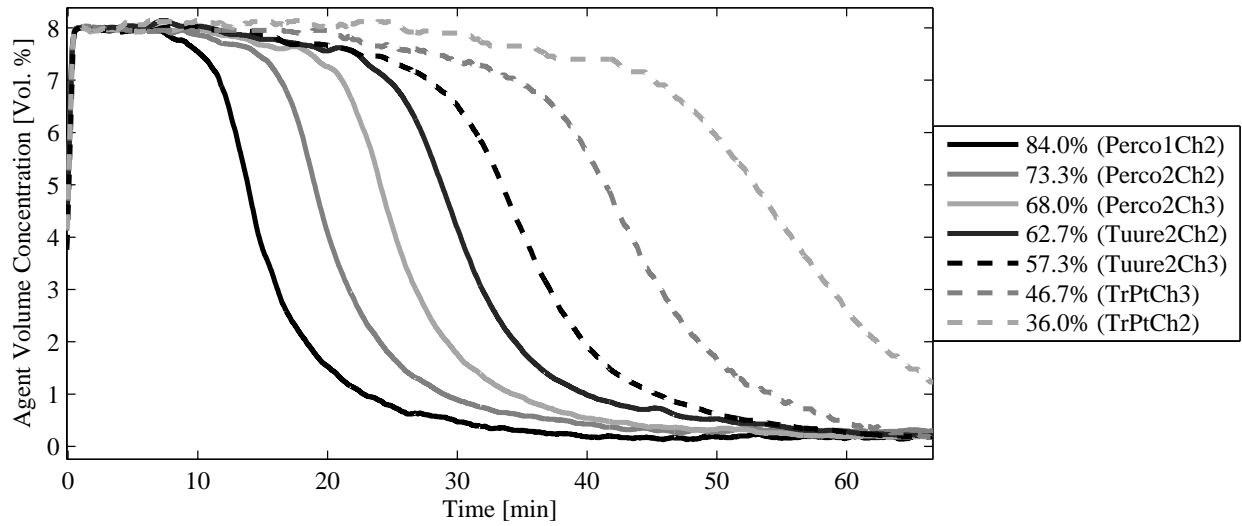


Figure C.16: Agent concentration data for test no. 17 (HFC-125)

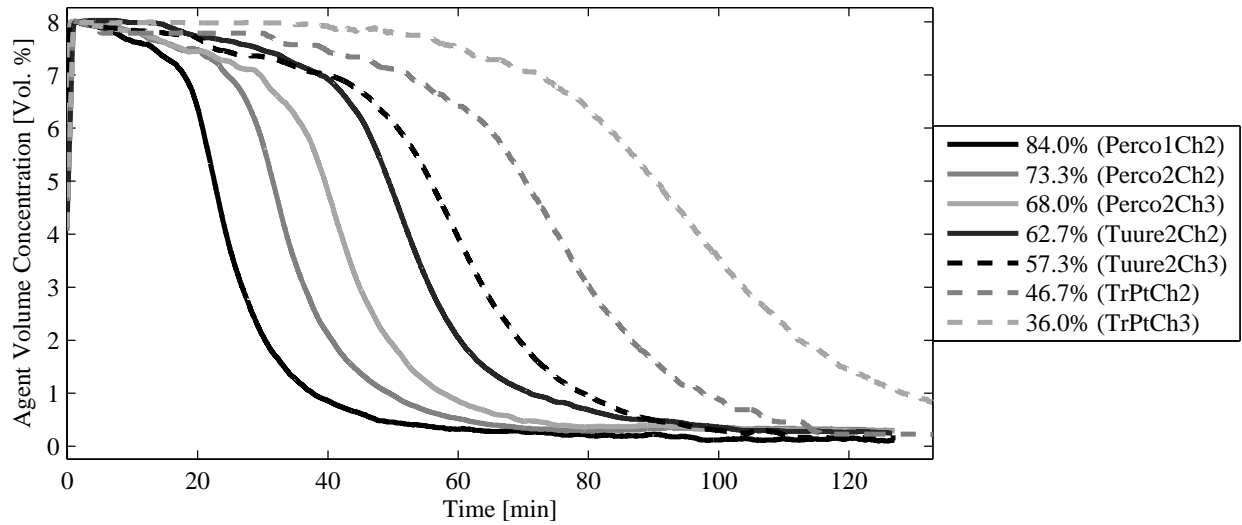


Figure C.17: Agent concentration data for test no. 18 (HFC-125)

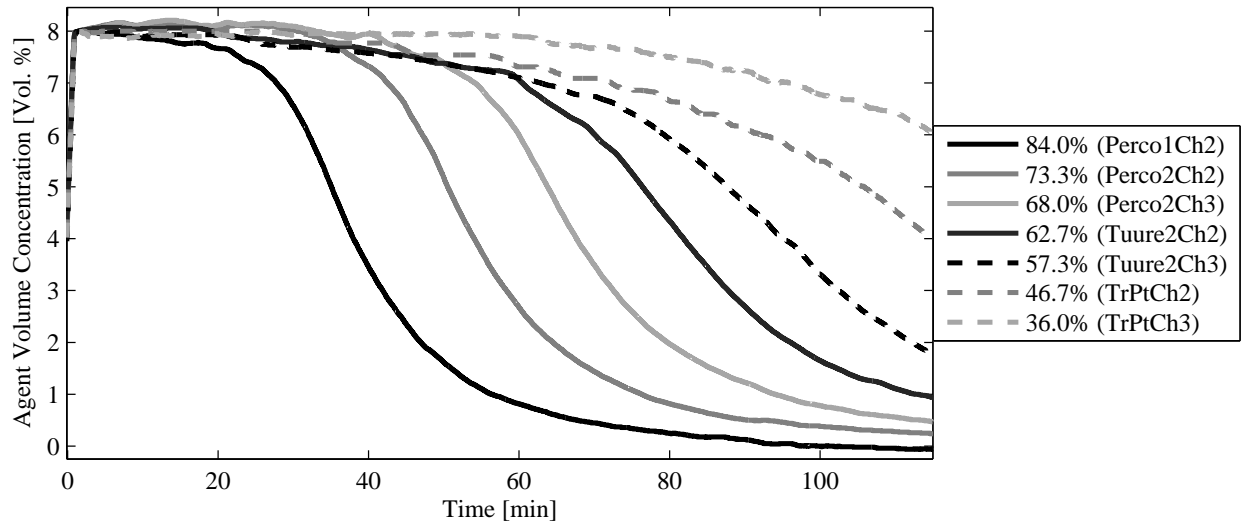


Figure C.18: Agent concentration data for test no. 19 (HFC-125)

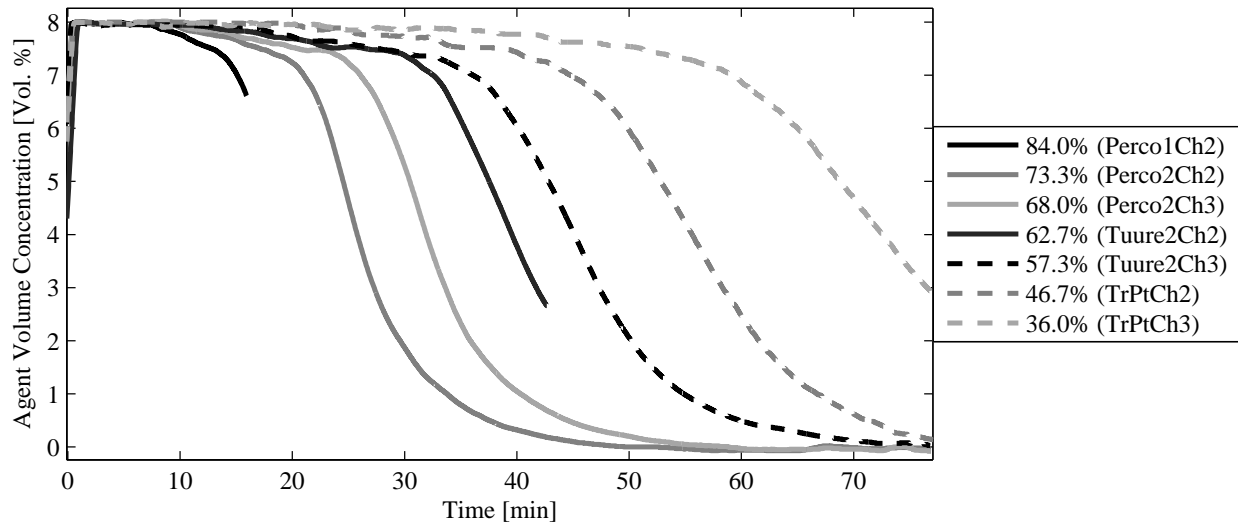


Figure C.19: Agent concentration data for test no. 20 (HFC-125)

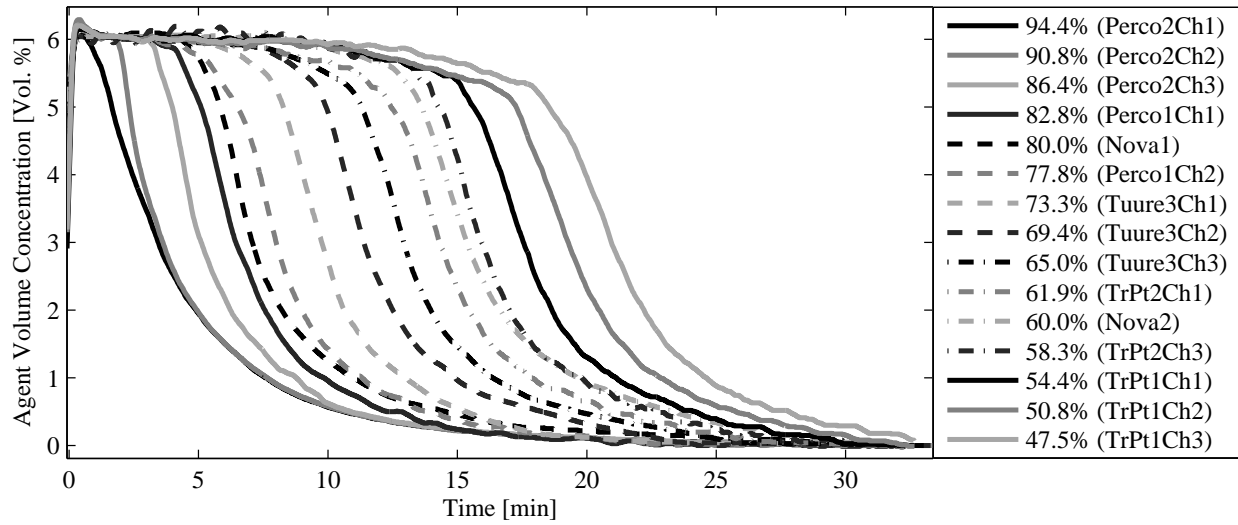


Figure C.20: Agent concentration data for test no. 21 (HFC-227ea)

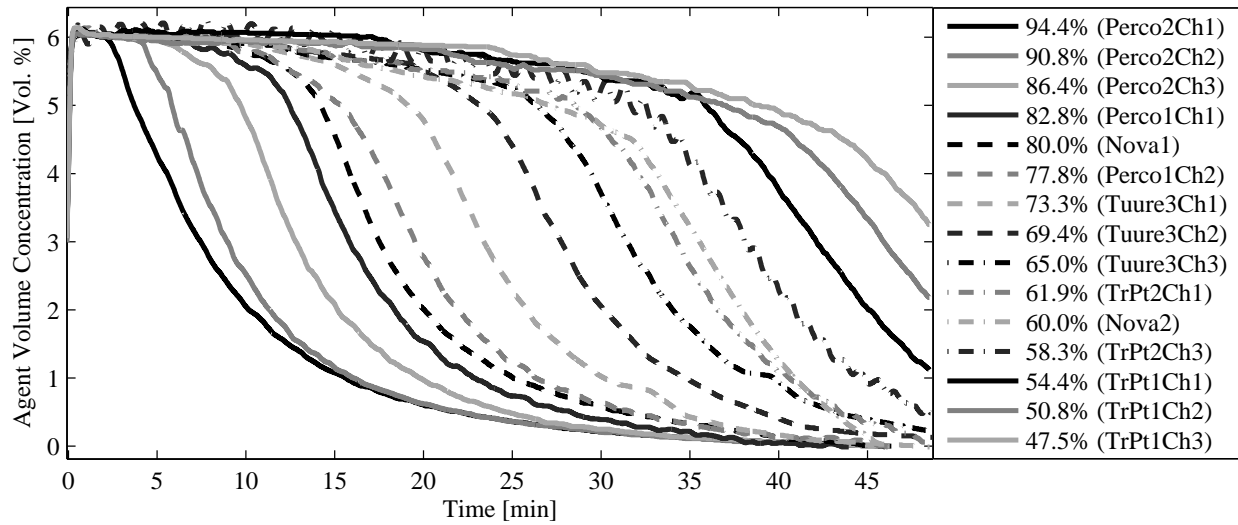


Figure C.21: Agent concentration data for test no. 22 (HFC-227ea)

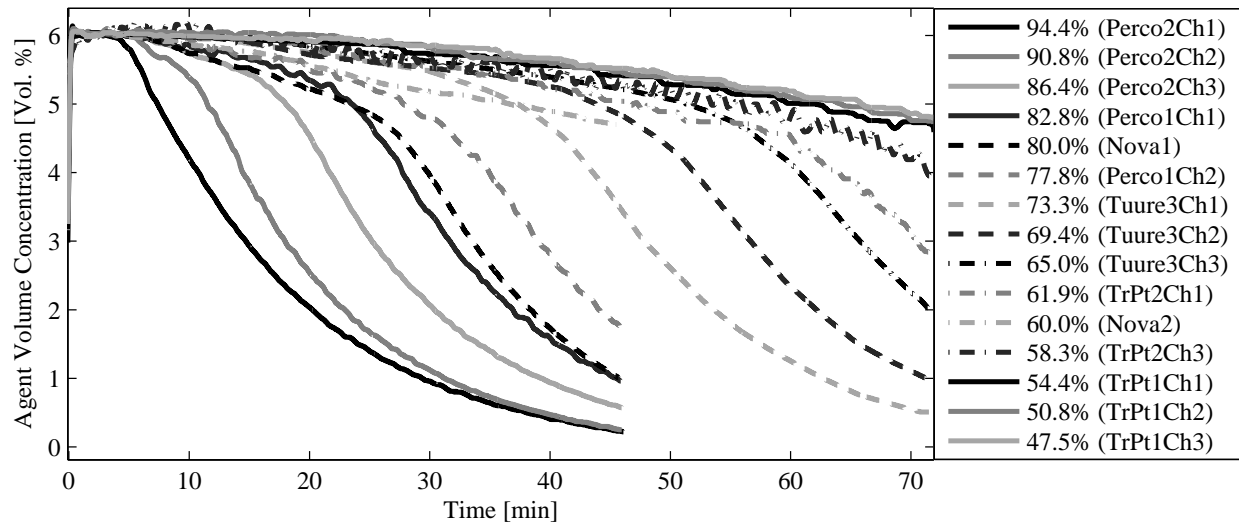


Figure C.22: Agent concentration data for test no. 23 (HFC-227ea)

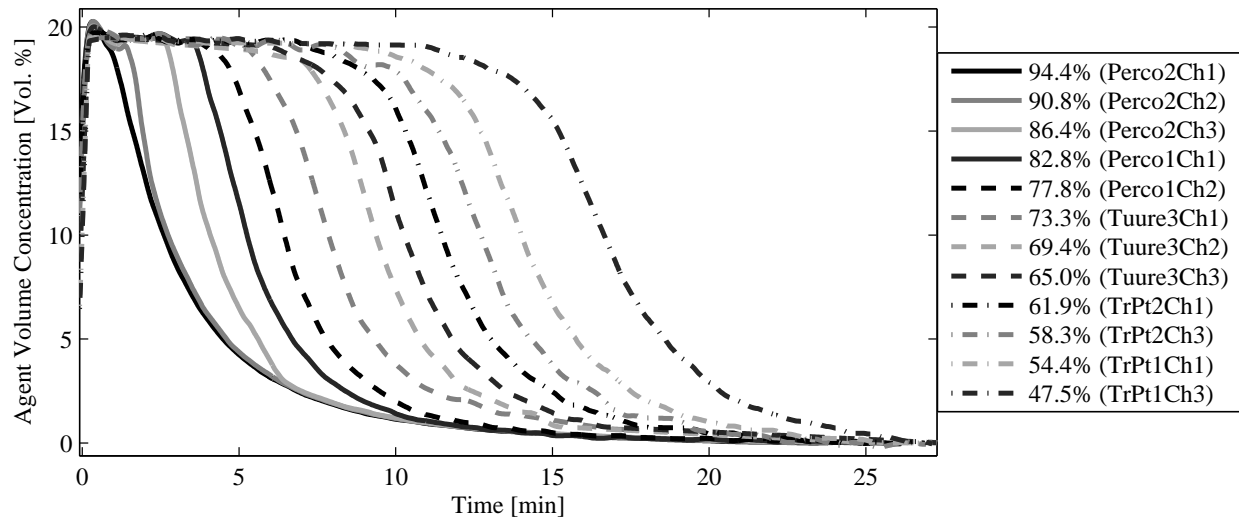


Figure C.23: Agent concentration data for test no. 28 (HFC-23)

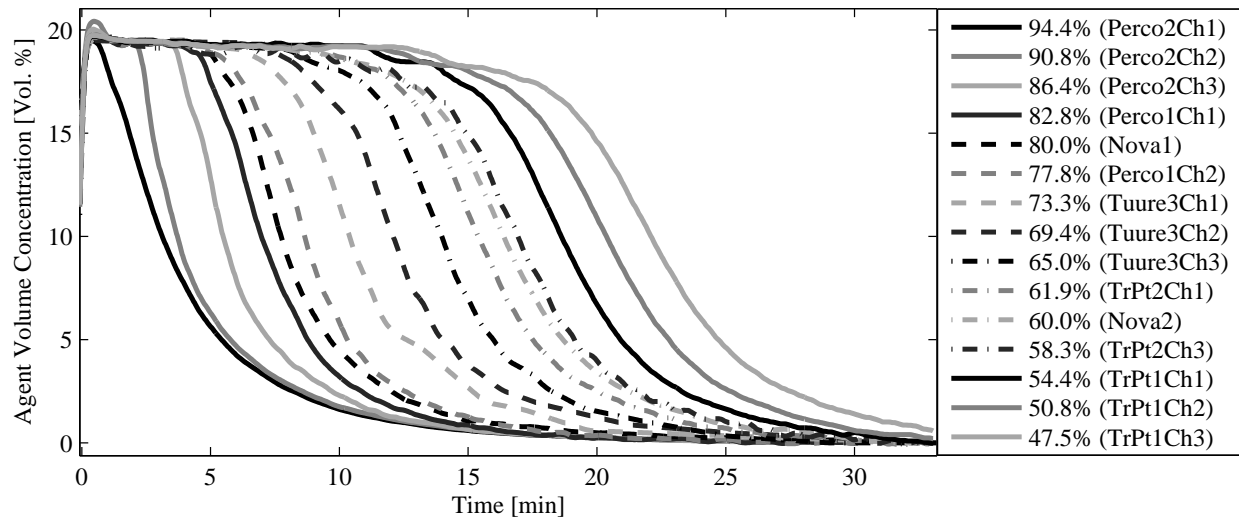


Figure C.24: Agent concentration data for test no. 29 (HFC-23)

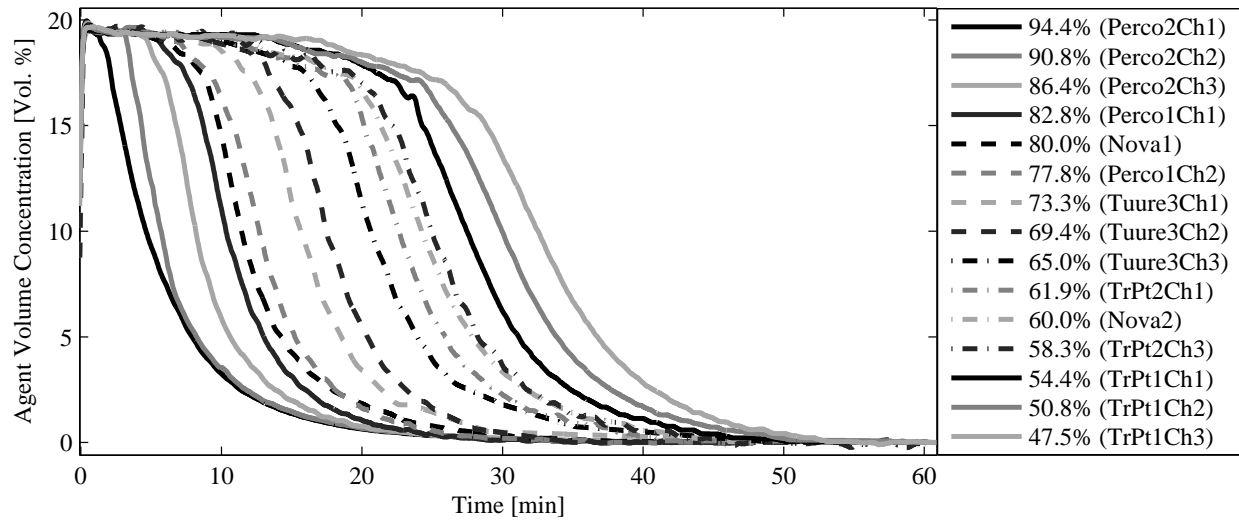


Figure C.25: Agent concentration data for test no. 30 (HFC-23)

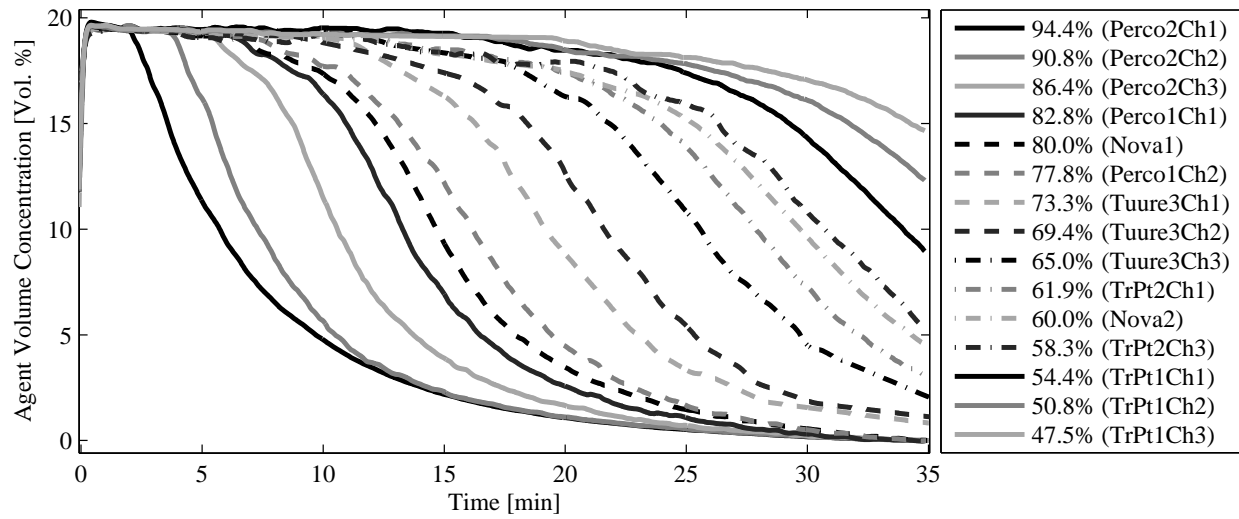


Figure C.26: Agent concentration data for test no. 31 (HFC-23)

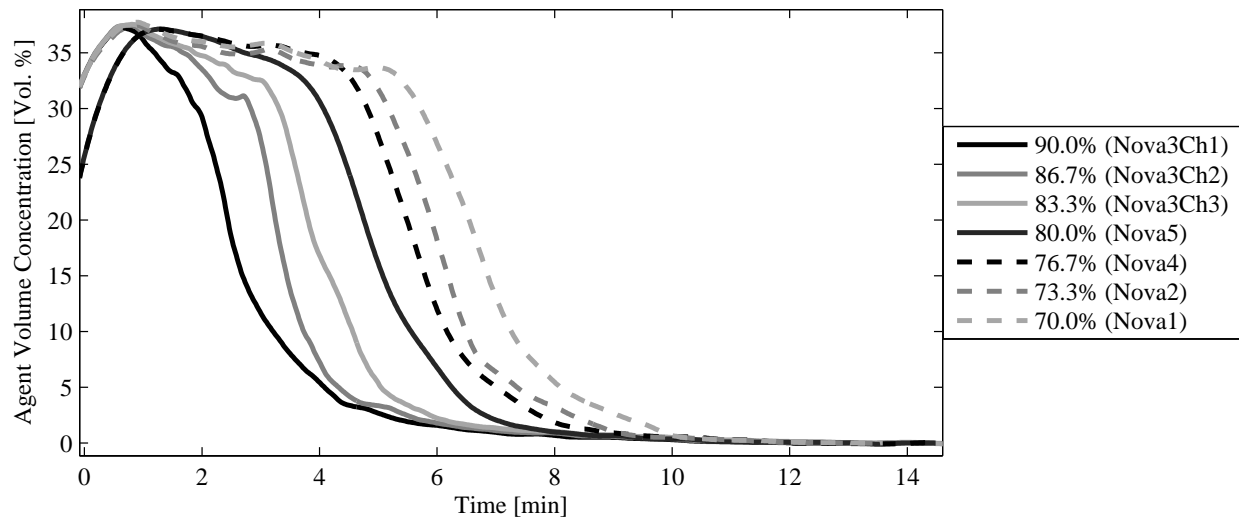


Figure C.27: Agent concentration data for test no. 32 (IG-55)

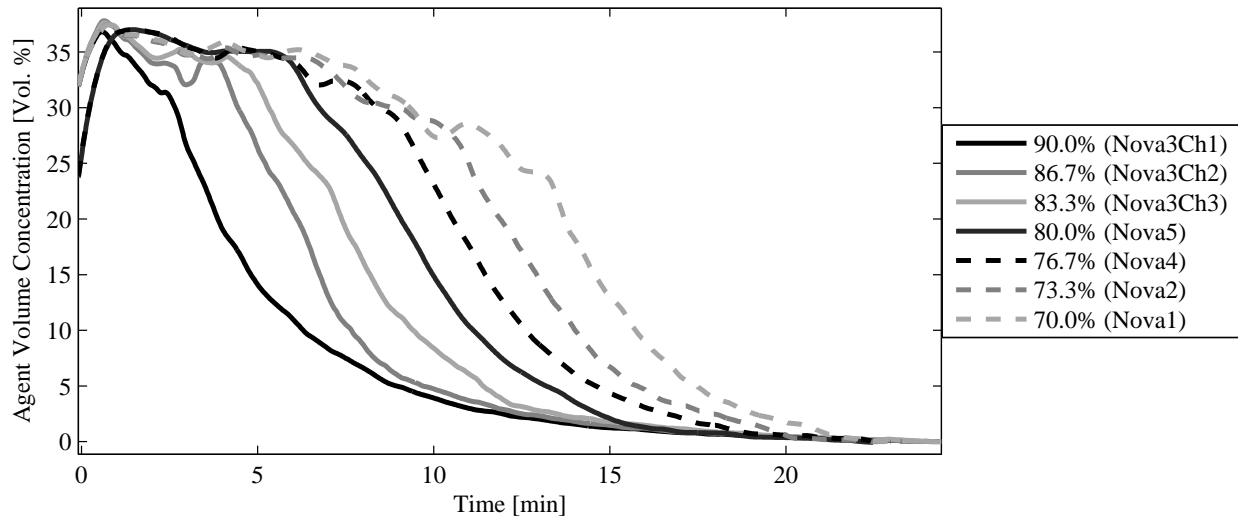


Figure C.28: Agent concentration data for test no. 34 (IG-55)

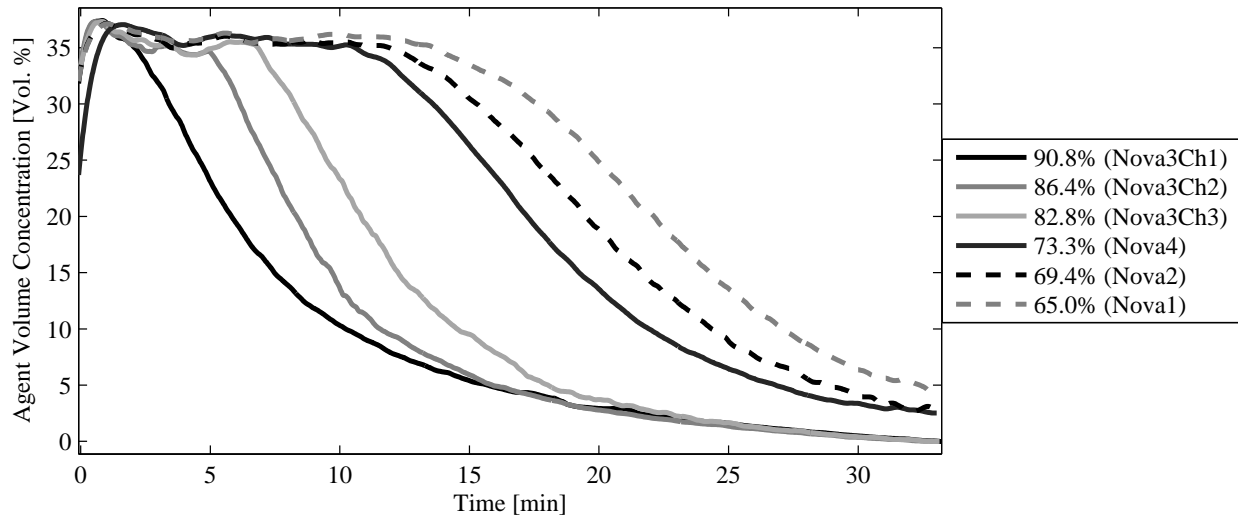


Figure C.29: Agent concentration data for test no. 35 (IG-55)

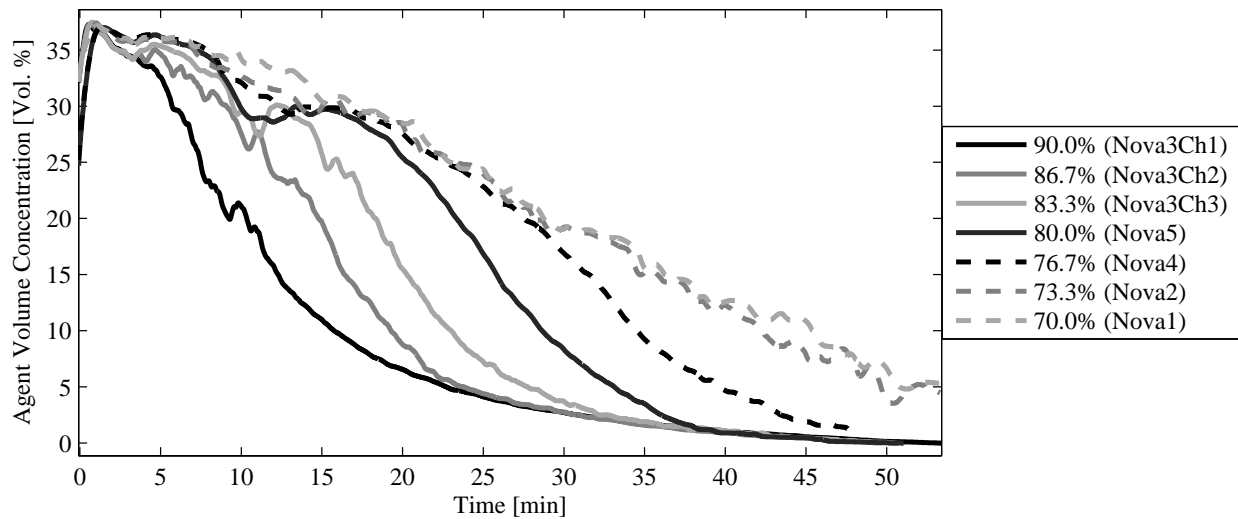


Figure C.30: Agent concentration data for test no. 36 (IG-55)

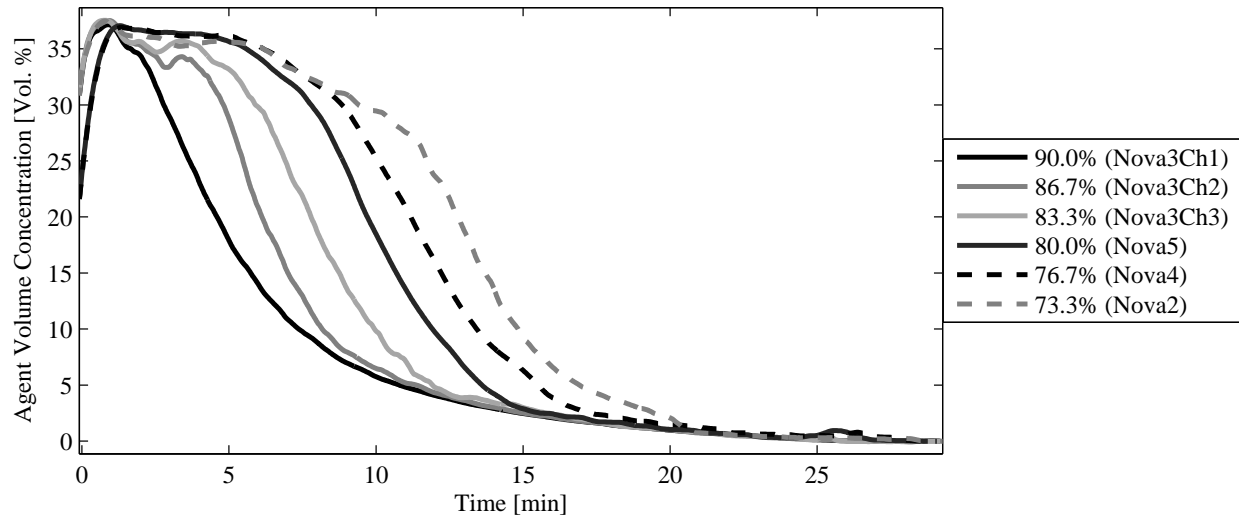


Figure C.31: Agent concentration data for test no. 38 (IG-55)

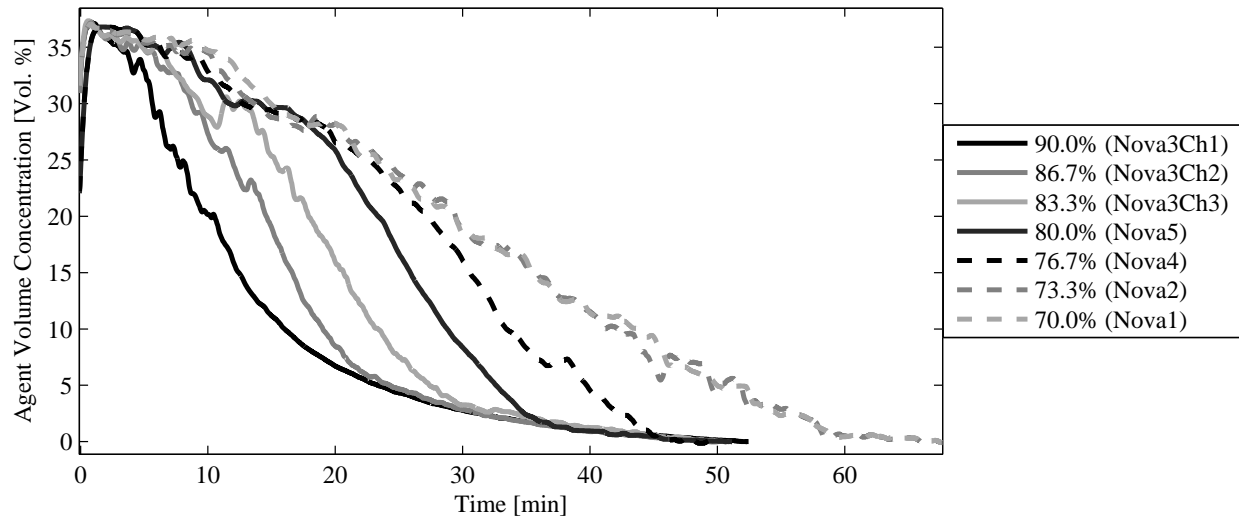


Figure C.32: Agent concentration data for test no. 40 (IG-55)

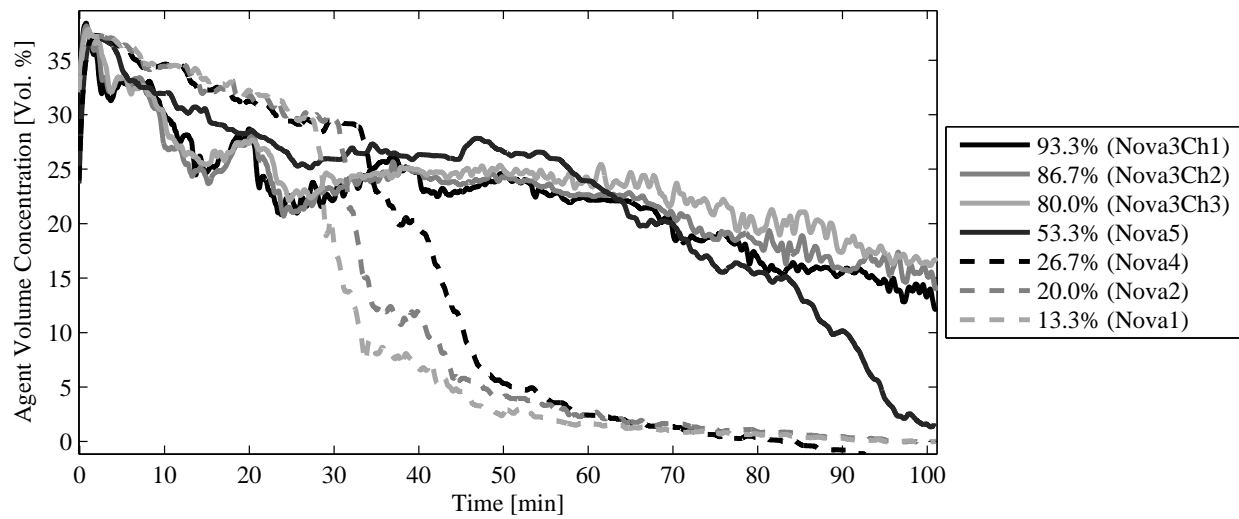


Figure C.33: Agent concentration data for test no. 42 (IG-100)

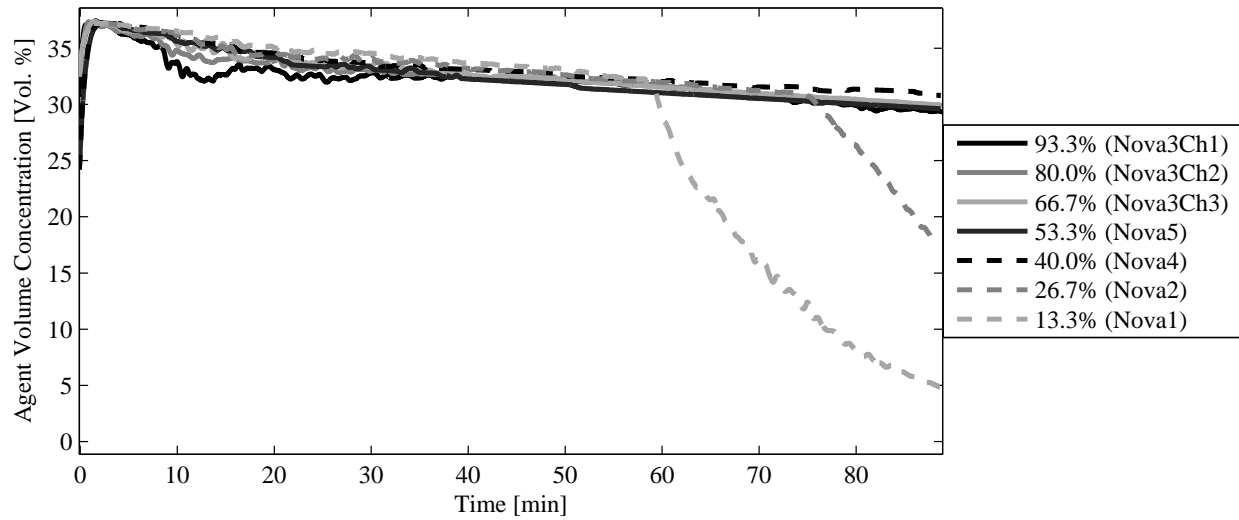


Figure C.34: Agent concentration data for test no. 43 (IG-100)

Appendix D

Ambient Pressure Data

During the period of agent discharge and throughout the subsequent hold time period transient fluctuations in ambient pressure within the experimental enclosure are experienced. For each conducted test, at least one pressure transducer was available to record this transient behavior. For a large fraction of the test matrix, as many as 6 different pressure transducers were available. The result is a very engaging and telling tale of the over- and under-pressures experienced throughout the period of agent discharge. Furthermore, the differential pressure inside the test enclosure, relative to that outside the test envelope, at the elevations of upper and lower leakages exposes the magnitude of the force driving agent draining throughout the hold time.

The figures contained within this appendix document all available sources of ambient pressure data for each conducted test. For a given test, when less than 10 minutes of data was retained a single plot is presented. Otherwise, two plots are presented; one focused on the period of agent discharge, and a second focusing on the small-magnitude pressures throughout the hold time period. In analyzing the ensuing figures reference Tables [A.1](#), [A.2](#), and [A.3](#) to understand the contextual variables for each conducted test.

The legend lists the plotted data series by instrument of origin as a single letter. Instruments ‘A’ and ‘B’ are Dwyer-Magnehelic, needle-indicating, pressure transducers with a full scale value of 11 inches of water column (2740 Pa). Typically, instrument ‘A’ represents a positive pressure transducer and ‘B’ represents a negative pressure transducer. For some tests, especially those conducted in 2005 and 2006, instrument ‘A’ represents a combined data trace of the output from both the positive and negative Magnehelic transducers. Instruments ‘A’ and ‘B’ are always installed at an elevation of 62” above the

floor.

Instruments ‘C’ through ‘F’ are Retrotec DM-2 digital manometers. These instruments are stand-alone devices that log to a PC via USB. Each instrument has 2 channels (C/D or E/F). Each can make measurements in the range of ± 1250 Pascals (± 0.15 Pa or 1% of reading, whichever is greater). Instruments ‘C’ & ‘D’ are always installed at the elevations of upper or lower leakages (offset 1 ft from the floor or ceiling). Instruments ‘E’ & ‘F’ are installed at 5-2/3 ft offsets from the floor or ceiling for tests 17 through 20. For chronological test numbers 21 through 26 (tests 28-31, 35, & 37; reference Table A.3) instruments ‘E’ & ‘F’ are installed 1 ft above the floor and 62” above the floor, respectively.

Generally, instruments ‘C’ & ‘D’ or ‘E’ & ‘F’ are both retained as each pair of instrument channels is derived from one of two, two-channel digital manometers. In the case of test number 30, no ‘F’ channel is present because this particular probe became disconnected upon agent discharge.

It should be noted that these data sets are originated from three, independent data acquisition systems. As such, data from the instrument pairs ‘A’ & ‘B’, ‘C’ & ‘D’, and ‘E’ & ‘F’ are shifted in time to appear as though the agent discharge commences at ~ 10 seconds. Discrepancies observed in the behavior between each pair of ambient pressure channels can sometimes be attributed to this time shift.

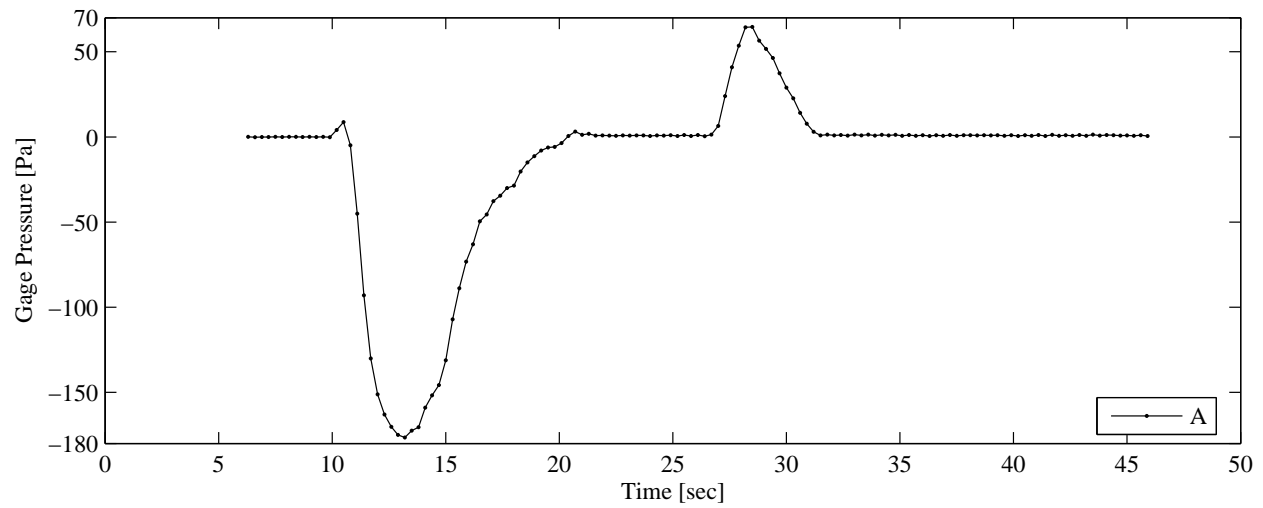


Figure D.1: Ambient pressure data during discharge for test no. 1 (HFC-227ea)

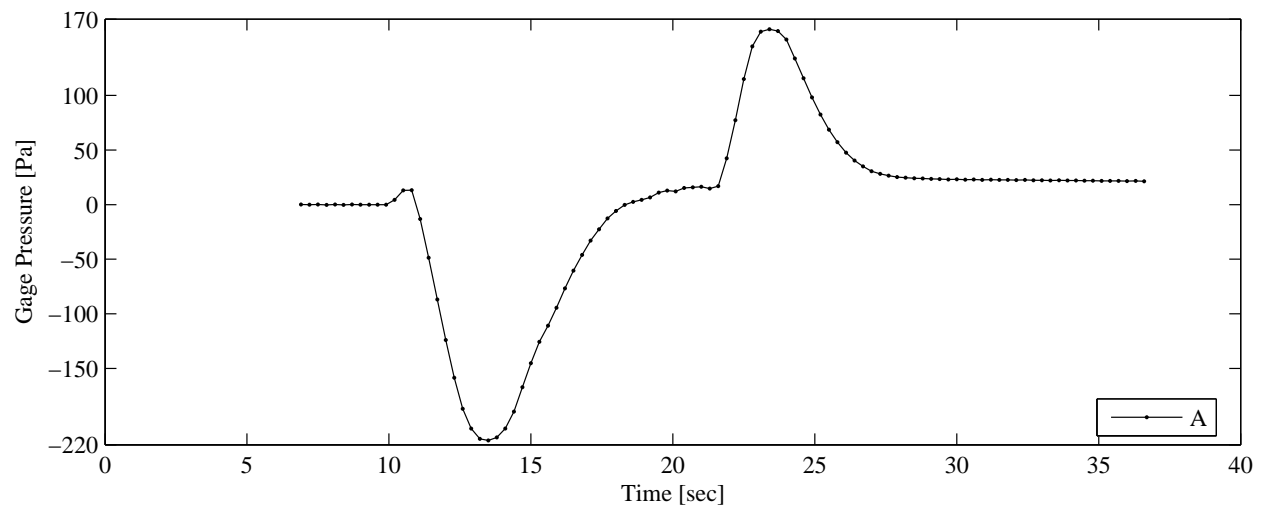


Figure D.2: Ambient pressure data during discharge for test no. 2 (HFC-227ea)

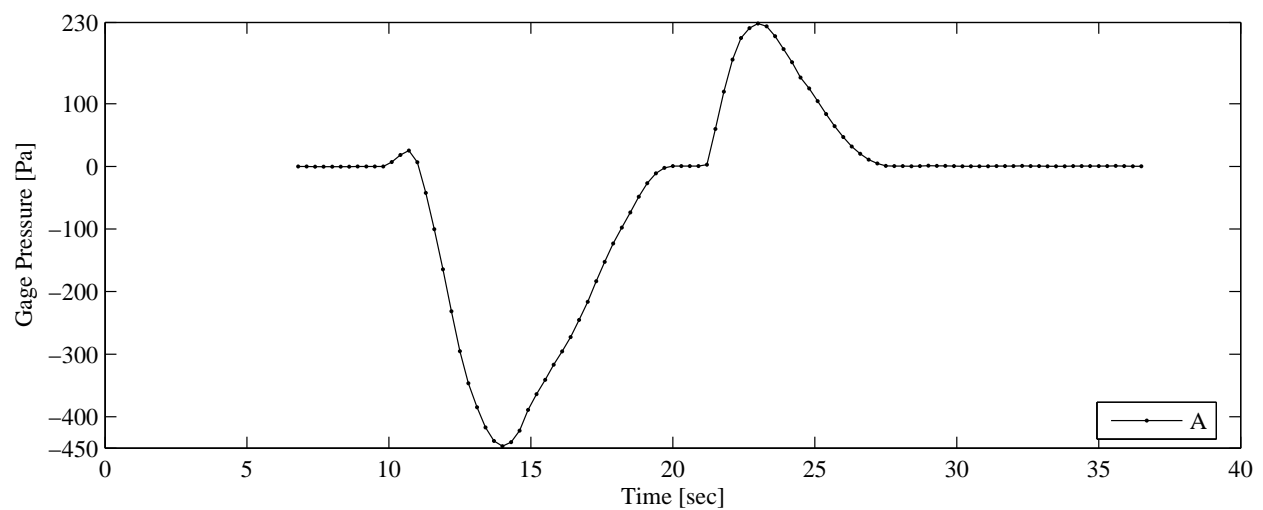


Figure D.3: Ambient pressure data during discharge for test no. 3 (HFC-227ea)

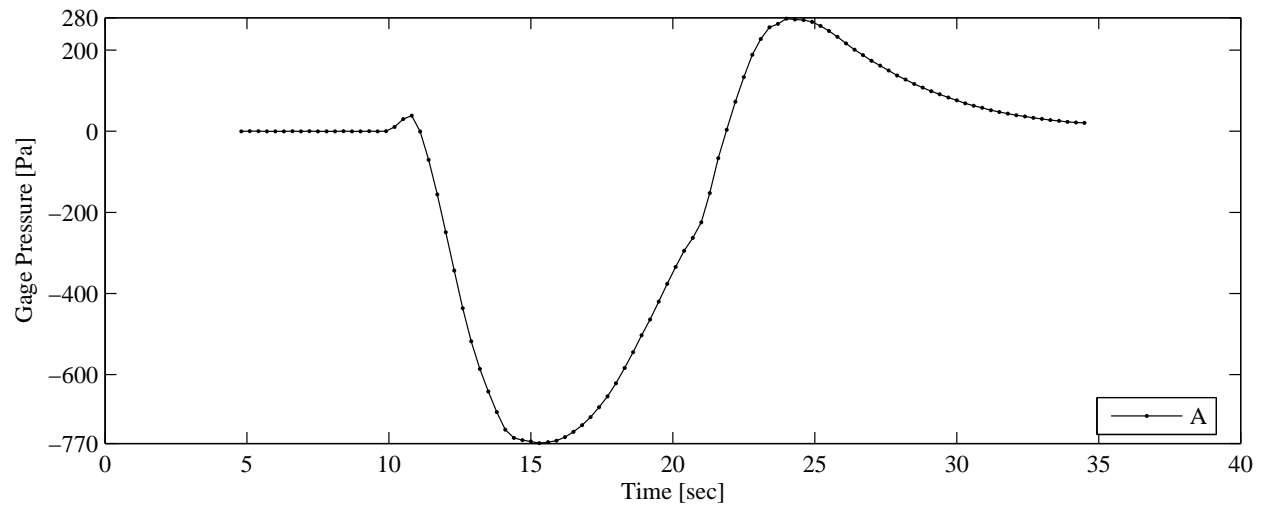


Figure D.4: Ambient pressure data during discharge for test no. 5 (HFC-227ea)

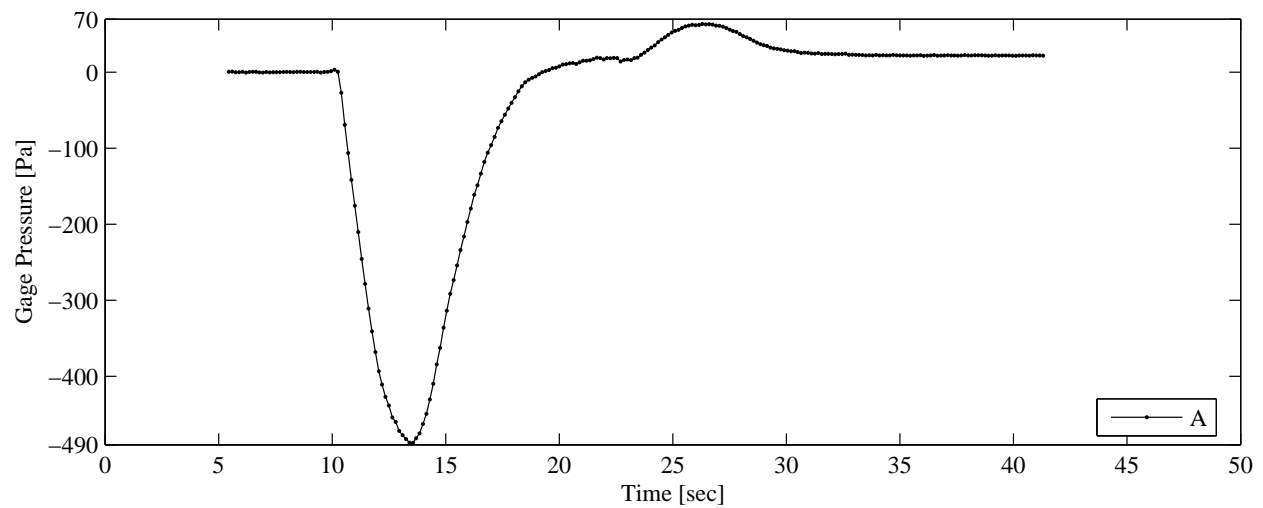


Figure D.5: Ambient pressure data during discharge for test no. 6 (FK-5-1-12)

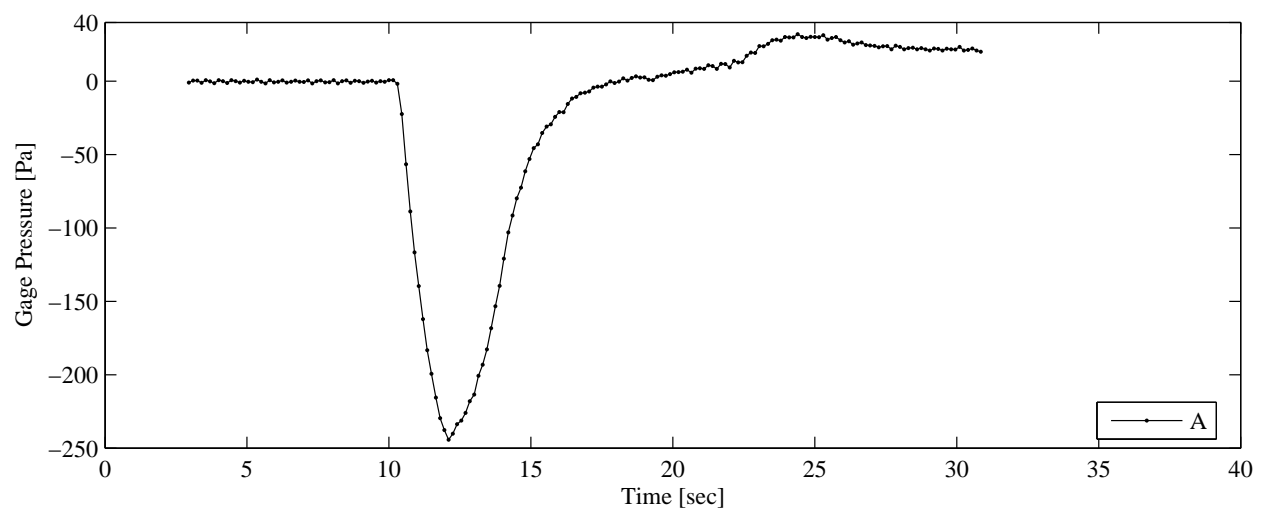


Figure D.6: Ambient pressure data during discharge for test no. 7 (FK-5-1-12)

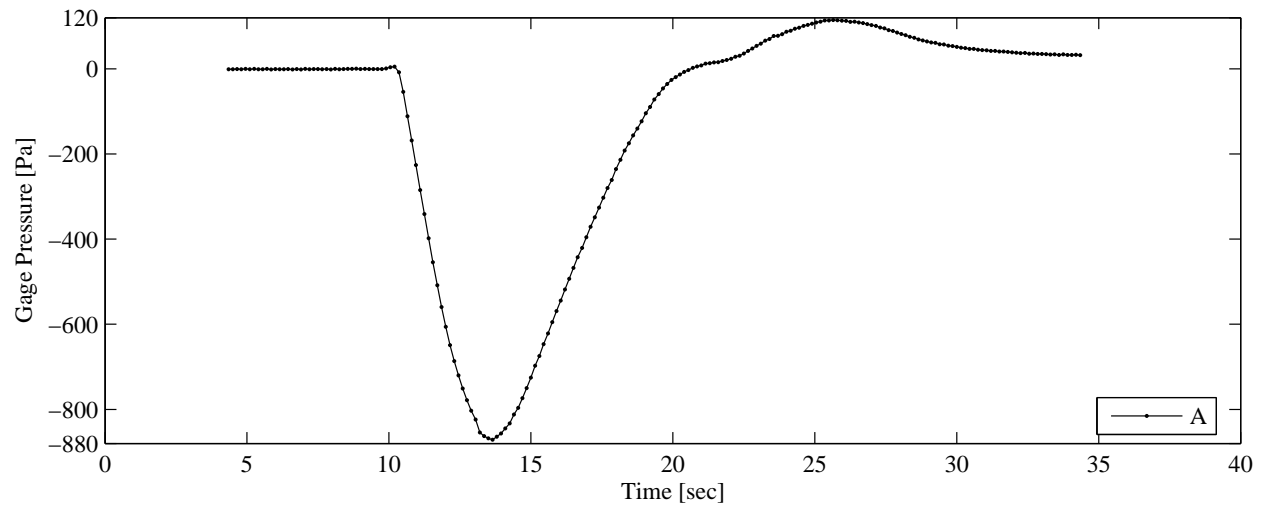


Figure D.7: Ambient pressure data during discharge for test no. 8 (FK-5-1-12)

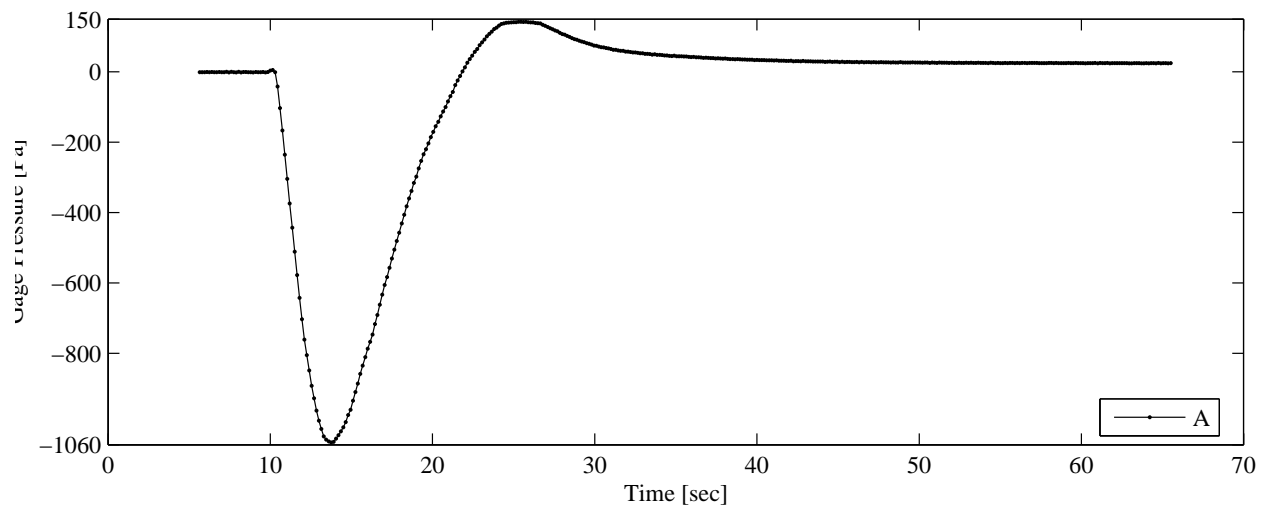


Figure D.8: Ambient pressure data during discharge for test no. 9 (FK-5-1-12)

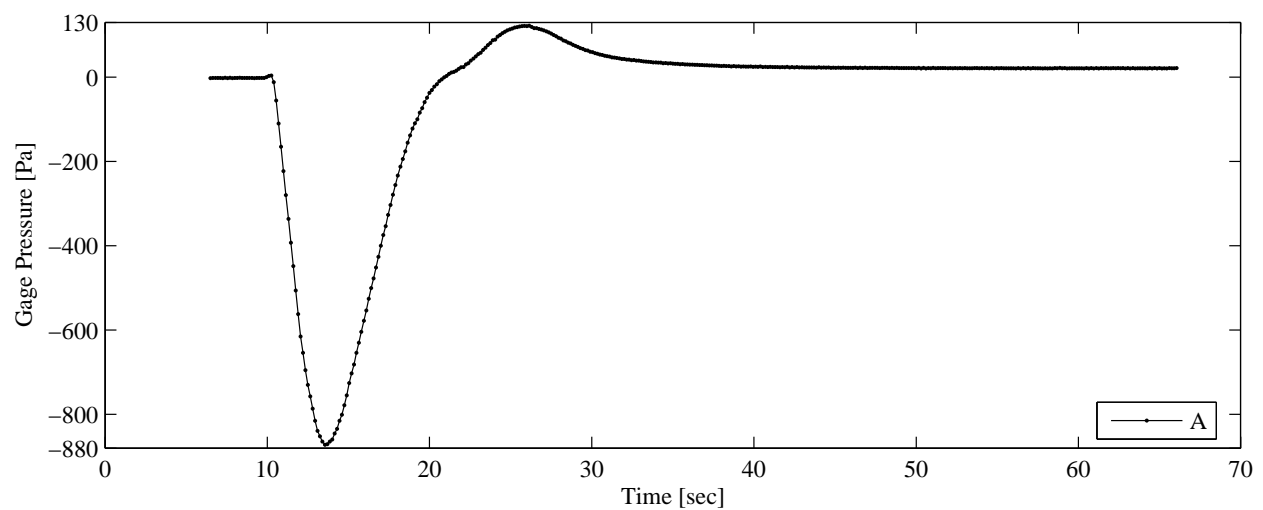


Figure D.9: Ambient pressure data during discharge for test no. 10 (FK-5-1-12)

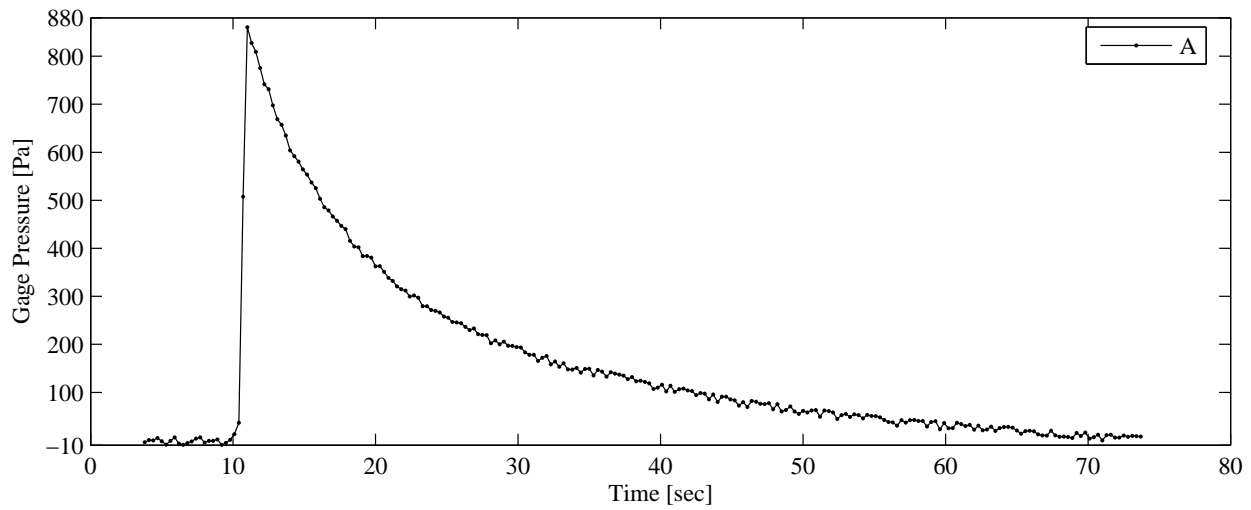


Figure D.10: Ambient pressure data during discharge for test no. 11 (IG-541)

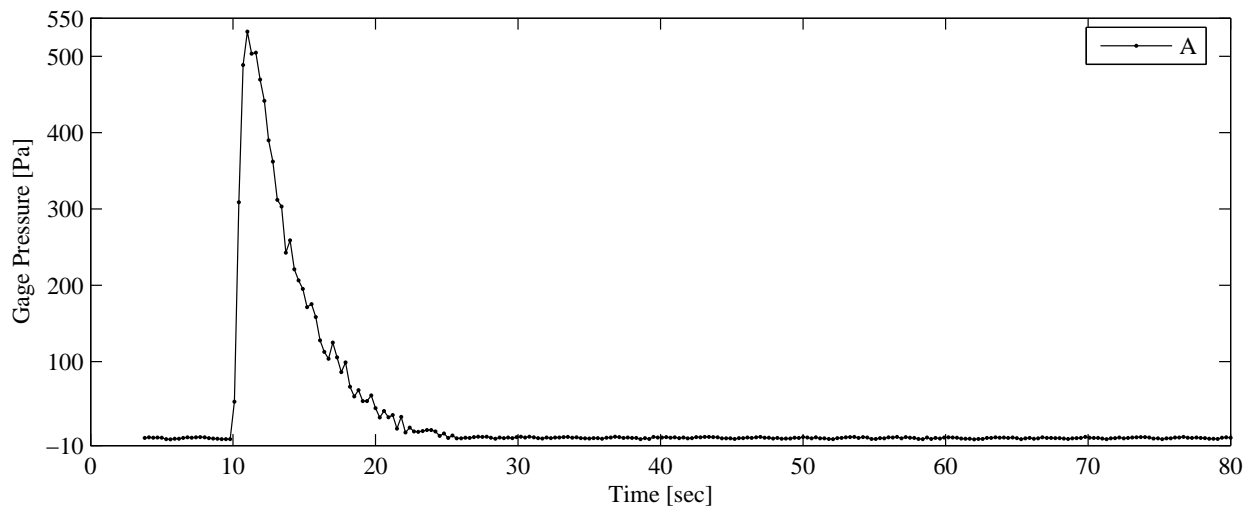


Figure D.11: Ambient pressure data during discharge for test no. 12 (IG-541)

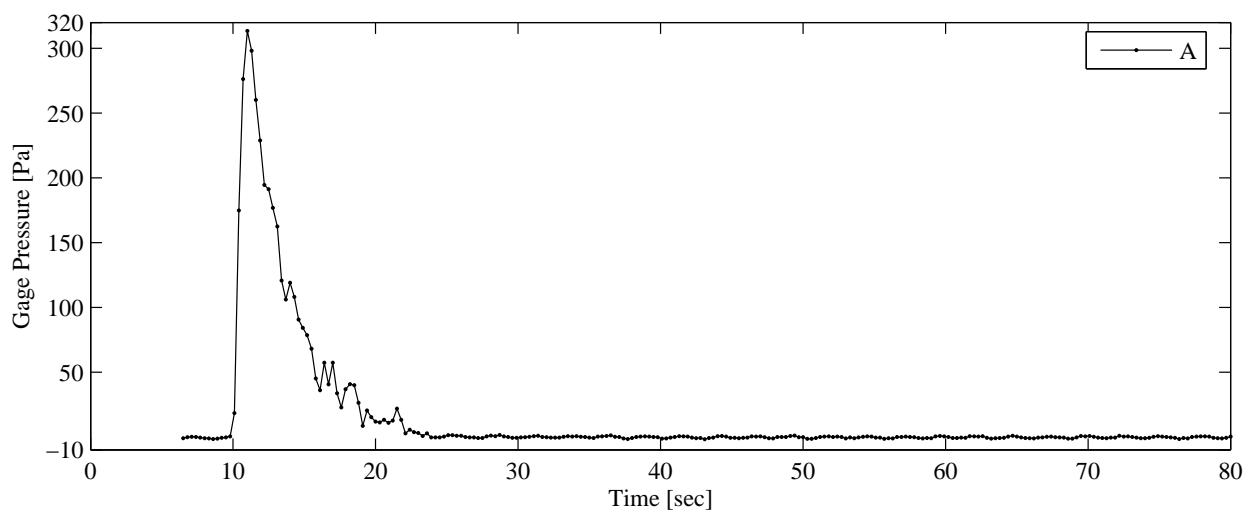


Figure D.12: Ambient pressure data during discharge for test no. 13 (IG-541)

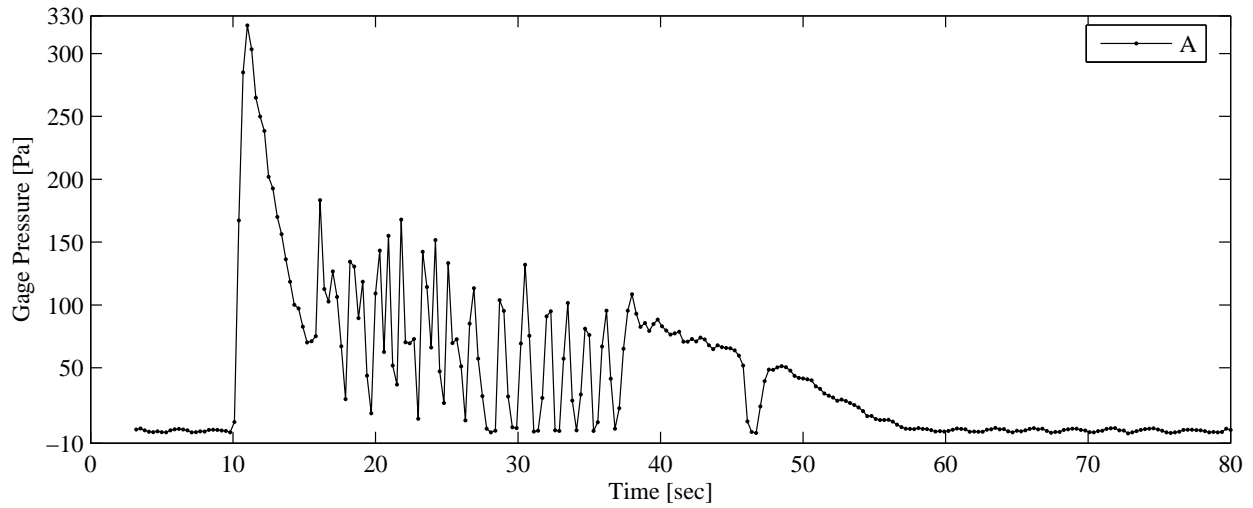


Figure D.13: Ambient pressure data during discharge for test no. 14 (IG-541)

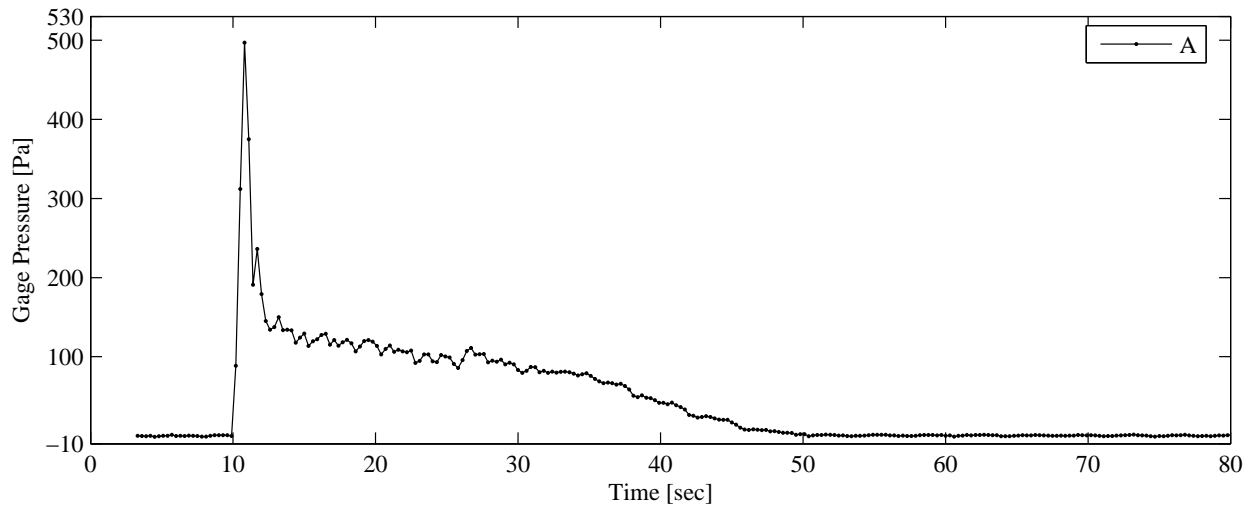


Figure D.14: Ambient pressure data during discharge for test no. 15 (IG-541)

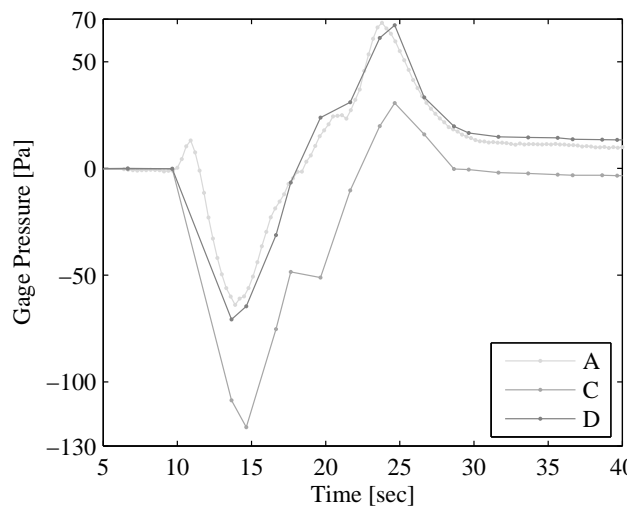


Figure D.15: Test no. 16 (HFC-125)

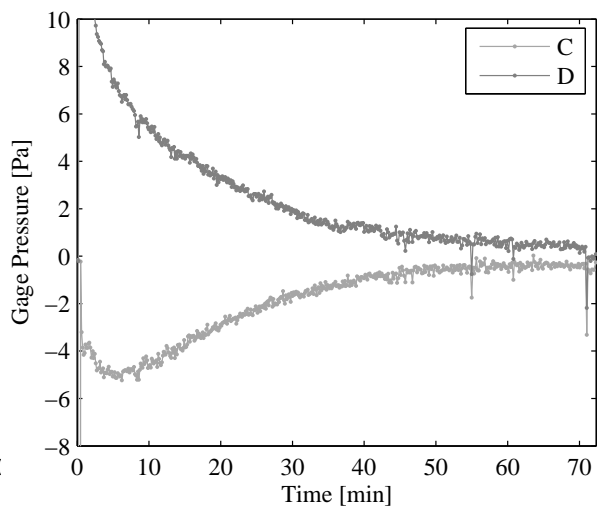


Figure D.16: Test No. 16 (HFC-125)

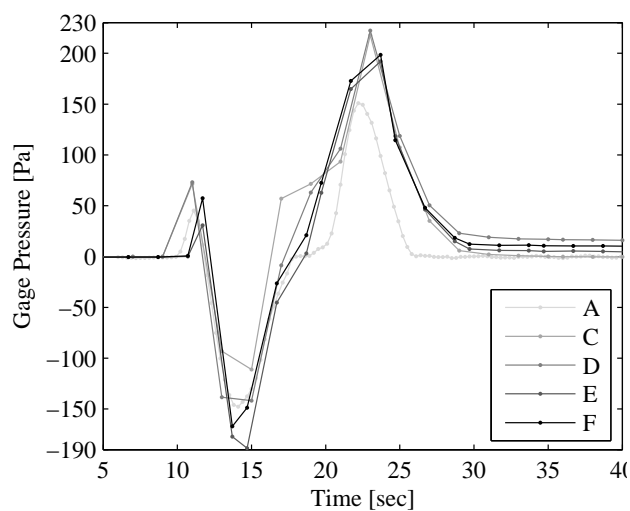


Figure D.17: Test no. 17 (HFC-125)

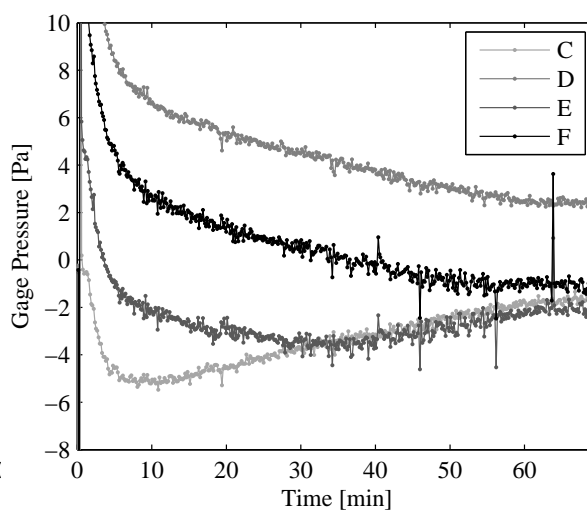


Figure D.18: Test No. 17 (HFC-125)

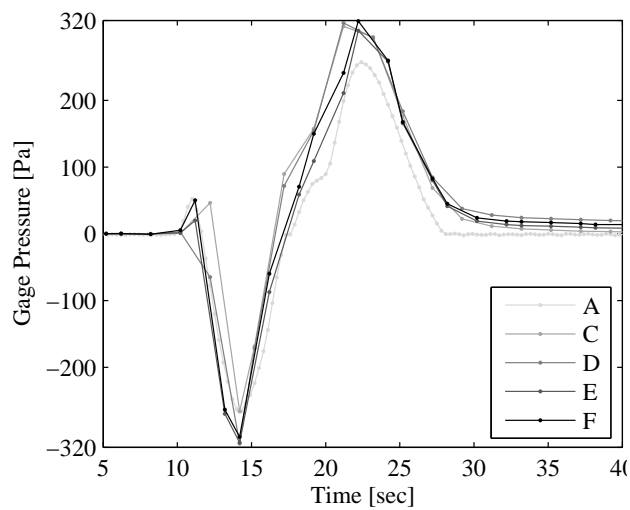


Figure D.19: Test no. 18 (HFC-125)

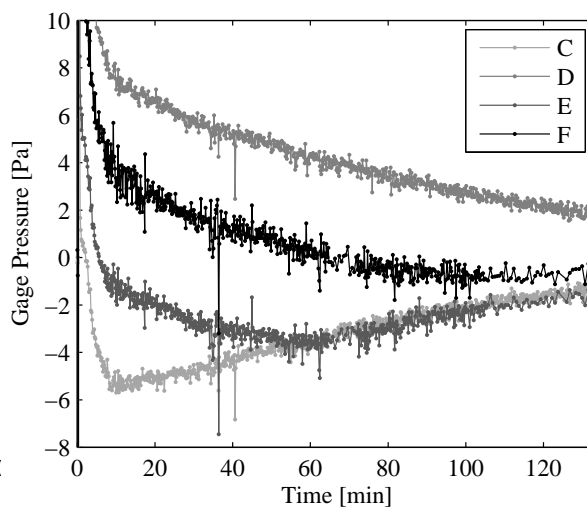


Figure D.20: Test No. 18 (HFC-125)

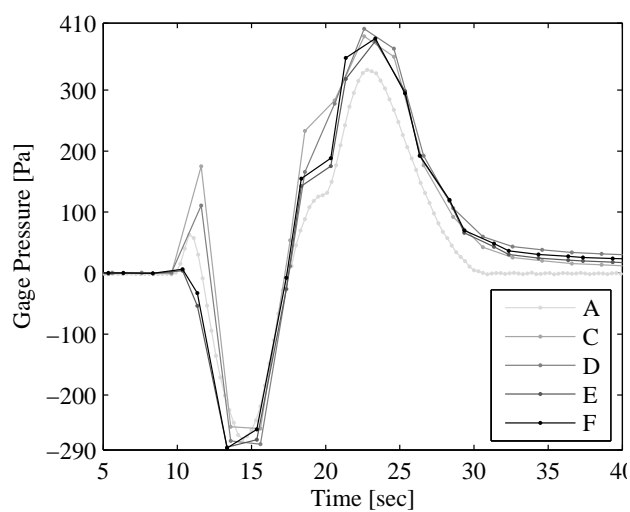


Figure D.21: Test no. 19 (HFC-125)

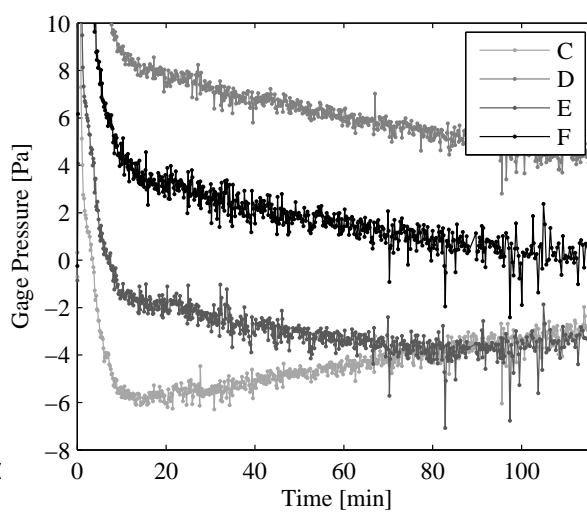


Figure D.22: Test No. 19 (HFC-125)

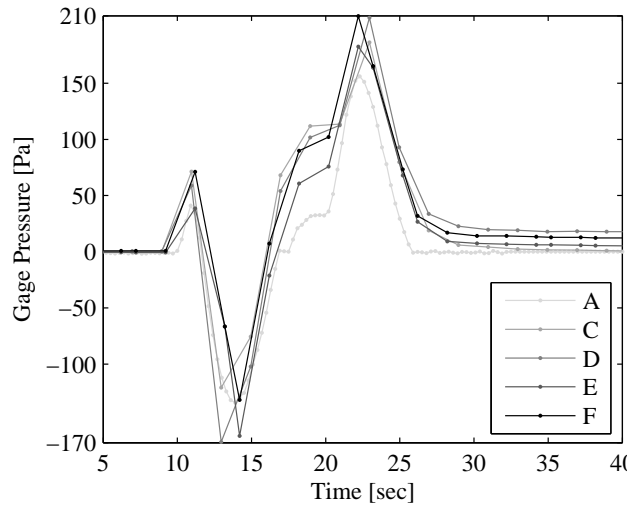


Figure D.23: Test no. 20 (HFC-125)

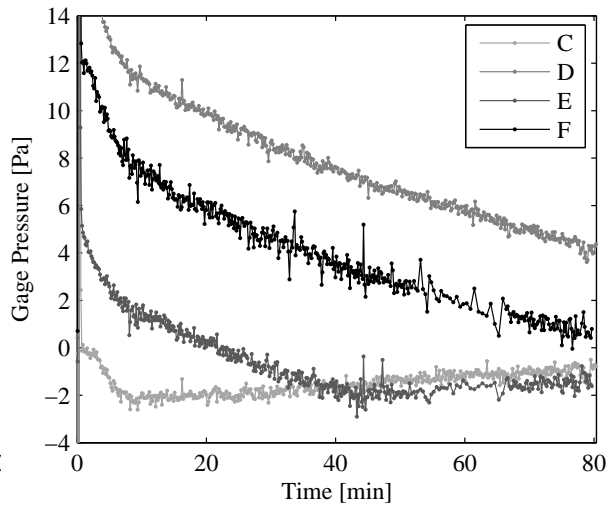


Figure D.24: Test No. 20 (HFC-125)

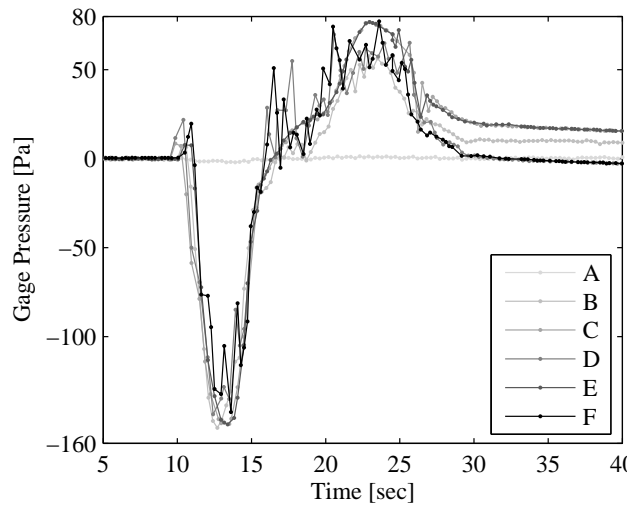


Figure D.25: Test no. 21 (HFC-227ea)

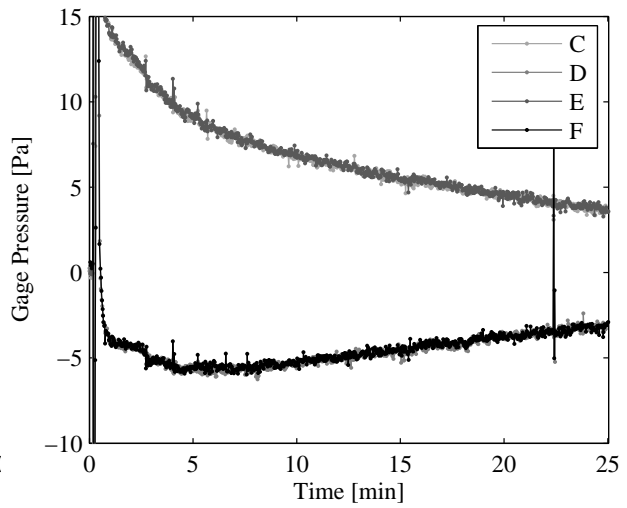


Figure D.26: Test No. 21 (HFC-227ea)

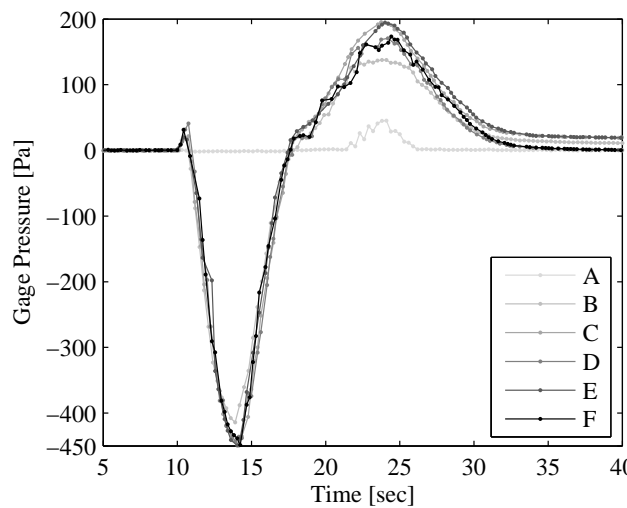


Figure D.27: Test no. 22 (HFC-227ea)

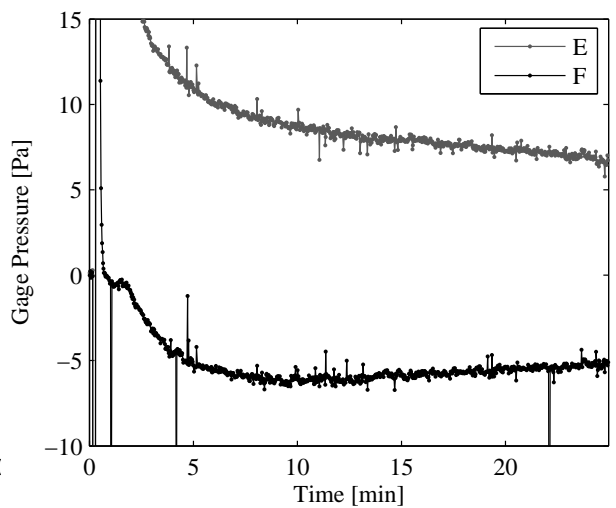


Figure D.28: Test No. 22 (HFC-227ea)

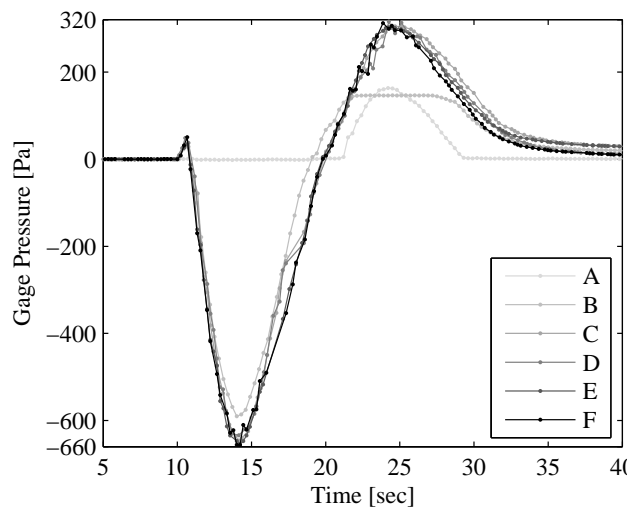


Figure D.29: Test no. 23 (HFC-227ea)

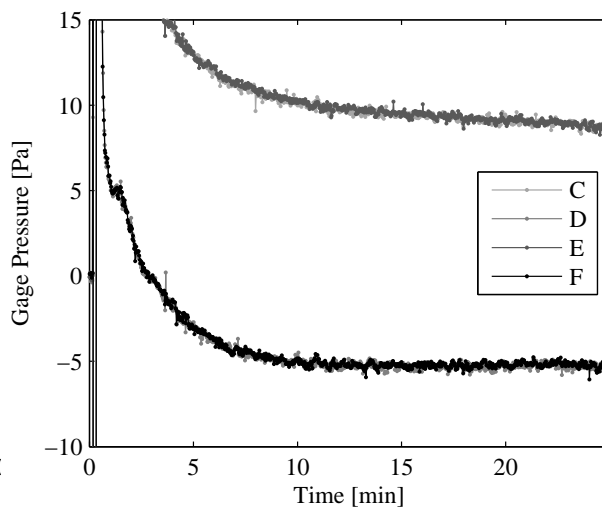


Figure D.30: Test No. 23 (HFC-227ea)

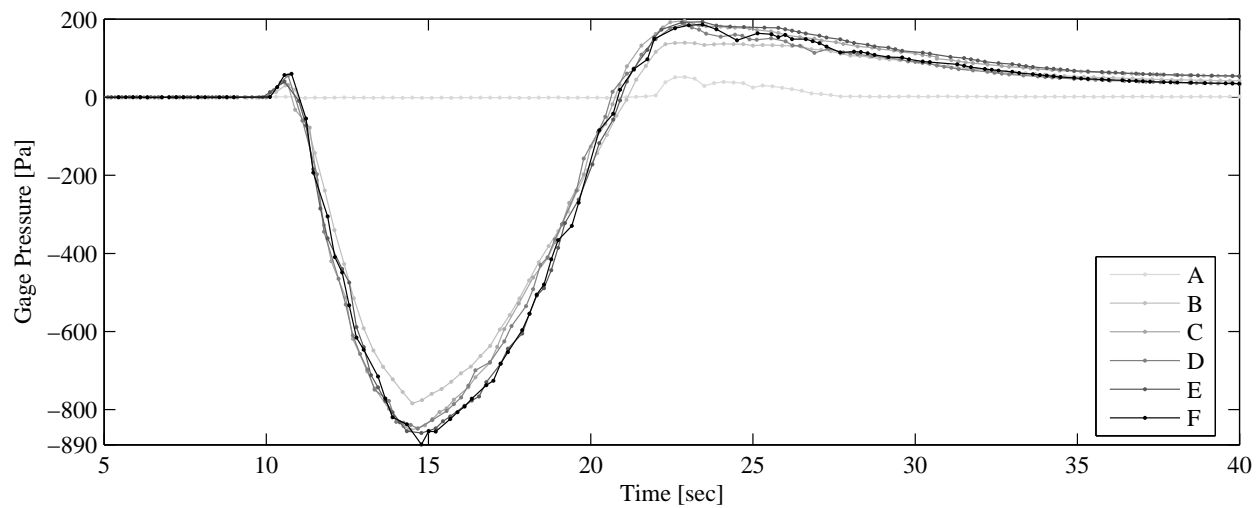


Figure D.31: Ambient pressure data during discharge for test no. 24 (HFC-227ea)

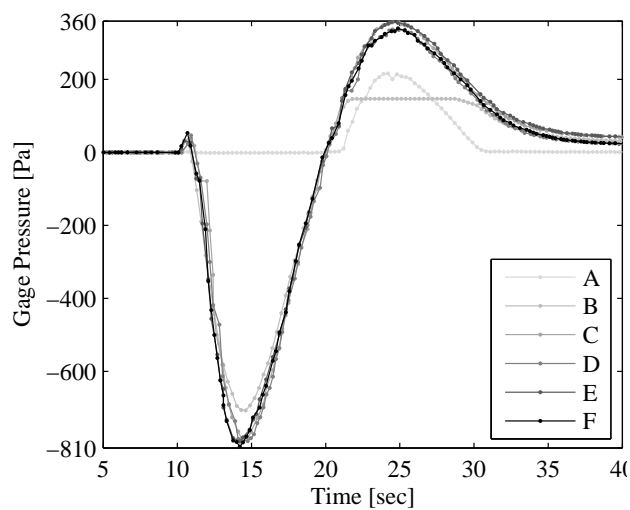


Figure D.32: Test no. 25 (HFC-227ea)

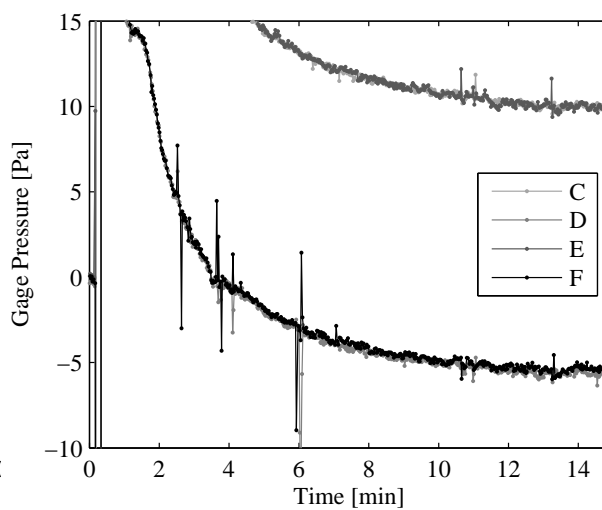


Figure D.33: Test No. 25 (HFC-227ea)

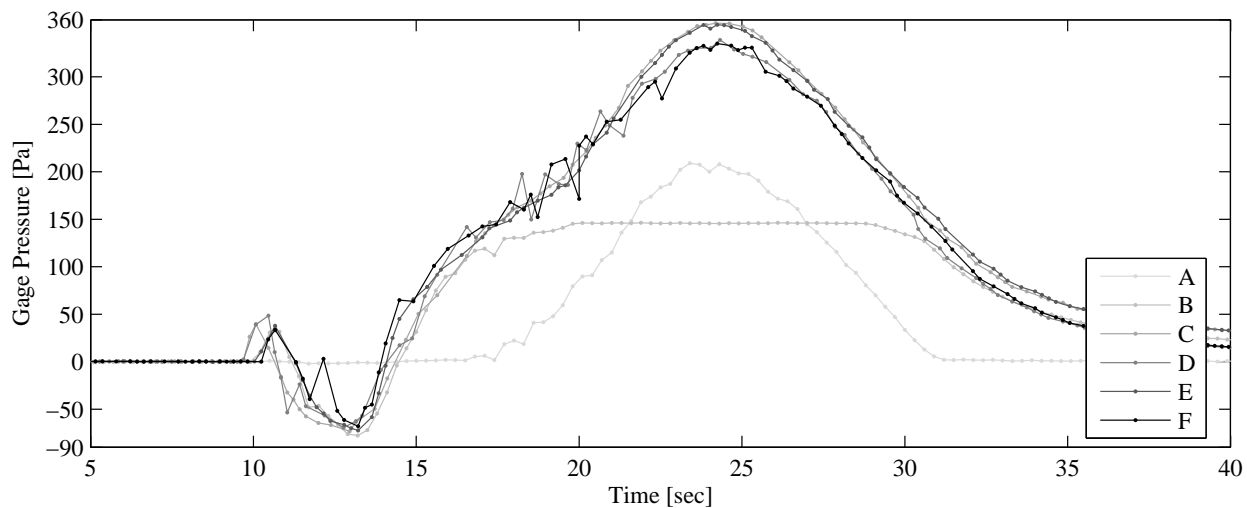


Figure D.34: Ambient pressure data during discharge for test no. 26 (HFC-227ea)

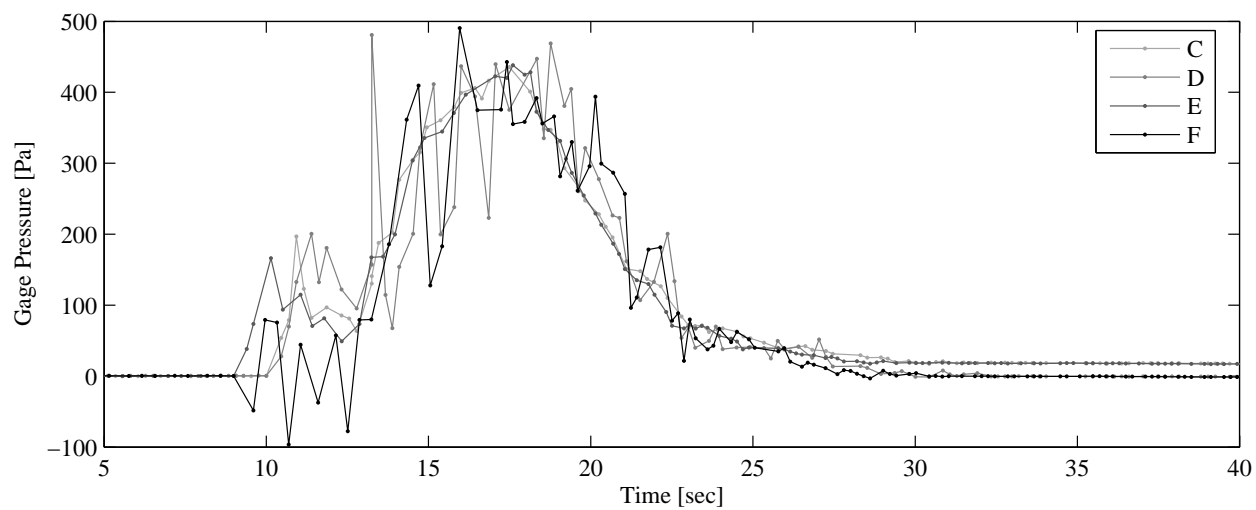


Figure D.35: Ambient pressure data during discharge for test no. 27 (HFC-23)

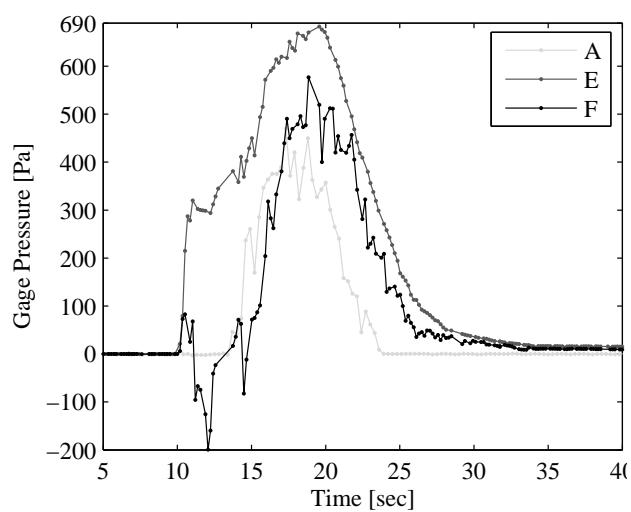


Figure D.36: Test no. 28 (HFC-23)

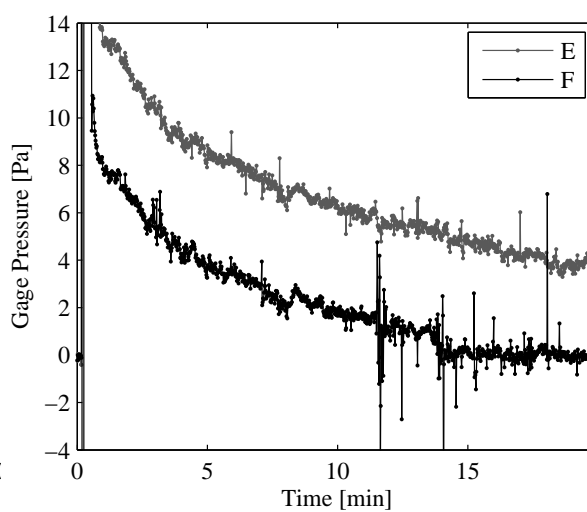


Figure D.37: Test No. 28 (HFC-23)

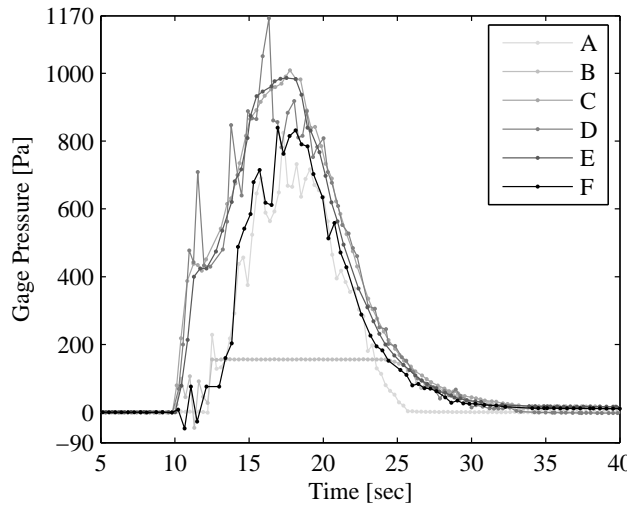


Figure D.38: Test no. 29 (HFC-23)

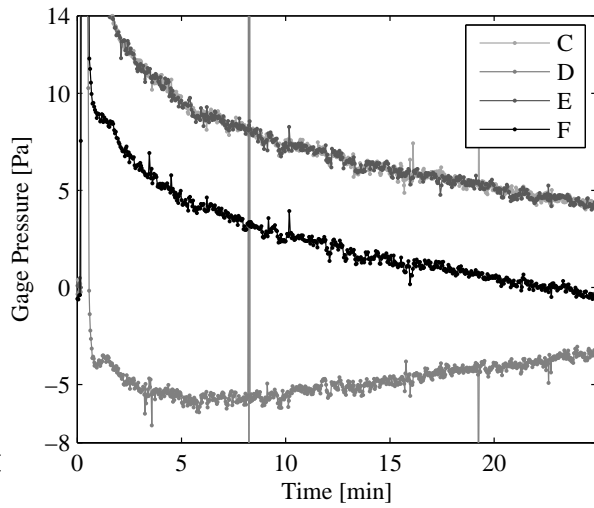


Figure D.39: Test No. 29 (HFC-23)

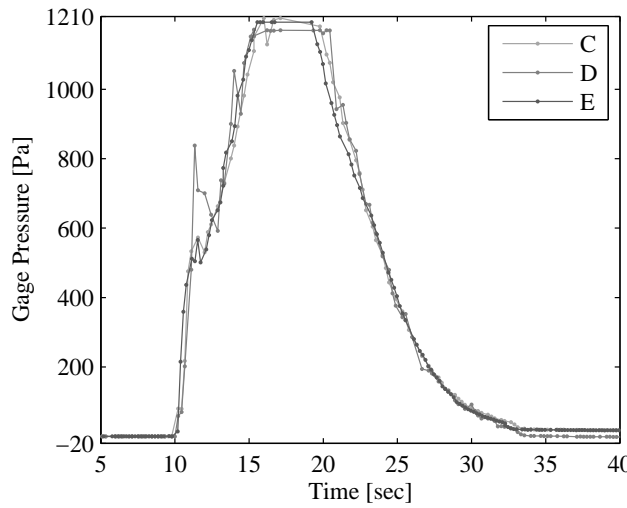


Figure D.40: Test no. 30 (HFC-23)

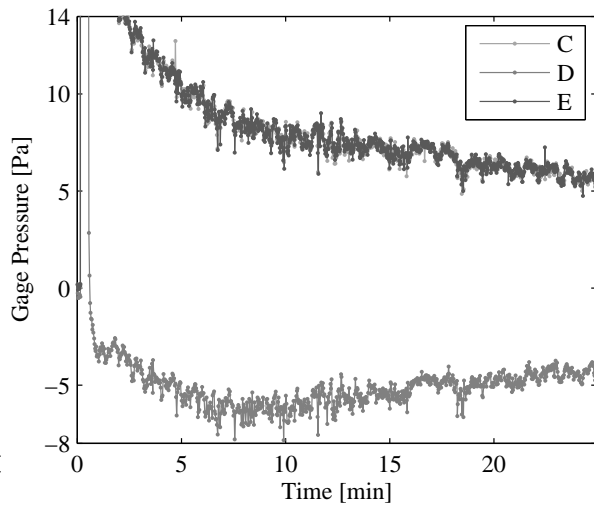


Figure D.41: Test No. 30 (HFC-23)

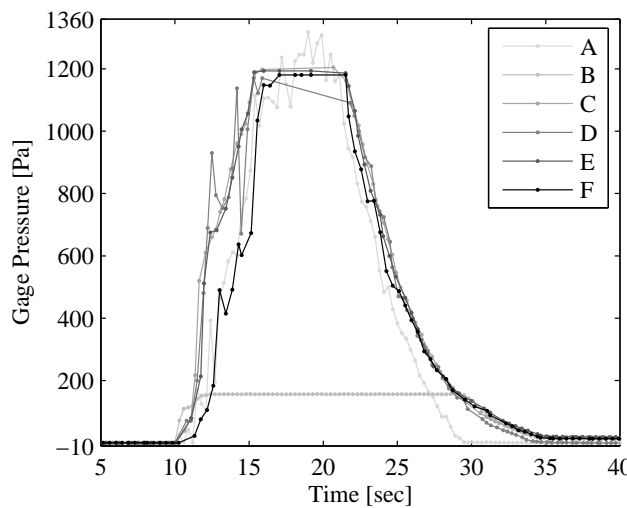


Figure D.42: Test no. 31 (HFC-23)

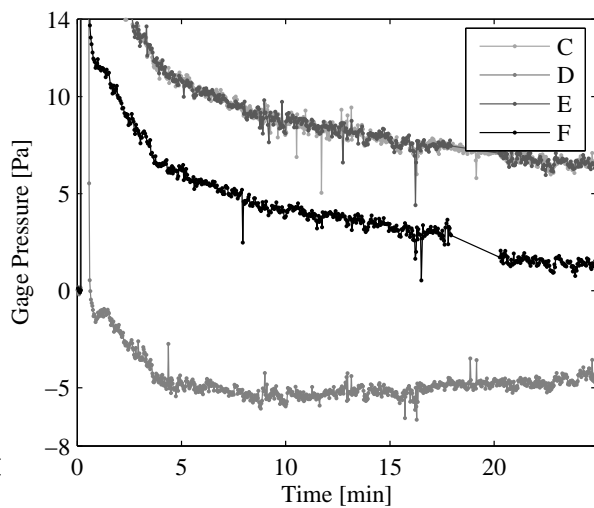


Figure D.43: Test No. 31 (HFC-23)

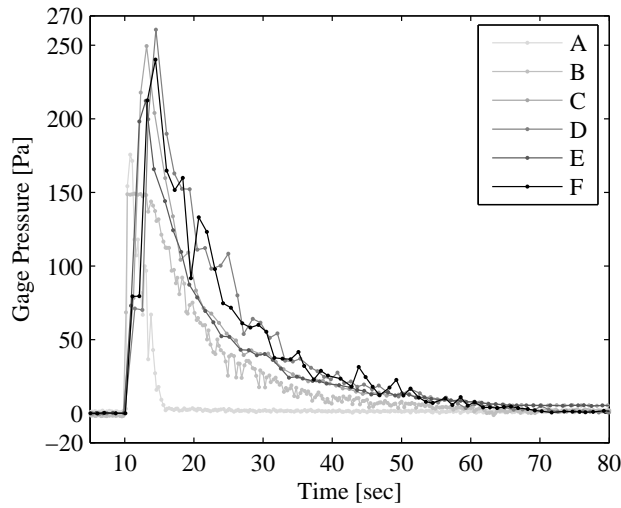


Figure D.44: Test no. 32 (IG-55)

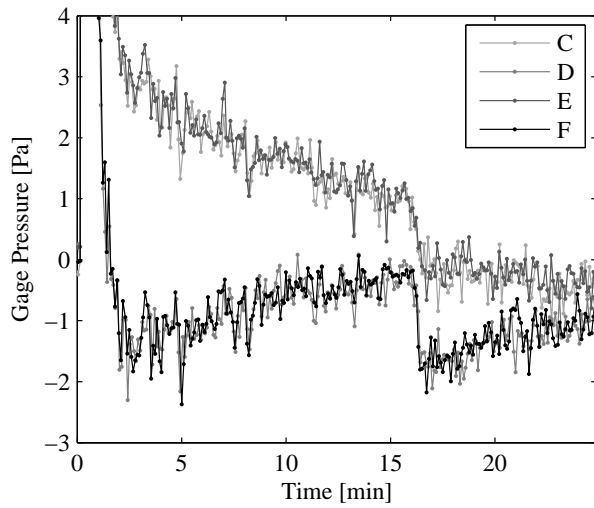


Figure D.45: Test No. 32 (IG-55)

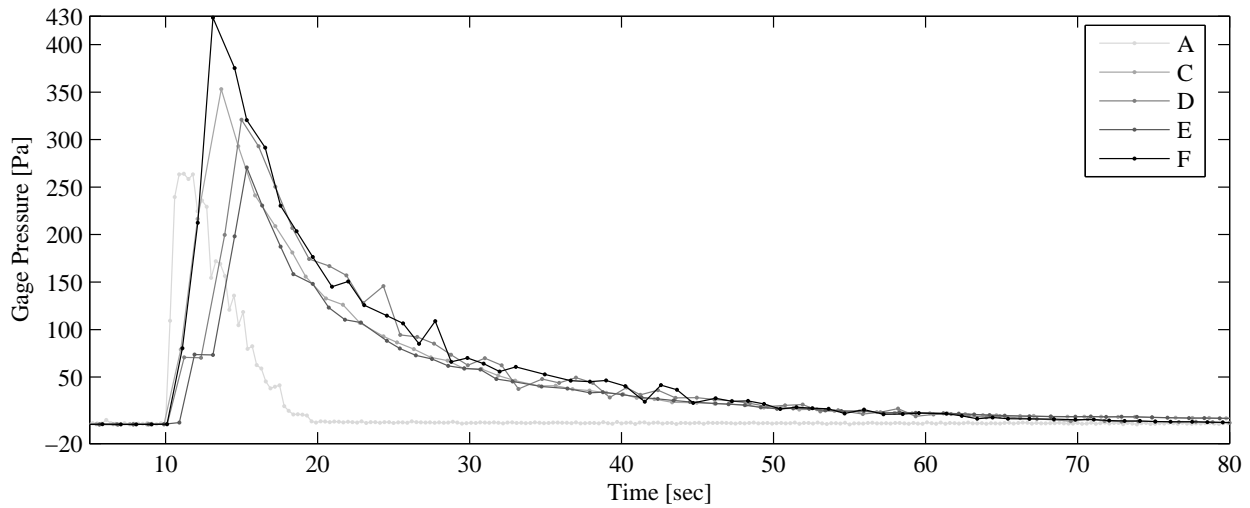


Figure D.46: Ambient pressure data during discharge for test no. 33 (IG-55)

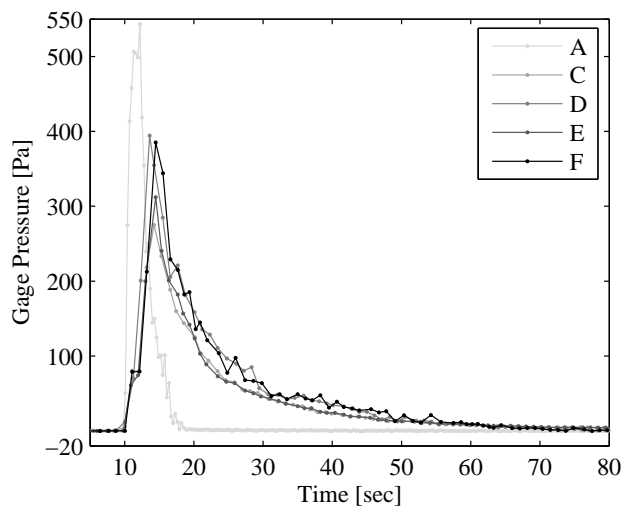


Figure D.47: Test no. 34 (IG-55)

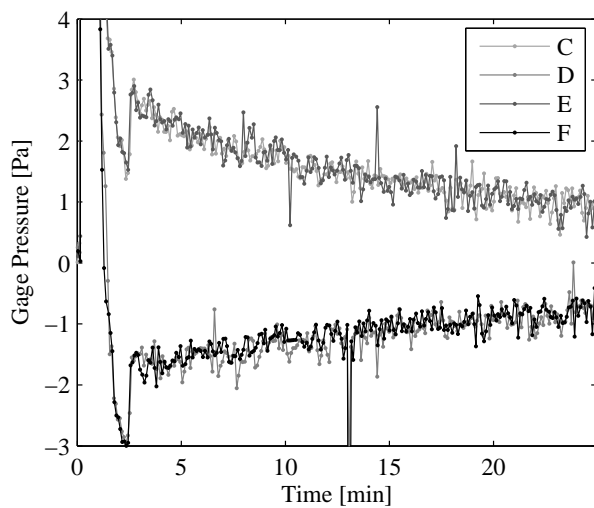


Figure D.48: Test No. 34 (IG-55)

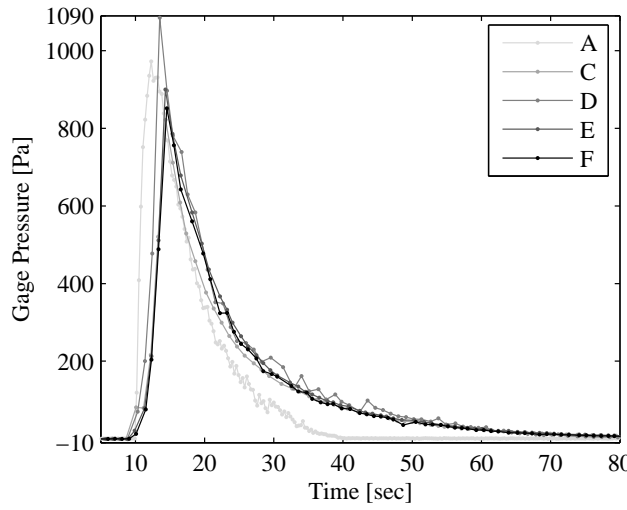


Figure D.49: Test no. 35 (IG-55)

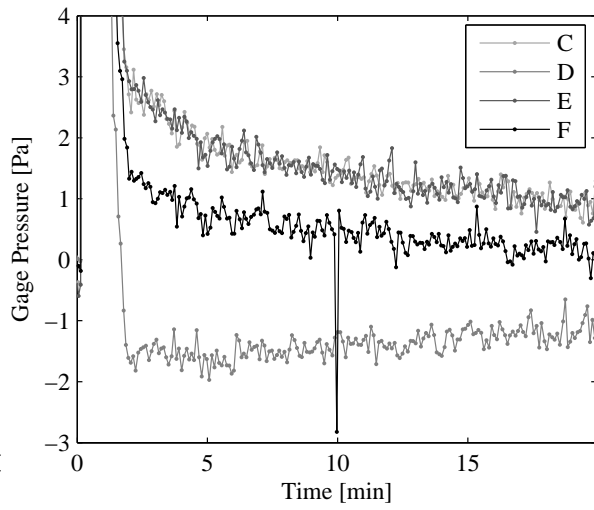


Figure D.50: Test No. 35 (IG-55)

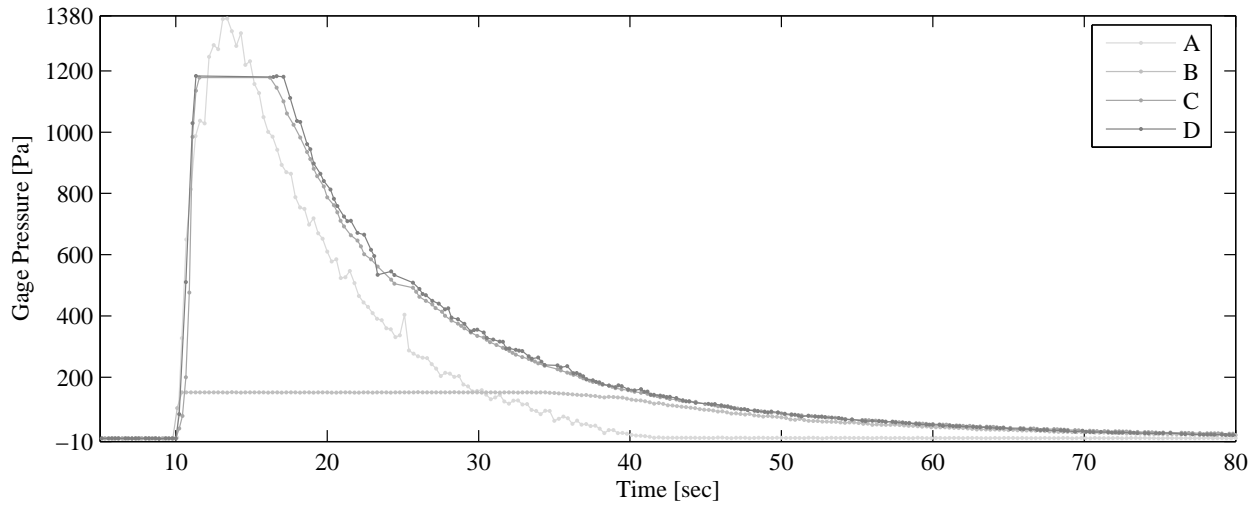


Figure D.51: Ambient pressure data during discharge for test no. 36 (IG-55)

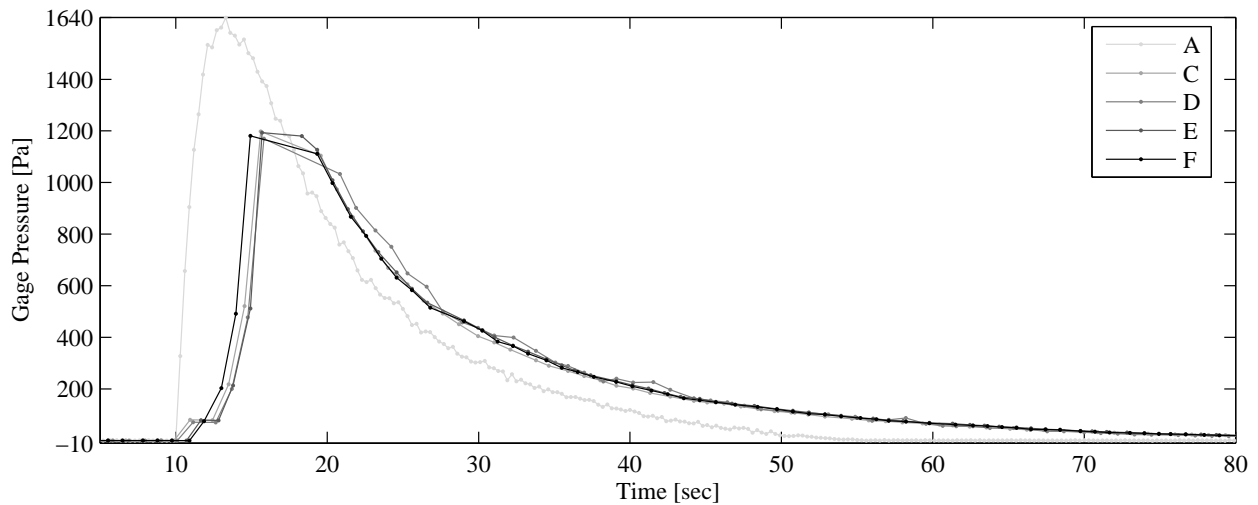


Figure D.52: Ambient pressure data during discharge for test no. 37 (IG-55)

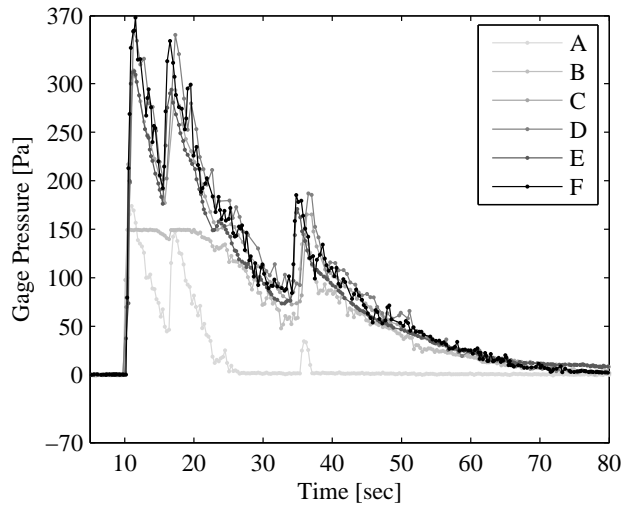


Figure D.53: Test no. 38 (IG-55P)

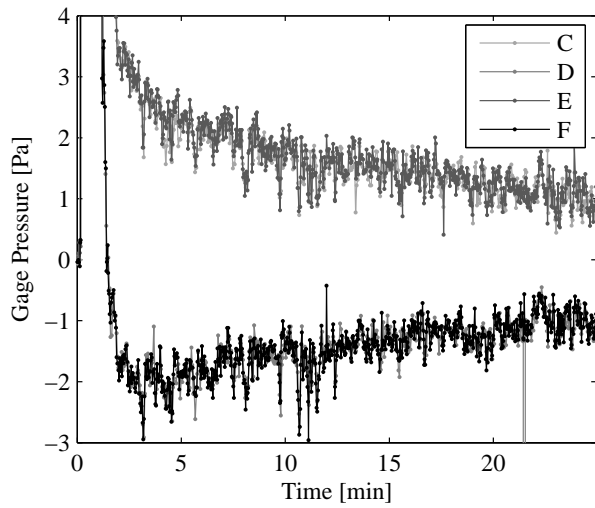


Figure D.54: Test No. 38 (IG-55P)

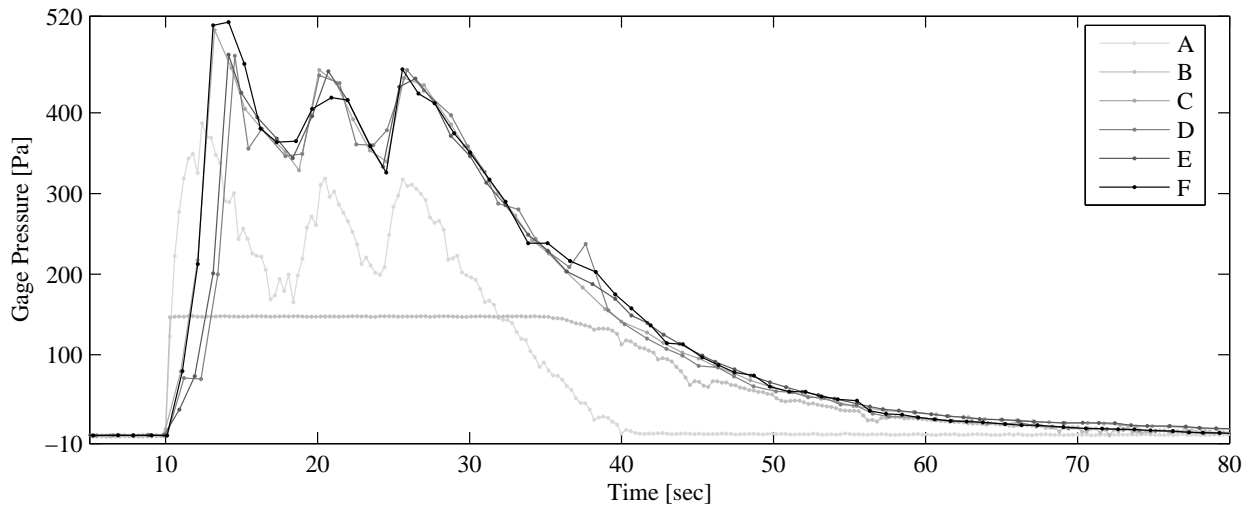


Figure D.55: Ambient pressure data during discharge for test no. 39 (IG-55P)

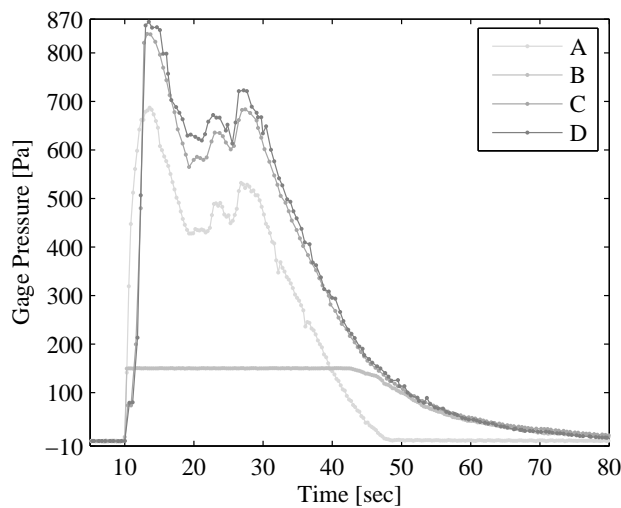


Figure D.56: Test no. 40 (IG-55P)

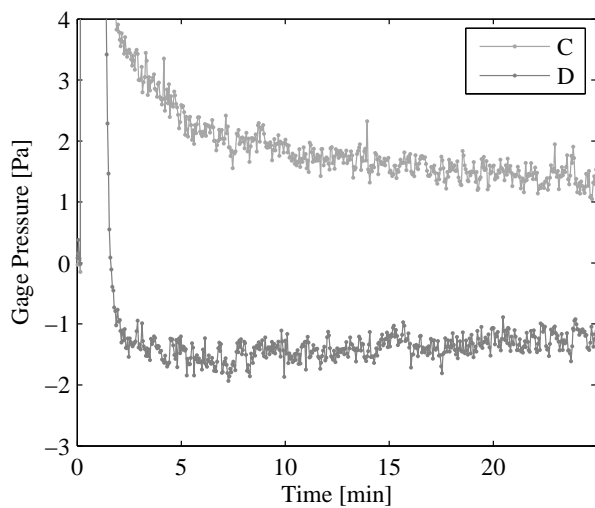


Figure D.57: Test No. 40 (IG-55P)

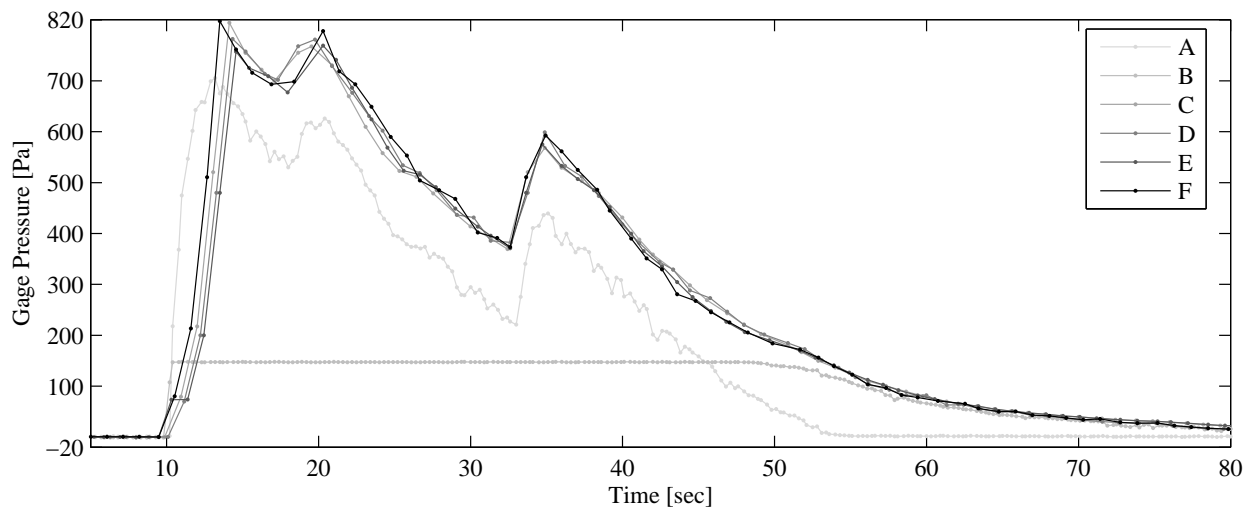


Figure D.58: Ambient pressure data during discharge for test no. 41 (IG-55P)

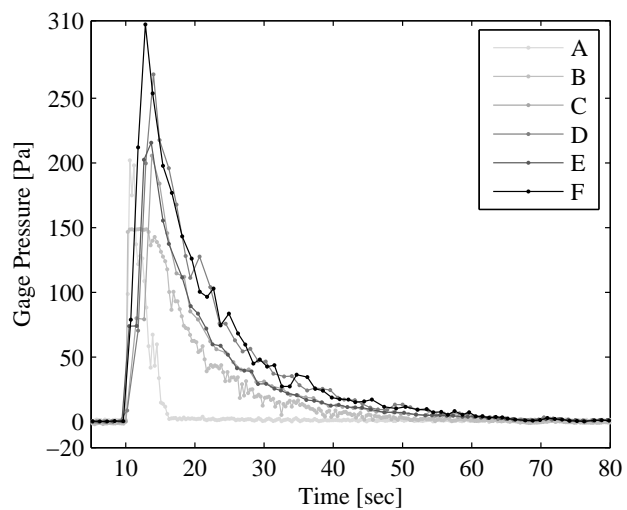


Figure D.59: Test no. 42 (IG-100)

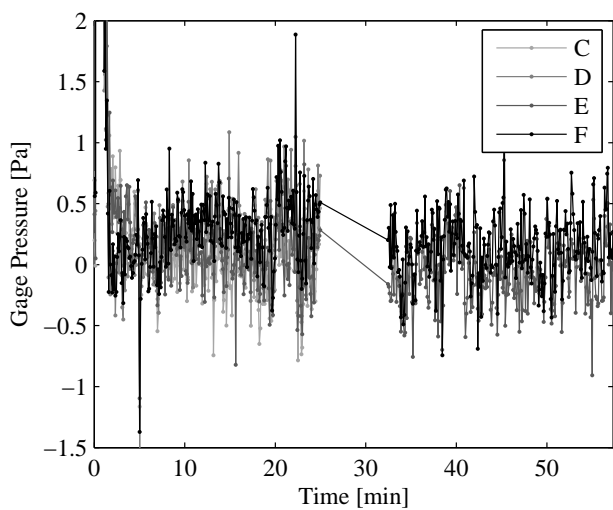


Figure D.60: Test No. 42 (IG-100)

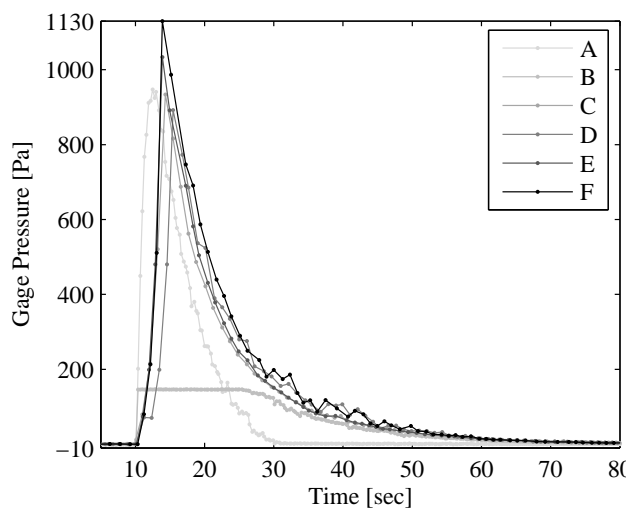


Figure D.61: Test no. 43 (IG-100)

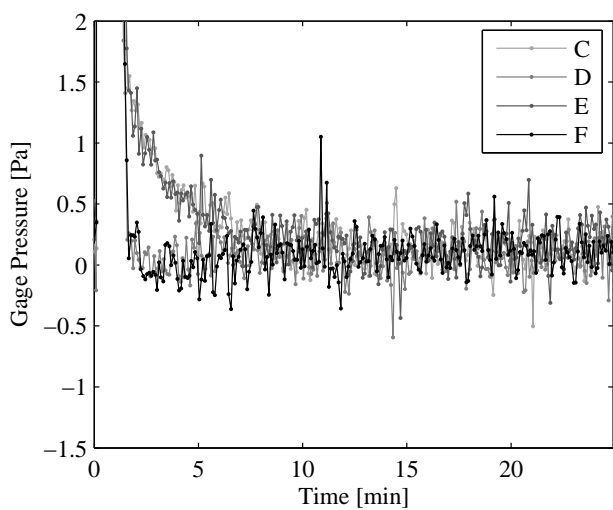


Figure D.62: Test No. 43 (IG-100)

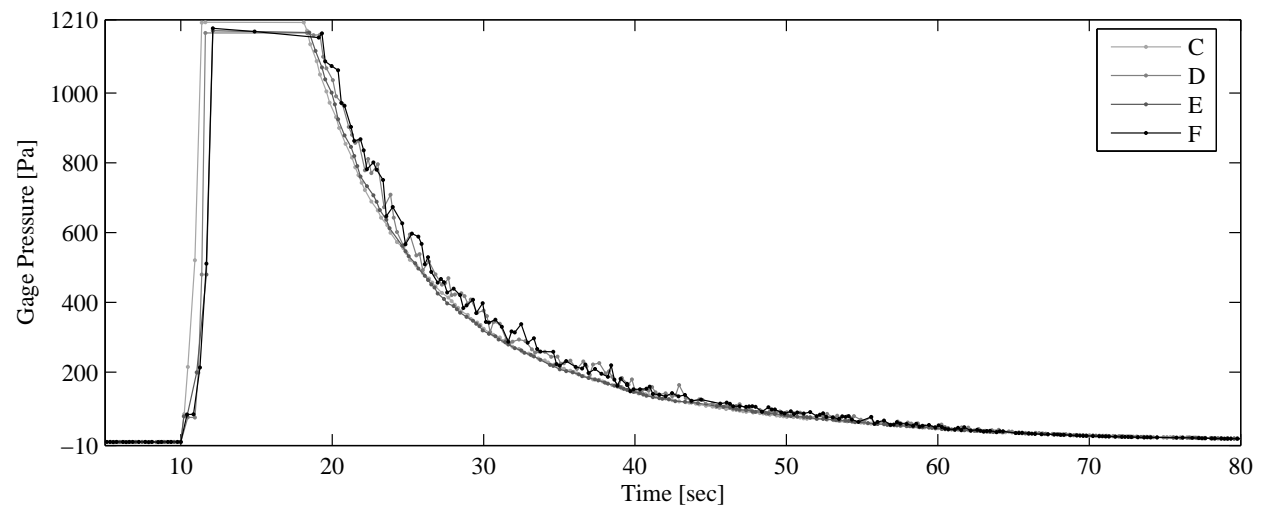


Figure D.63: Ambient pressure data during discharge for test no. 44 (IG-100)

Appendix E

Nozzle Pressure Data

Every conducted experiment begins is initiated via manual activation of the charged total flooding fire suppression system. For the various agent types used, a different system design was installed. The system is comprised of the number and type of pressurized agent storage cylinders, the dip tube and valve assembly, the cylinders to pipe network manifold (if used), the elevation change, equivalent length and diameter of the agent delivery pipe network and the discharge nozzle (within the experimental envelope). Depending on the agent type, delivery method, and hardware used the agent discharge characteristics can vary significantly.

The following of this appendix presents all the retained the nozzle pressure data. This instrument was tapped into the delivery piping approximately 6" upstream of the terminating nozzle. This data is invaluable in diagnosing system design and agent delivery issues. These data sets are of additional value in assessing the duration of discharge, a system variable that is regulated by prescriptive industry design standards.

When analyzing the ensuing figures please reference Table [A.2](#) for further information regarding the system configuration and hardware used. Note as well that the pressure transducer failed on test 30 moments after the peak nozzle pressure pulse passed.

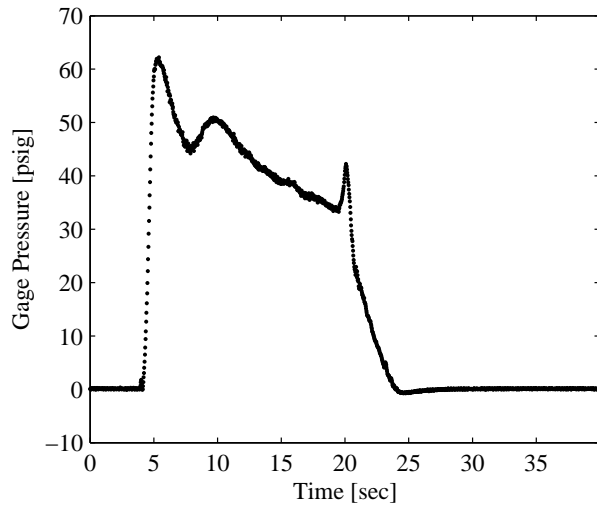


Figure E.1: Test no. 1 (HFC-227ea)

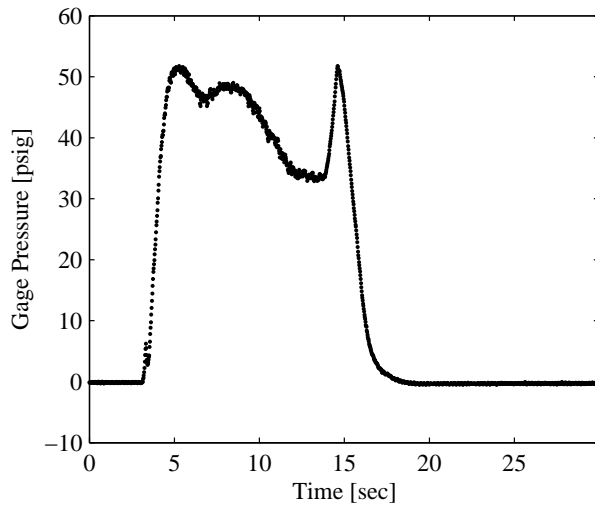


Figure E.2: Test no. 2 (HFC-227ea)

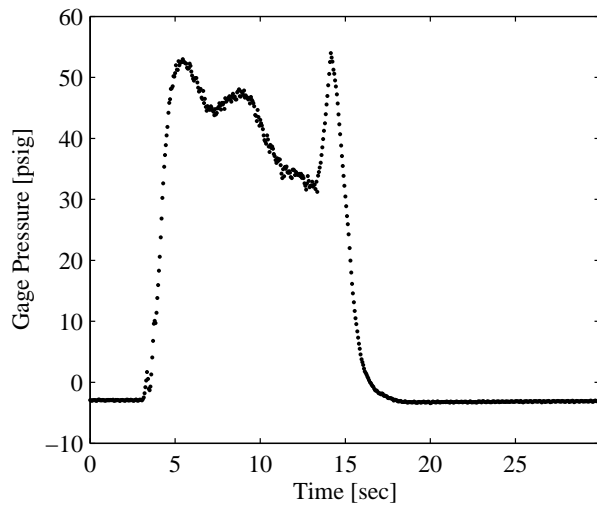


Figure E.3: Test no. 3 (HFC-227ea)

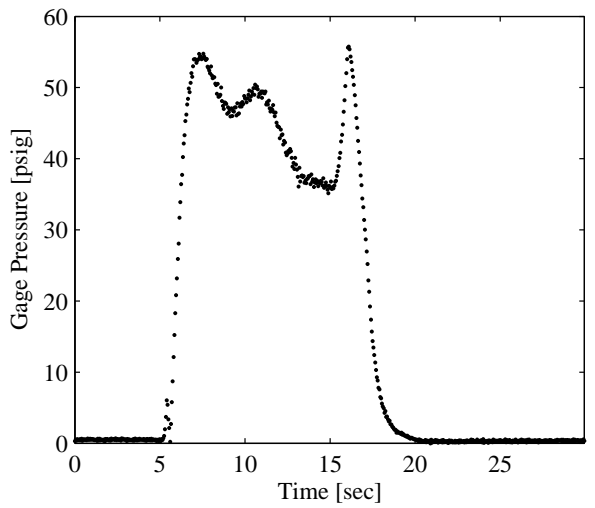


Figure E.4: Test no. 4 (HFC-227ea)

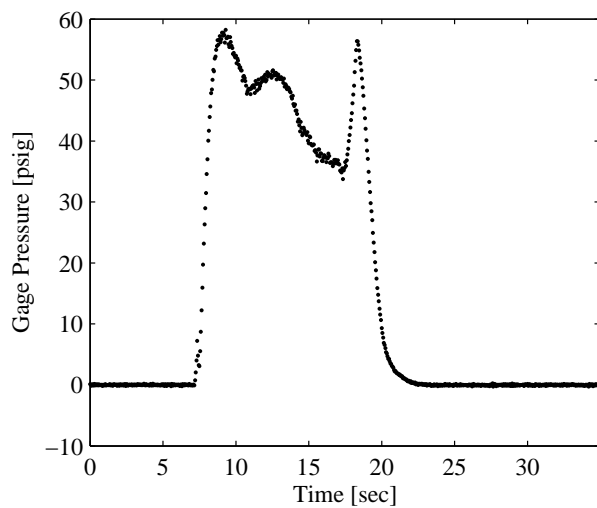


Figure E.5: Test no. 5 (HFC-227ea)

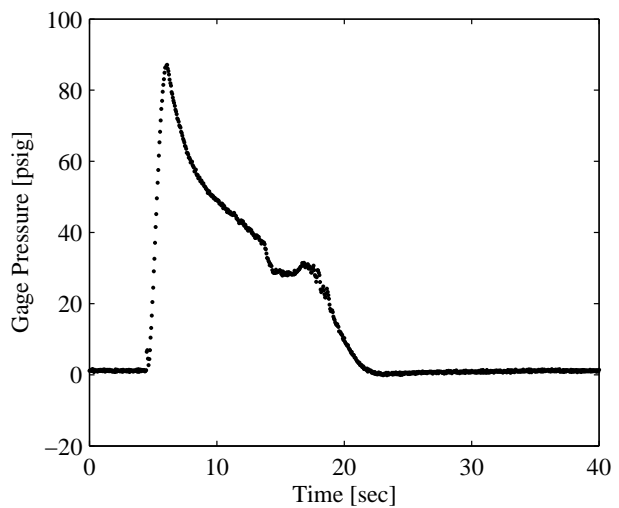


Figure E.6: Test no. 6 (FK-5-1-12)

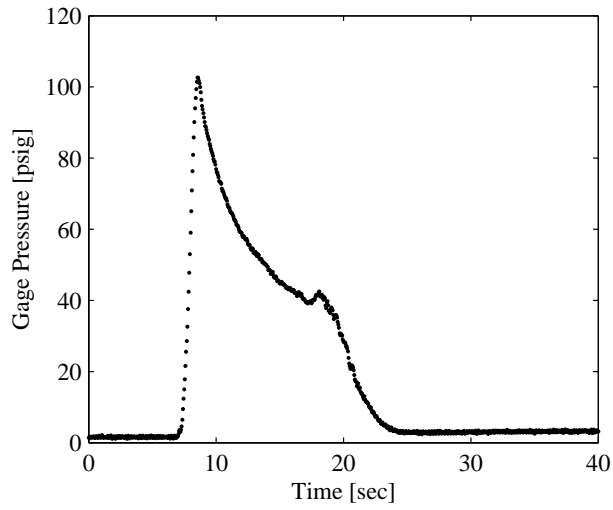


Figure E.7: Test no. 7 (FK-5-1-12)

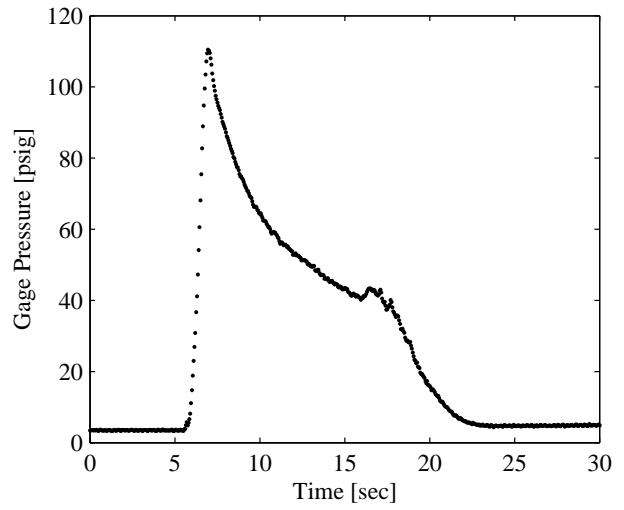


Figure E.8: Test no. 8 (FK-5-1-12)

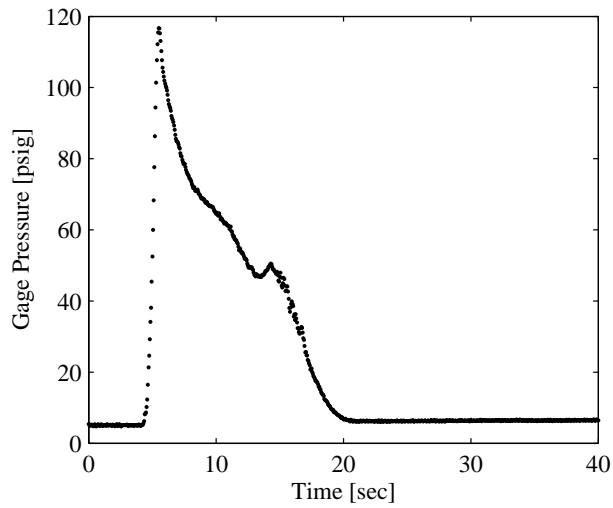


Figure E.9: Test no. 9 (FK-5-1-12)

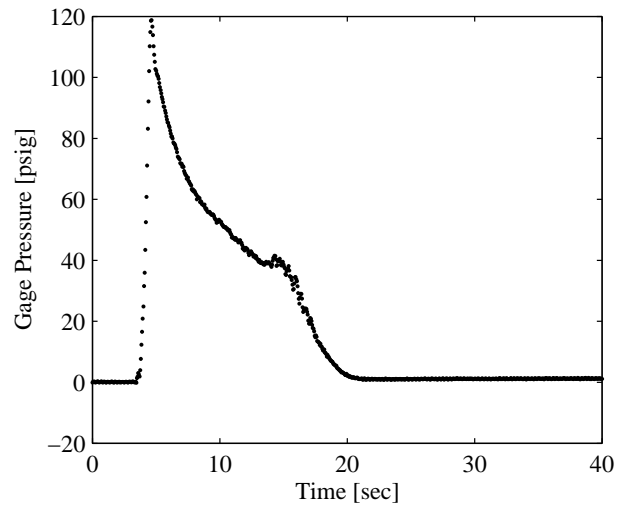


Figure E.10: Test no. 10 (FK-5-1-12)

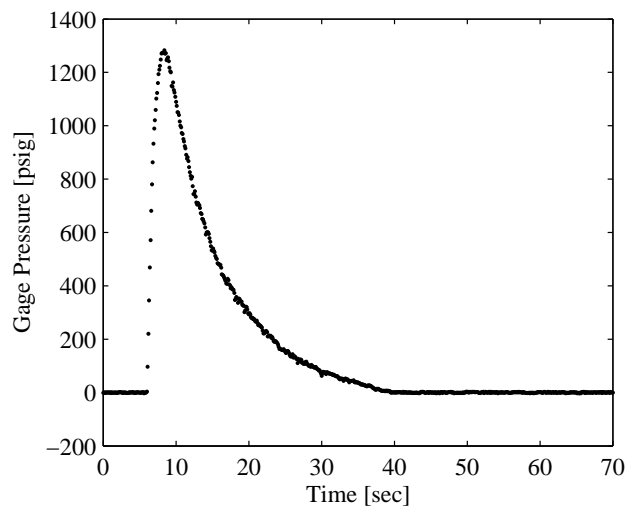


Figure E.11: Test no. 11 (IG-541)

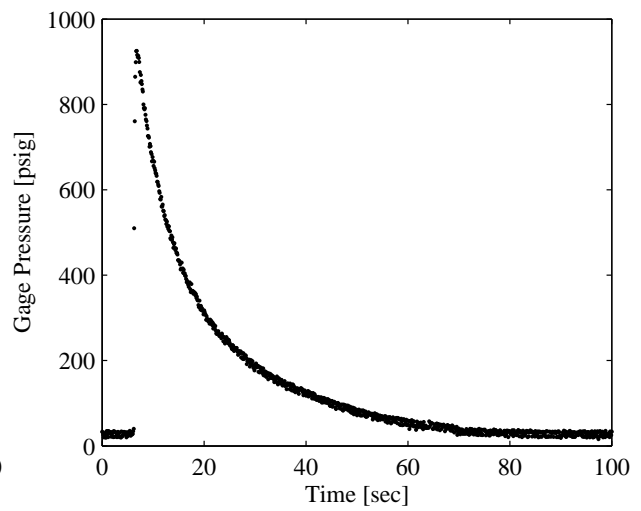


Figure E.12: Test no. 12 (IG-541)

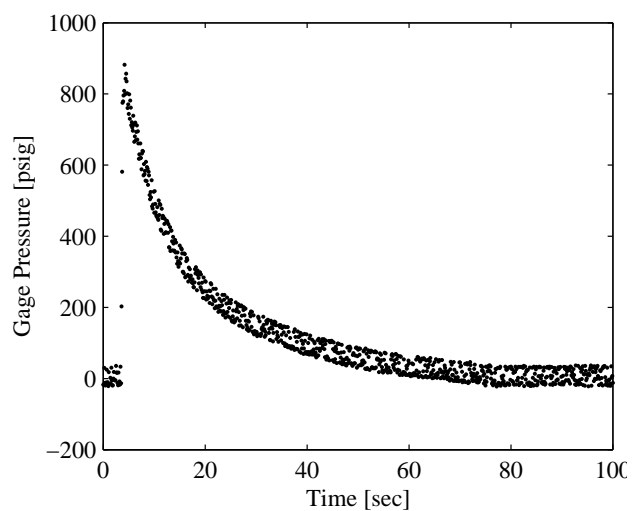


Figure E.13: Test no. 13 (IG-541)

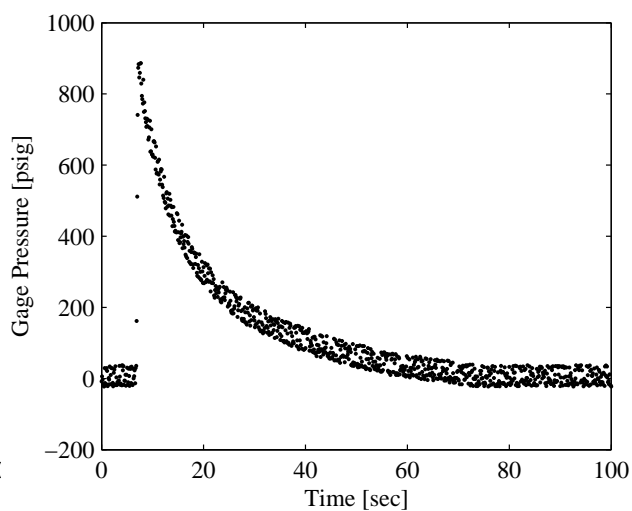


Figure E.14: Test no. 14 (IG-541)

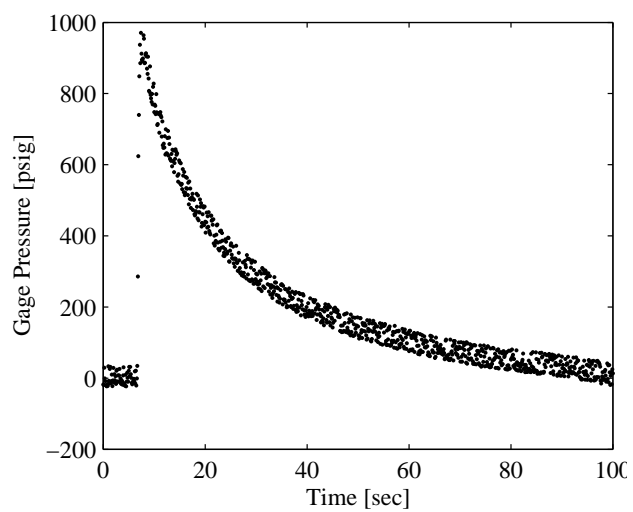


Figure E.15: Test no. 15 (IG-541)

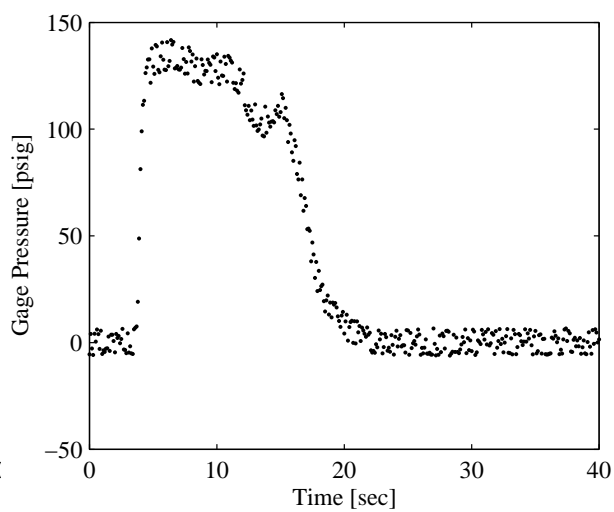


Figure E.16: Test no. 16 (HFC-125)

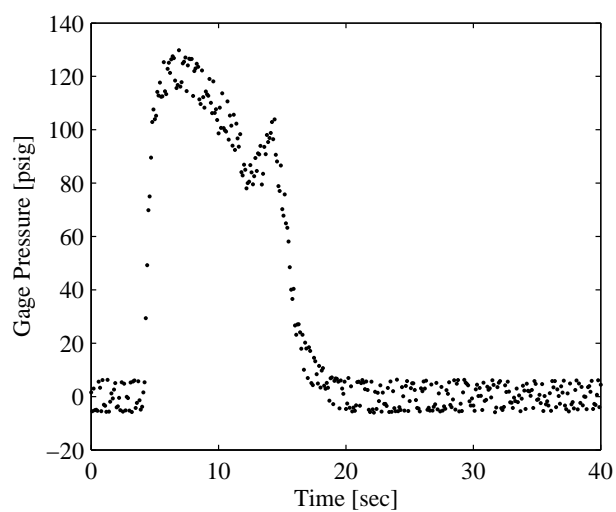


Figure E.17: Test no. 17 (HFC-125)

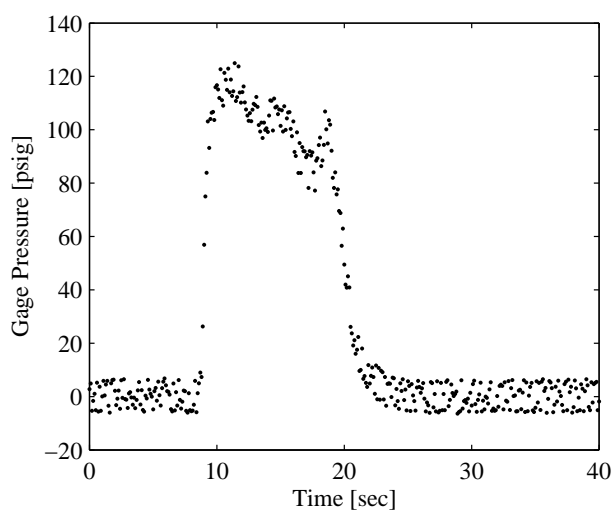


Figure E.18: Test no. 18 (HFC-125)

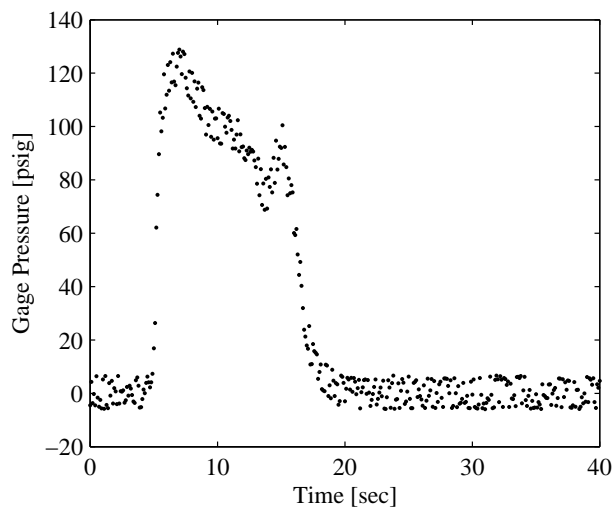


Figure E.19: Test no. 19 (HFC-125)

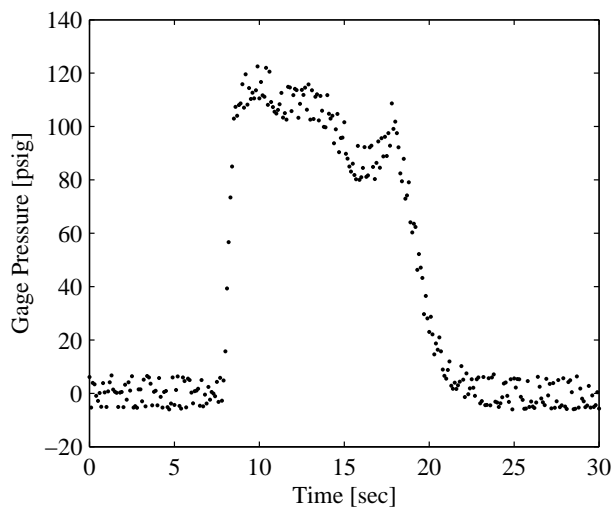


Figure E.20: Test no. 20 (HFC-125)

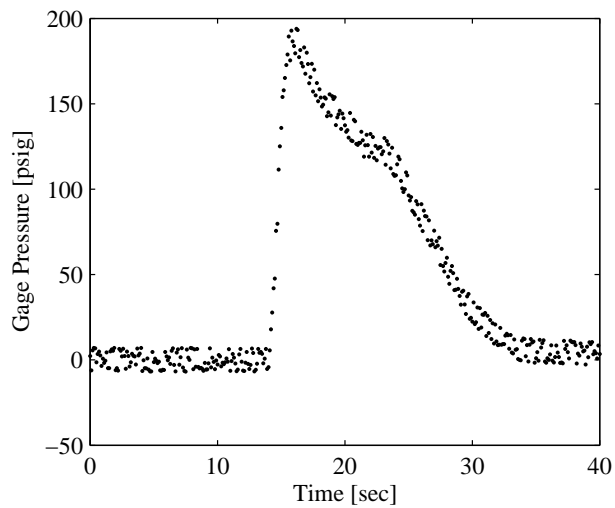


Figure E.21: Test no. 21 (HFC-227ea)

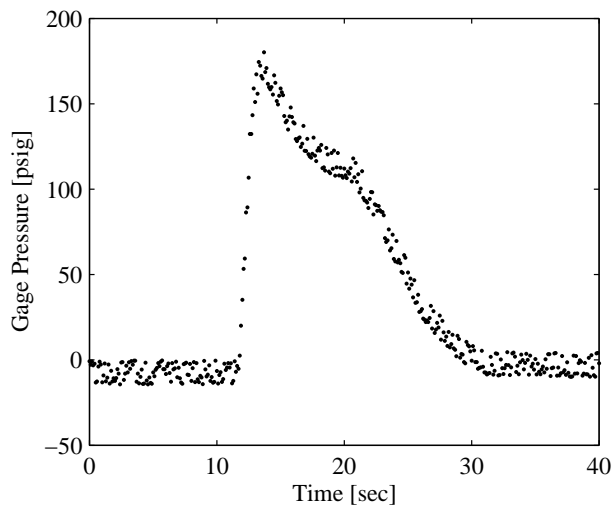


Figure E.22: Test no. 22 (HFC-227ea)

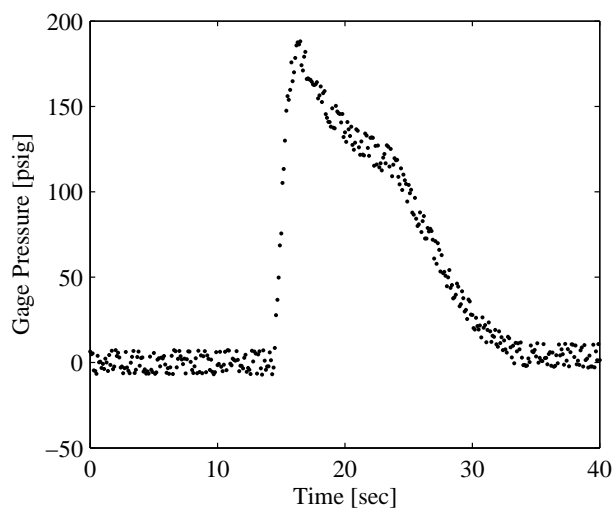


Figure E.23: Test no. 23 (HFC-227ea)

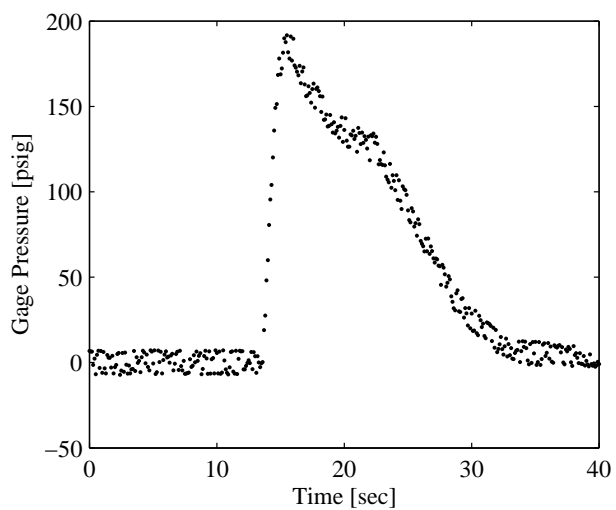


Figure E.24: Test no. 24 (HFC-227ea)

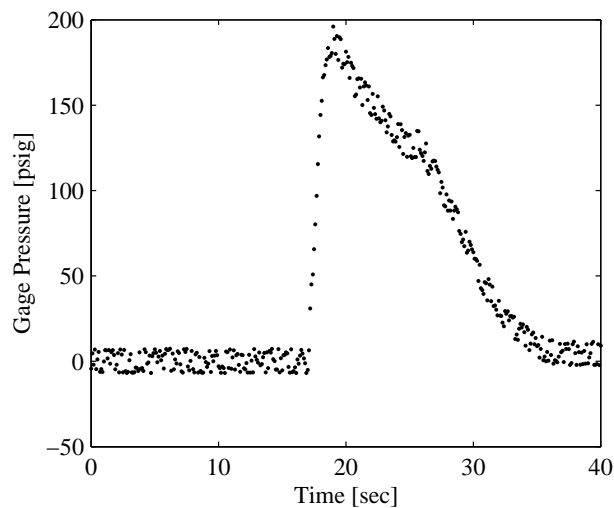


Figure E.25: Test no. 25 (HFC-227ea)

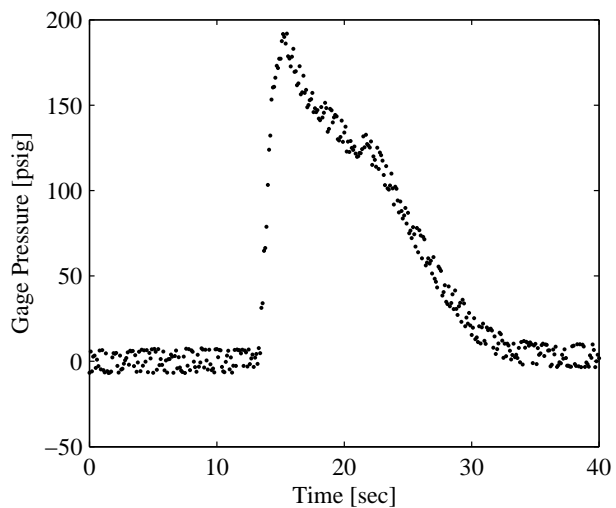


Figure E.26: Test no. 26 (HFC-227ea)

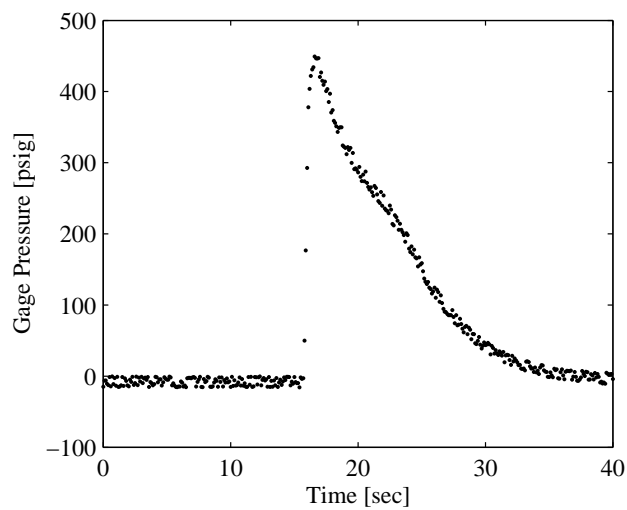


Figure E.27: Test no. 28 (HFC-23)

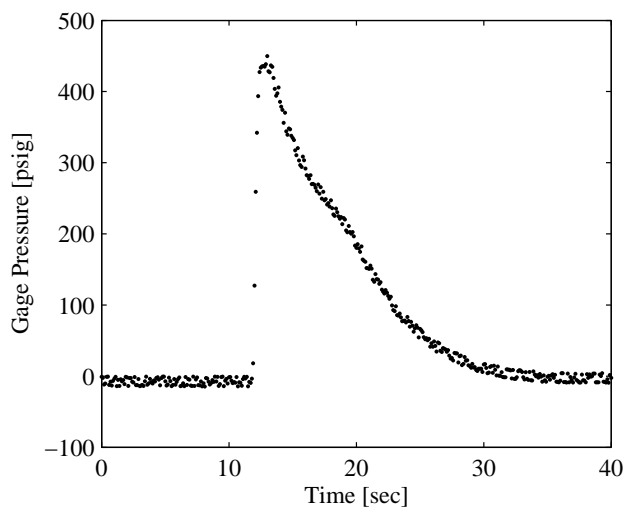


Figure E.28: Test no. 29 (HFC-23)

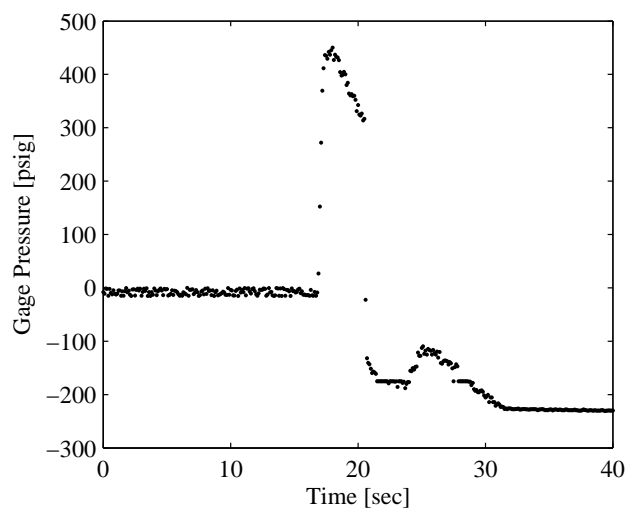


Figure E.29: Test no. 30 (HFC-23)

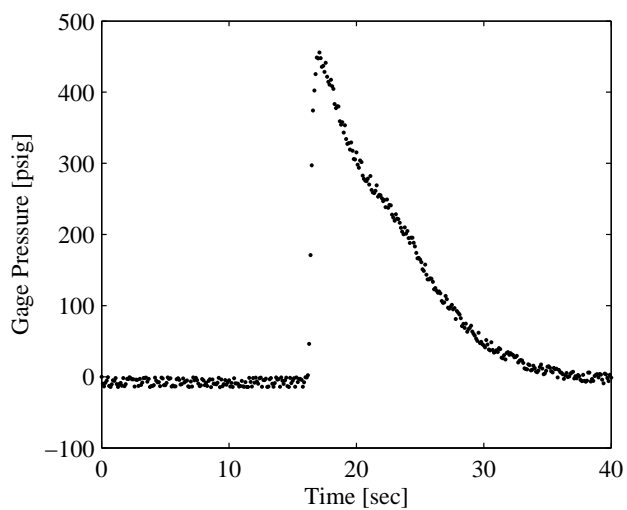


Figure E.30: Test no. 31 (HFC-23)

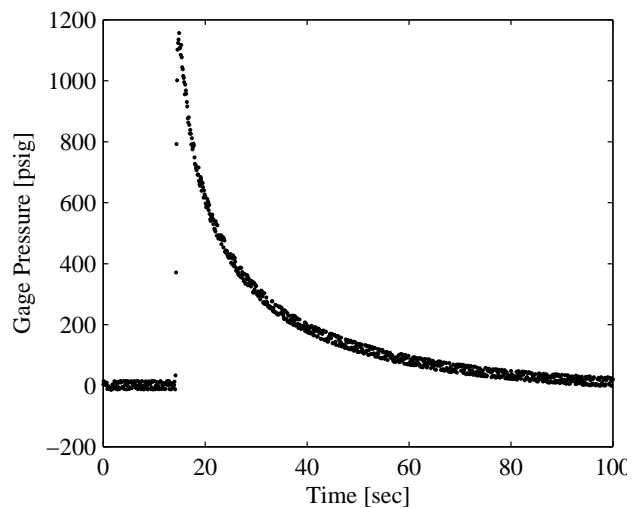


Figure E.31: Test no. 32 (IG-55)

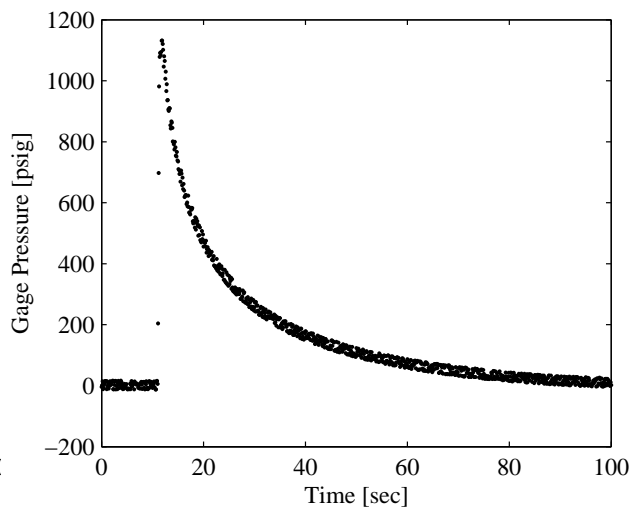


Figure E.32: Test no. 33 (IG-55)

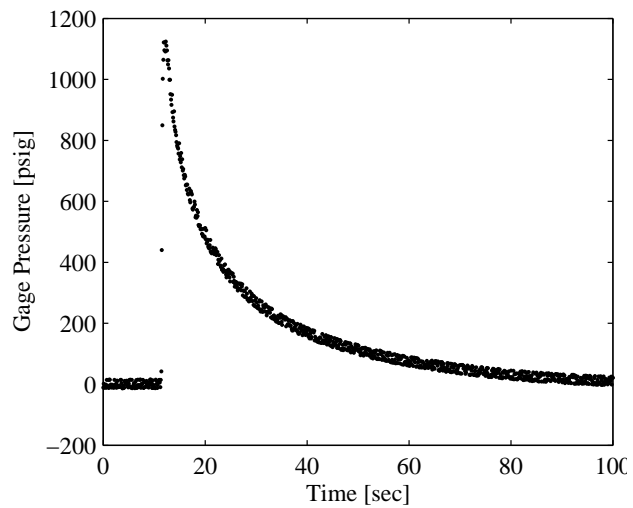


Figure E.33: Test no. 34 (IG-55)

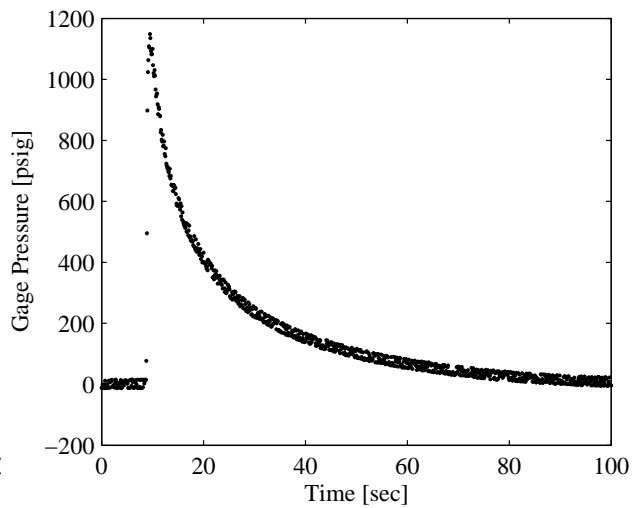


Figure E.34: Test no. 36 (IG-55)

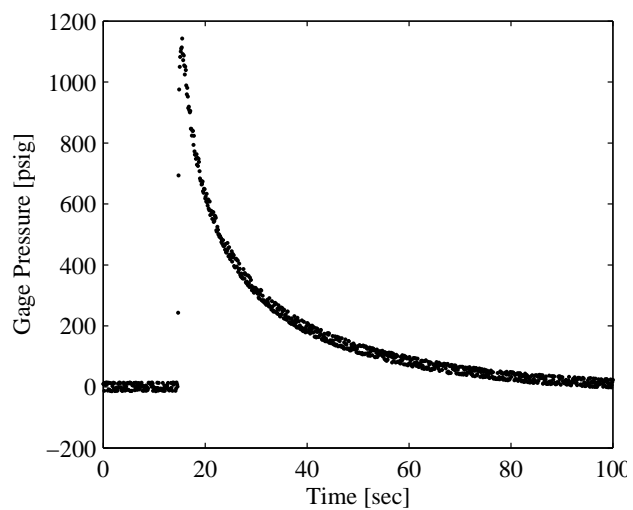


Figure E.35: Test no. 37 (IG-55)

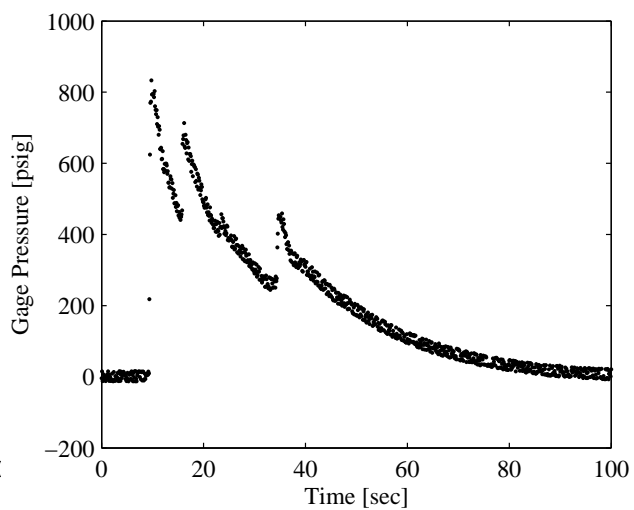


Figure E.36: Test no. 38 (IG-55P)

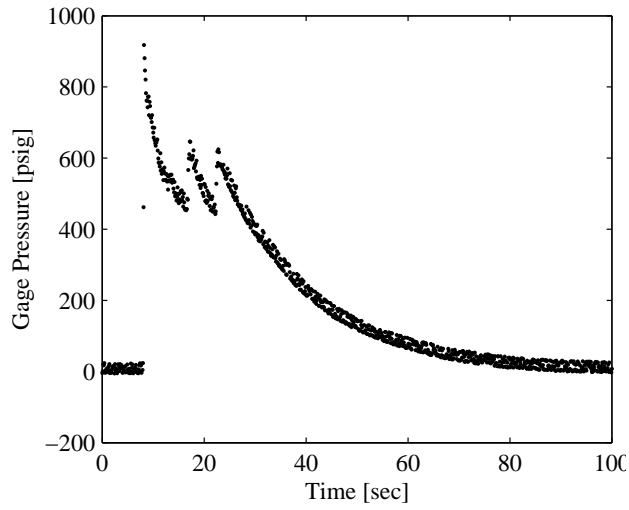


Figure E.37: Test no. 39 (IG-55P)

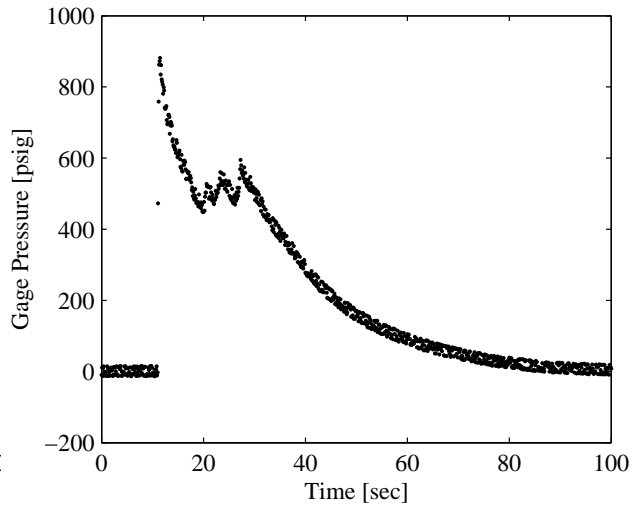


Figure E.38: Test no. 40 (IG-55P)

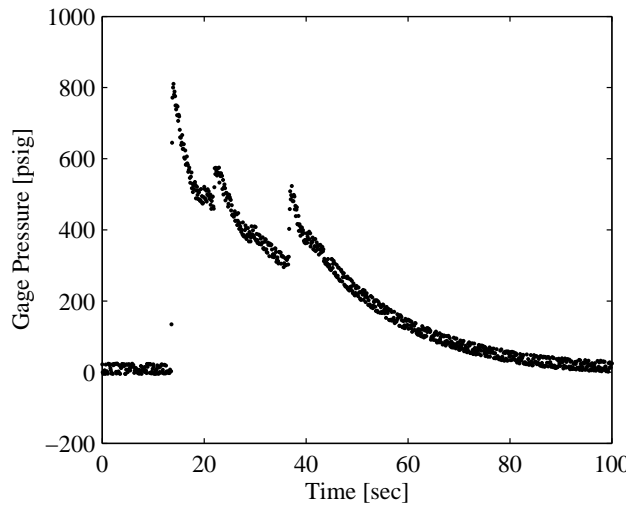


Figure E.39: Test no. 41 (IG-55P)

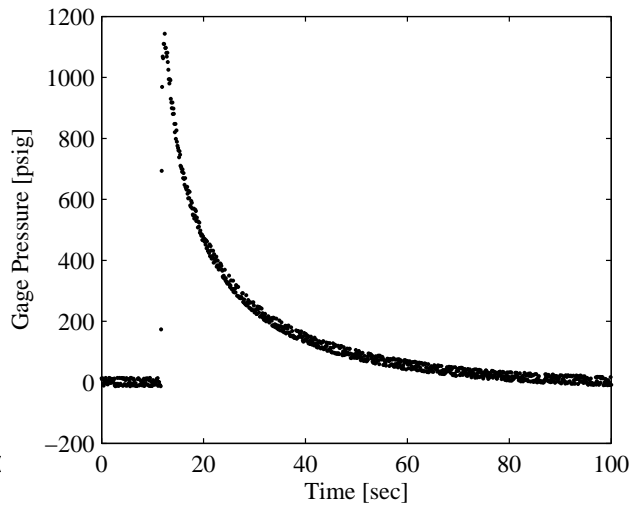


Figure E.40: Test no. 42 (IG-100)

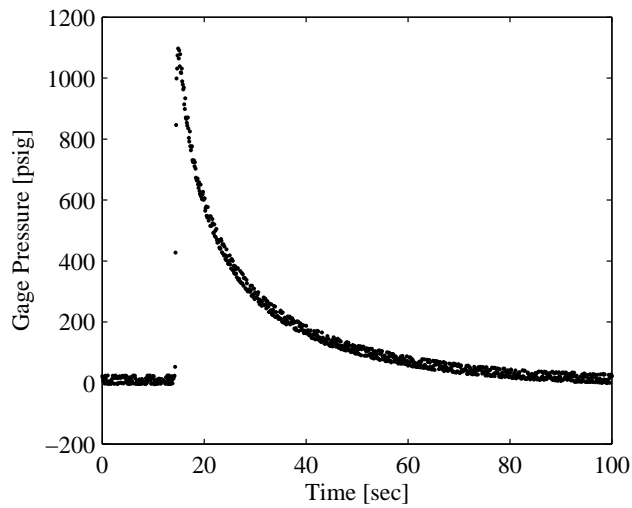


Figure E.41: Test no. 43 (IG-100)

Appendix F

Ambient Temperature Data

Although temperature gradients are not considered in the subject hold time theories, some of the enclosure’s ambient temperature profile is documented herein. Most experiments from ‘05 and ‘06 had at least one temperature source provided. Up to five temperature data sources were retained from the majority of the 2007 test campaign. This appendix presents all available temperature data from all tests conducted. Reference Tables [A.1](#), [A.2](#), and [A.3](#) for further experiment configuration information on each conducted test.

Each temperature probe is given in the figure legend by means of a single letter. Instrument ‘A’ is a 1/8” diameter probe of unknown location (somewhere inside the experimental envelope).

Instrument ‘B’ is an exposed, 1/16th in diameter bead, type K, thermocouple. It was installed halfway through the enclosure’s wall, suspended in the center of one of the 1 inch diameter leakages (manually controlled), at the top-center of the northern-most enclosure wall. It serves as an indicator for both the temperature of leaking gas through this upper enclosure orifice and the direction of gas flow (inwards or outwards). Instrument ‘B’ has been deleted from the data sets for test 23, 29, 30, and 31 due to a plug being mounted on the inside of the 1” dia. hole in which this probe was installed (due to the maladjusted leakage configuration this probe no longer experiences gas involved with the agent draining behavior).

Instruments ‘C’, ‘D’, and ‘E’ are all 1/16”, ungrounded, sheathed, type K, thermocouple probes. As well, they are each installed inside the test enclosure, offset ~1 inch from the north wall at elevations of 1’, 8’ and 15’ above the floor, respectively. They give a rough temperature profile within the test enclosure throughout agent discharge and the hold time period.

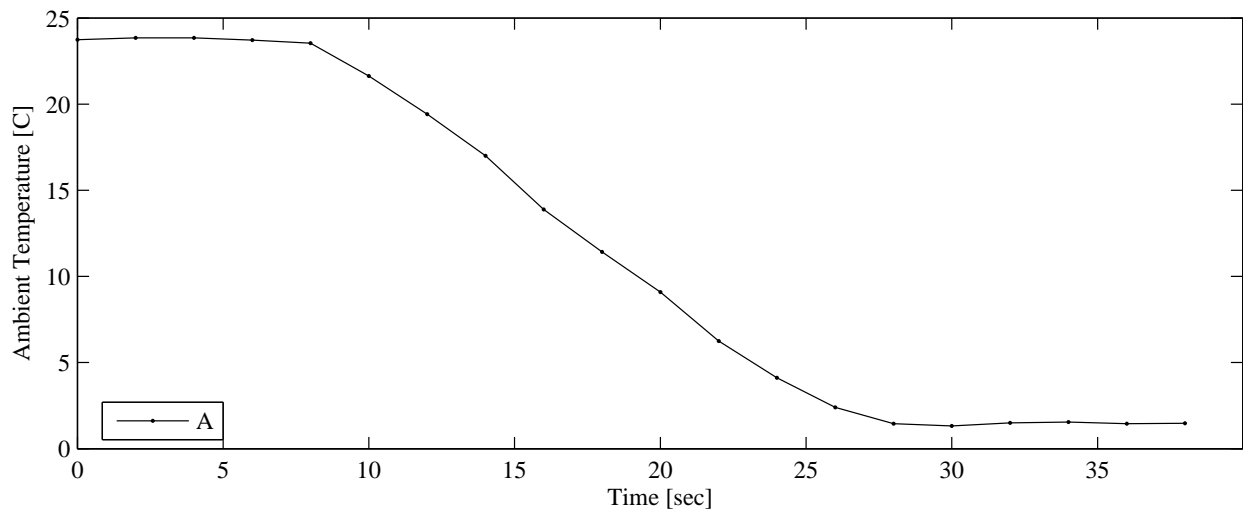


Figure F.1: Ambient temperature data for test no. 1 (HFC-227ea)

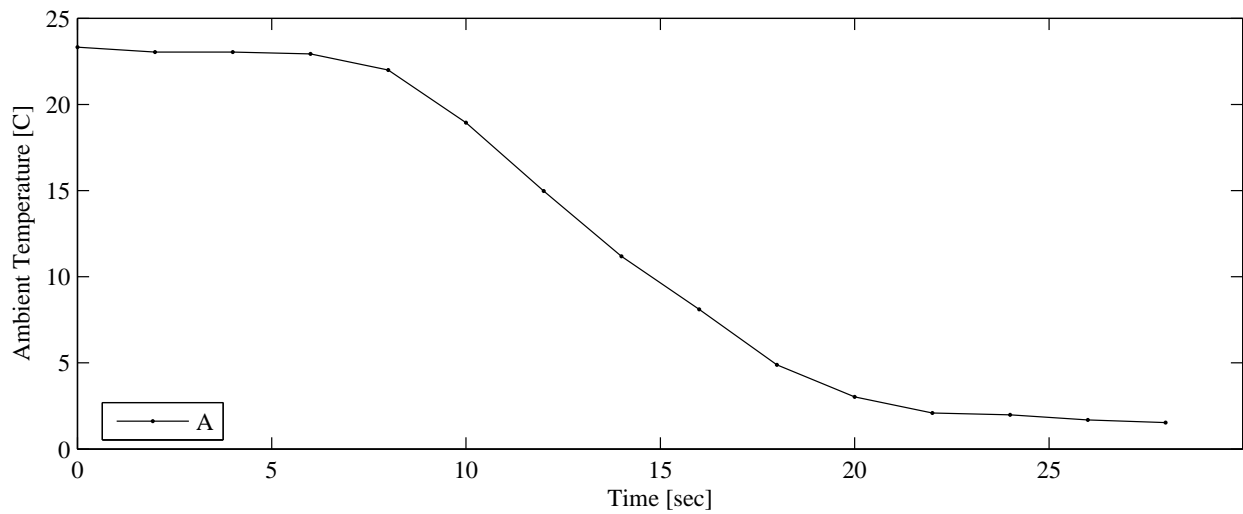


Figure F.2: Ambient temperature data for test no. 2 (HFC-227ea)

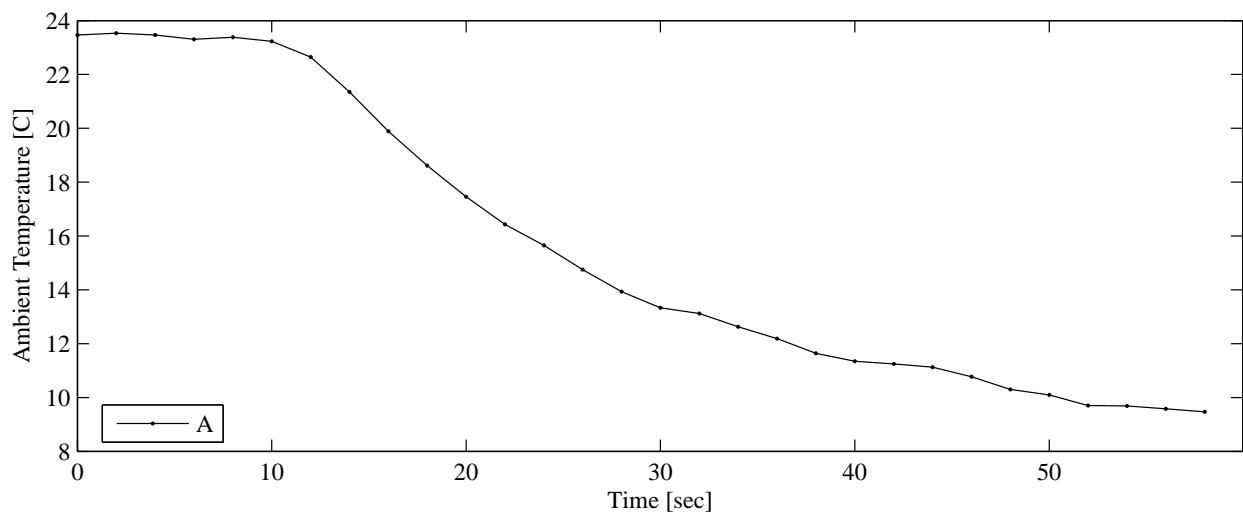


Figure F.3: Ambient temperature data for test no. 7 (FK-5-1-12)

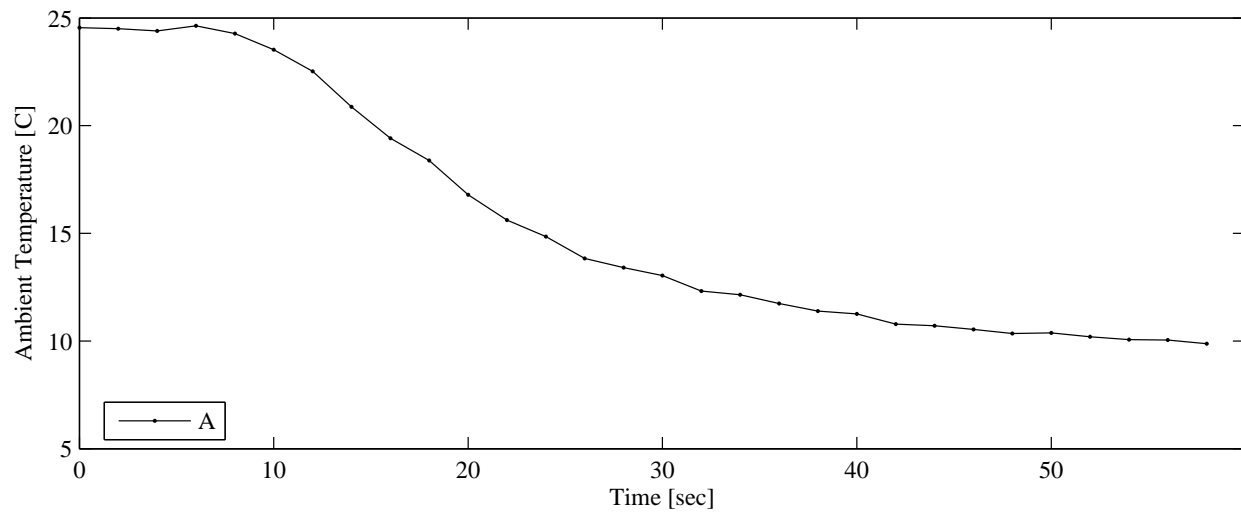


Figure F.4: Ambient temperature data for test no. 8 (FK-5-1-12)

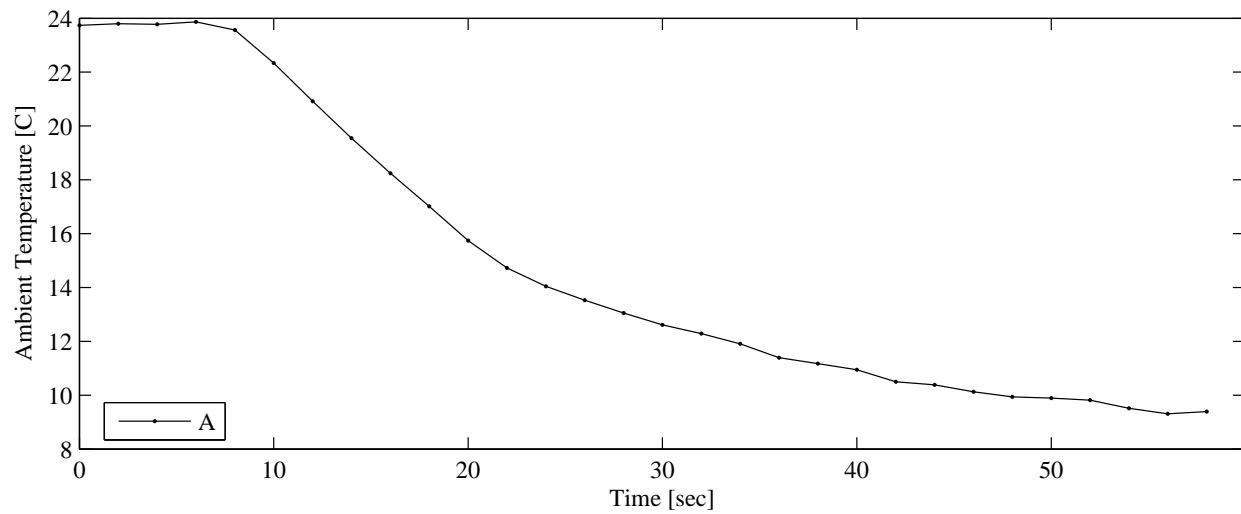


Figure F.5: Ambient temperature data for test no. 9 (FK-5-1-12)

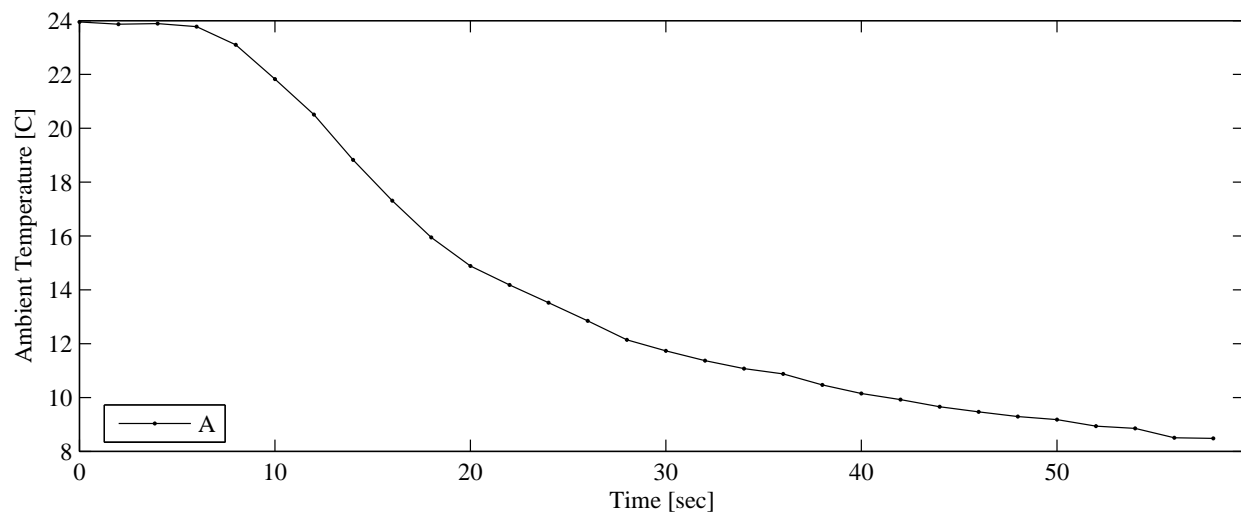


Figure F.6: Ambient temperature data for test no. 10 (FK-5-1-12)

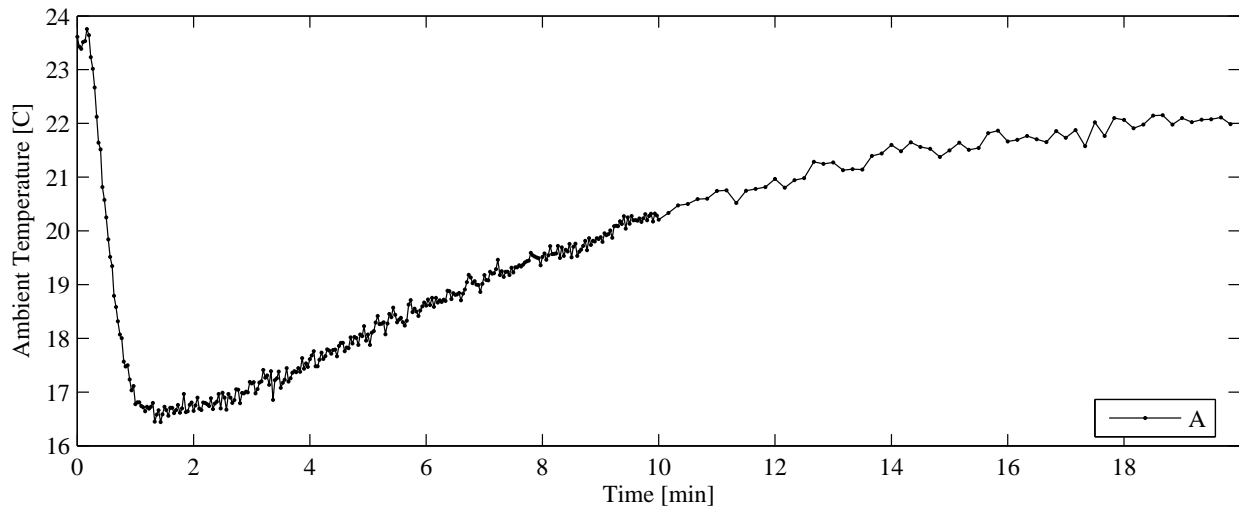


Figure F.7: Ambient temperature data for test no. 11 (IG-541)

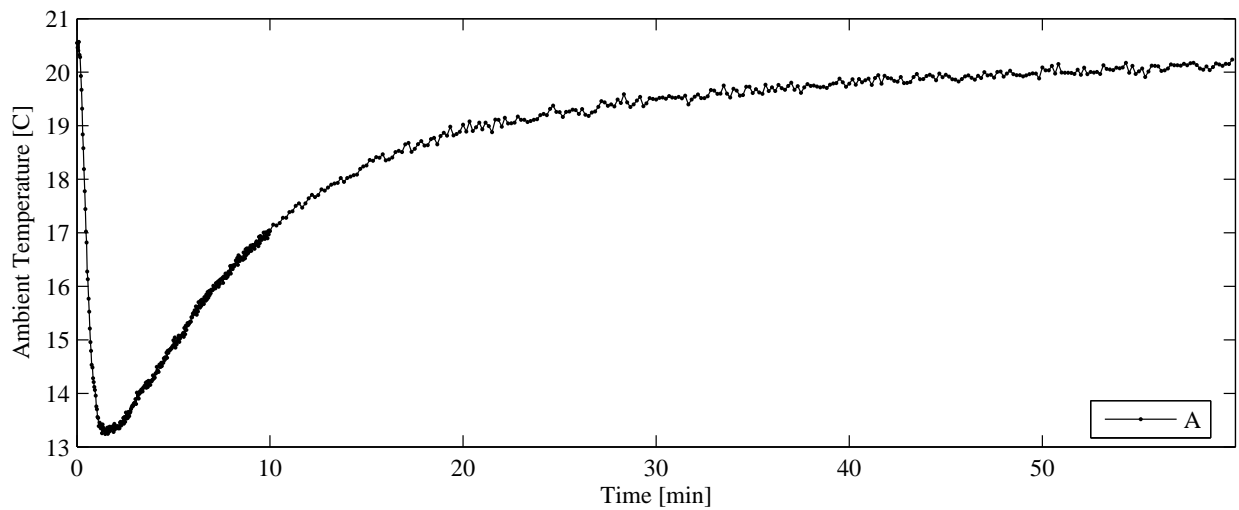


Figure F.8: Ambient temperature data for test no. 13 (IG-541)

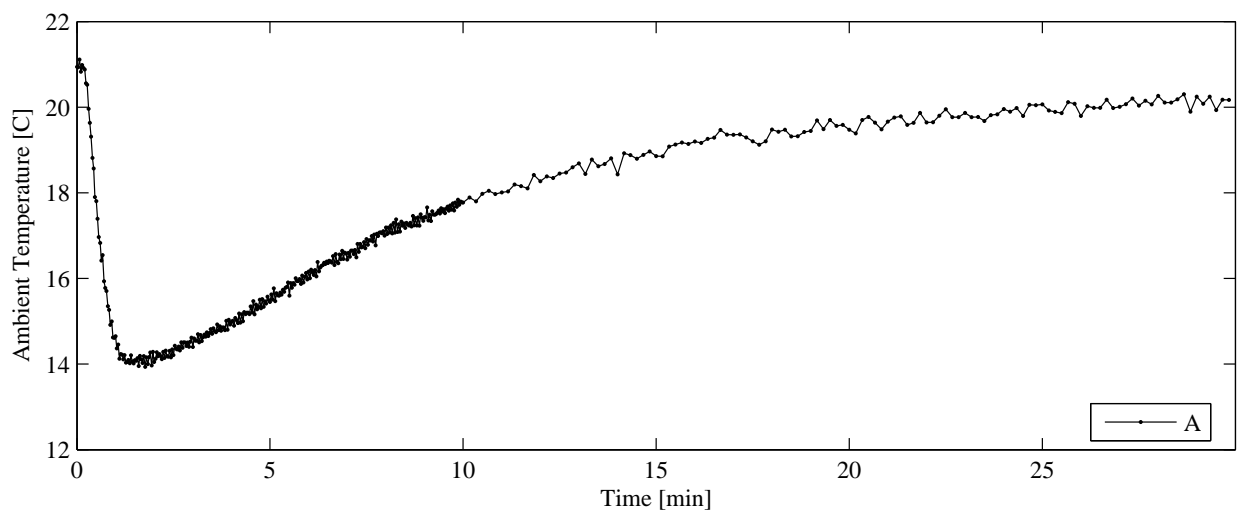


Figure F.9: Ambient temperature data for test no. 14 (IG-541)

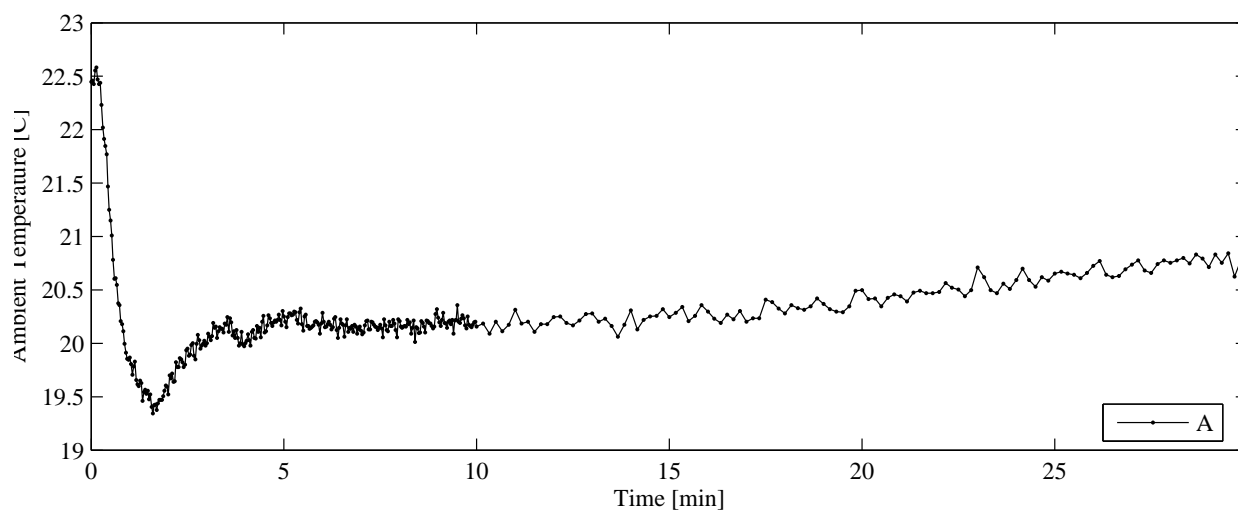


Figure F.10: Ambient temperature data for test no. 15 (IG-541)

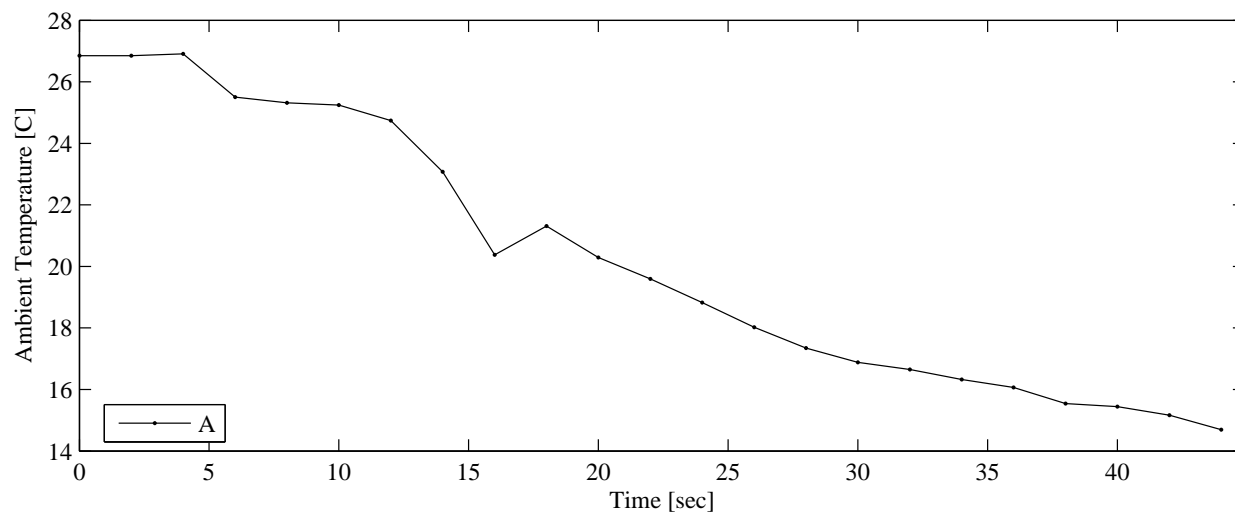


Figure F.11: Ambient temperature data for test no. 17 (HFC-125)

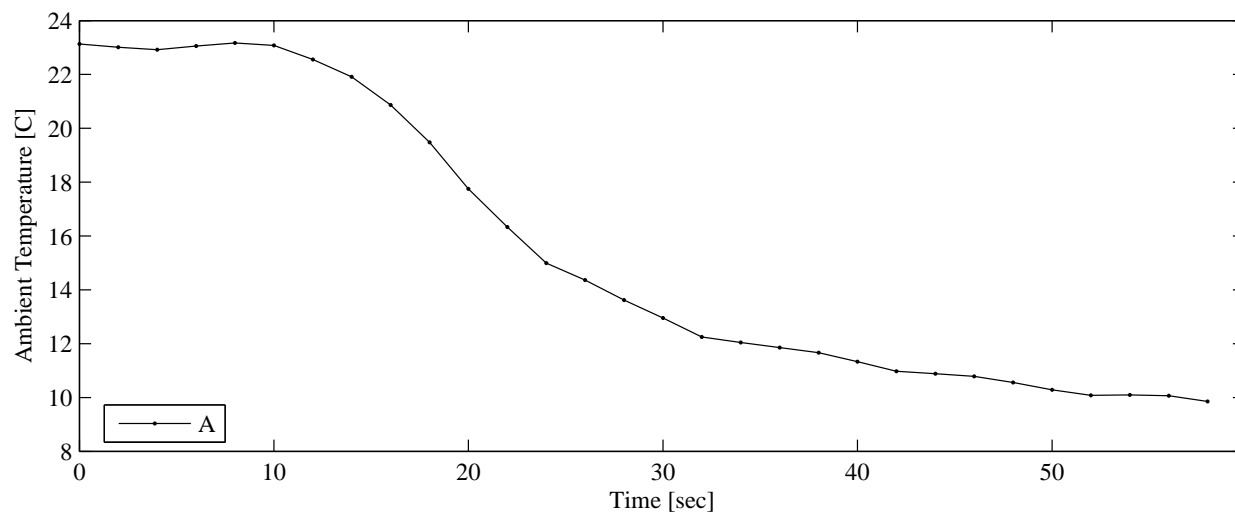


Figure F.12: Ambient temperature data for test no. 18 (HFC-125)

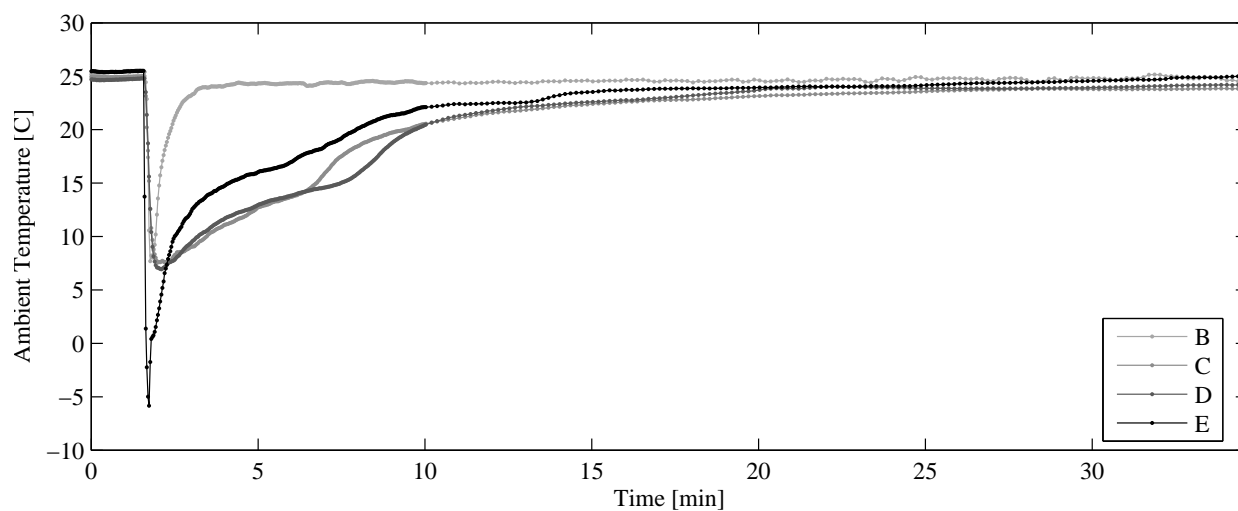


Figure F.13: Ambient temperature data for test no. 21 (HFC-227ea)

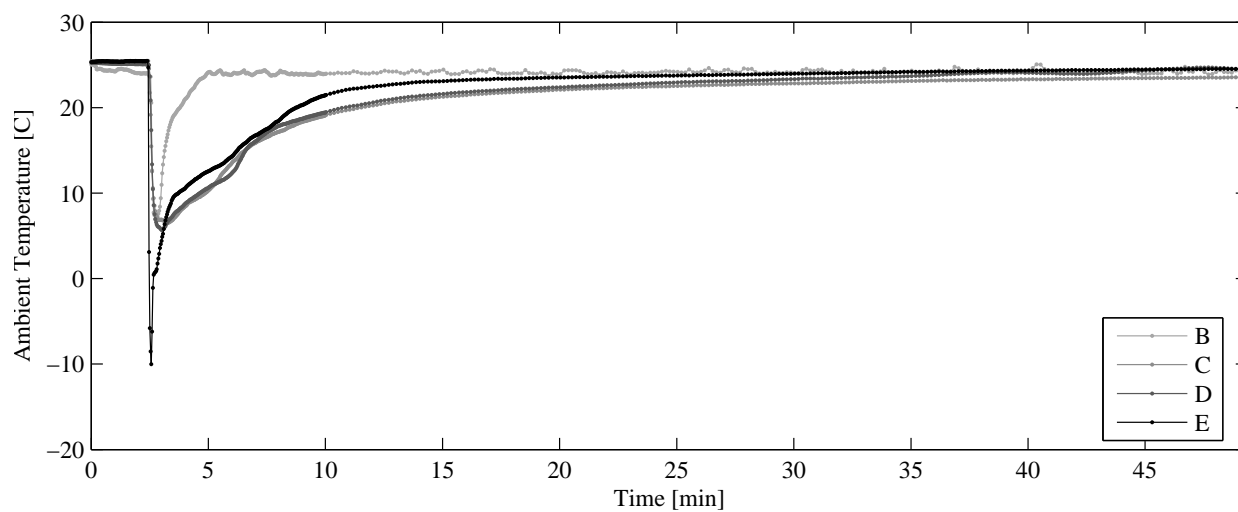


Figure F.14: Ambient temperature data for test no. 22 (HFC-227ea)

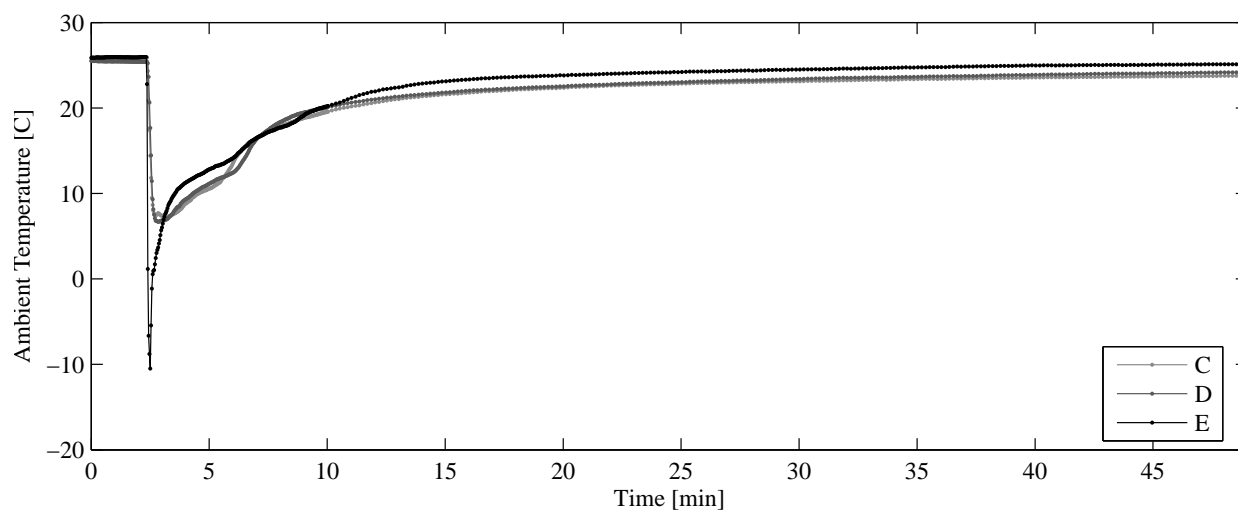


Figure F.15: Ambient temperature data for test no. 23 (HFC-227ea)

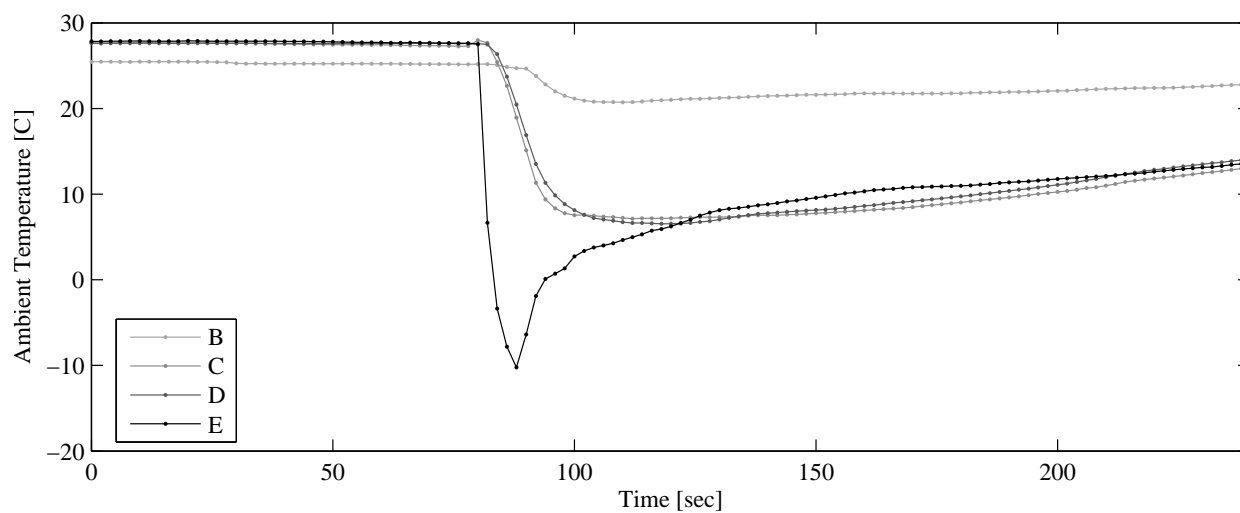


Figure F.16: Ambient temperature data for test no. 24 (HFC-227ea)

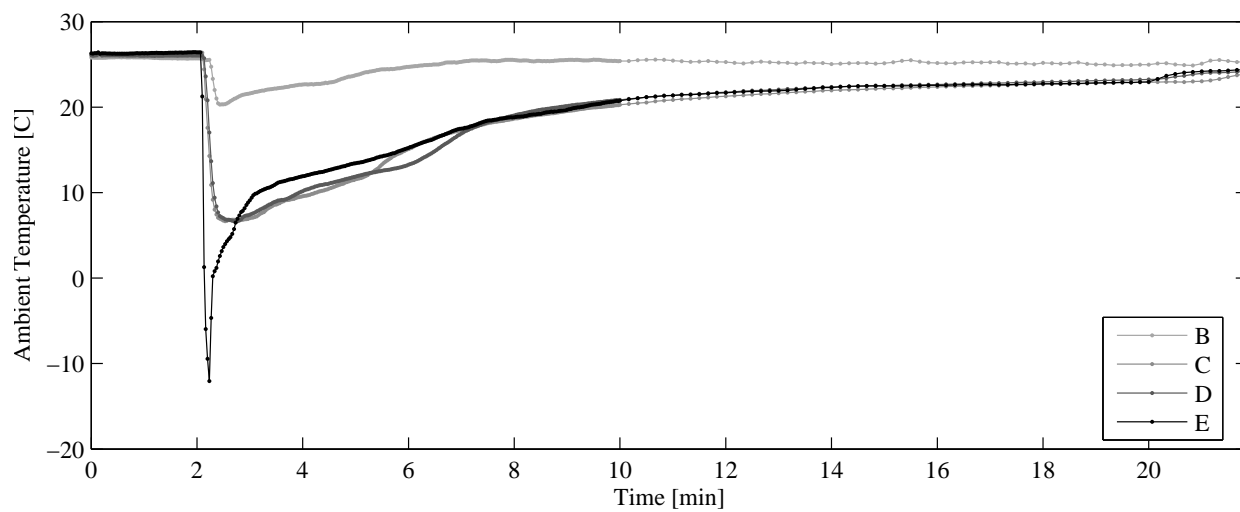


Figure F.17: Ambient temperature data for test no. 25 (HFC-227ea)

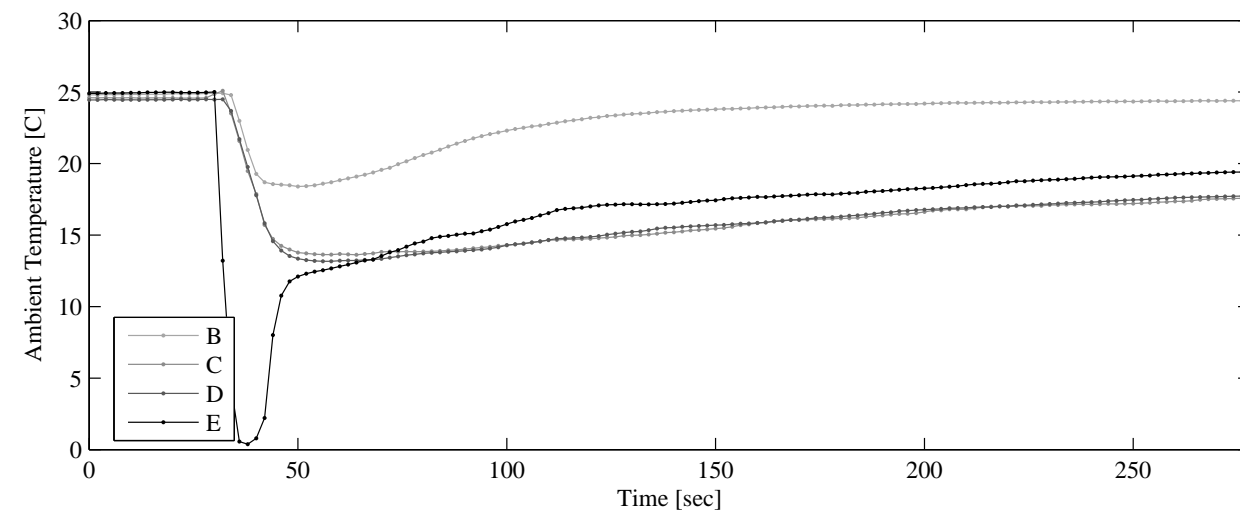


Figure F.18: Ambient temperature data for test no. 26 (HFC-227ea)

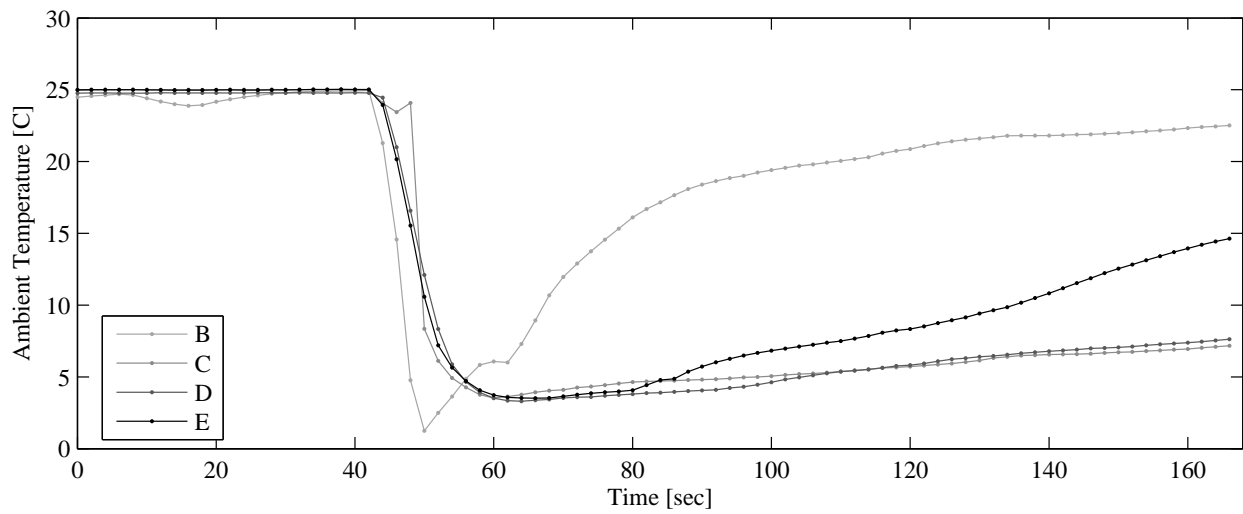


Figure F.19: Ambient temperature data for test no. 27 (HFC-23)

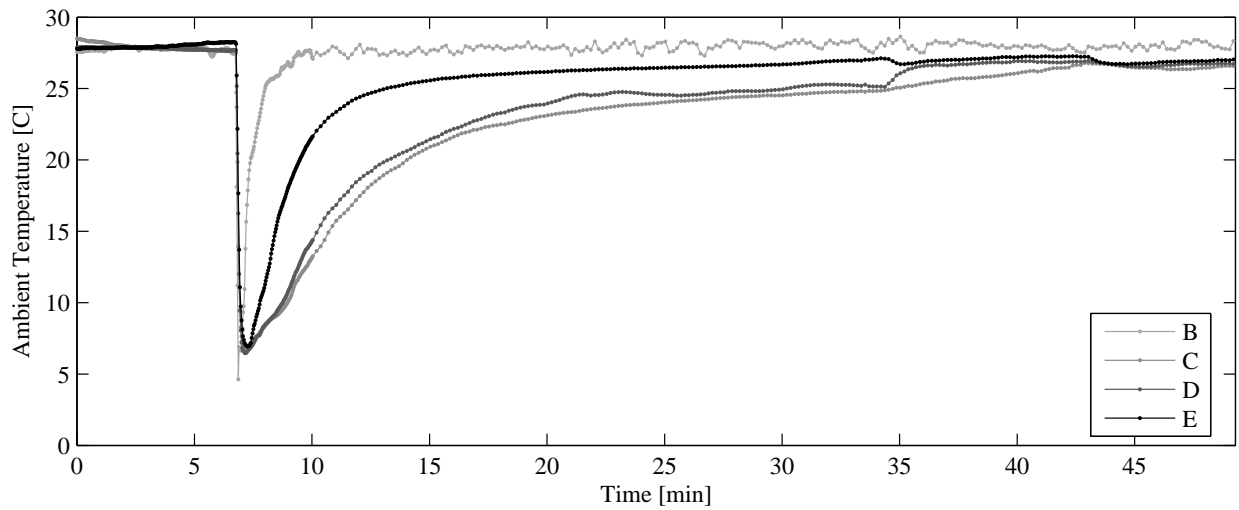


Figure F.20: Ambient temperature data for test no. 28 (HFC-23)

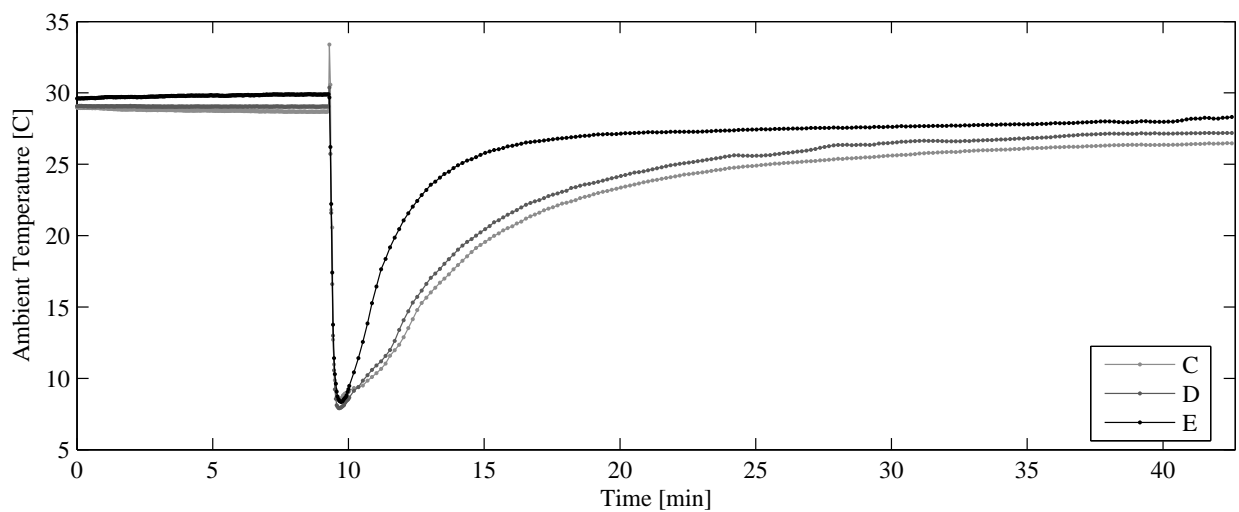


Figure F.21: Ambient temperature data for test no. 29 (HFC-23)

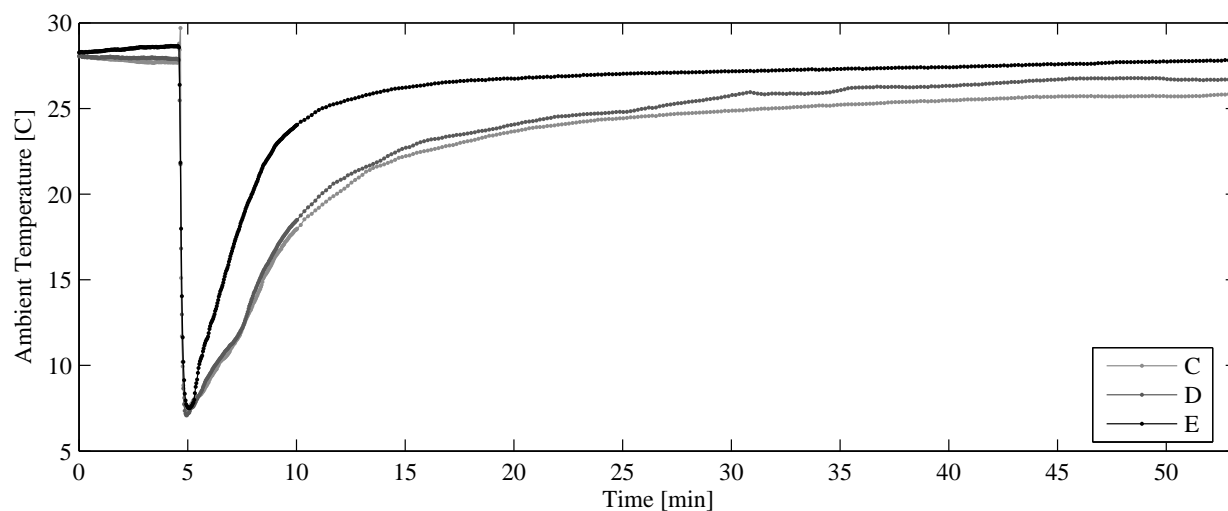


Figure F.22: Ambient temperature data for test no. 30 (HFC-23)

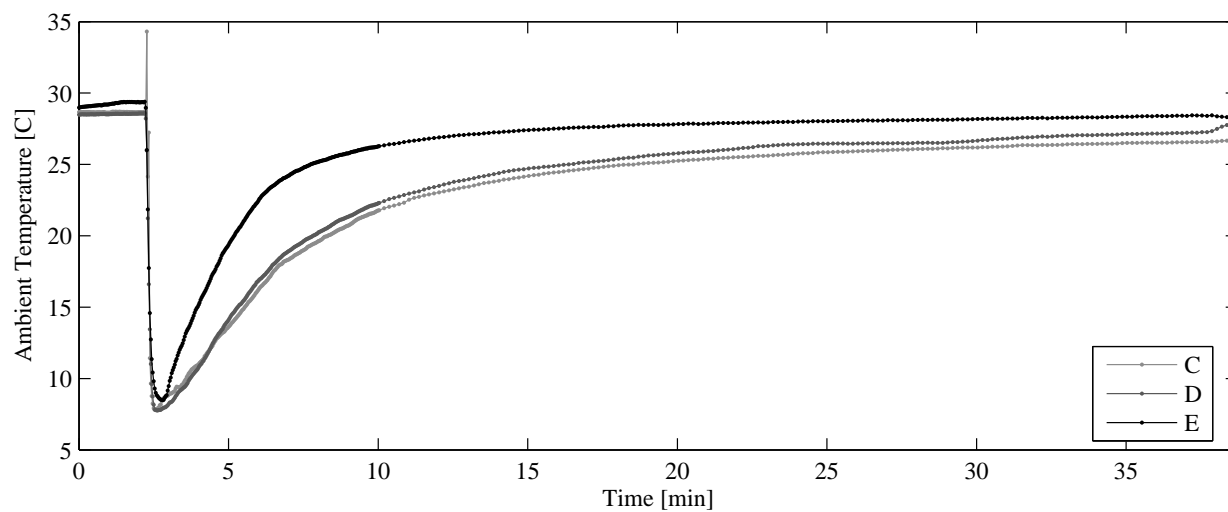


Figure F.23: Ambient temperature data for test no. 31 (HFC-23)

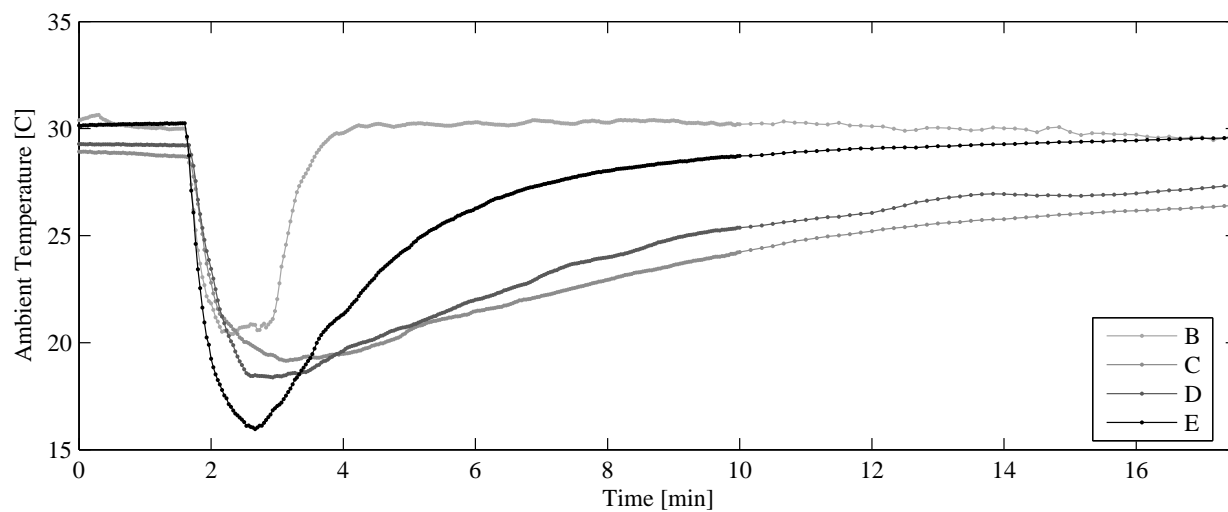


Figure F.24: Ambient temperature data for test no. 32 (IG-55)

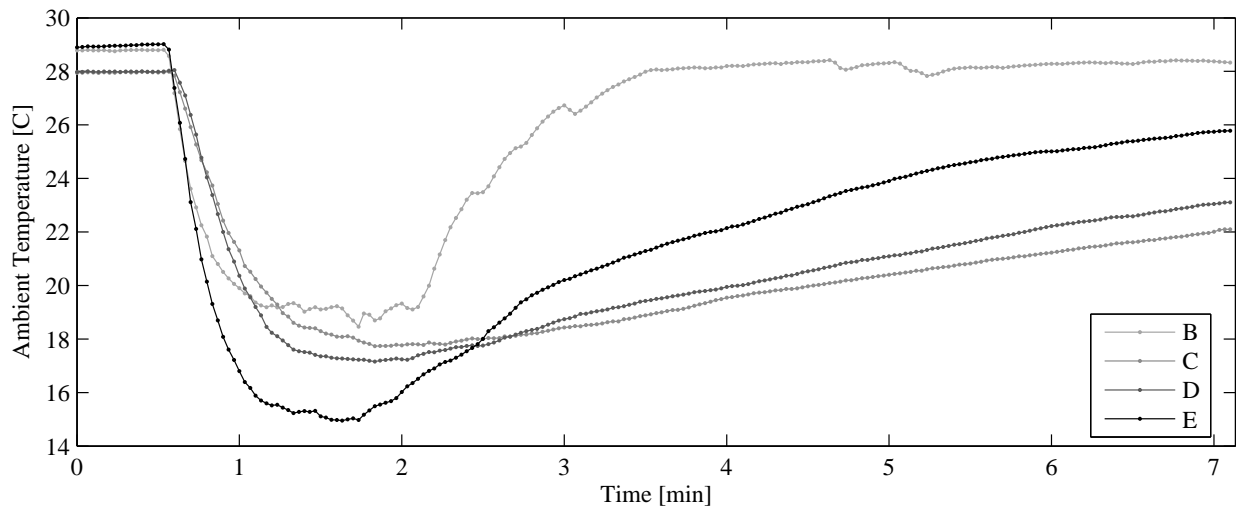


Figure F.25: Ambient temperature data for test no. 33 (IG-55)

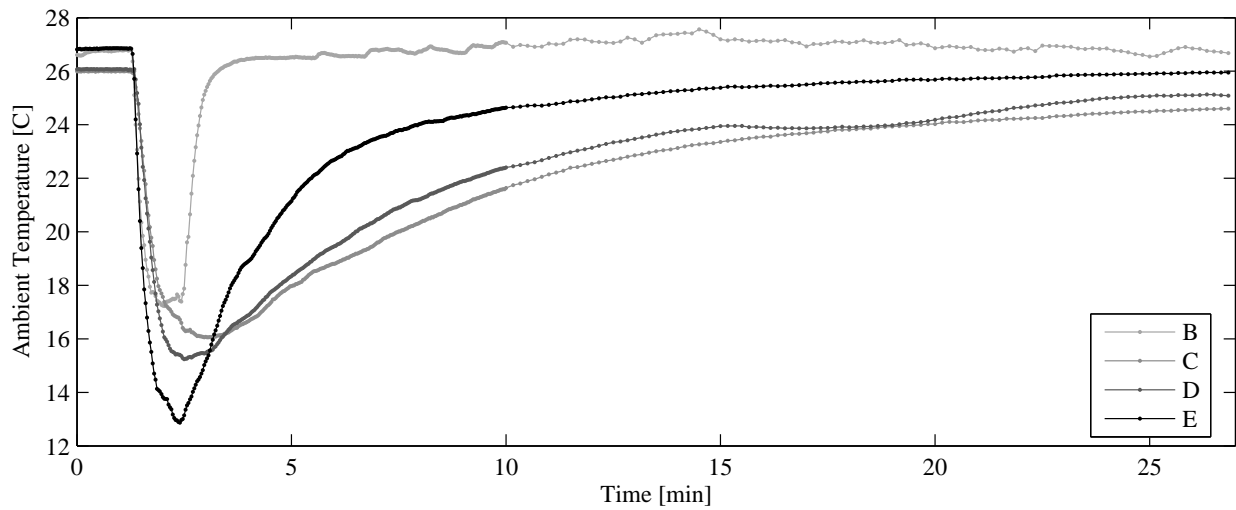


Figure F.26: Ambient temperature data for test no. 34 (IG-55)

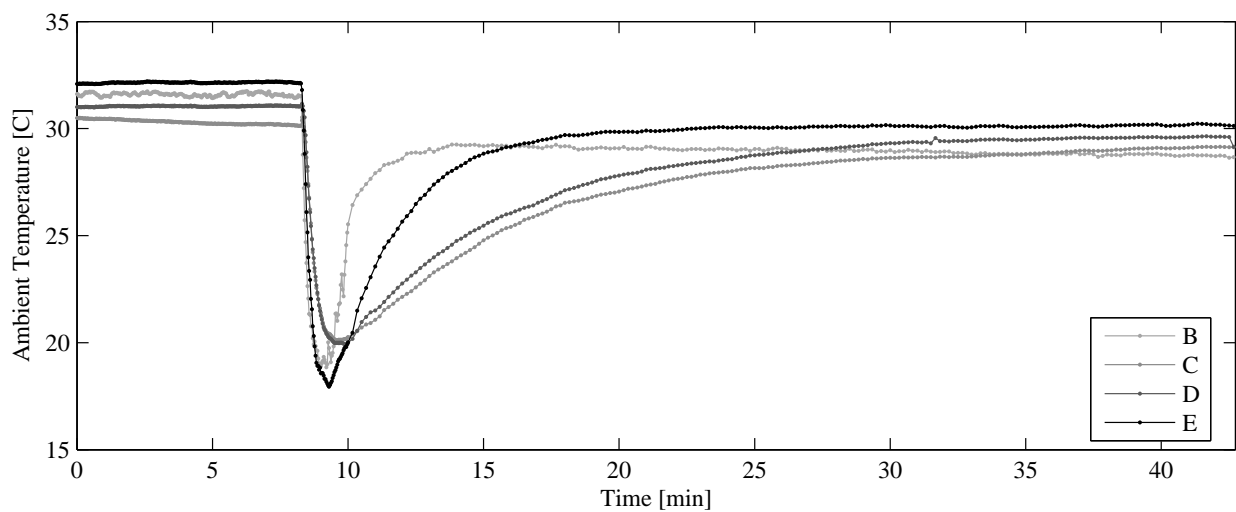


Figure F.27: Ambient temperature data for test no. 35 (IG-55)

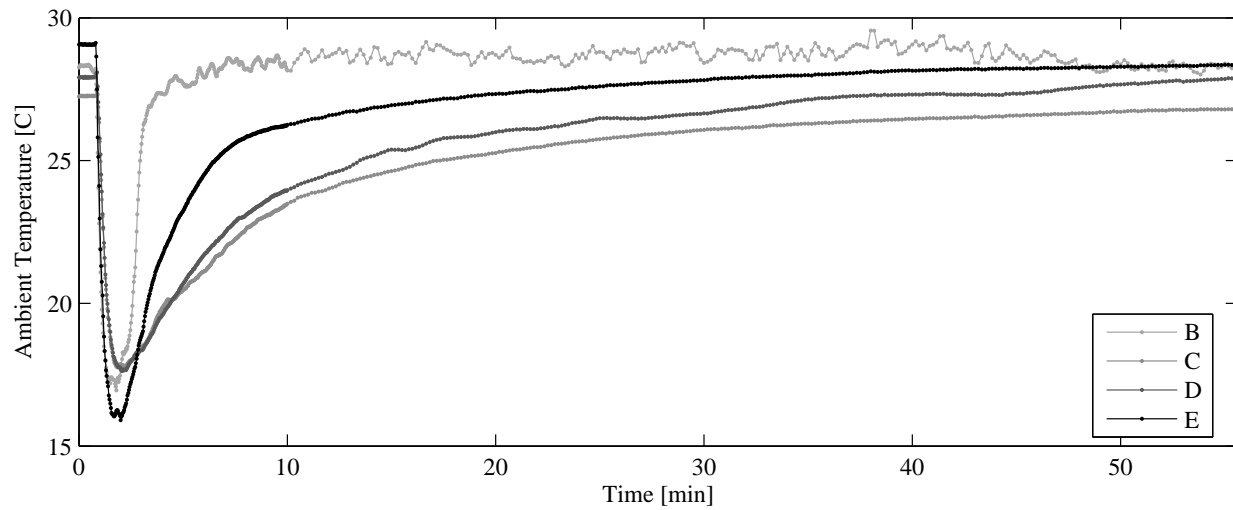


Figure F.28: Ambient temperature data for test no. 36 (IG-55)

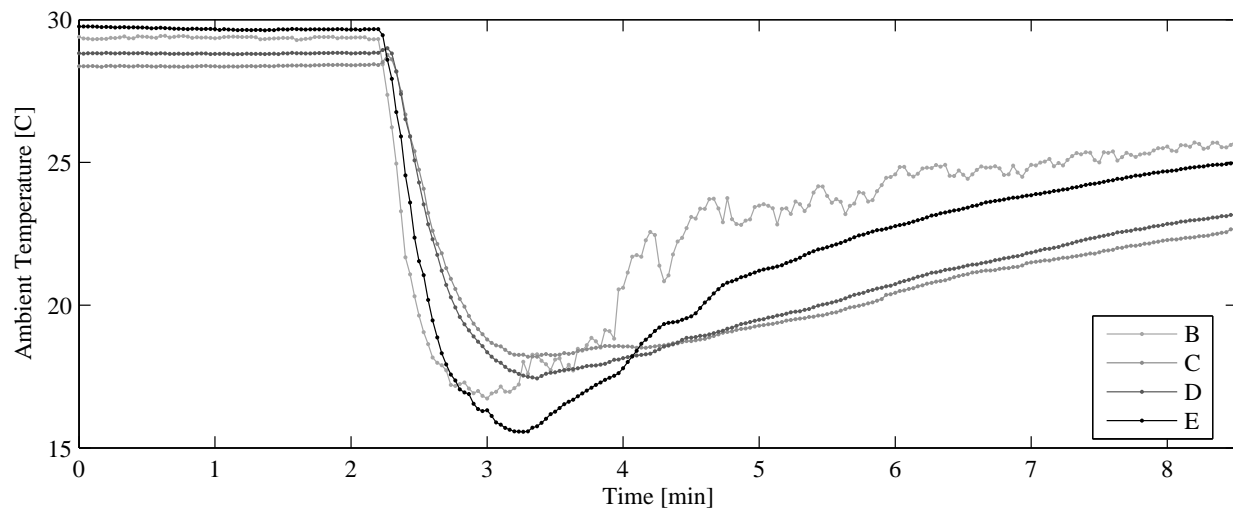


Figure F.29: Ambient temperature data for test no. 37 (IG-55)

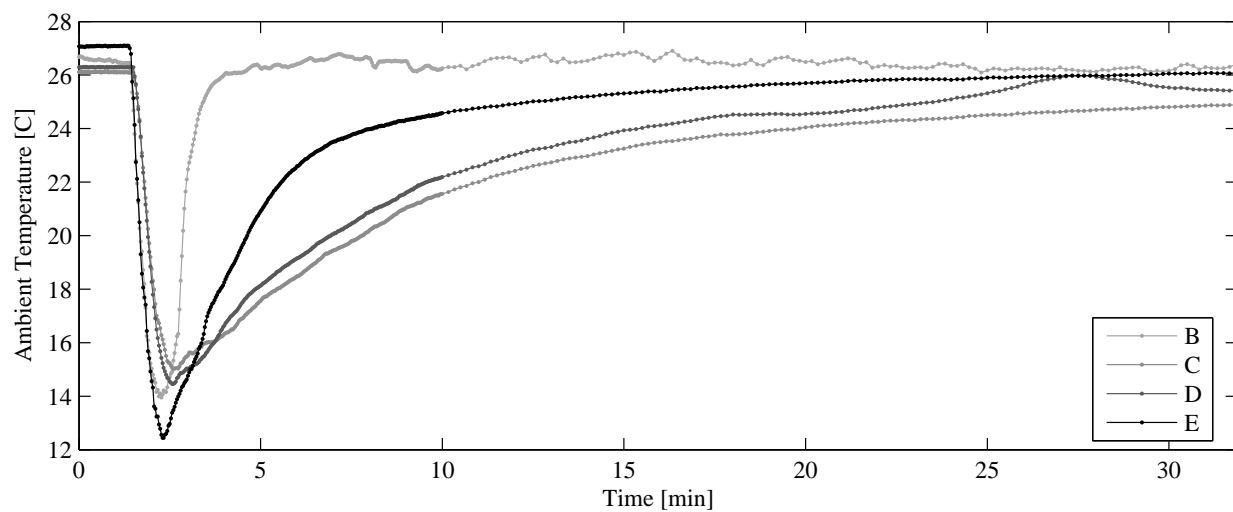


Figure F.30: Ambient temperature data for test no. 38 (IG-55P)

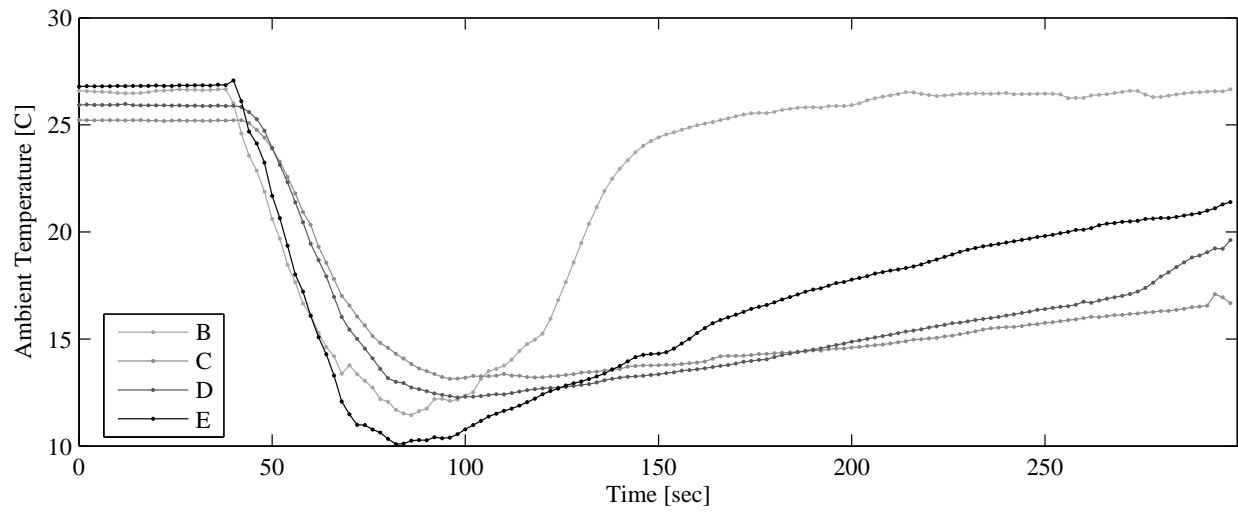


Figure F.31: Ambient temperature data for test no. 39 (IG-55P)

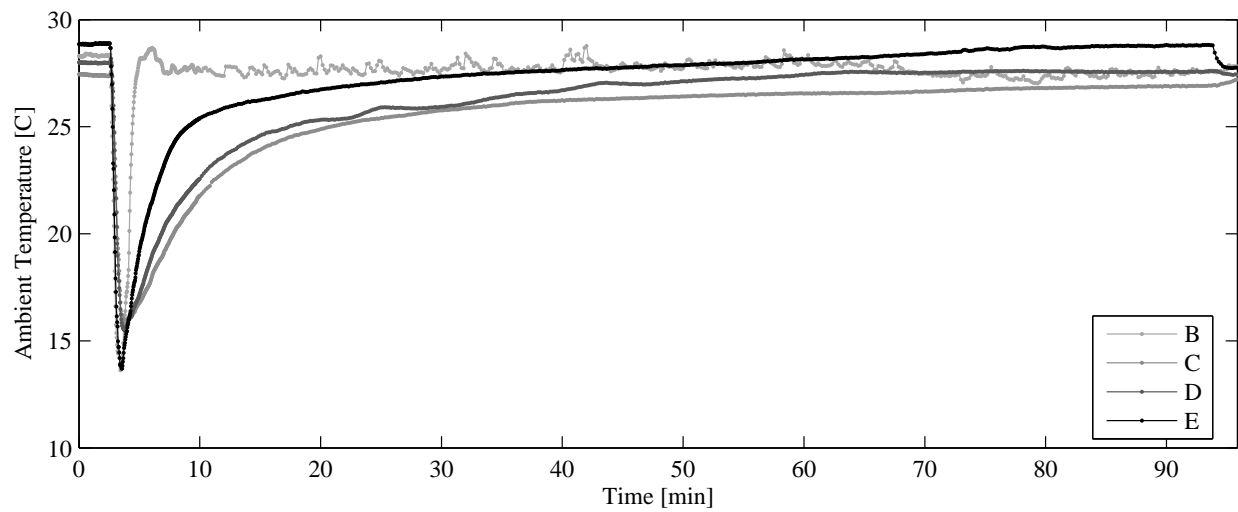


Figure F.32: Ambient temperature data for test no. 40 (IG-55P)

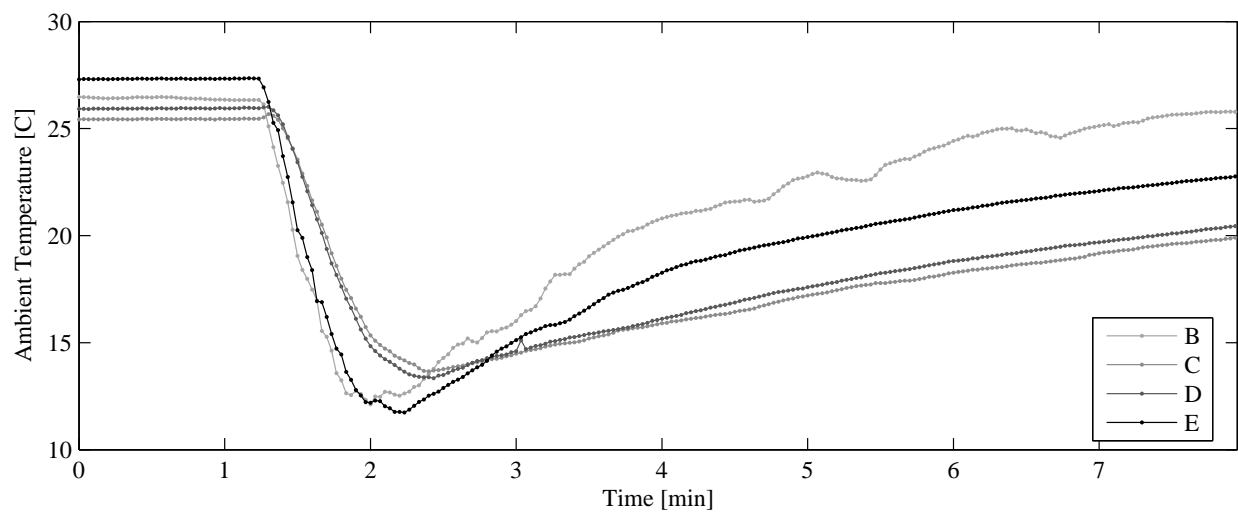


Figure F.33: Ambient temperature data for test no. 41 (IG-55P)

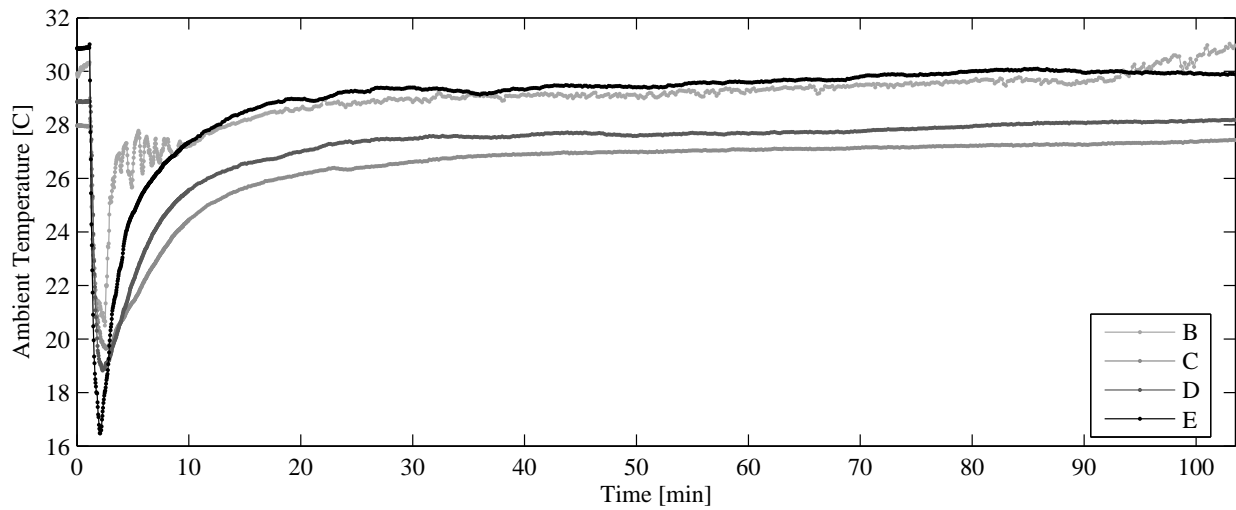


Figure F.34: Ambient temperature data for test no. 42 (IG-100)

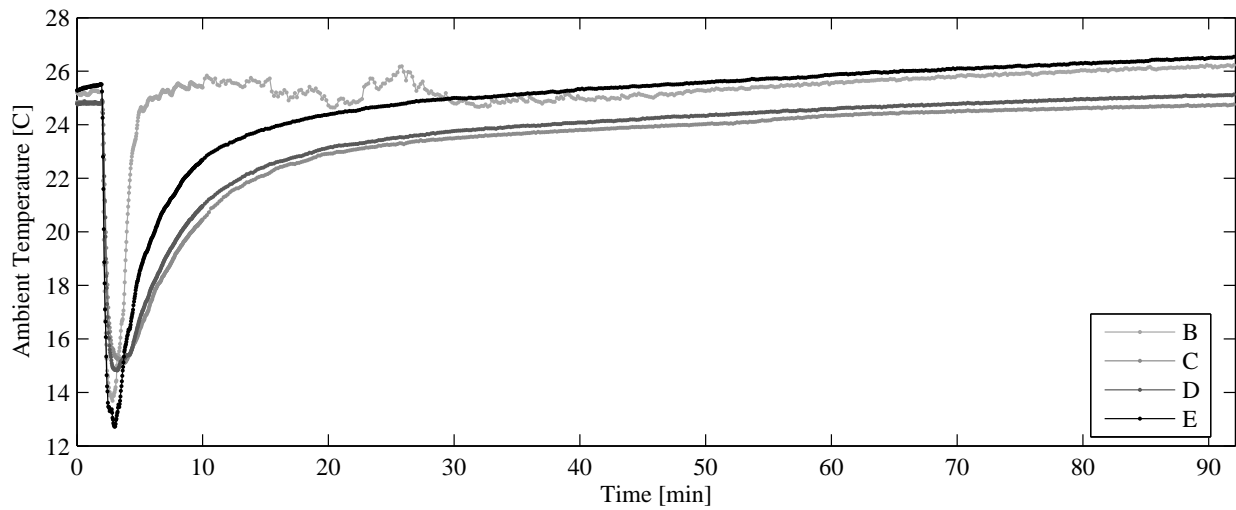


Figure F.35: Ambient temperature data for test no. 43 (IG-100)

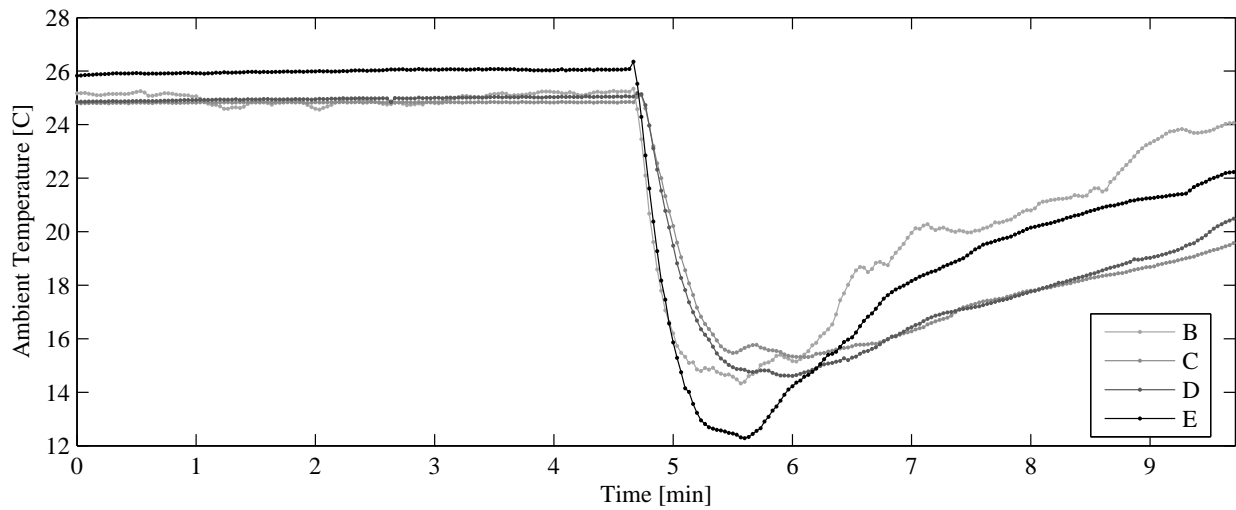


Figure F.36: Ambient temperature data for test no. 44 (IG-100)

Appendix G

The Lower Leakage Fraction

As demonstrated in Figure 2.3, each of the subject hold time models are most sensitive to the *lower leakage fraction* (LLF), an input parameter given as F in Chapters 2 and 3. It is formulated in terms of the upper and lower leakage areas as Equation (2.2). The LLF can also be given in terms of the driving pressure and density of the gases flowing through the upper and lower leakages for the ideal case where all gases are at standard temperature and pressure (STP) as Equation (2.4), or

$$F = \frac{1}{1 + \sqrt{\frac{\rho_{high}\Delta P_{low}}{\rho_{low}\Delta P_{high}}}}.$$

The following figures of this appendix are the result applying the correlating equation above to the data sets given in Appendix D. A single figure is presented for each pair of data traces, in every test where they were installed at the elevations of upper and lower controlled leakages (each DM-2 instrument offered two channels, paired in time). The instruments given in Appendix D as ‘C’ and ‘D’ constitute Inst. #1 while Inst. #2 is derived from instruments ‘E’ and ‘F’.

For all agent types the LLF is defined as the ratio of the lower enclosure leakage area to that of the summed upper and lower leakages,

$$F = \frac{A_{low}}{(A_{high} + A_{low})}.$$

In the case of pure nitrogen, given as IG-100, the densities of gases flowing through upper and lower enclosure orifices are reversed. The LLF is still

formulated as above, yet the direction of gases flowing through upper and lower orifices is assumed to be in reverse, resulting in

$$F = \frac{1}{1 + \sqrt{\frac{\rho_{low} \Delta P_{low}}{\rho_{high} \Delta P_{high}}}},$$

where the magnitudes of the driving pressure differentials P_{low} and P_{high} are an absolute value of the differential pressure across the enclosure boundary. Beyond this, in referencing Figures G.24-G.27 the plotted IG-100 data is incredibly noisy. This is somewhat misfortunate in that the one lighter-than-air agent utilized herein imposes such a subtle force of buoyancy that the data obtained from the pressure transducers are unable to result in a distinctive LLF correlation (due to precision and accuracy limitations).

Reference Tables A.1, A.2, and A.3 for information on each experiments' configuration parameters.

As stated, the following figures are formulated through adoption of an ideal condition where temperature transients do not exist. It follows that the agent draining behavior, when unadulterated by bias pressures due to HVAC systems, wind or other, would necessarily result in a purely buoyancy driven condition. This scenario depends upon a consistent balance between the volumetric gas flows between the summed upper leakages and that of the lower leakages ($Q_{high} = Q_{low}$).

As the audience expects, this is not the scenario in real life. The transient temperature data sets are presented in Appendix F. In comparing the temperature data for any given experiment to the correlated, effective LLF in the ensuing figures one can gain a greater insight into the duration of time for which the correlation is invalid. Typically, about the first 10 minutes of each following figure is invalid and could have been left uncharted as the assumption used to formulate Equation (2.4) is not valid. In fact, because all agent types result in a temperature drop that then gradually warms to the ambient temperature surrounding the test enclosure, a prolonged amount of gas expansion exists within. This ultimately allows the agent-air mixture inside the enclosure, to both vent outwards and not allow an influx of fresh air for a period of time while warming. Naturally, this effect gradually wears off and a stable, correlated value of the lower leakage fraction, F , results.

It should be noted that this exercise is not in vain. Because this project seeks to understand the validity of various hold time models as implemented and interpreted by today's global jurisdictions the steady-state LLF values

exhibited in this exercise are directly implemented in performing hold time calculations throughout this study. In this way the empirical hold time is analyzed against a calculated hold time prediction that utilizes the most accurate input information that would be realizable to design technicians in the field (a multi-phase door fan test procedure can achieve this same leakage information).

As stated, the LLF is the most sensitive input parameter to every subject hold time model. Thus, the steady-state LLF demonstrated in the following figures is averaged and used in preparation of the Figures [2.10](#), [2.11](#), and [3.9](#) and all the figures given in Appendix [J](#).

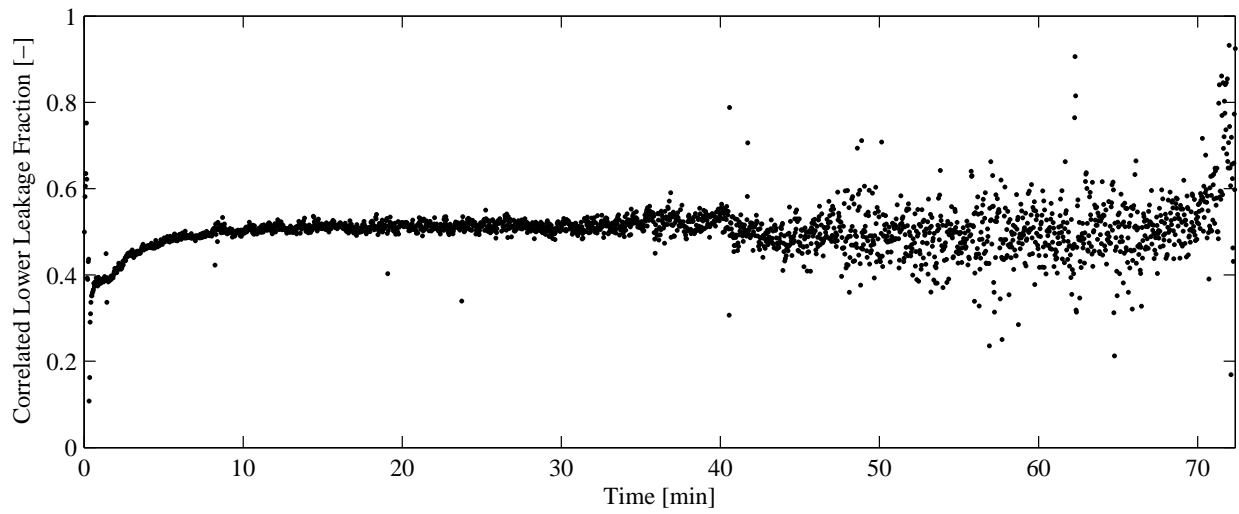


Figure G.1: Correlated lower leakage fraction for test no. 16 - Inst. #1 (HFC-125)

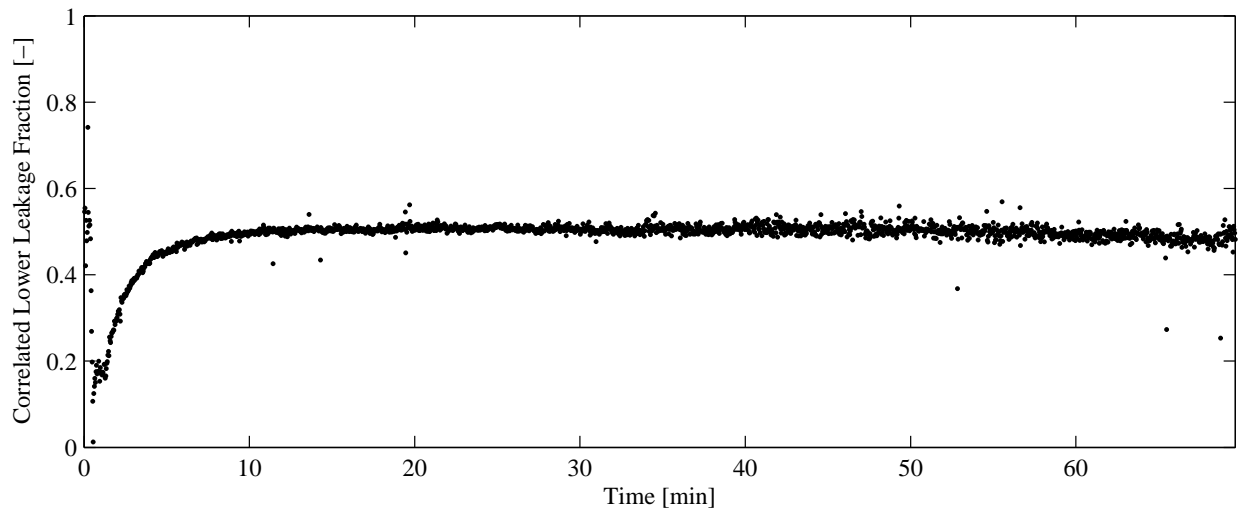


Figure G.2: Correlated lower leakage fraction for test no. 17 - Inst. #1 (HFC-125)

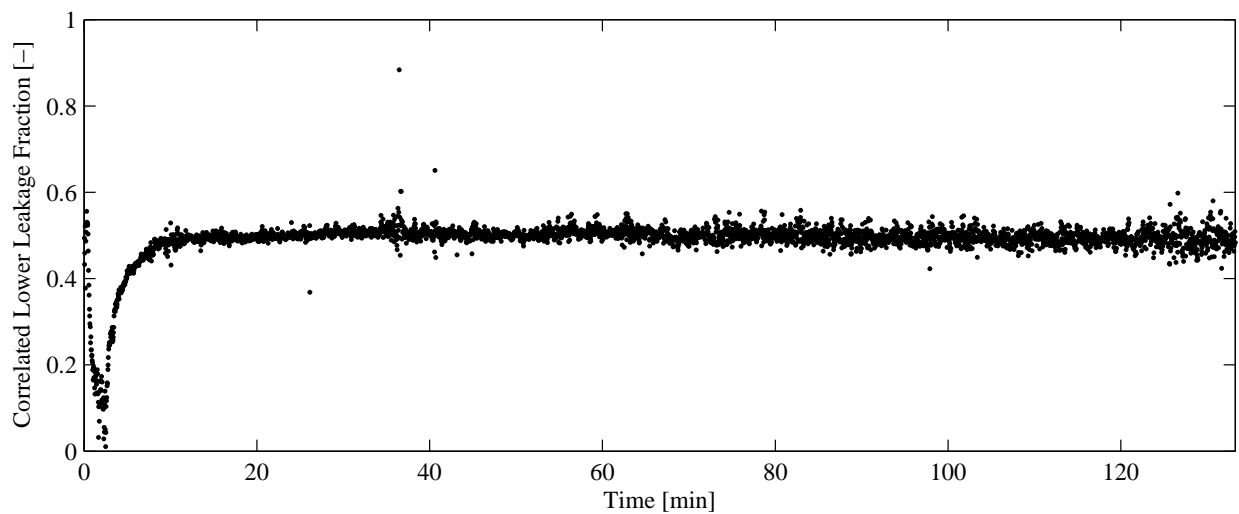


Figure G.3: Correlated lower leakage fraction for test no. 18 - Inst. #1 (HFC-125)

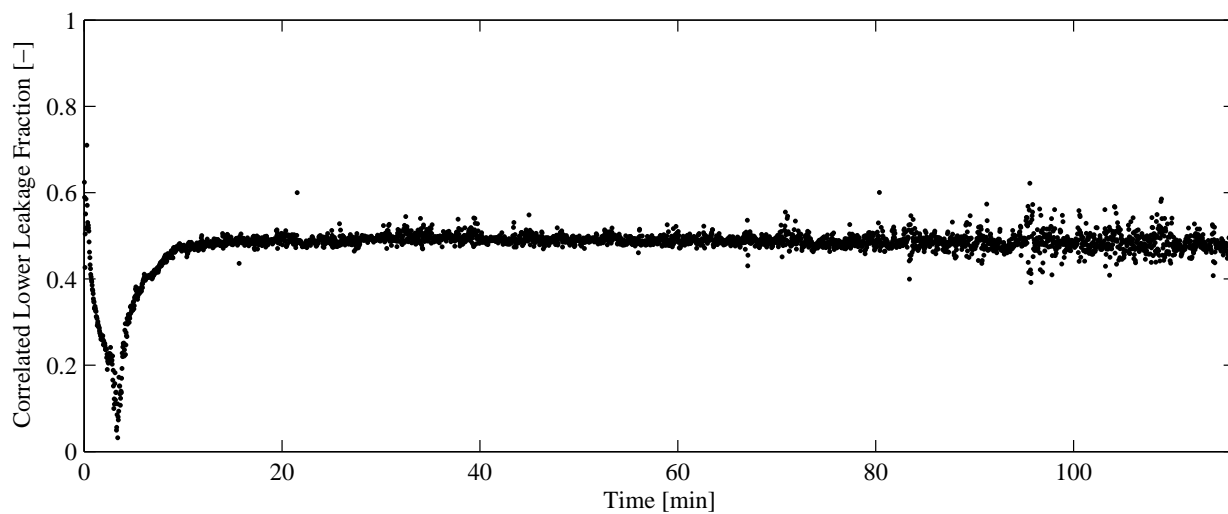


Figure G.4: Correlated lower leakage fraction for test no. 19 - Inst. #1 (HFC-125)

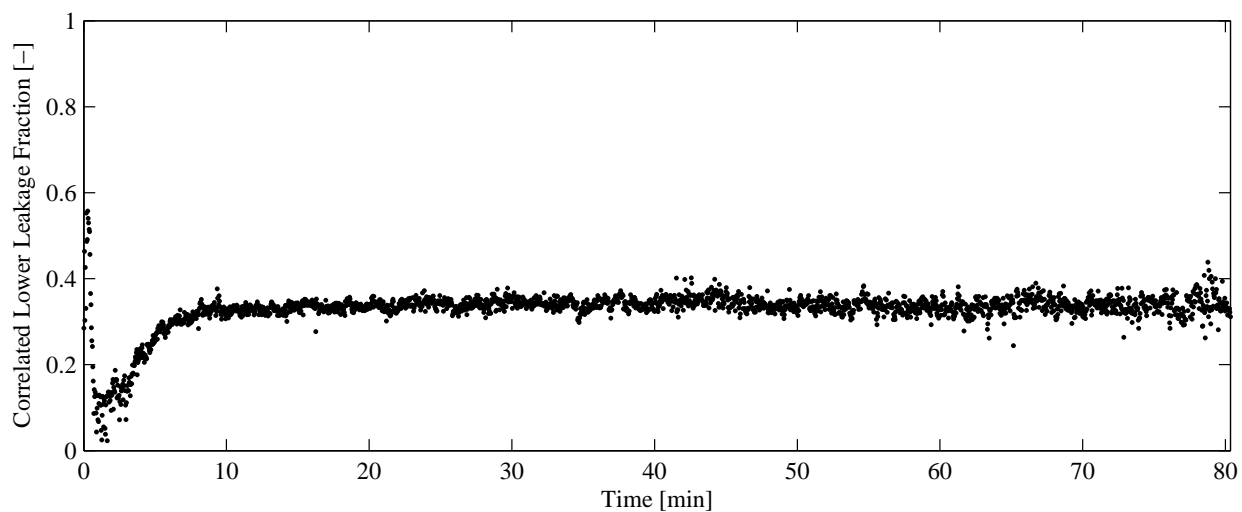


Figure G.5: Correlated lower leakage fraction for test no. 20 - Inst. #1 (HFC-125)

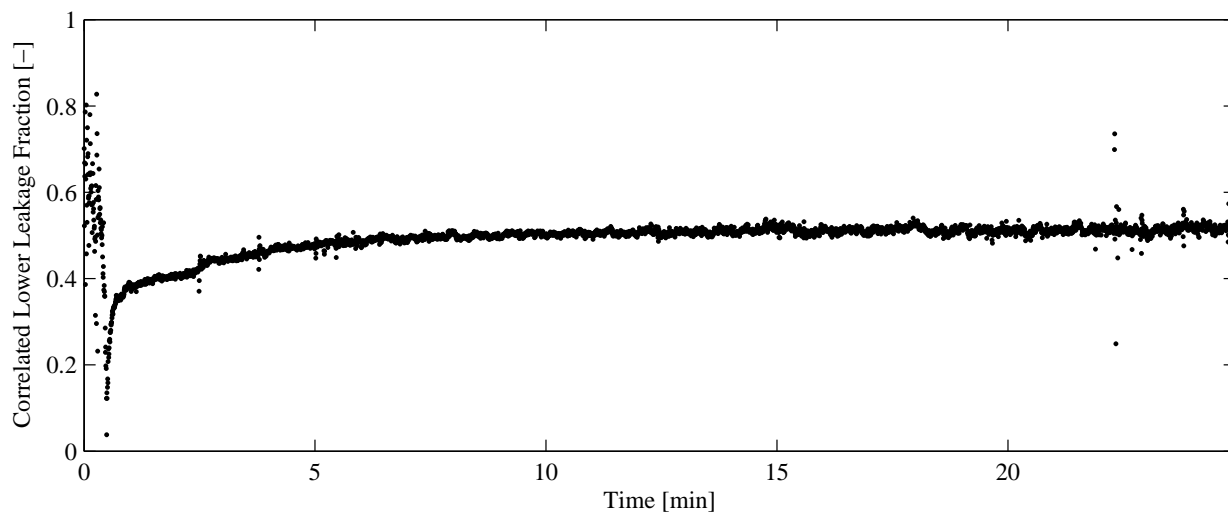


Figure G.6: Correlated lower leakage fraction for test no. 21 - Inst. #1 (HFC-227ea)

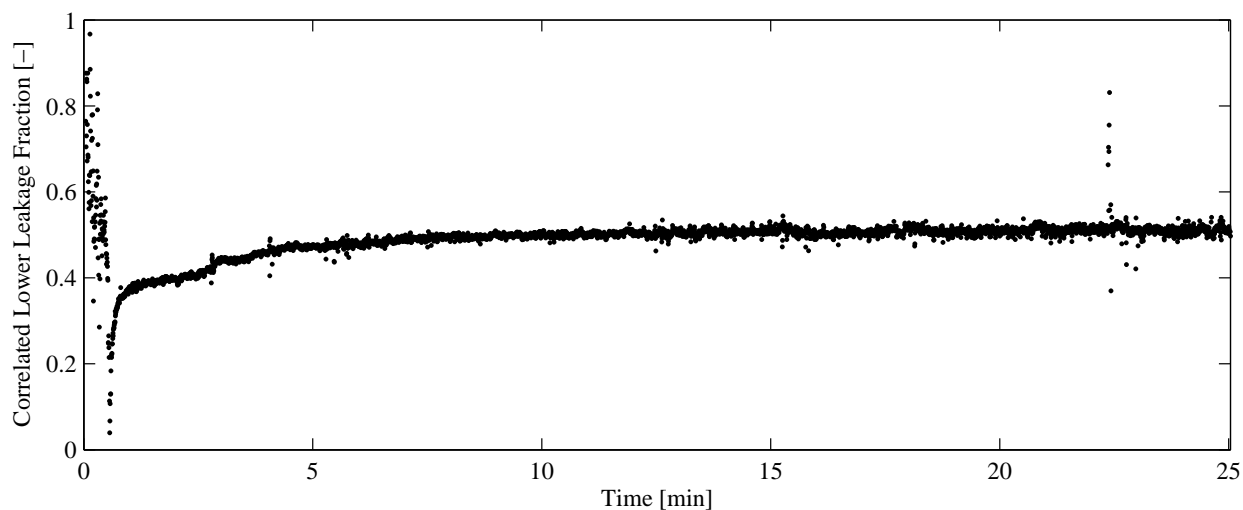


Figure G.7: Correlated lower leakage fraction for test no. 21 - Inst. #2 (HFC-227ea)

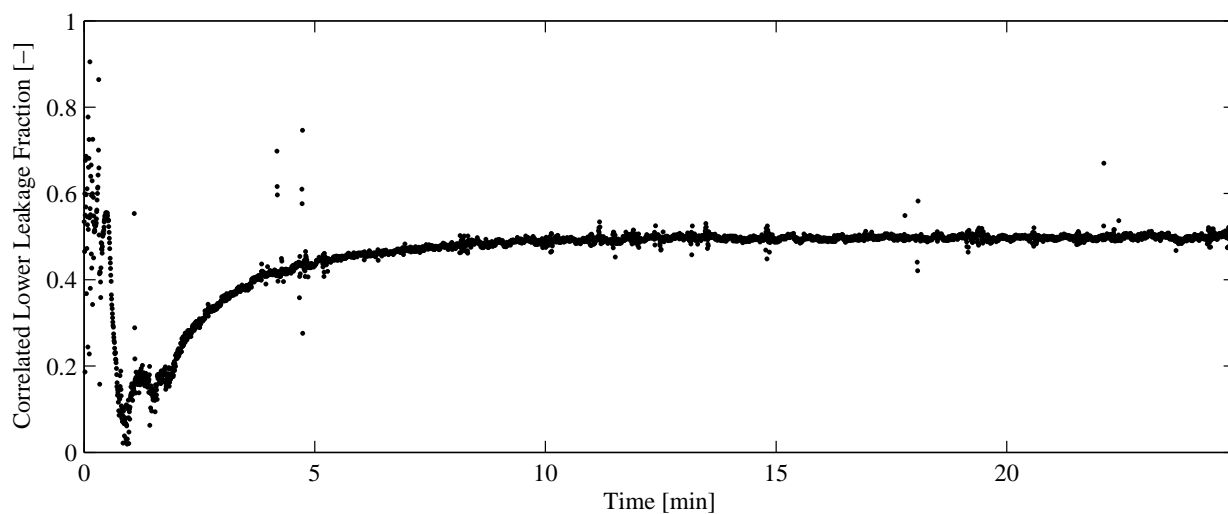


Figure G.8: Correlated lower leakage fraction for test no. 22 - Inst. #2 (HFC-227ea)

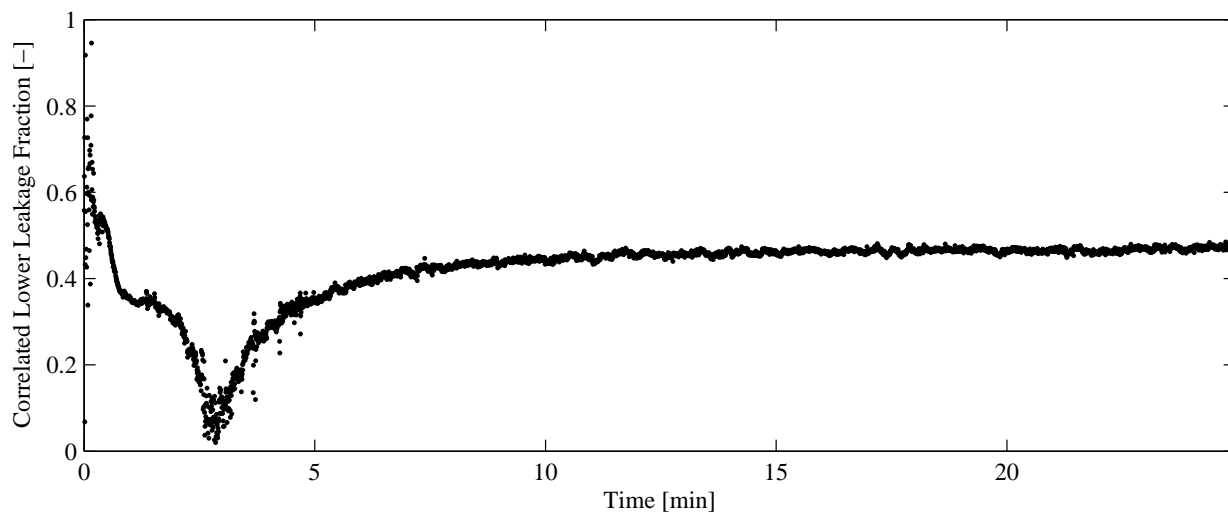


Figure G.9: Correlated lower leakage fraction for test no. 23 - Inst. #1 (HFC-227ea)

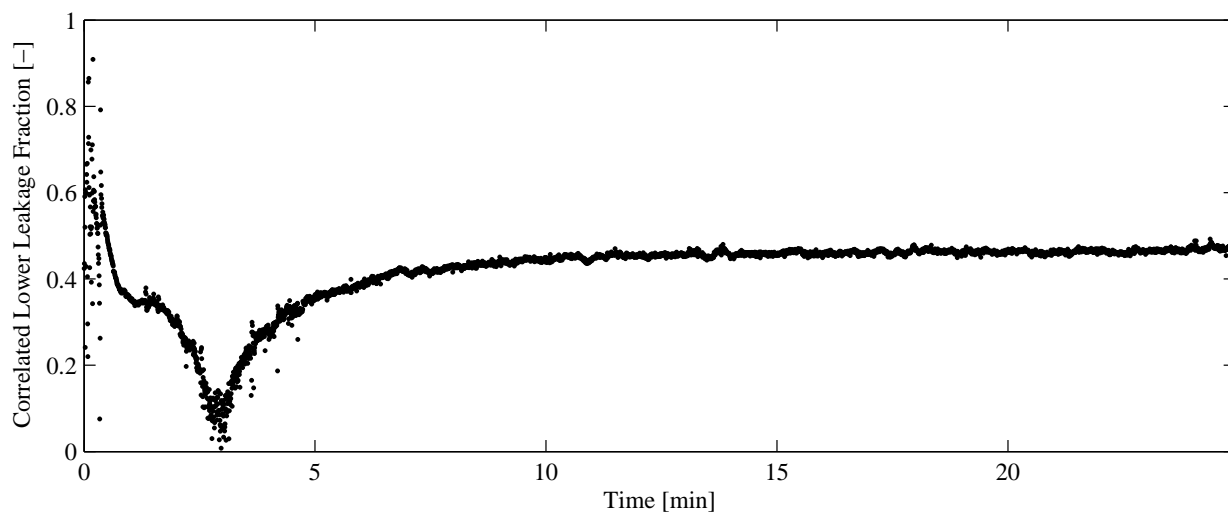


Figure G.10: Correlated lower leakage fraction for test no. 23 - Inst. #2 (HFC-227ea)

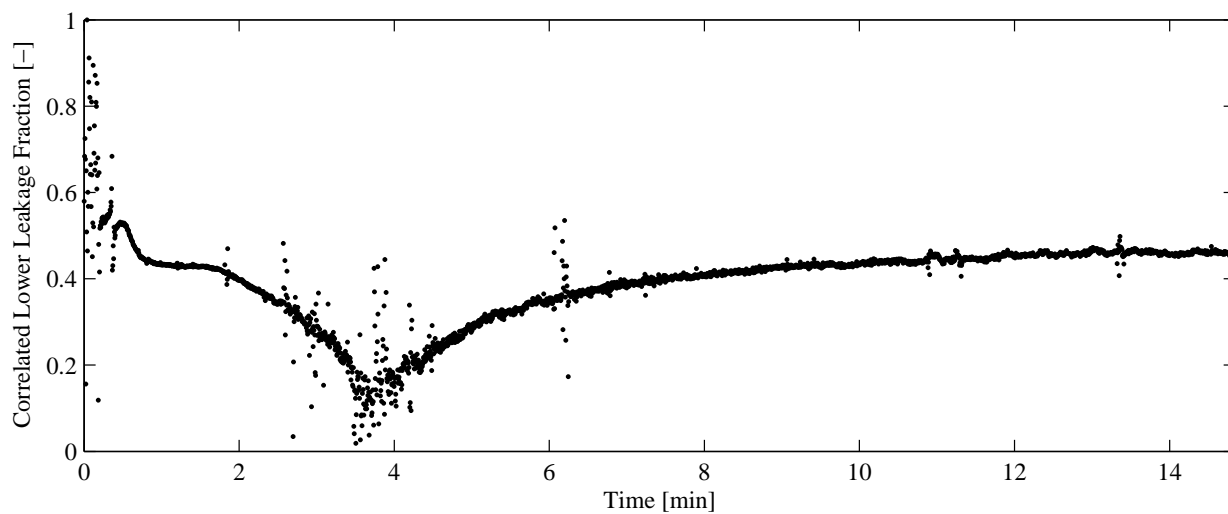


Figure G.11: Correlated lower leakage fraction for test no. 25 - Inst. #1 (HFC-227ea)

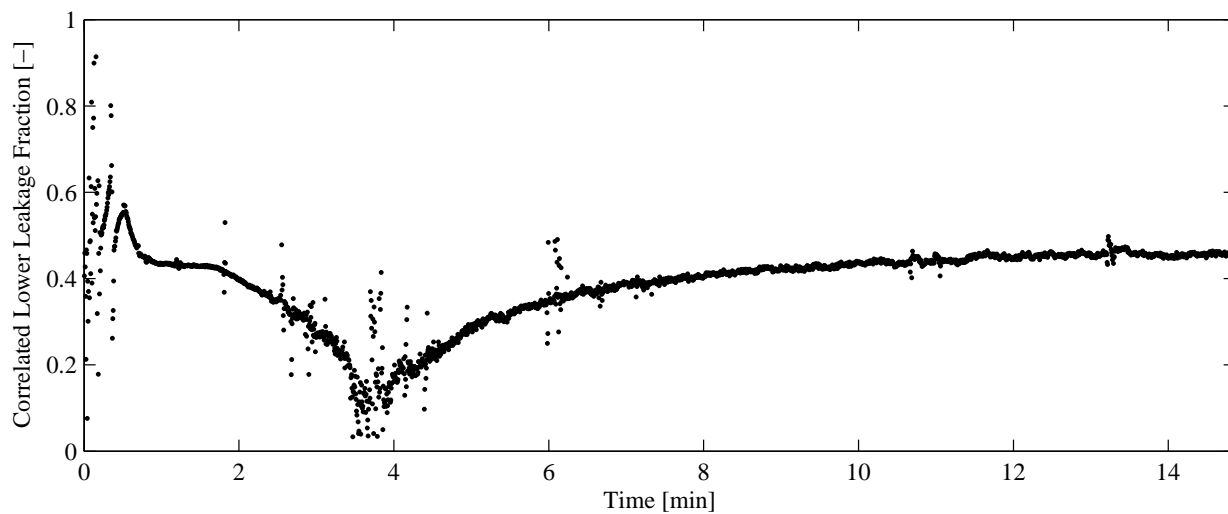


Figure G.12: Correlated lower leakage fraction for test no. 25 - Inst. #2 (HFC-227ea)

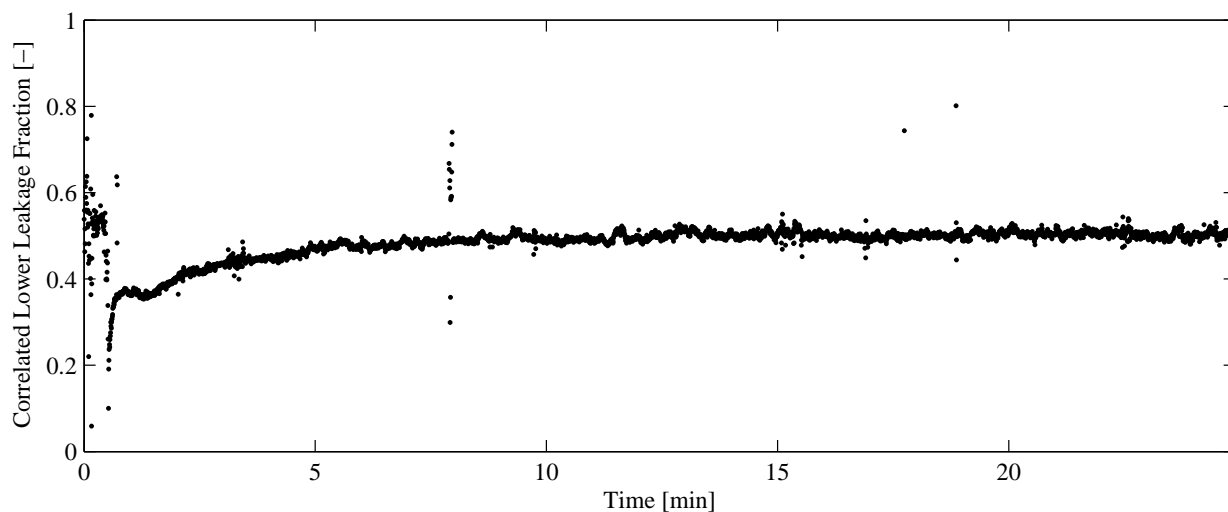


Figure G.13: Correlated lower leakage fraction for test no. 29 - Inst. #1 (HFC-23)

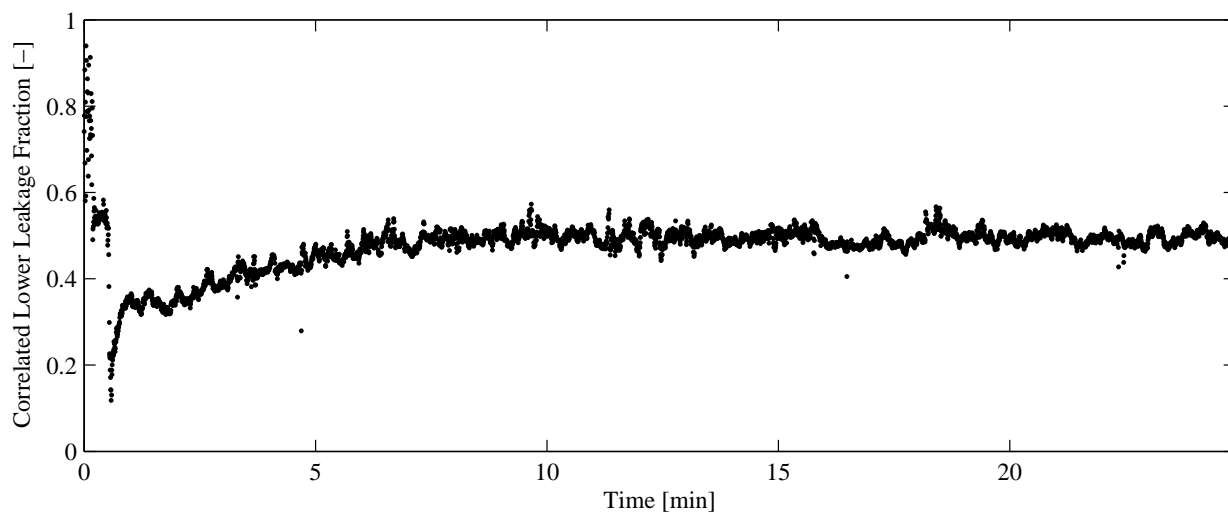


Figure G.14: Correlated lower leakage fraction for test no. 30 - Inst. #1 (HFC-23)

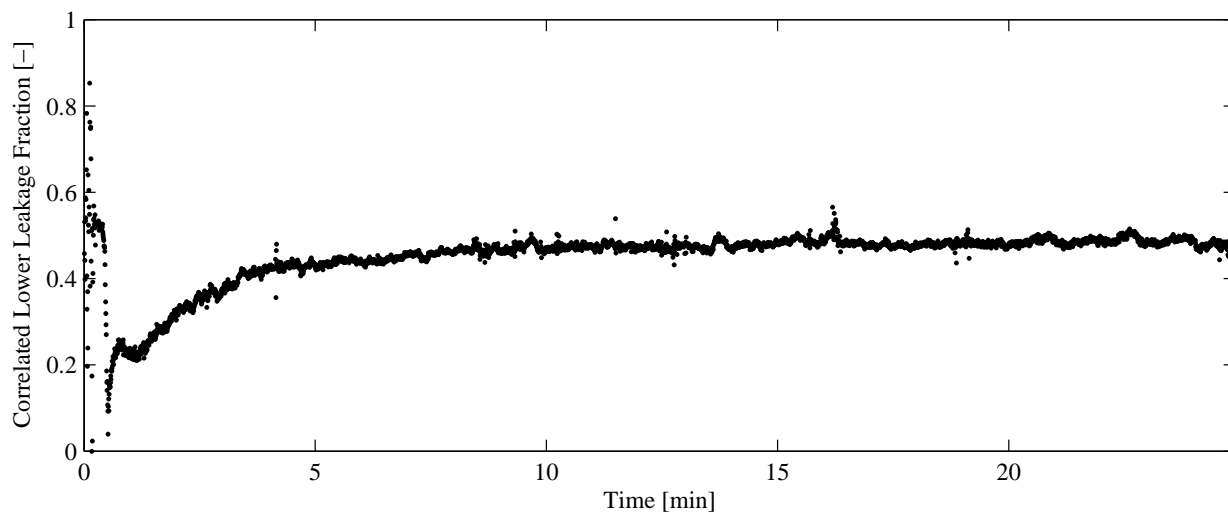


Figure G.15: Correlated lower leakage fraction for test no. 31 - Inst. #1 (HFC-23)

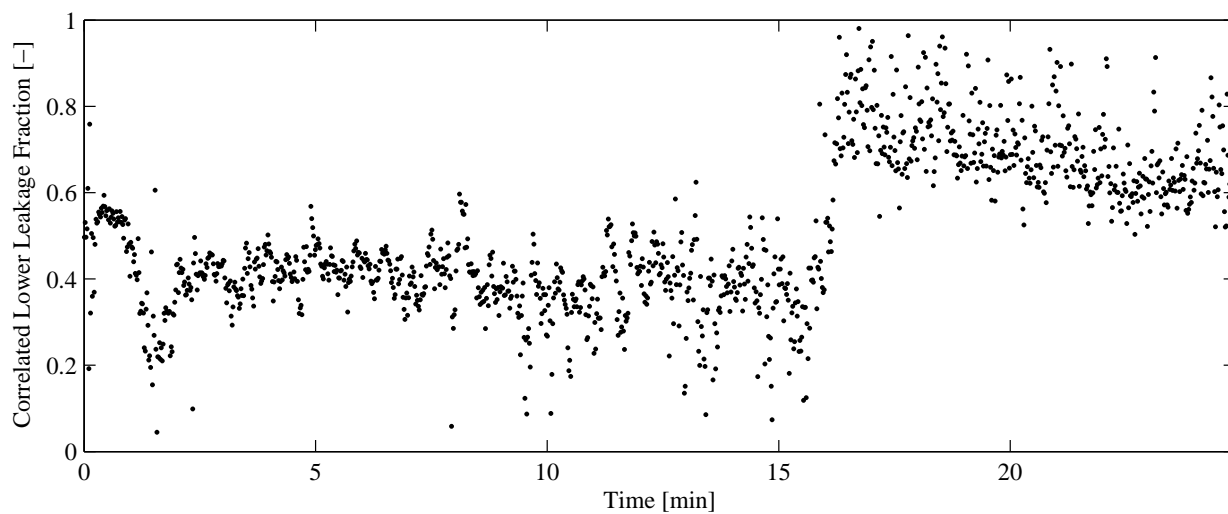


Figure G.16: Correlated lower leakage fraction for test no. 32 - Inst. #1 (IG-55)

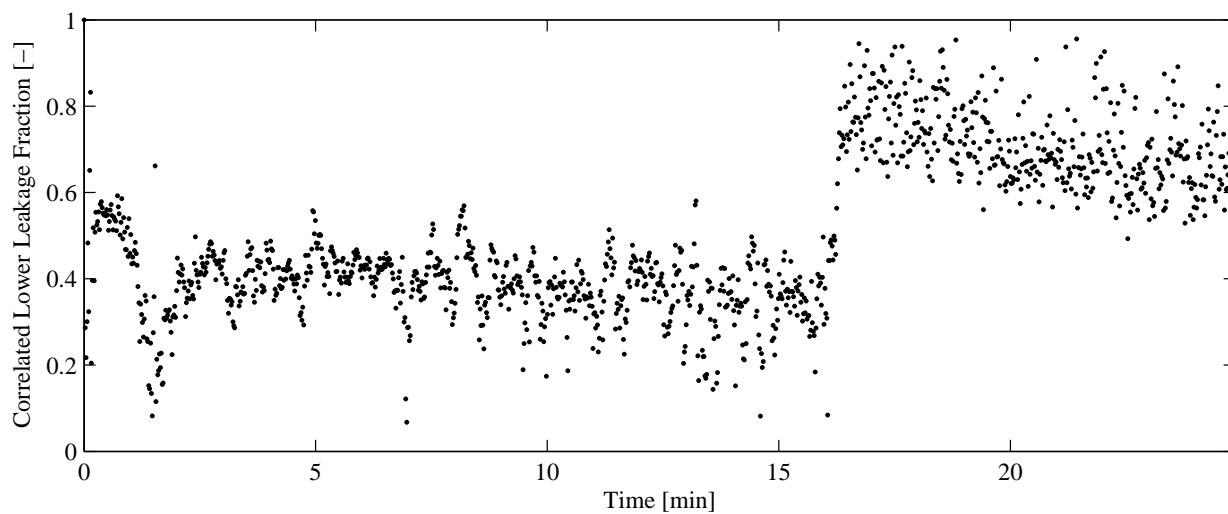


Figure G.17: Correlated lower leakage fraction for test no. 32 - Inst. #2 (IG-55)

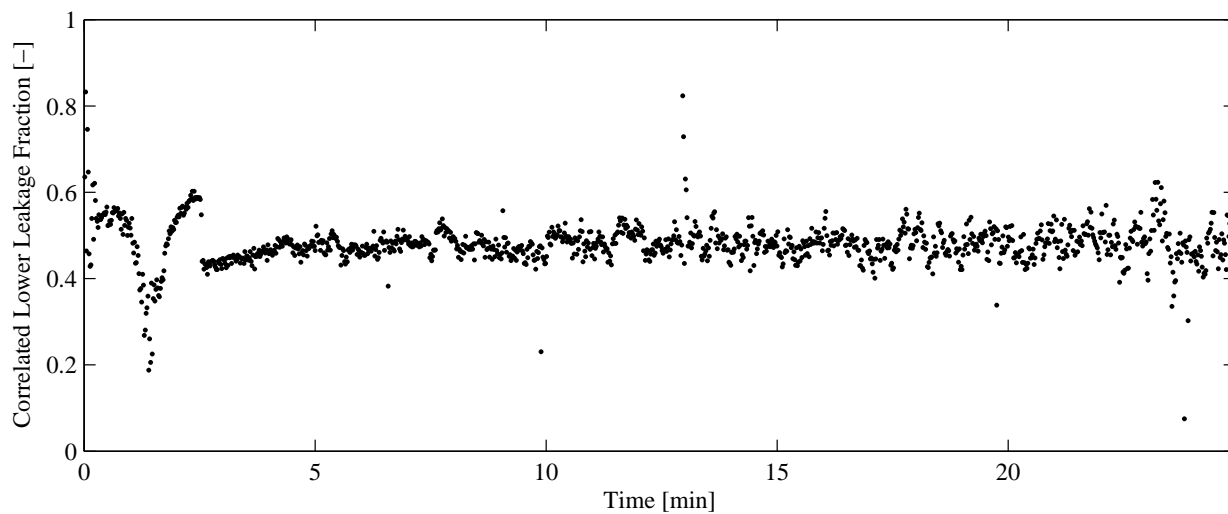


Figure G.18: Correlated lower leakage fraction for test no. 34 - Inst. #1 (IG-55)

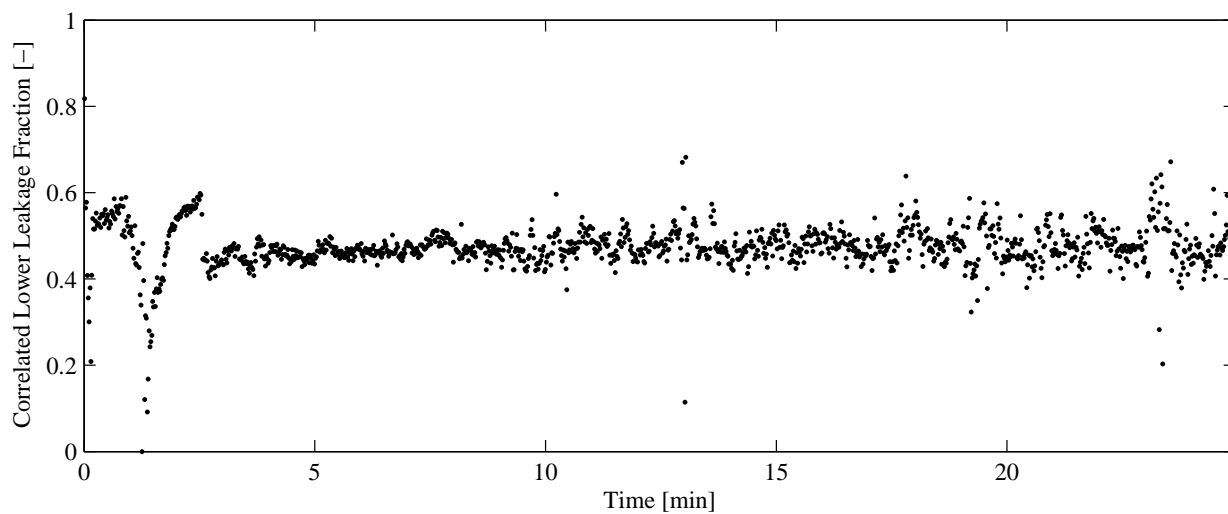


Figure G.19: Correlated lower leakage fraction for test no. 34 - Inst. #2 (IG-55)

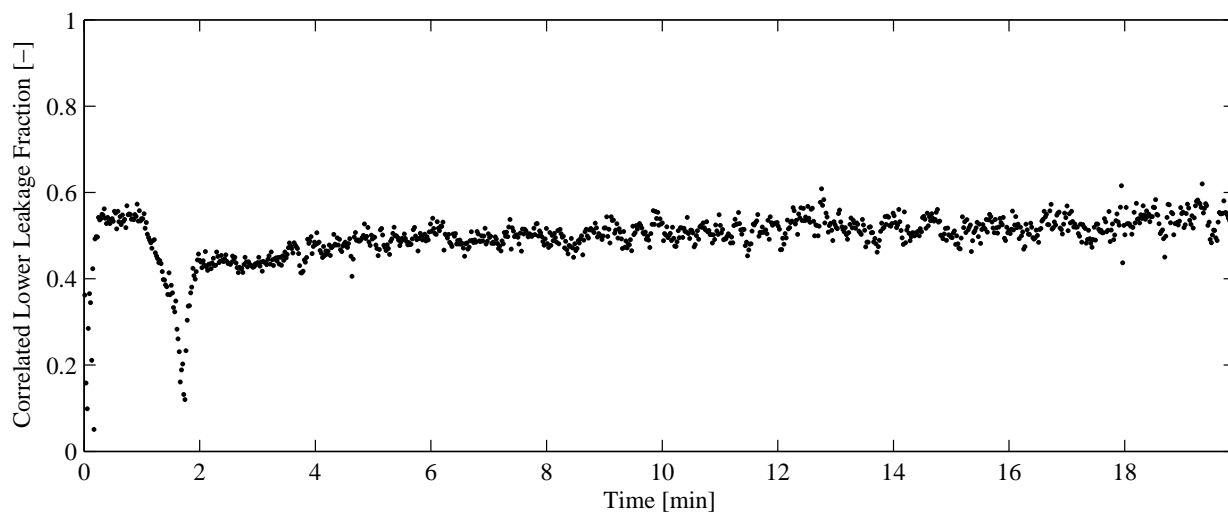


Figure G.20: Correlated lower leakage fraction for test no. 35 - Inst. #1 (IG-55)

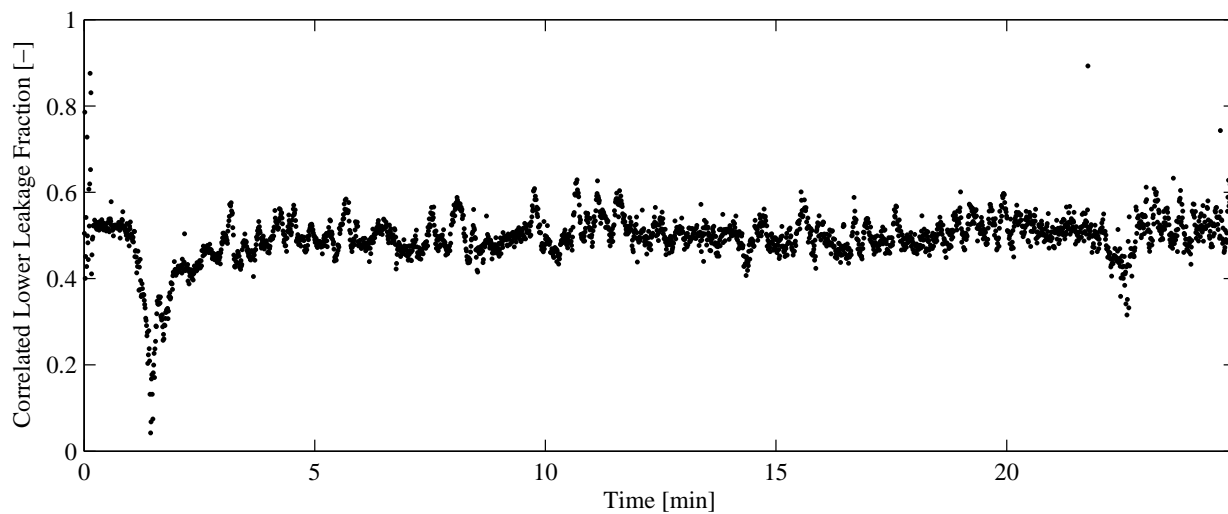


Figure G.21: Correlated lower leakage fraction for test no. 38 - Inst. #1 (IG-55P)

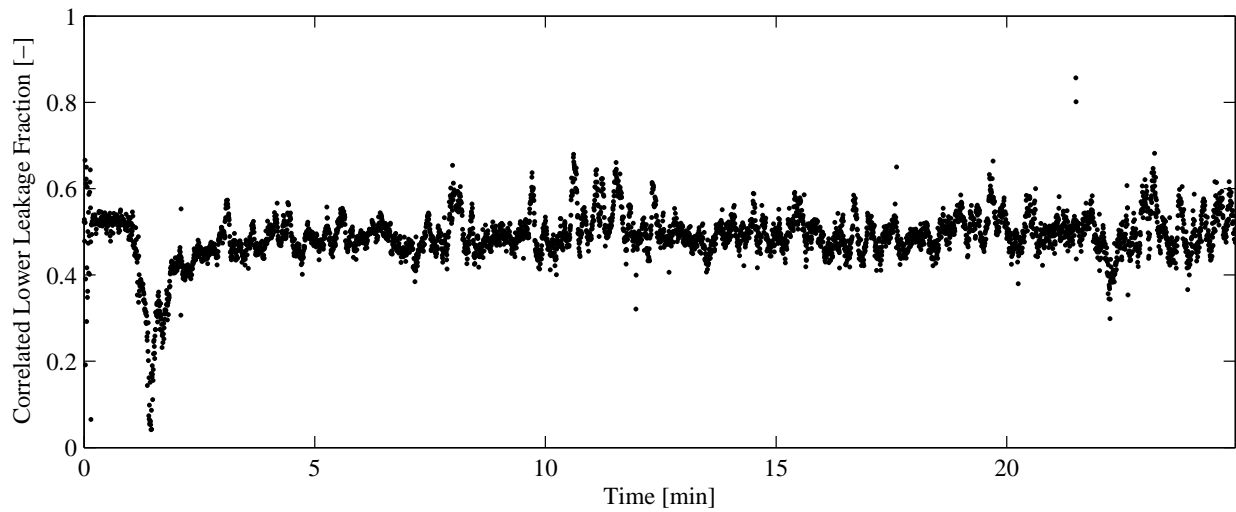


Figure G.22: Correlated lower leakage fraction for test no. 38 - Inst. #2 (IG-55P)

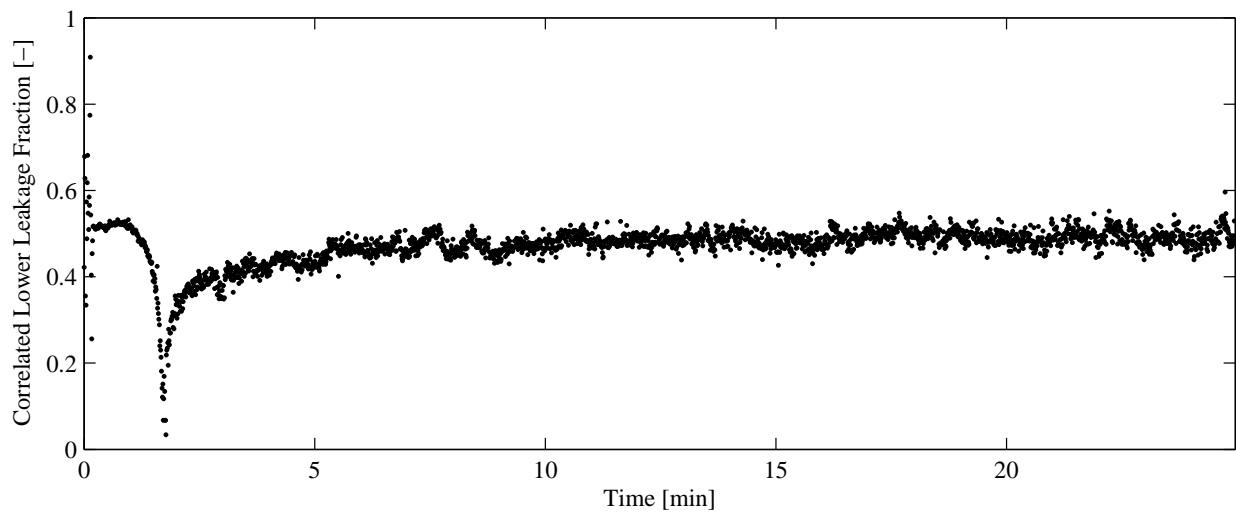


Figure G.23: Correlated lower leakage fraction for test no. 40 - Inst. #1 (IG-55P)

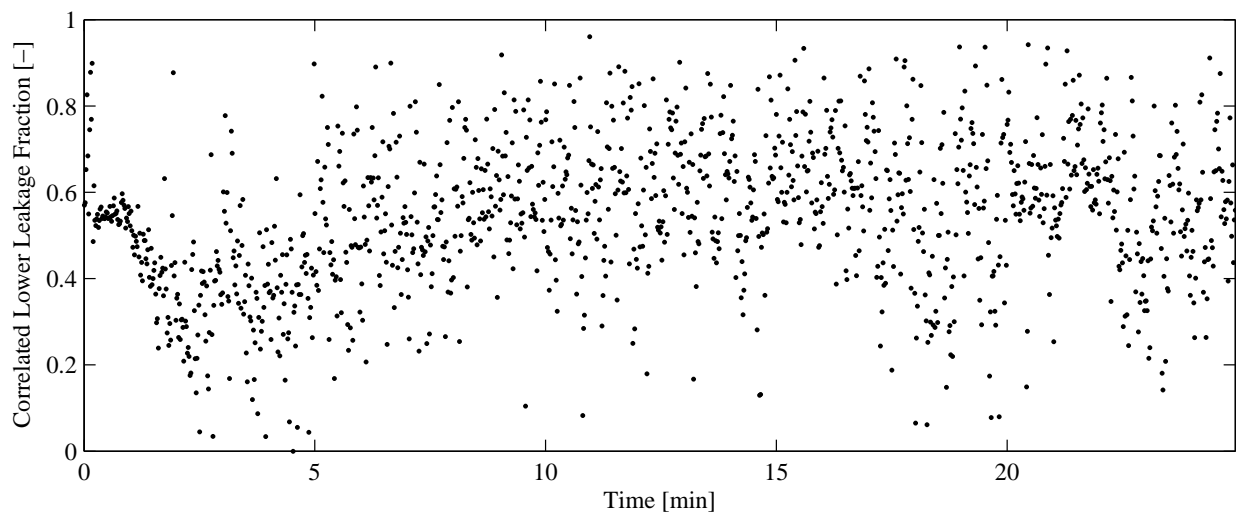


Figure G.24: Correlated lower leakage fraction for test no. 42 - Inst. #1 (IG-100)

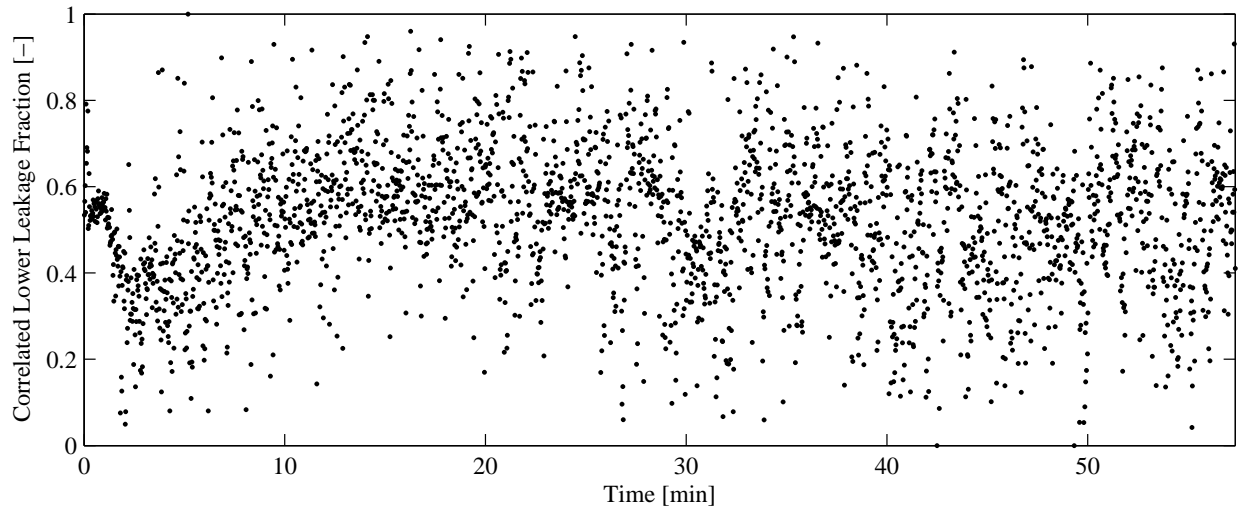


Figure G.25: Correlated lower leakage fraction for test no. 42 - Inst. #2 (IG-100)

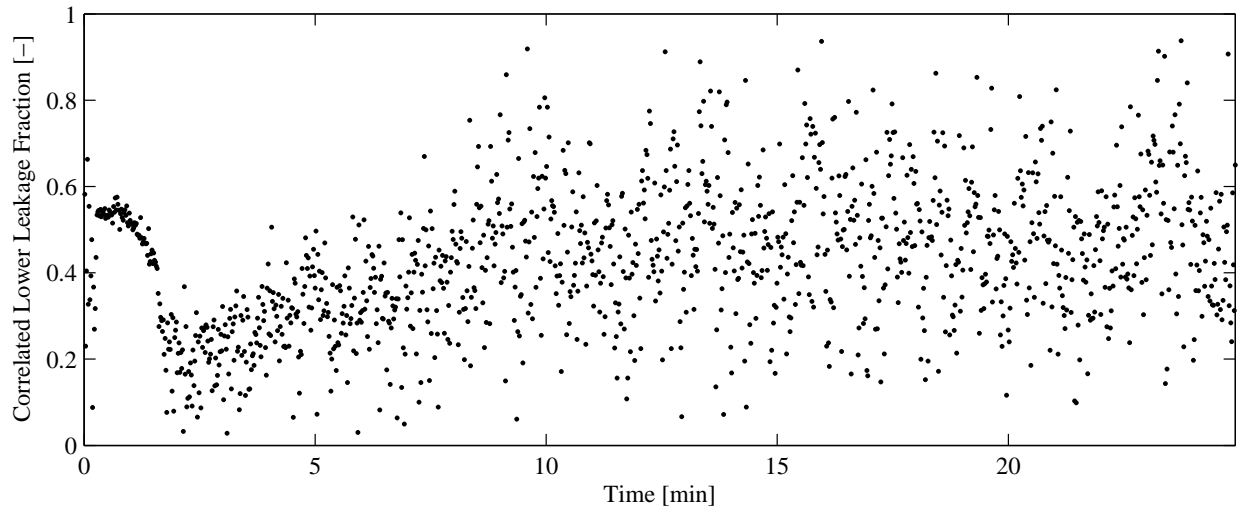


Figure G.26: Correlated lower leakage fraction for test no. 43 - Inst. #1 (IG-100)

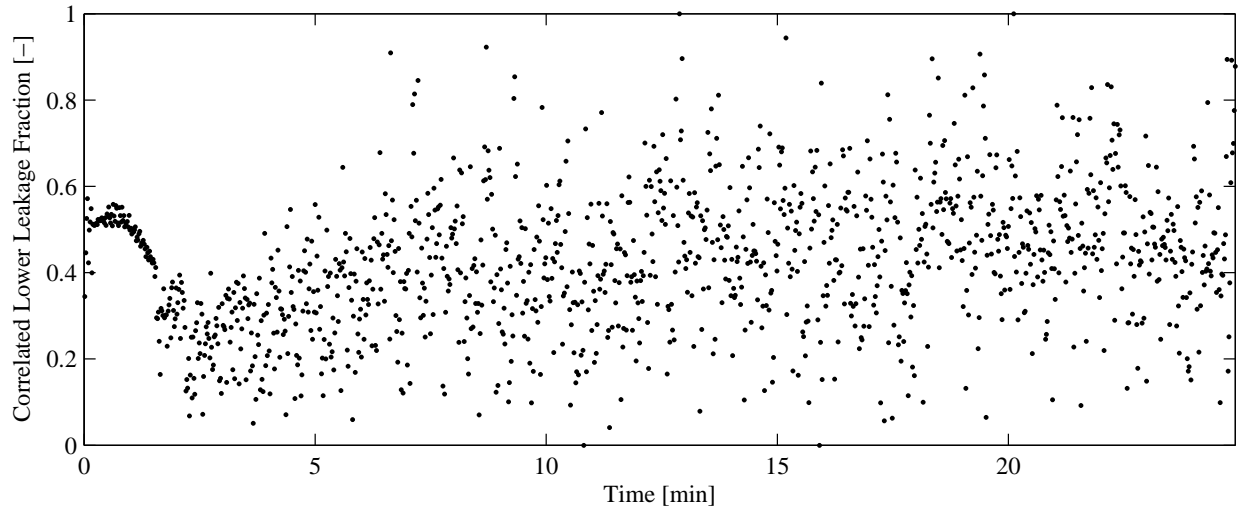


Figure G.27: Correlated lower leakage fraction for test no. 43 - Inst. #2 (IG-100)

Appendix H

The Agent Concentration Profile

Agent draining models come in two categories based upon the assumption taken for gas species diffusivity. When assumed to occur instantaneously, a homogeneous mix of agent and air of gradually decaying concentration exists within the enclosure. Such a model is termed the *continuous mixing model*. When gas diffusion is assumed nonexistent or to occur in instantaneously-mixed, predefined ratios, the draining agent-air mixture and inflowing fresh air are assumed to stratify. Models in this category are termed the *sharp descending interface*, *wide descending interface*, and *thick descending interface*.

The analysis provided in this document analyzes the data only in the stratifying regime. Agents that do not exhibit a predictable degree of stratification generally do not drain from the design envelope as readily as other agent types (typically those with vapor densities much heavier than atmospheric air). Due to the heightened risk of rapid agent draining, the focus throughout is placed on understanding the predictability of hold times for stratifying agent types.

The following pages of this appendix provide figures that translate the agent concentration data of Appendix C onto elevation-concentration axes. The same axes are used to demonstrate the ideal elevation-concentration assumptions for each of the descending interface models in Figures 2.8 and 3.4. The accuracy of the assumptions taken can be evaluated through direct comparison of the assumed profile and that exhibited in the ensuing figures.

Reference Tables A.1, A.2, and A.3 for information on each experiments' configuration parameters.

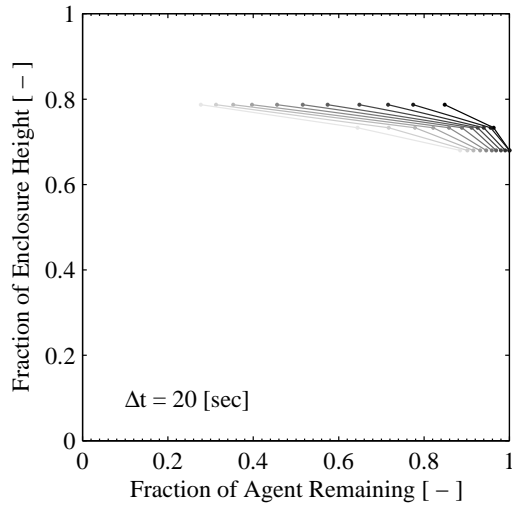


Figure H.1: Test no. 1 (HFC-227ea)

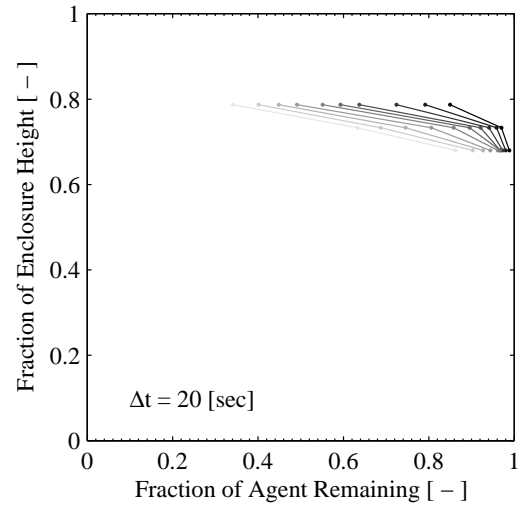


Figure H.2: Test no. 2 (HFC-227ea)

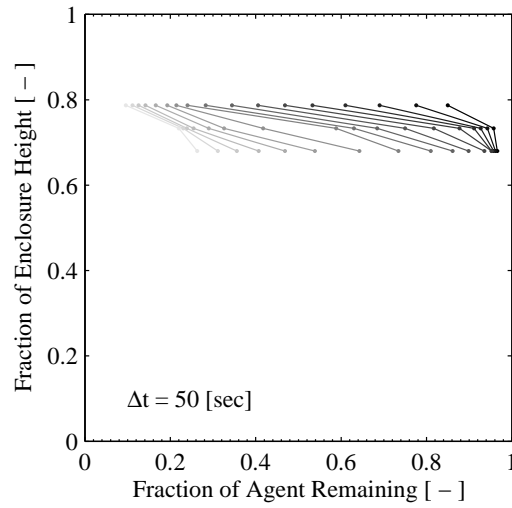


Figure H.3: Test no. 3 (HFC-227ea)

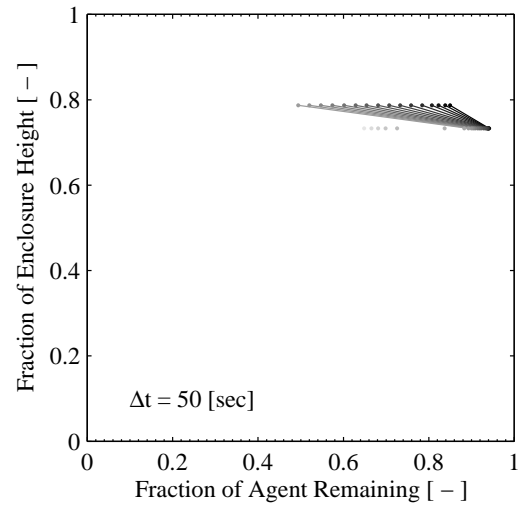


Figure H.4: Test no. 5 (HFC-227ea)

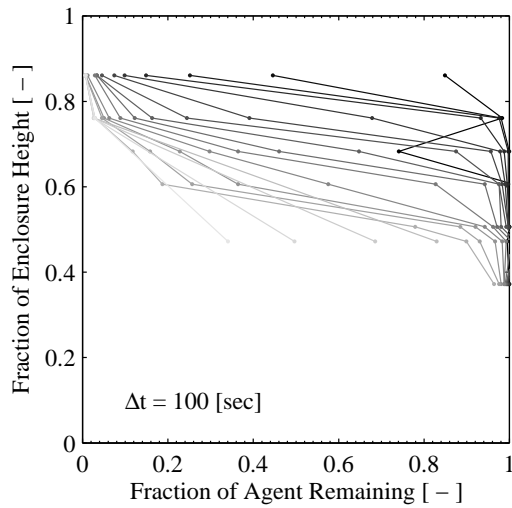


Figure H.5: Test no. 6 (FK-5-1-12)

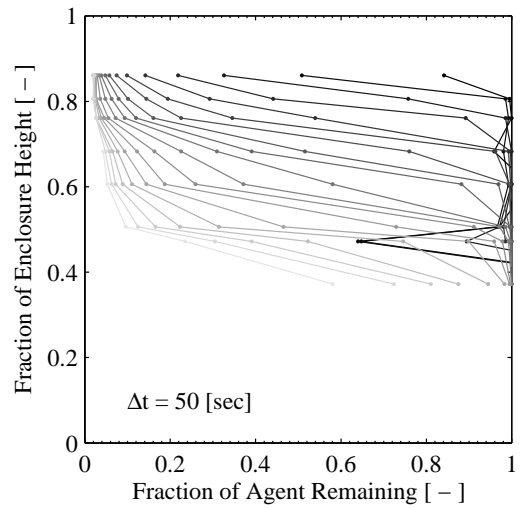


Figure H.6: Test no. 7 (FK-5-1-12)

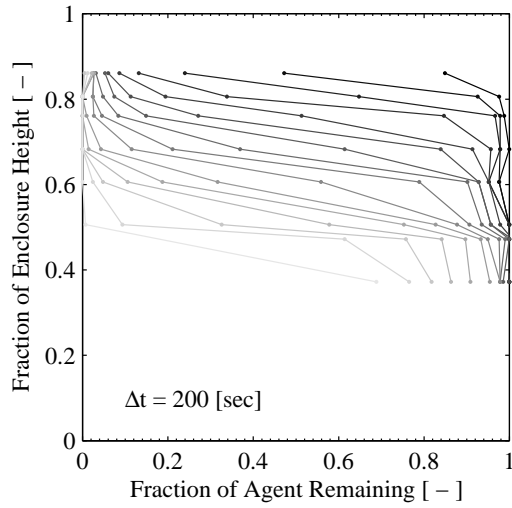


Figure H.7: Test no. 8 (FK-5-1-12)

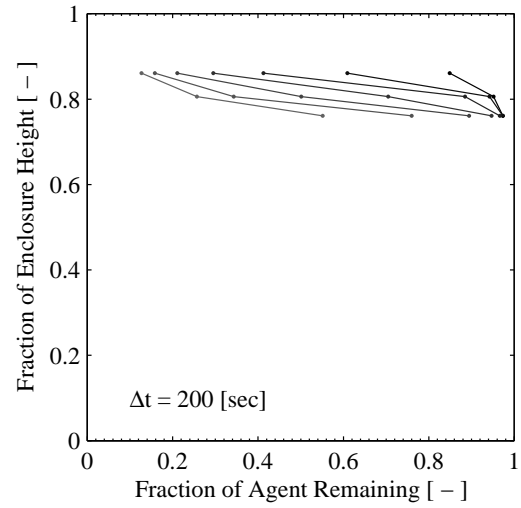


Figure H.8: Test no. 9 (FK-5-1-12)

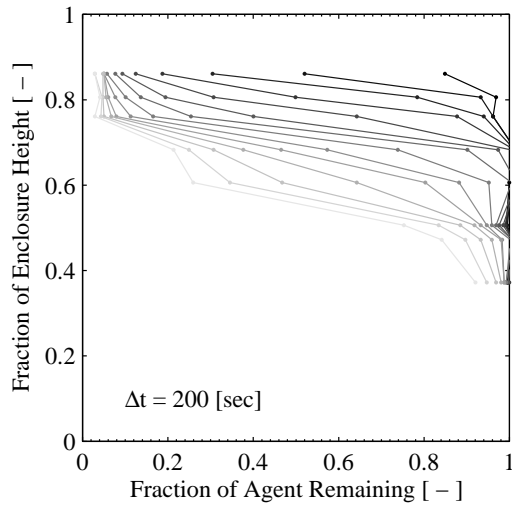


Figure H.9: Test no. 10 (FK-5-1-12)

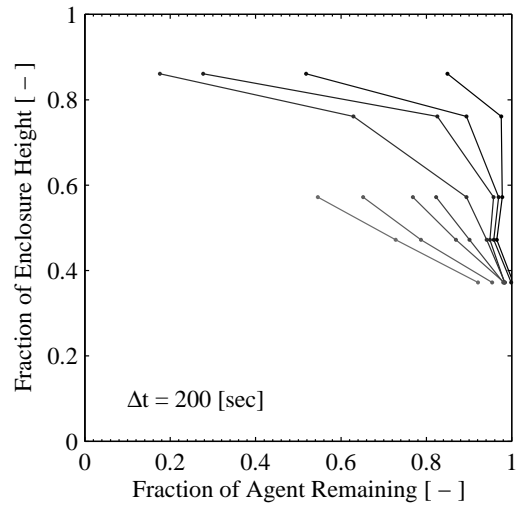


Figure H.10: Test no. 11 (IG-541)

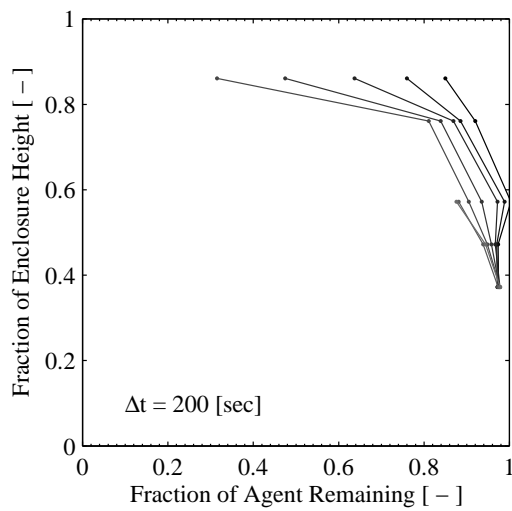


Figure H.11: Test no. 12 (IG-541)

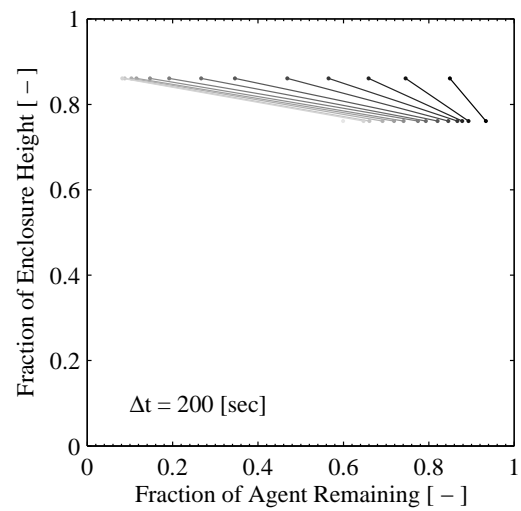


Figure H.12: Test no. 13 (IG-541)

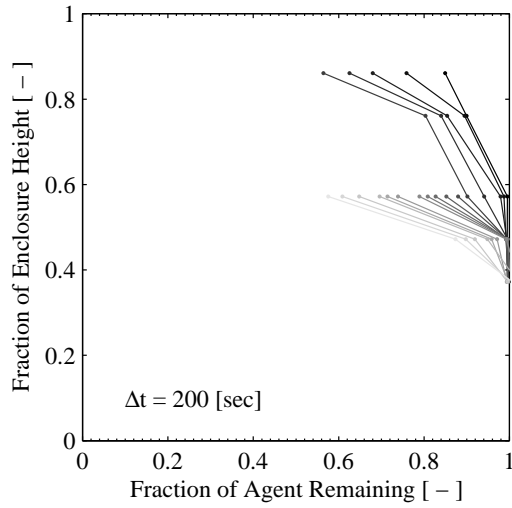


Figure H.13: Test no. 14 (IG-541)

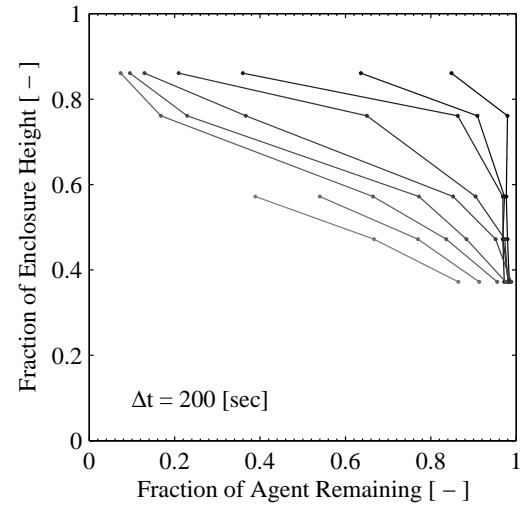


Figure H.14: Test no. 15 (IG-541)

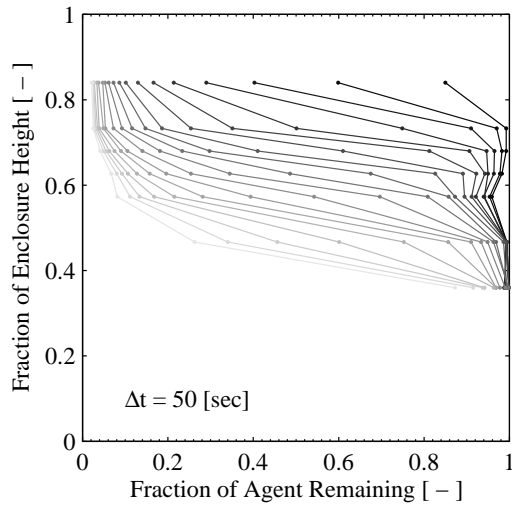


Figure H.15: Test no. 16 (HFC-125)

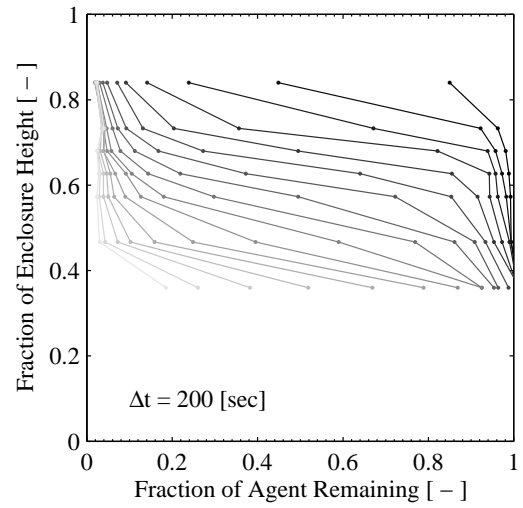


Figure H.16: Test no. 17 (HFC-125)

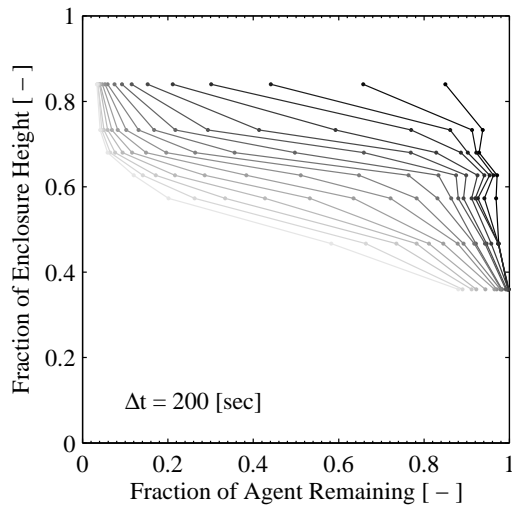


Figure H.17: Test no. 18 (HFC-125)

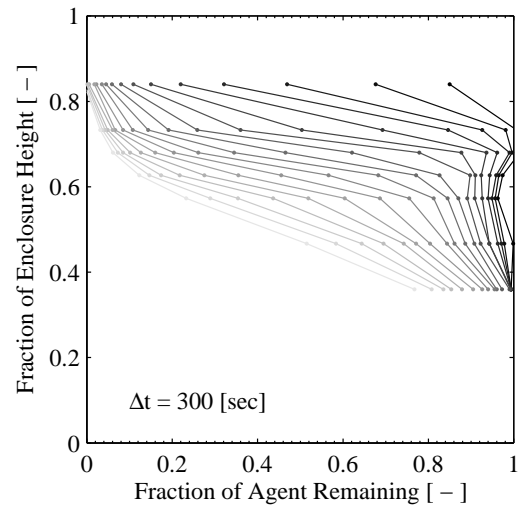


Figure H.18: Test no. 19 (HFC-125)

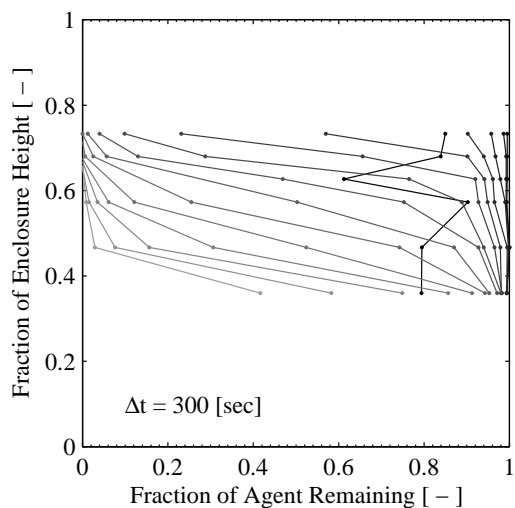


Figure H.19: Test no. 20 (HFC-125)

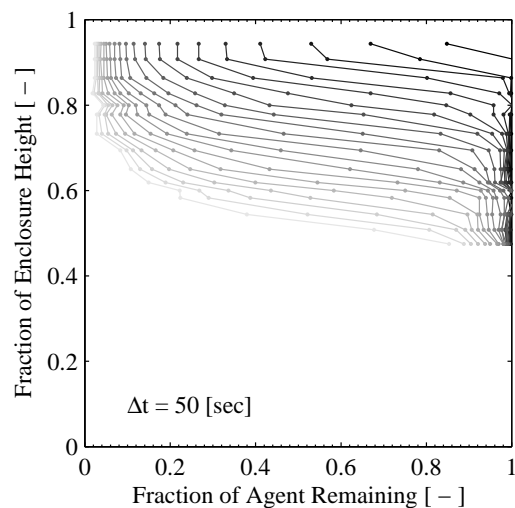


Figure H.20: Test no. 21 (HFC-227ea)

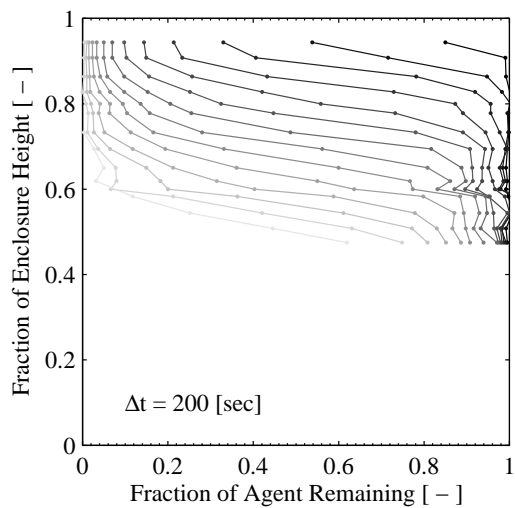


Figure H.21: Test no. 22 (HFC-227ea)

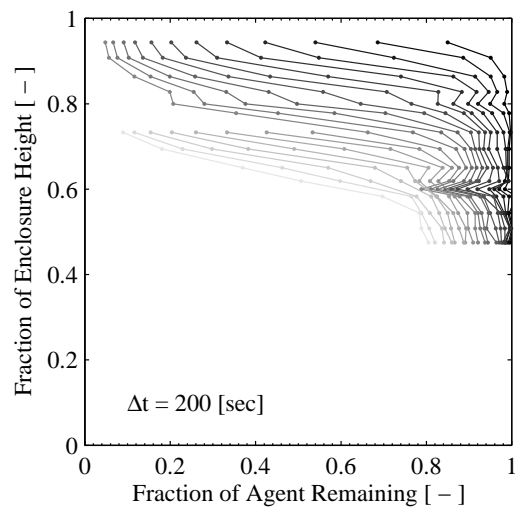


Figure H.22: Test no. 23 (HFC-227ea)

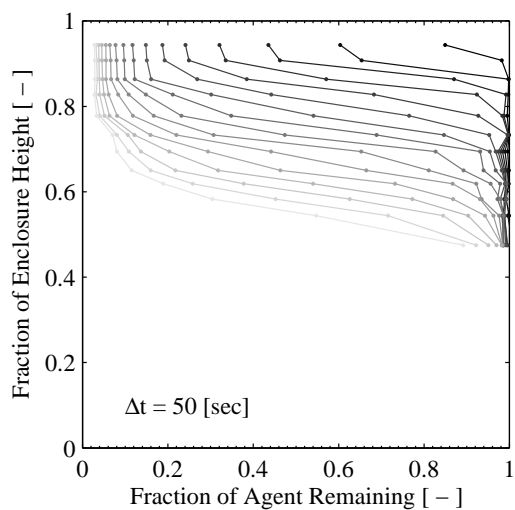


Figure H.23: Test no. 28 (HFC-23)

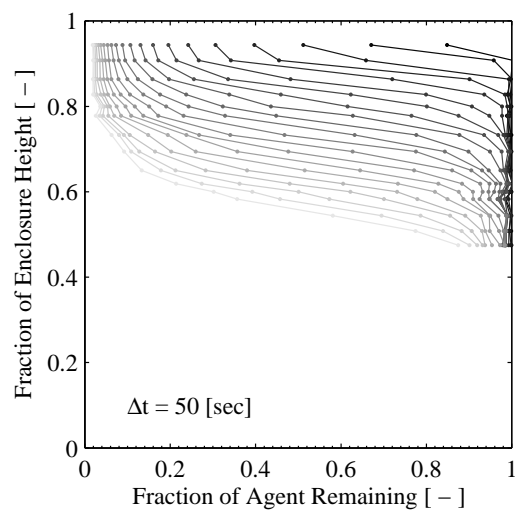


Figure H.24: Test no. 29 (HFC-23)

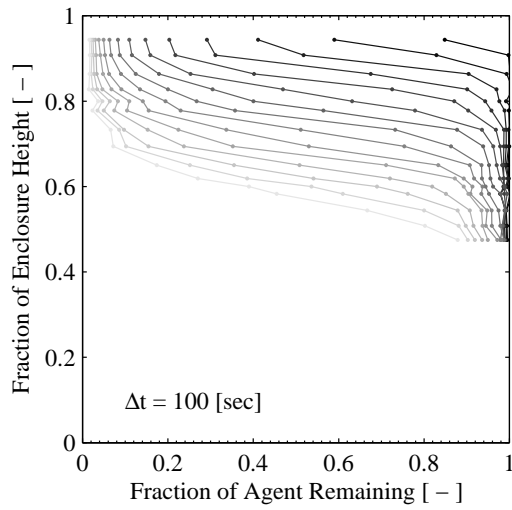


Figure H.25: Test no. 30 (HFC-23)

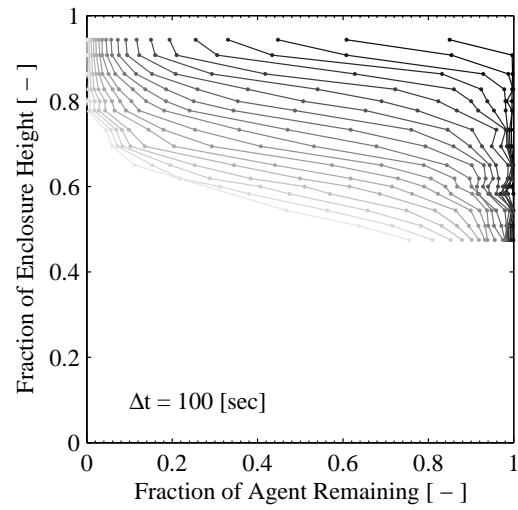


Figure H.26: Test no. 31 (HFC-23)

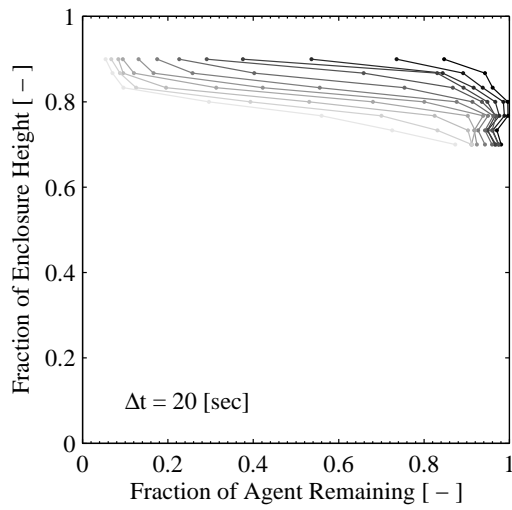


Figure H.27: Test no. 32 (IG-55)

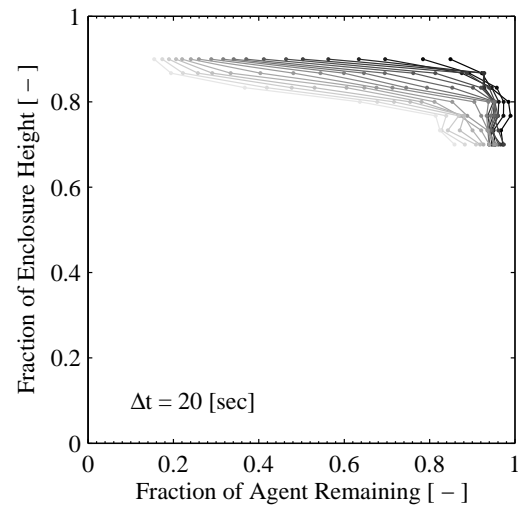


Figure H.28: Test no. 34 (IG-55)

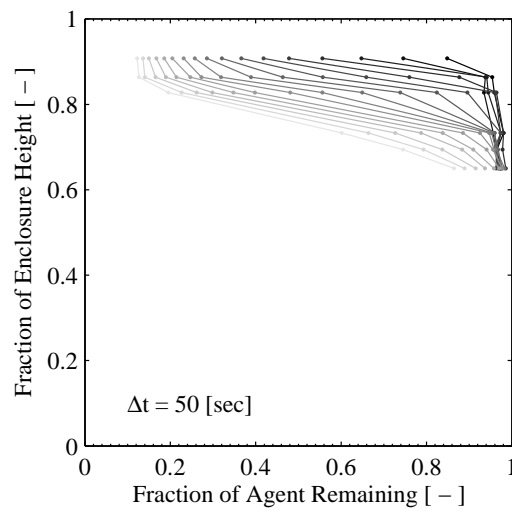


Figure H.29: Test no. 35 (IG-55)

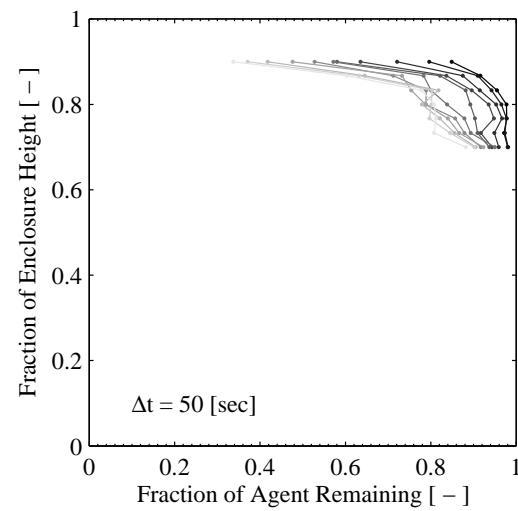


Figure H.30: Test no. 36 (IG-55)

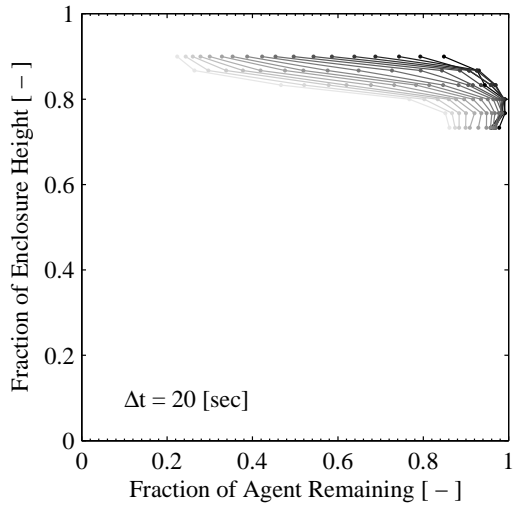


Figure H.31: Test no. 38 (IG-55P)

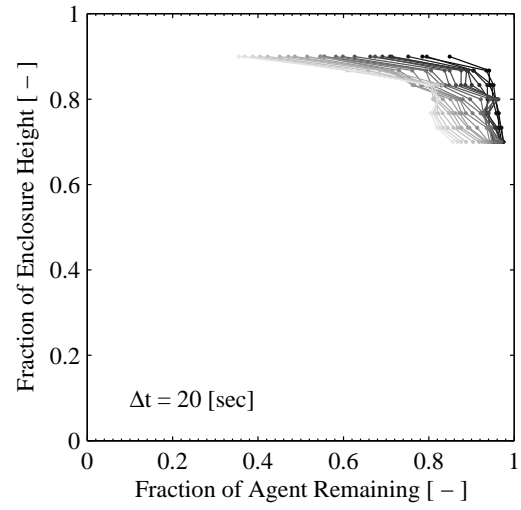


Figure H.32: Test no. 40 (IG-55P)

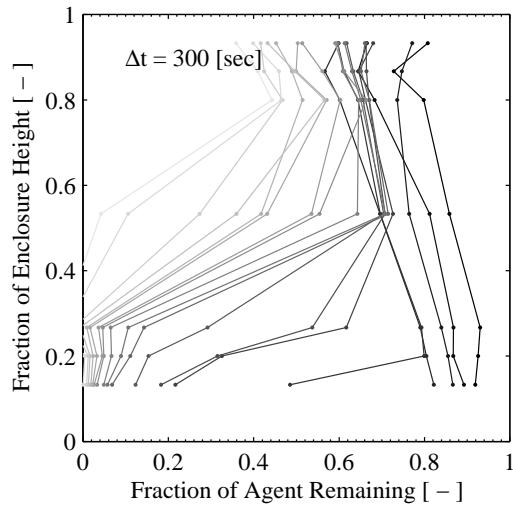


Figure H.33: Test no. 42 (IG-100)

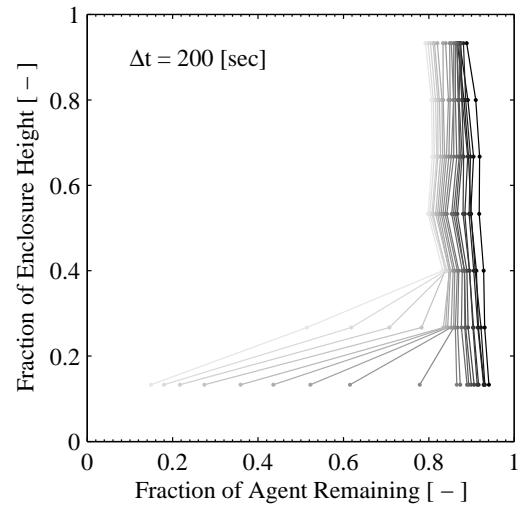


Figure H.34: Test no. 43 (IG-100)

Appendix I

The Regressed Agent Profile Slope

This appendix documents a test-by-test regression of the observed experimental agent concentration profile as depicted in Appendix H. The regressed parameter is the slope of the linearized elevation-concentration profile as a function of time. This parameter is referred to as the slope, represented as,

$$\omega = \frac{(\Delta H/H_{max})}{(\Delta C/C_{max})},$$

or the normalized change in elevation, H , over the normalized change in agent concentration, C . Throughout this appendix the regressed slope, or dimensionless interface thickness (when assuming that the denominator, $(\Delta C/C_{max})$, always equals 1), is always plotted as a positive magnitude.

The new stratifying hold time model presented in Chapter 3 relies upon the assumed existence of a characteristic maximum slope, which is obtained for use from the experimental data sets as regressed in the following. The regression procedure is detailed in Section 3.4, primarily as demonstrated by Figure 3.5.

Reference Tables A.1, A.2, and A.3 for information on each experiments' configuration parameters.

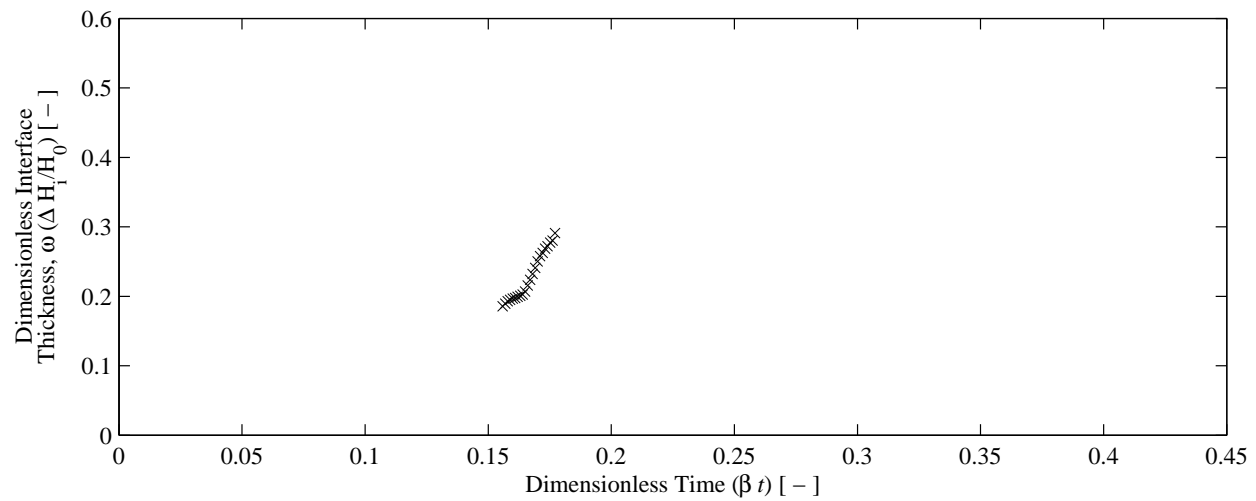


Figure I.1: Transient regressed agent profile slope for test no. 1 (HFC-227ea)

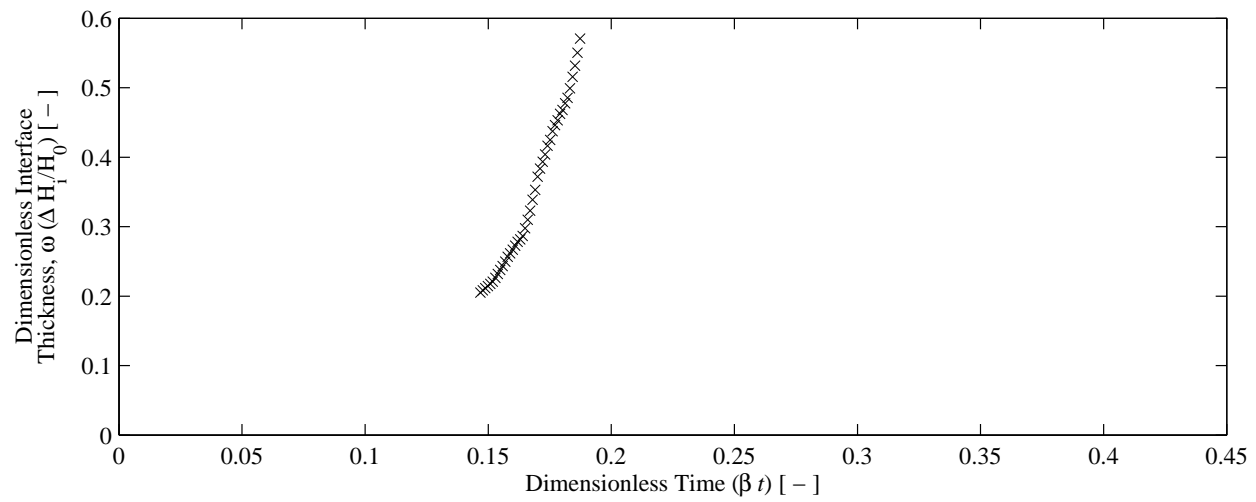


Figure I.2: Transient regressed agent profile slope for test no. 2 (HFC-227ea)

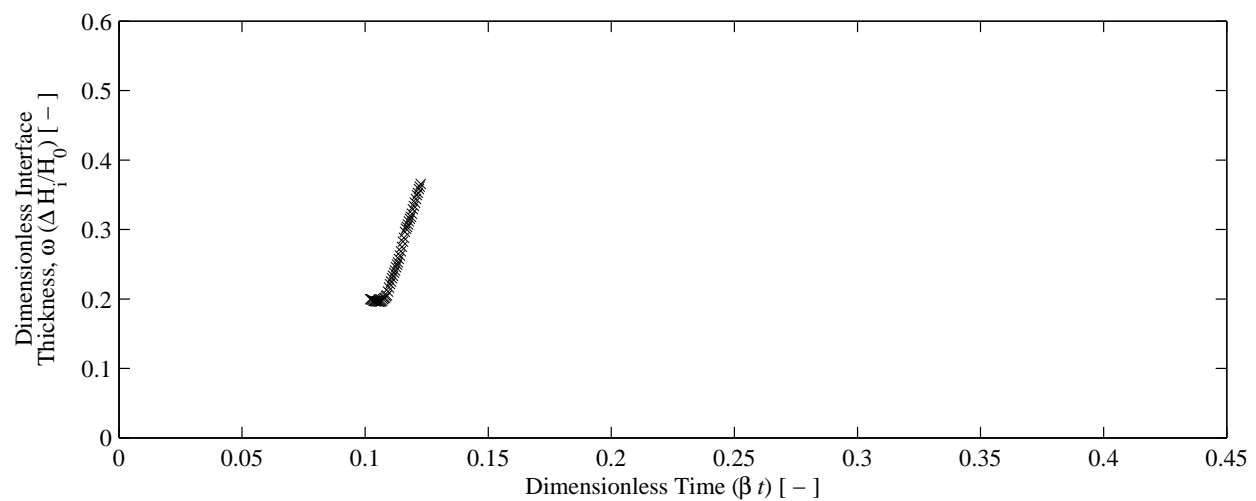


Figure I.3: Transient regressed agent profile slope for test no. 3 (HFC-227ea)

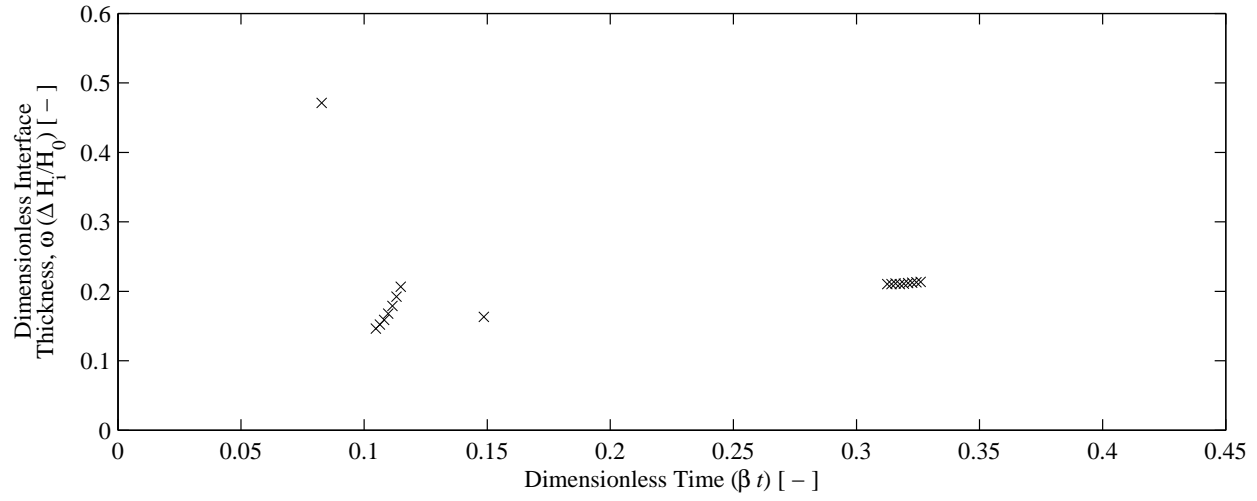


Figure I.4: Transient regressed agent profile slope for test no. 7 (FK-5-1-12)

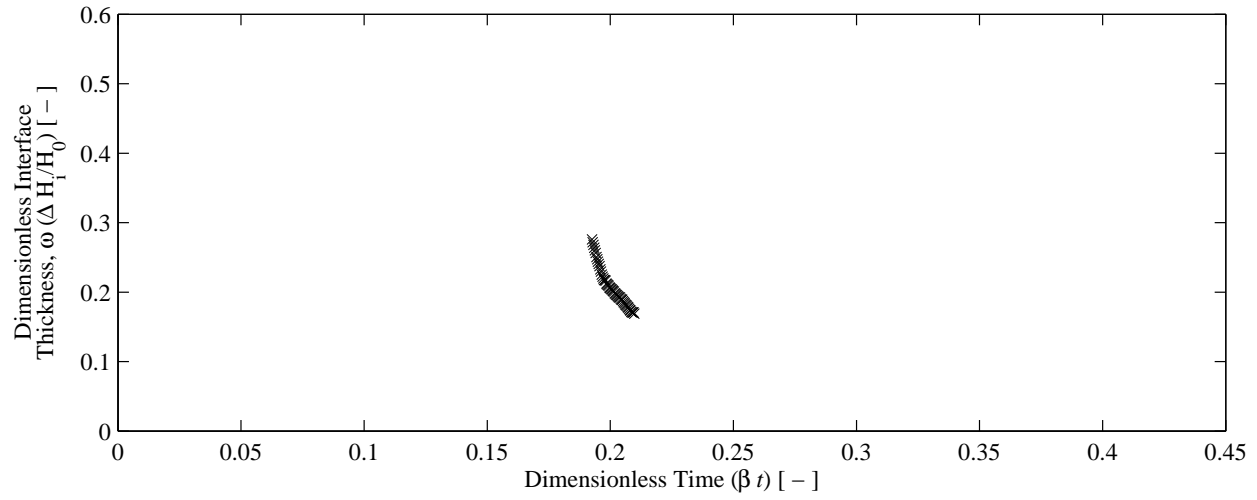


Figure I.5: Transient regressed agent profile slope for test no. 8 (FK-5-1-12)

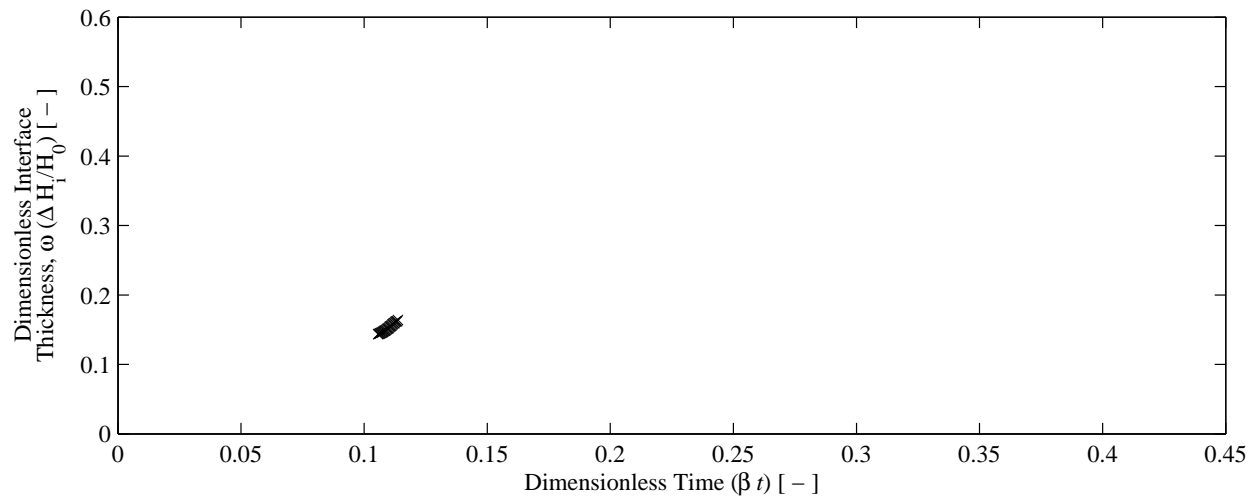


Figure I.6: Transient regressed agent profile slope for test no. 9 (FK-5-1-12)

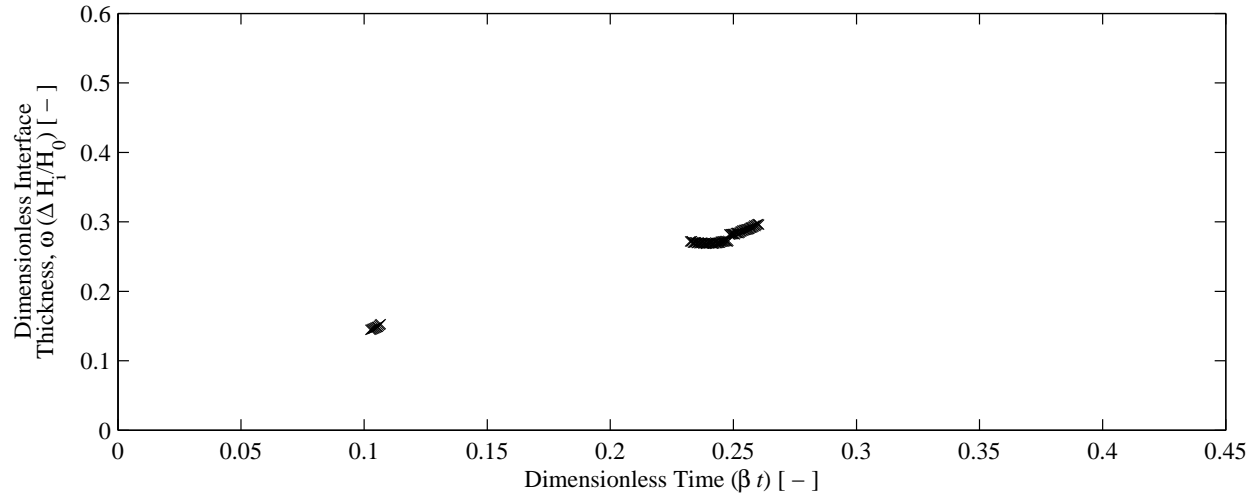


Figure I.7: Transient regressed agent profile slope for test no. 10 (FK-5-1-12)

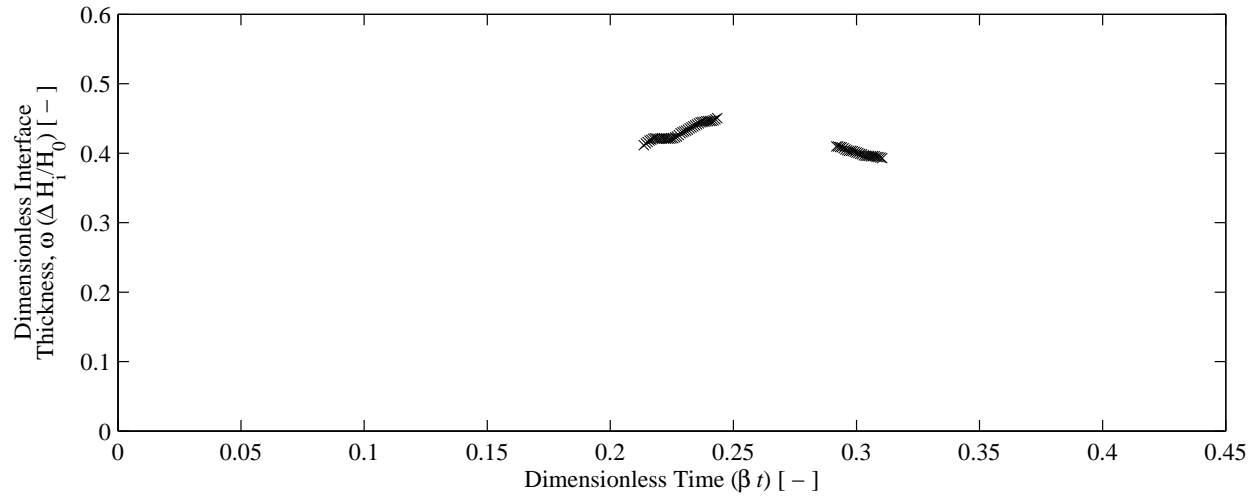


Figure I.8: Transient regressed agent profile slope for test no. 15 (IG-541)

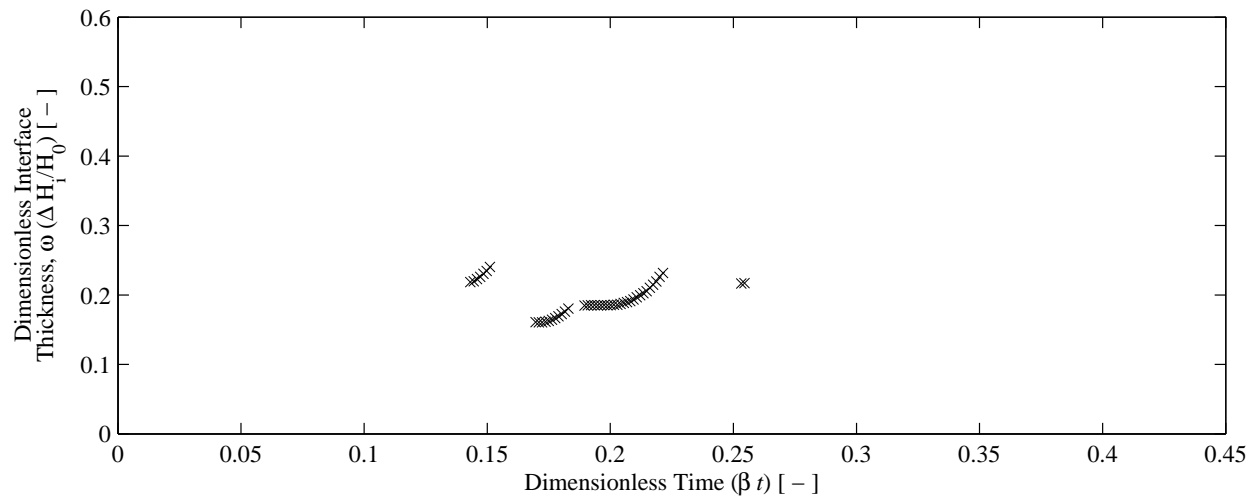


Figure I.9: Transient regressed agent profile slope for test no. 16 (HFC-125)

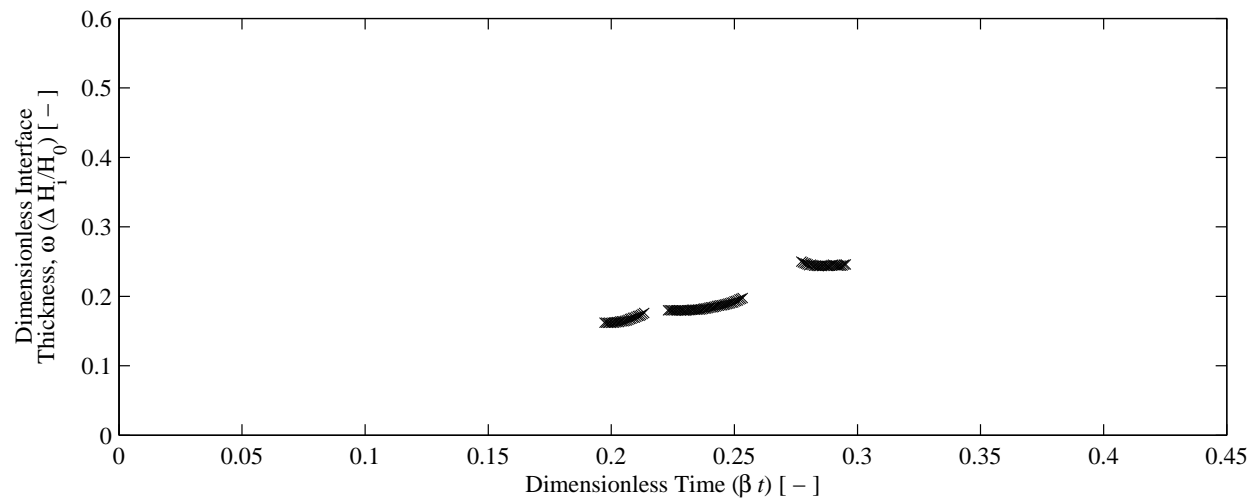


Figure I.10: Transient regressed agent profile slope for test no. 17 (HFC-125)

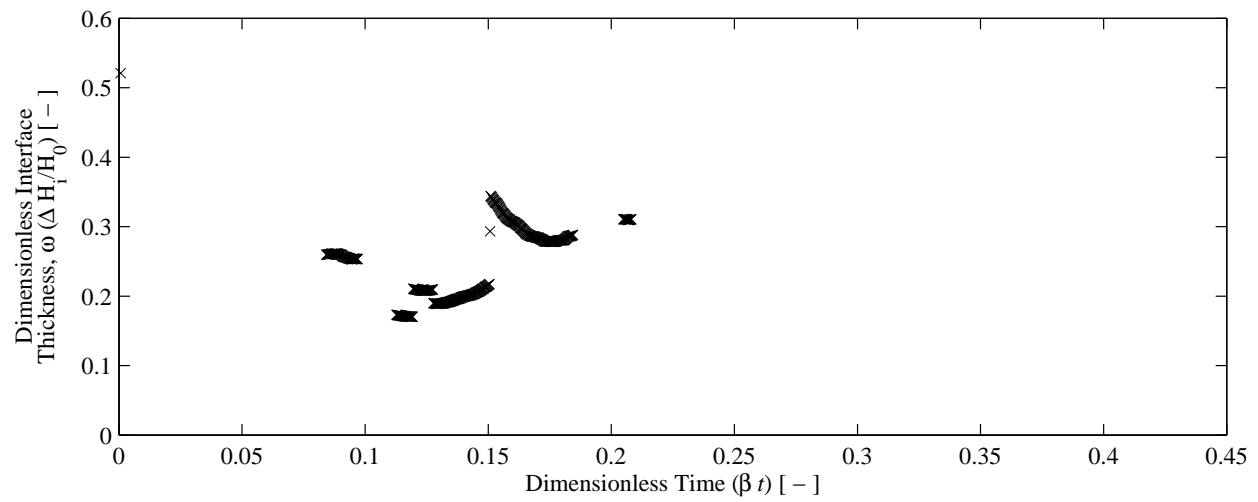


Figure I.11: Transient regressed agent profile slope for test no. 18 (HFC-125)

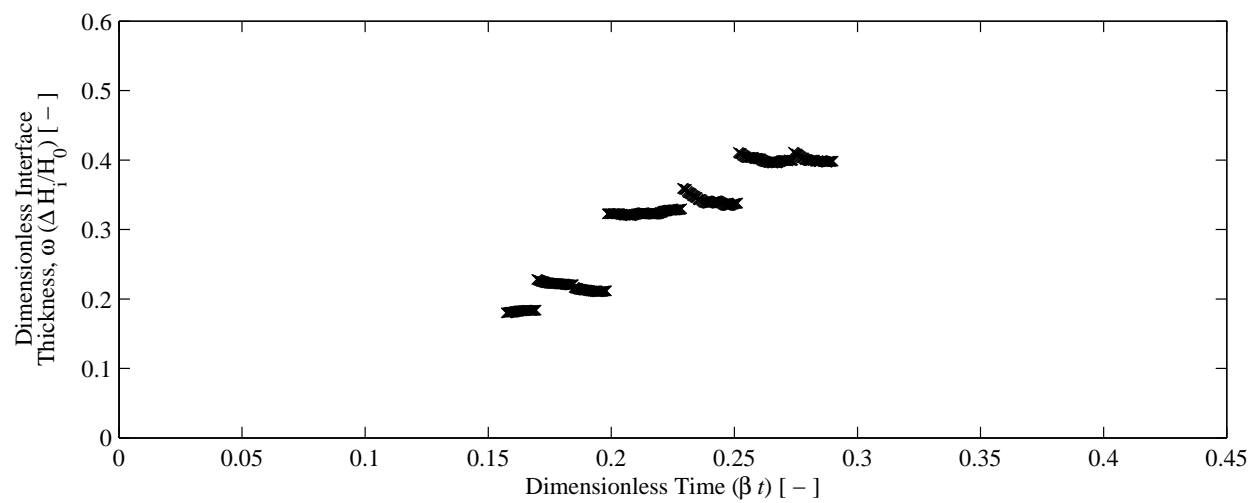


Figure I.12: Transient regressed agent profile slope for test no. 19 (HFC-125)

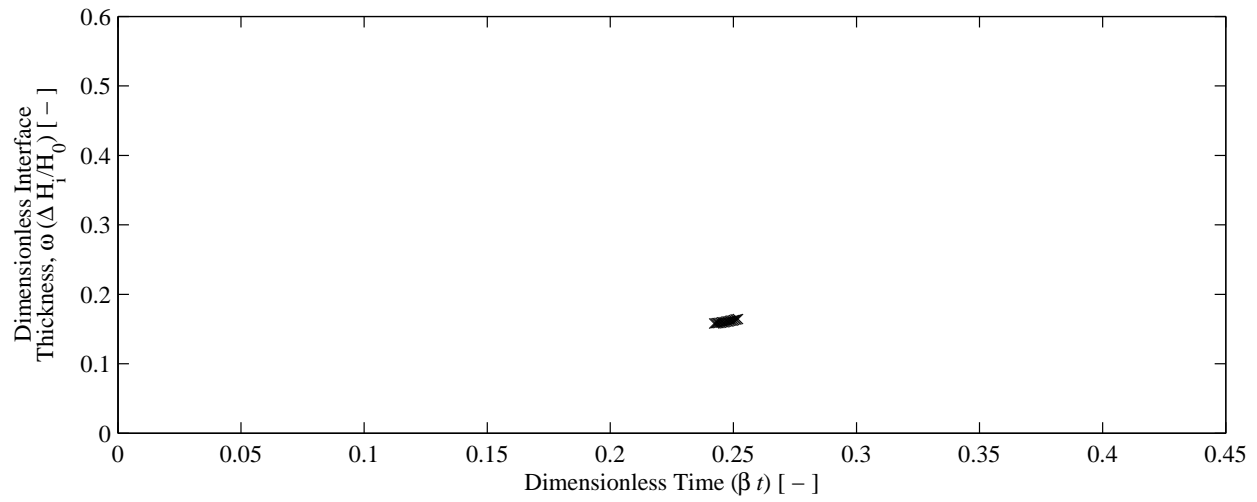


Figure I.13: Transient regressed agent profile slope for test no. 20 (HFC-125)

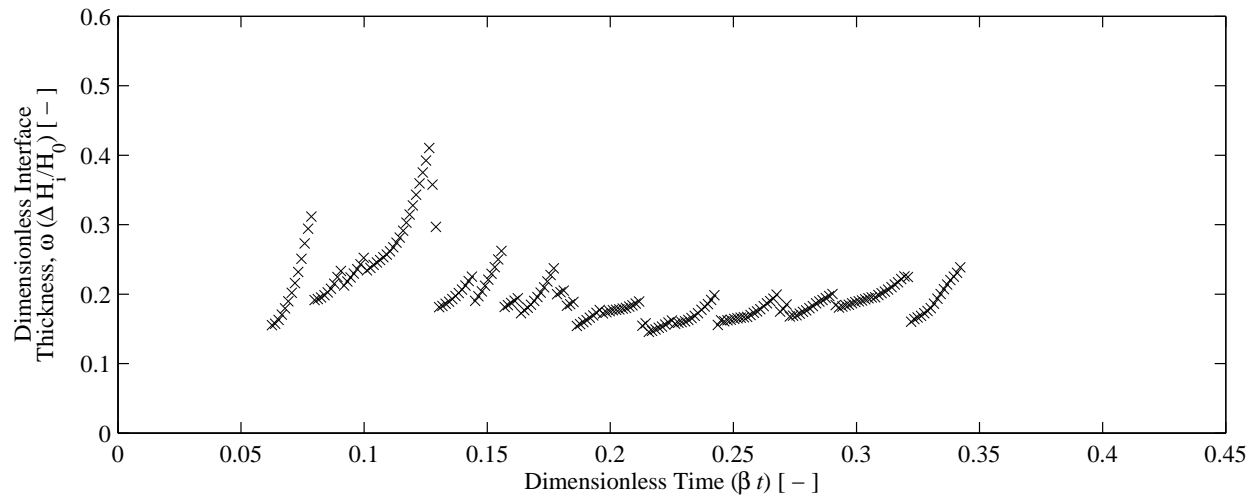


Figure I.14: Transient regressed agent profile slope for test no. 21 (HFC-227ea)

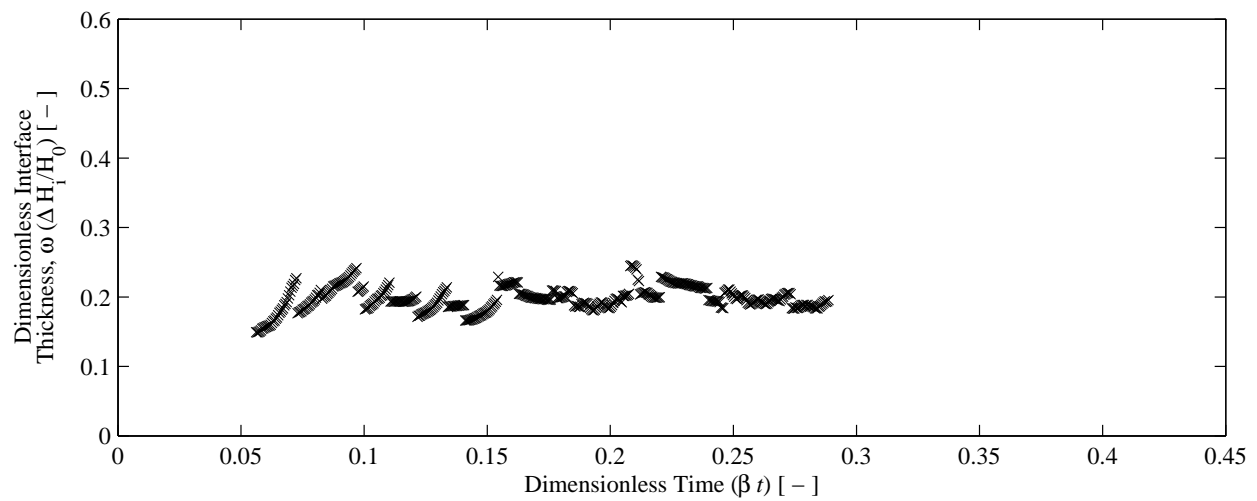


Figure I.15: Transient regressed agent profile slope for test no. 22 (HFC-227ea)

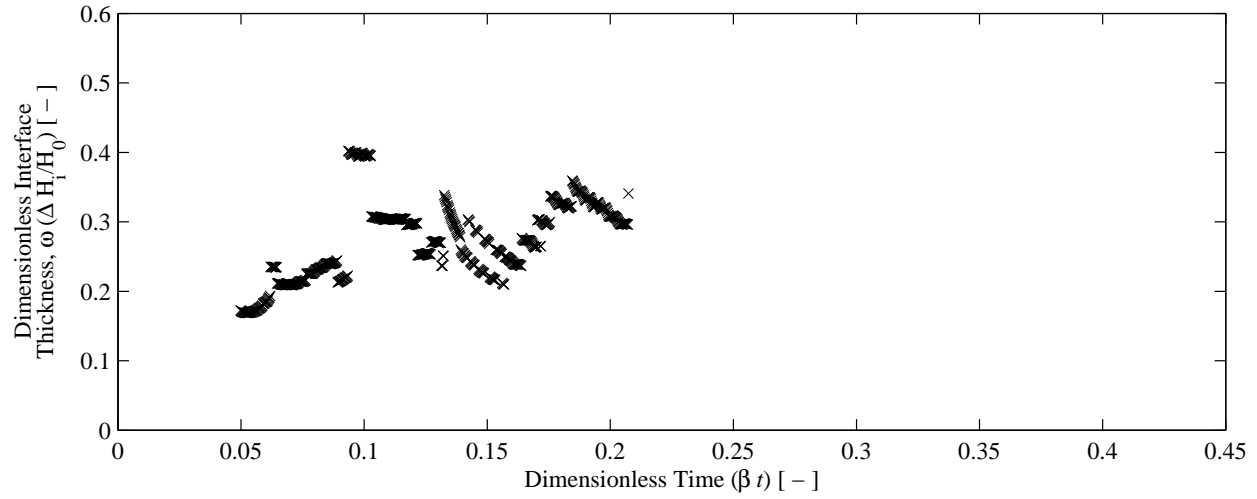


Figure I.16: Transient regressed agent profile slope for test no. 23 (HFC-227ea)

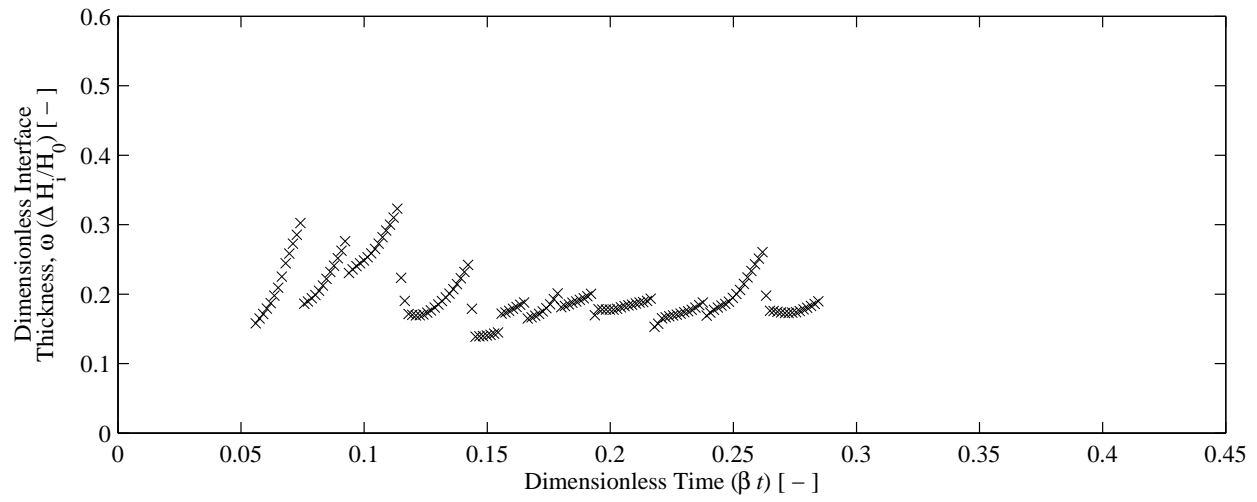


Figure I.17: Transient regressed agent profile slope for test no. 28 (HFC-23)

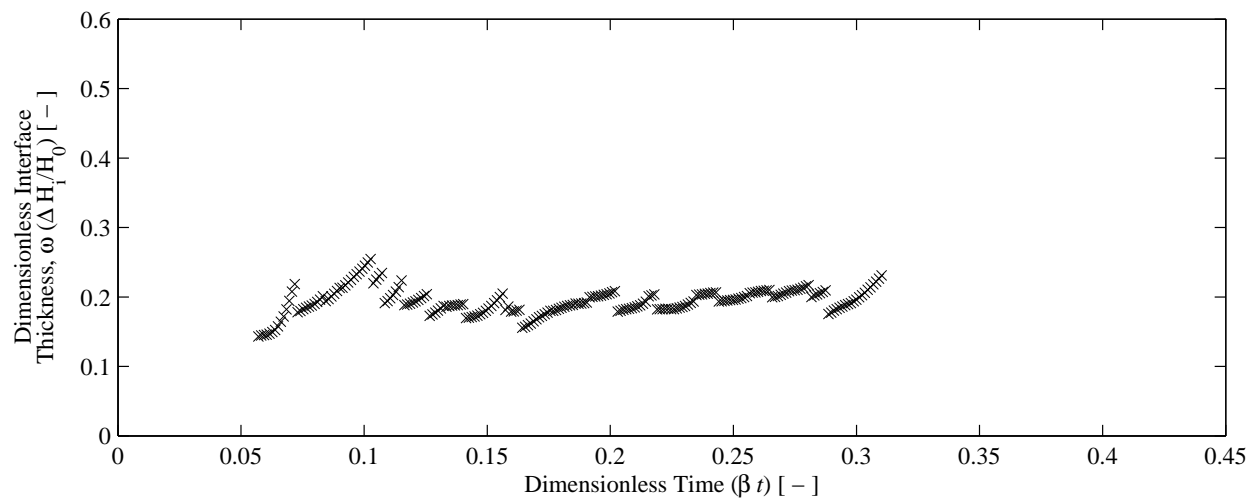


Figure I.18: Transient regressed agent profile slope for test no. 29 (HFC-23)

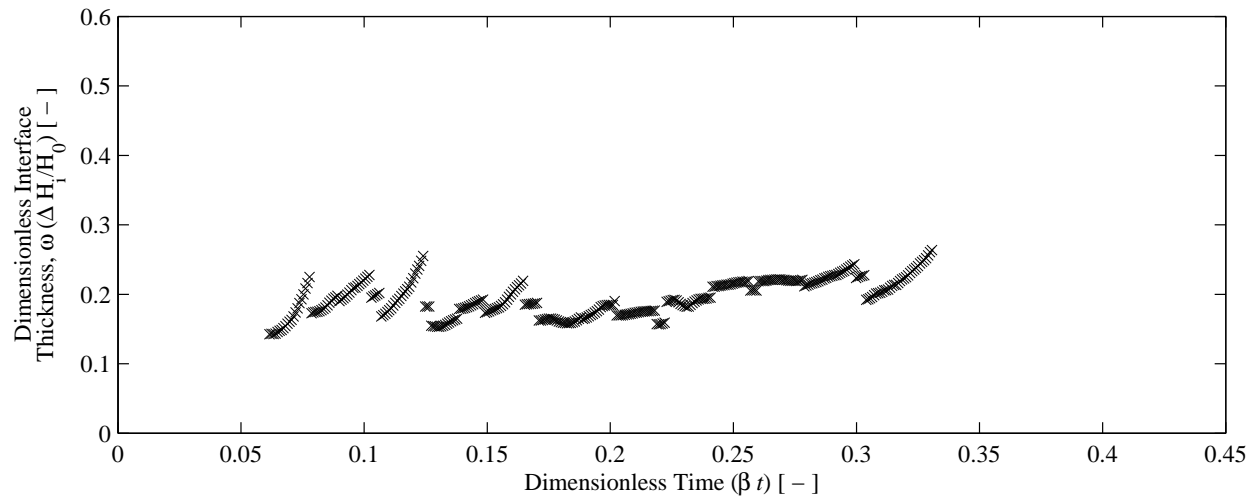


Figure I.19: Transient regressed agent profile slope for test no. 30 (HFC-23)

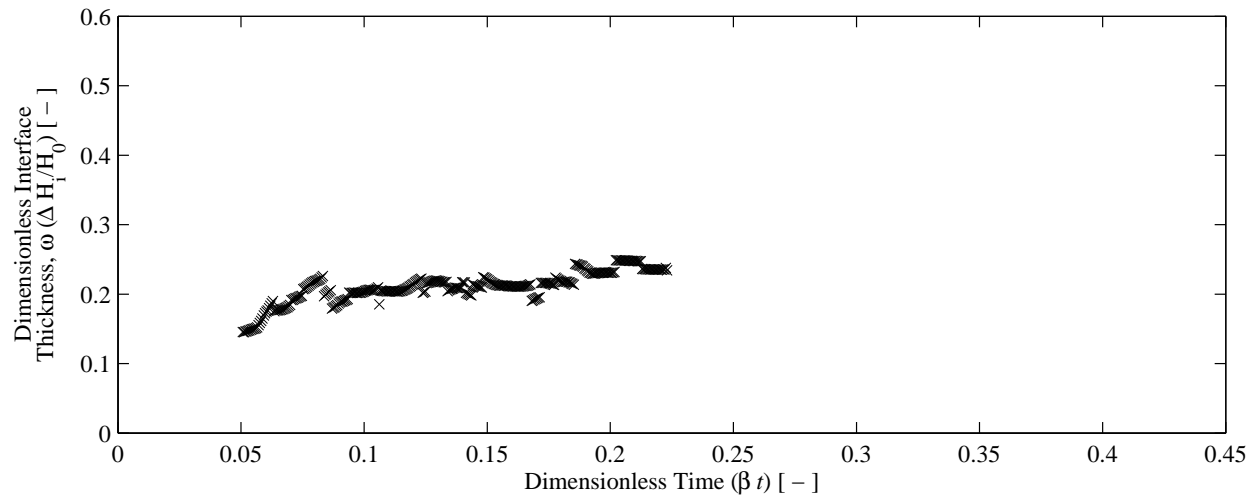


Figure I.20: Transient regressed agent profile slope for test no. 31 (HFC-23)

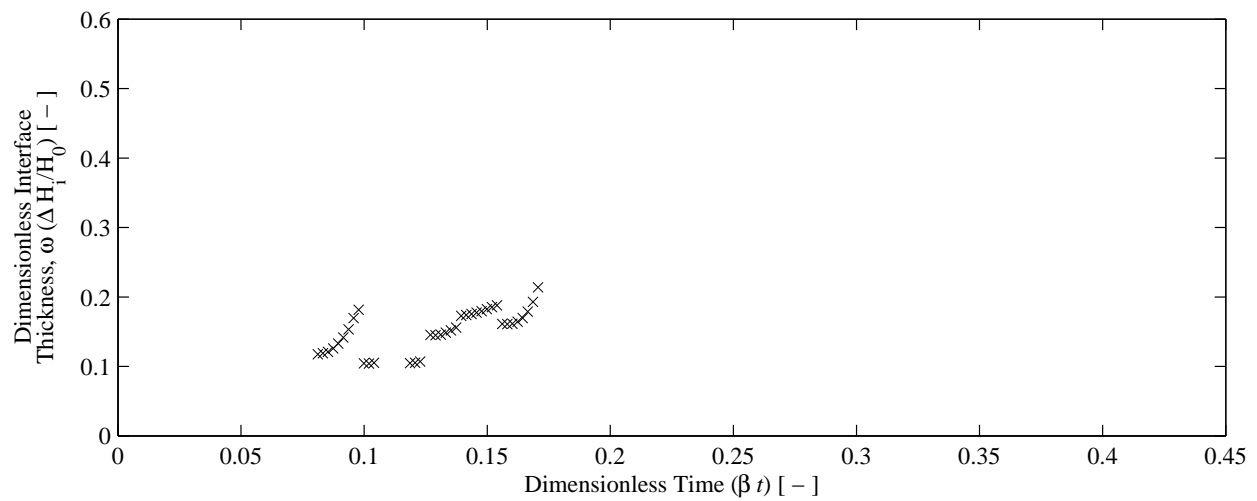


Figure I.21: Transient regressed agent profile slope for test no. 32 (IG-55)

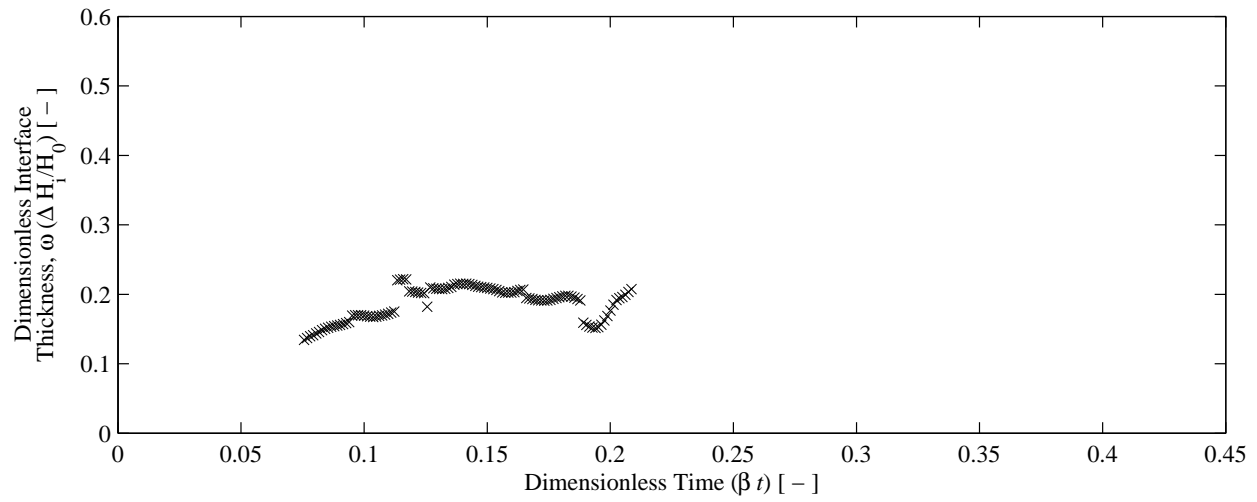


Figure I.22: Transient regressed agent profile slope for test no. 34 (IG-55)

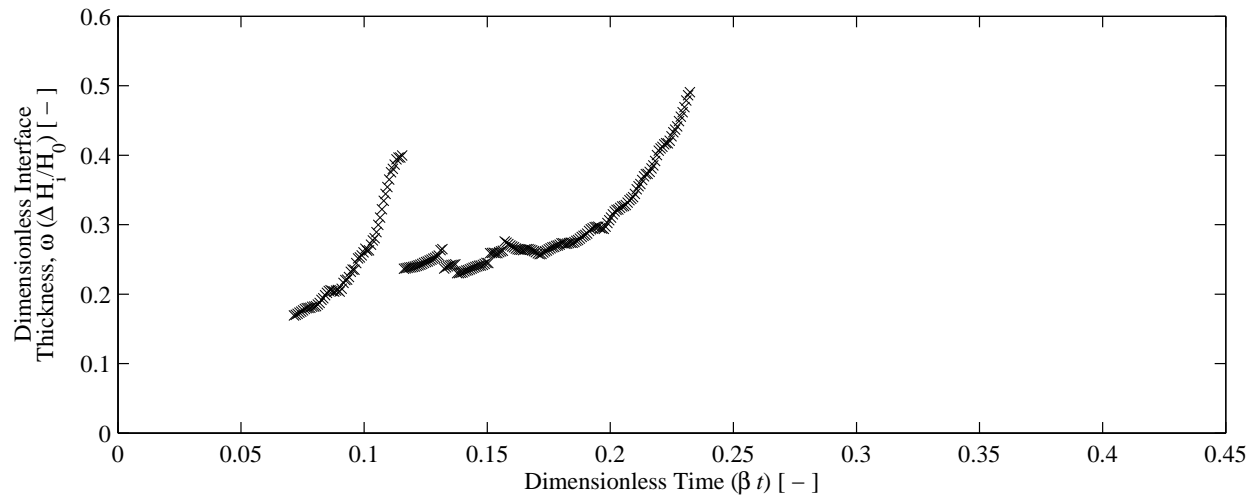


Figure I.23: Transient regressed agent profile slope for test no. 35 (IG-55)

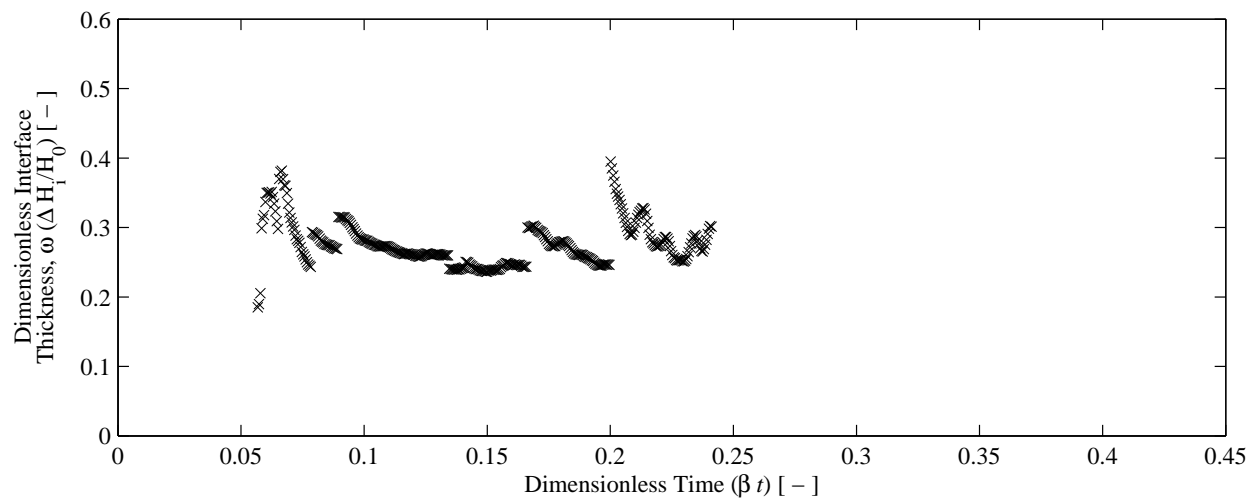


Figure I.24: Transient regressed agent profile slope for test no. 36 (IG-55)

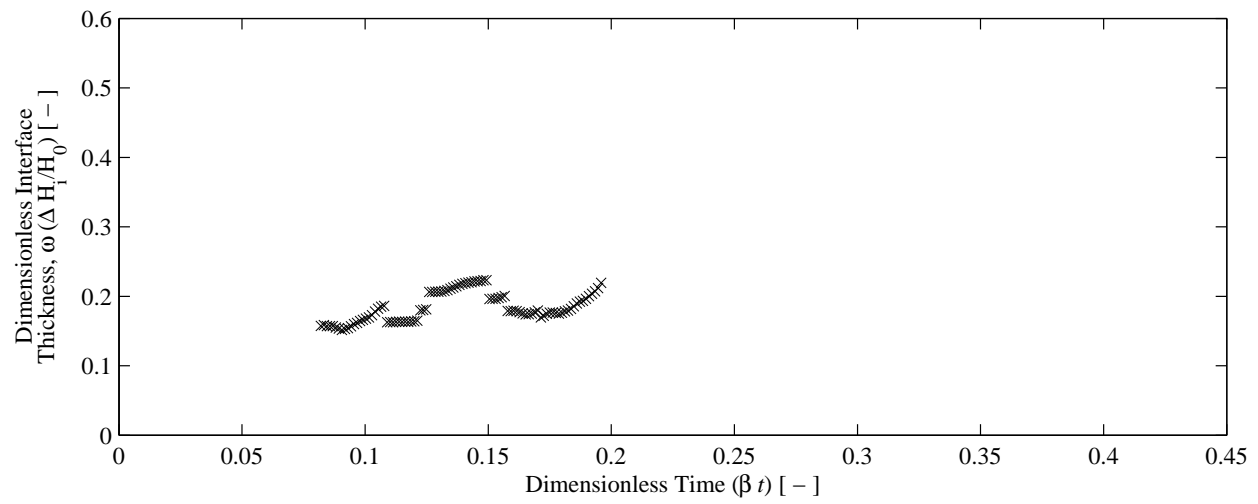


Figure I.25: Transient regressed agent profile slope for test no. 38 (IG-55P)

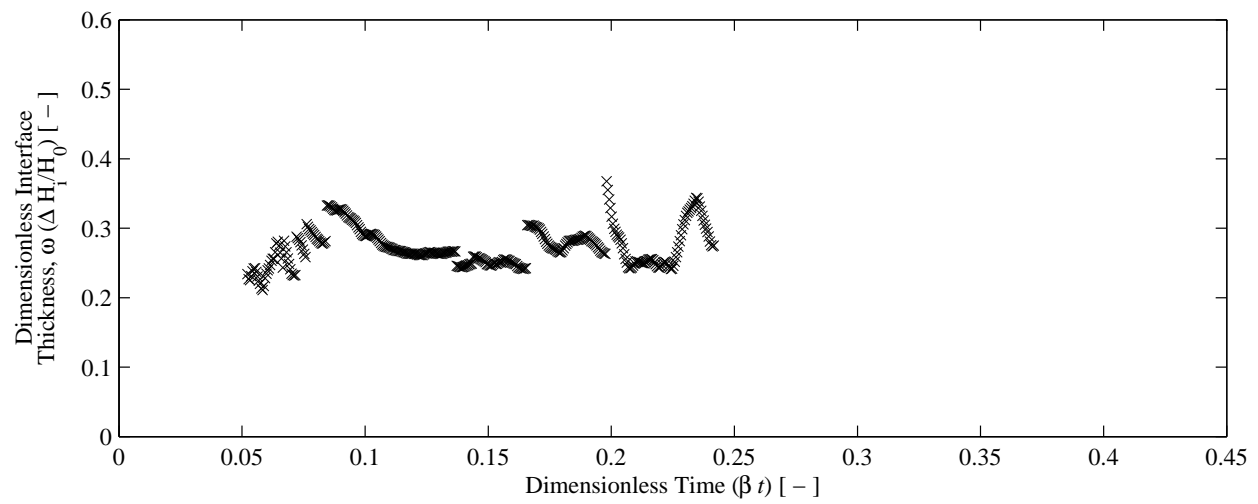


Figure I.26: Transient regressed agent profile slope for test no. 40 (IG-55P)

Appendix J

Hold Time Model Evaluation

The following of this appendix presents an expanded catalog of the quintessential hold time model evaluation charts as previously utilized in Chapters [2](#) and [3](#). The hold time calculations made for and construction of these dimensionless validation plots is also detailed in the referenced chapters. Previously, Figures [2.10](#), [2.11](#) and [3.9](#) present all the available data together. This appendix separates the data sets onto different axes by agent type and then groups them together again on the last page.

Reference Tables [A.1](#), [A.2](#), and [A.3](#) for information on each experiments' configuration parameters.

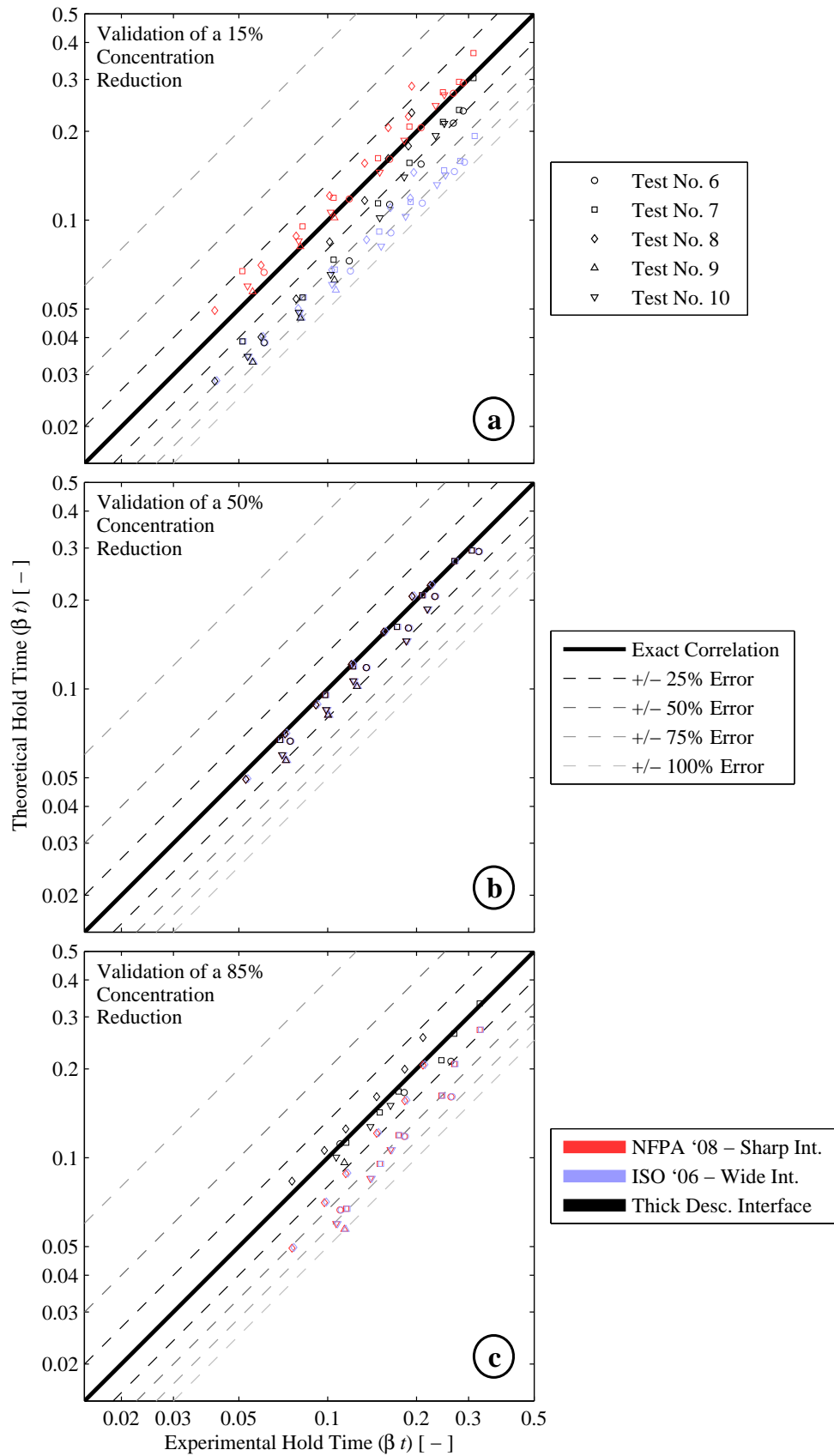


Figure J.1: The predicted theoretical hold time at 15%, 50%, and 85% concentration reduction thresholds, evaluated at any elevation, compared to the observed behavior of all the FK-5-1-12 tests conducted.

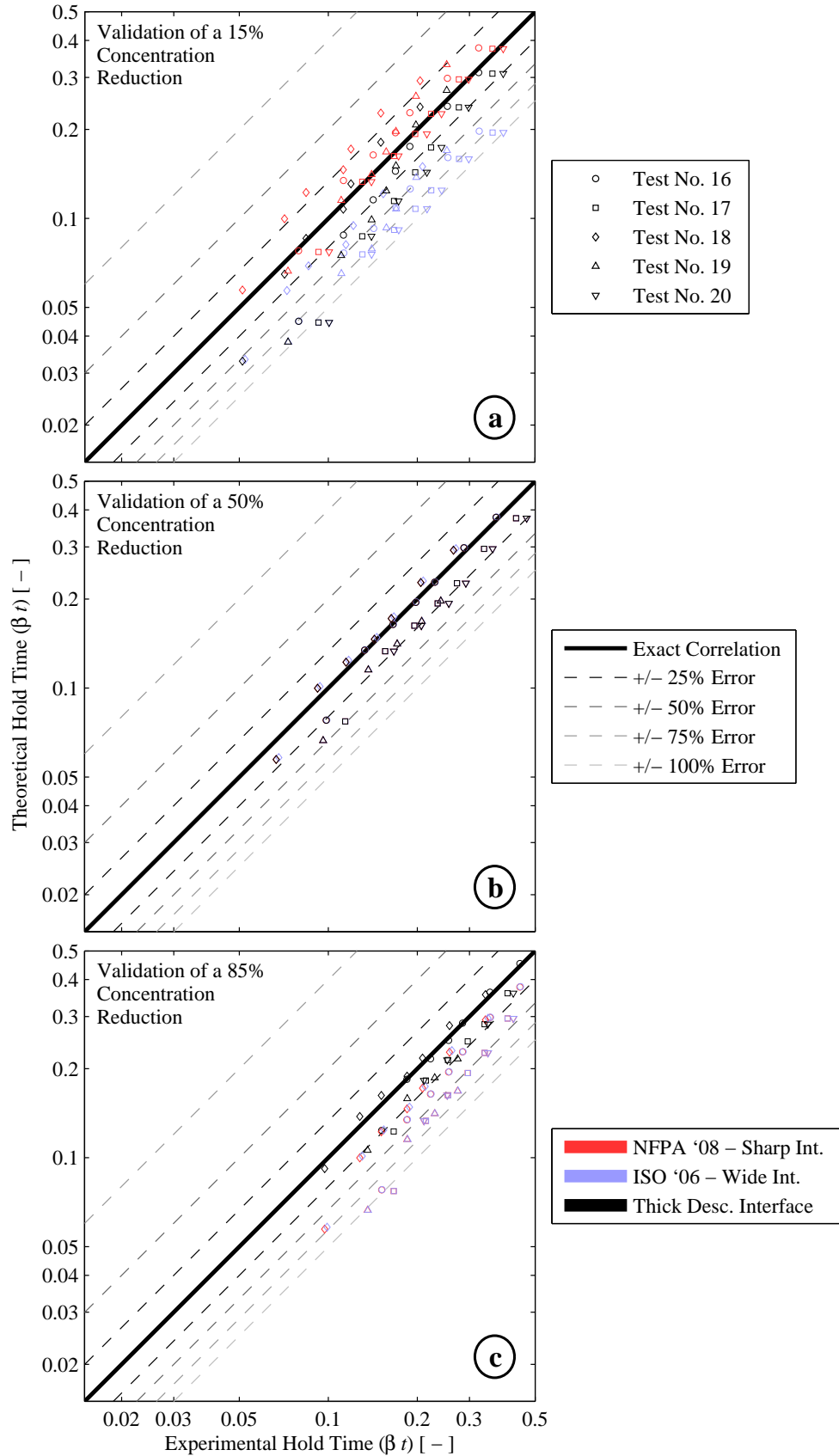


Figure J.2: The predicted theoretical hold time at 15%, 50%, and 85% concentration reduction thresholds, evaluated at any elevation, compared to the observed behavior of all the HFC-125 tests conducted.

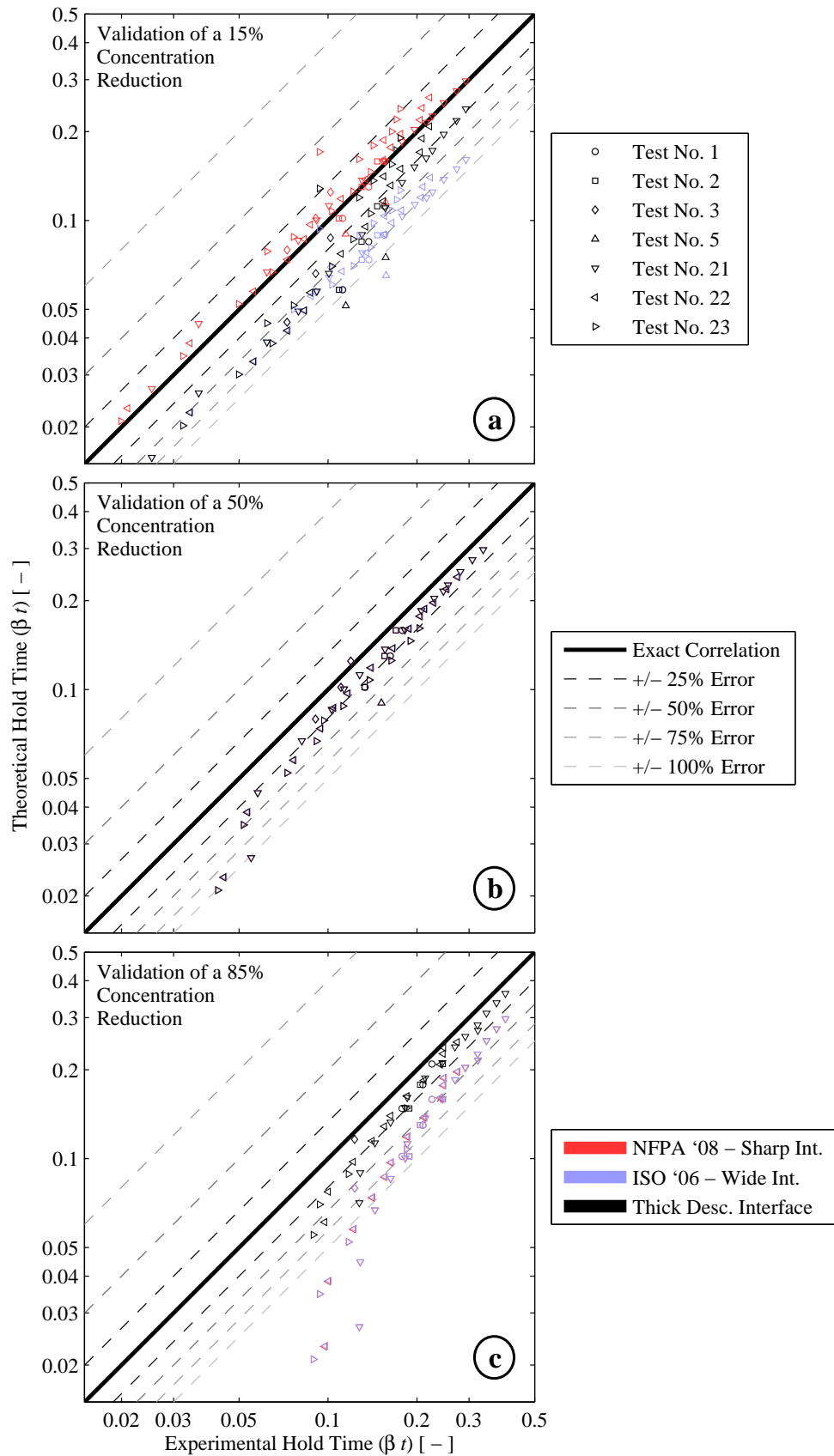


Figure J.3: The predicted theoretical hold time at 15%, 50%, and 85% concentration reduction thresholds, evaluated at any elevation, compared to the observed behavior of all the HFC-227ea tests conducted.

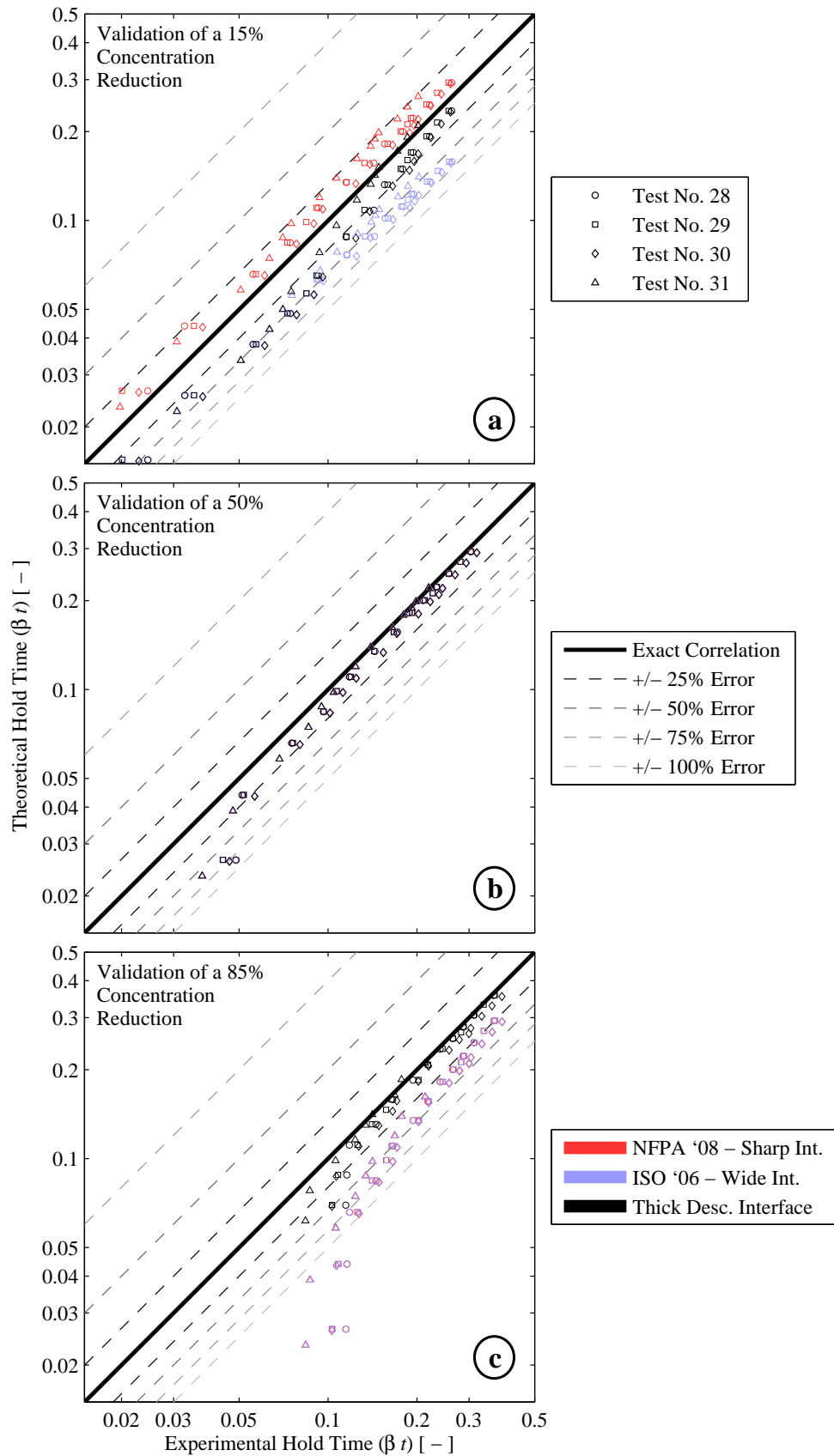


Figure J.4: The predicted theoretical hold time at 15%, 50%, and 85% concentration reduction thresholds, evaluated at any elevation, compared to the observed behavior of all the HFC-23 tests conducted.

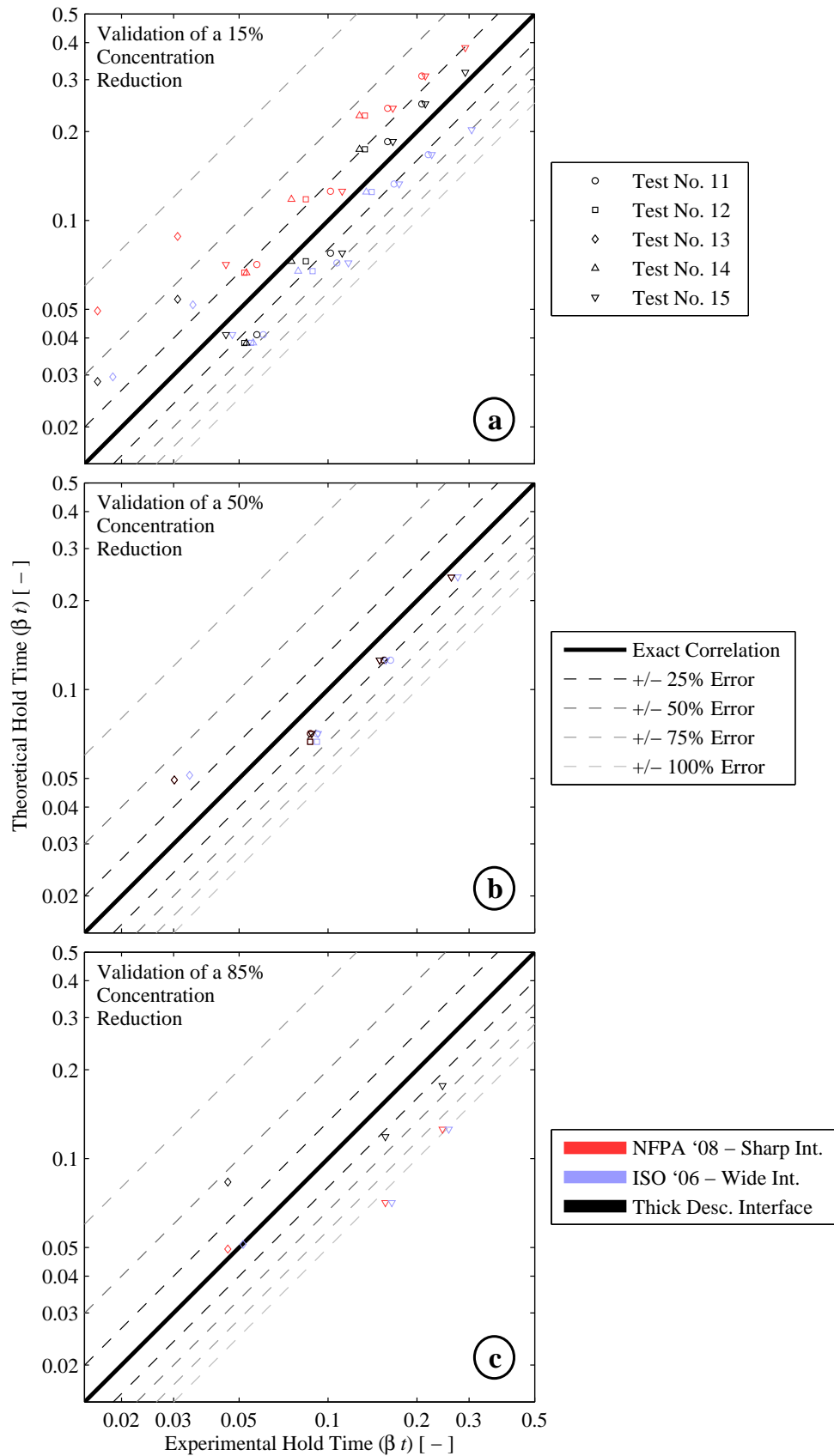


Figure J.5: The predicted theoretical hold time at 15%, 50%, and 85% concentration reduction thresholds, evaluated at any elevation, compared to the observed behavior of all the IG-541 tests conducted.

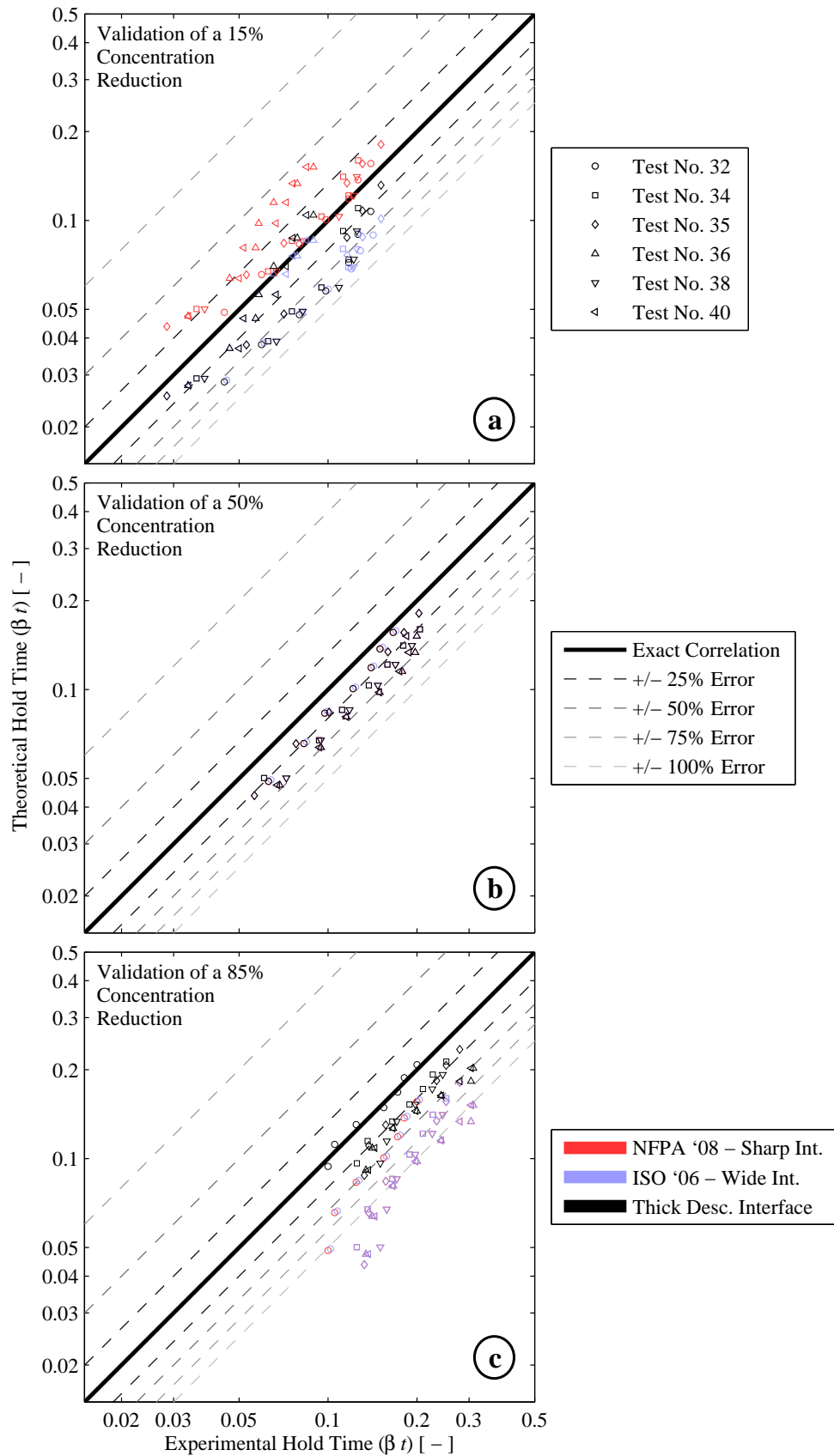


Figure J.6: The predicted theoretical hold time at 15%, 50%, and 85% concentration reduction thresholds, evaluated at any elevation, compared to the observed behavior of all the IG-55 tests conducted.

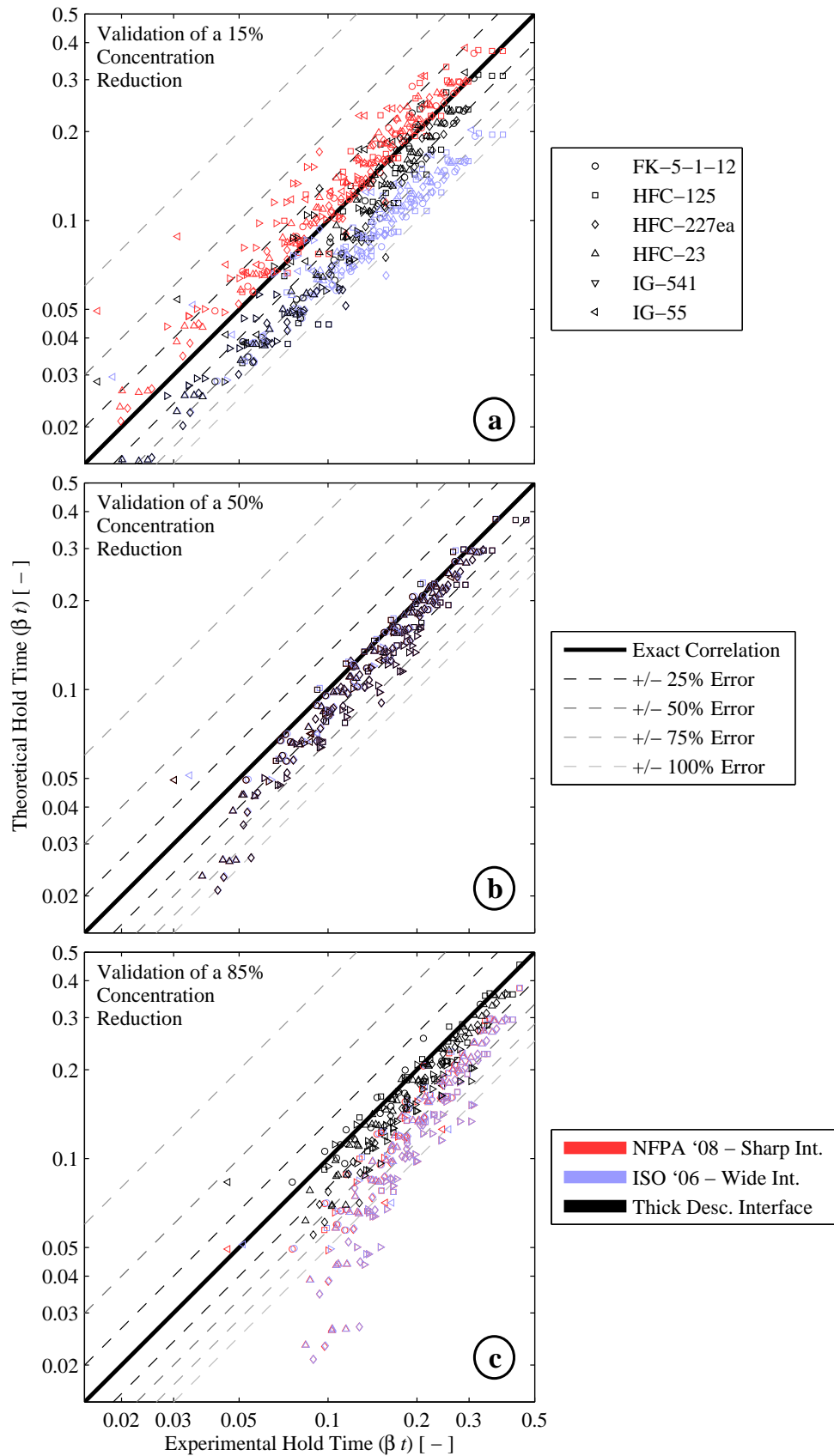


Figure J.7: The predicted theoretical hold time at 15%, 50%, and 85% concentration reduction thresholds, evaluated at any elevation, compared to the observed behavior of all clean agent types tested (pure N₂ not included).